



UNIVERSIDADE ESTADUAL DE CAMPINAS

INSTITUTO DE QUÍMICA

VINÍCIUS DINIZ

**Advanced Hybrid Materials for Direct Potable Reuse as Alternatives to Activated
Carbon for Removal of Contaminants of Emerging Concern**

**Materiais Híbridos Avançados para Reuso Potável Direto como Alternativas ao
Carvão Ativado para a Remoção de Contaminantes Emergentes**

CAMPINAS

2025

VINÍCIUS DINIZ

Advanced Hybrid Materials for Direct Potable Reuse as Alternatives to Activated
Carbon for Removal of Contaminants of Emerging Concern

Materiais Híbridos Avançados para Reuso Potável Direto como Alternativas ao Carvão
Ativado para a Remoção de Contaminantes Emergentes

Tese de Doutorado apresentada ao Instituto de Química da
Universidade Estadual de Campinas como parte dos
requisitos exigidos para a obtenção do título de Doutor em
Ciências

Doctor's Thesis presented to the Institute of Chemistry of
the University of Campinas as part of the requirements to
obtain the title of Doctor in Sciences

Supervisora: Prof^a Dr^a Susanne Rath

O arquivo digital corresponde à versão final da Tese defendida pelo aluno Vinícius Diniz
e orientada pela Prof^a. Dr^a. Susanne Rath.

CAMPINAS

2025

Ficha catalográfica
Universidade Estadual de Campinas (UNICAMP)
Biblioteca do Instituto de Química
Simone Luiz Alves - CRB 8/9094

D615a Diniz, Vinicius, 1994-
Advanced hybrid materials for direct potable reuse as alternatives to
activated carbon for removal of contaminants of emerging concern / Vinicius
Diniz. – Campinas, SP : [s.n.], 2025.

Orientador: Susanne Rath.
Tese (doutorado) – Universidade Estadual de Campinas (UNICAMP),
Instituto de Química.

1. Água - Reúso. 2. Carbono ativado. 3. Contaminantes emergentes. 4.
Cromatografia líquida. 5. Polímeros porosos. 6. Dióxido de titânio. I. Rath,
Susanne, 1962-. II. Universidade Estadual de Campinas (UNICAMP).
Instituto de Química. III. Título.

Informações complementares

Título em outro idioma: Materiais híbridos avançados para reuso potável direto como
alternativas ao carvão ativado para a remoção de contaminantes emergentes

Palavras-chave em inglês:

Water reuse

Carbon, activated

Emerging contaminants

Liquid chromatography

Porous polymers

Titanium dioxide

Área de concentração: Química Analítica

Titulação: Doutor em Ciências

Banca examinadora:

Susanne Rath [Orientador]

José Alberto Fracassi da Silva

Davi Gasparini Fernandes Cunha

José Carlos Mierzwa

José Roberto Guimarães

Data de defesa: 11-03-2025

Programa de Pós-Graduação: Química

Objetivos de Desenvolvimento Sustentável (ODS)

ODS: 6. Água potável e saneamento

Identificação e informações acadêmicas do(a) aluno(a)

- ORCID do autor: <https://orcid.org/0000-0002-2108-7702>

- Currículo Lattes do autor: <http://lattes.cnpq.br/3015961866891481>

BANCA EXAMINADORA

Profa. Dra. Susanne Rath (Orientadora)

Prof. Dr. José Alberto Fracassi da Silva (Instituto de química - UNICAMP)

Prof. Dr. Davi Gasparini Fernandes Cunha (Escola de Engenharia de São Carlos - USP)

Prof. Dr. José Carlos Mierzwa (Escola Politécnica - USP)

Prof. Dr. José Roberto Guimarães (Faculdade de Engenharia Civil, Arquitetura e Urbanismo - UNICAMP)

A Ata da defesa assinada pelos membros da Comissão Examinadora, consta no SIGA/Sistema de Fluxo de Dissertação/Tese e na Secretaria do Programa da Unidade.

Este exemplar corresponde à redação final da Tese de Doutorado defendida pelo(a) aluno(a) **Vinicius Diniz**, aprovada pela Comissão Julgadora em 11 de Março de 2025.

I wholeheartedly dedicate this thesis to my parents (Ivo and Cidinha) and my partner (Gabriela), whose unwavering support made it possible for me to pursue my dreams.

Dedico esta tese de todo o coração aos meus pais (Ivo e Cidinha) e à minha parceira (Gabriela), cujo apoio inabalável tornou possível a realização dos meus sonhos

Acknowledgements

Although my name appears on the cover of this thesis, this work is the result of the unwavering support and contributions of many individuals, for which I am deeply grateful. While it is impossible to thank everyone who has been part of this journey, I extend my sincere appreciation to each of you. A few individuals, however, deserve special mention.

First and foremost, I wish to express my deepest gratitude to my parents, Ivo and Cidinha, for their unconditional love and support, which have been with me since birth and throughout my pursuit of this doctorate. Your belief in me has been invaluable.

To my younger sister, Maria Eduarda, thank you for your faith in my abilities. I look forward to supporting you as you embark on your own journey, and I cannot wait to be in the front row at your viva in the years to come.

I am forever grateful to my grandparents, Edna and Jurandir, for helping to raise me and supporting me alongside my parents. Without your love and guidance, none of this would have been possible. I also wish to remember my late grandfather, Moíses, who called me "doctor" long before I ever imagined pursuing this path. His belief in me has always been a source of inspiration.

A special thanks to my supervisor, Prof. Susanne Rath, whose unwavering guidance since my master's degree has been essential to my growth as a researcher. Your wisdom and mentorship have shaped me both as a scientist and as a person, and I am profoundly grateful.

I also extend my heartfelt thanks to Dr. Colin Crick, who welcomed me into his lab at QMUL for 16 months. Your belief in me, as an international student eager to advance my skills in materials science, and your guidance throughout my time there have had a lasting impact on me both personally and professionally.

I would like to thank Prof. Jarbas Rohwedder for his assistance with the microwave-assisted syntheses and Raman analysis, and for his insights into the flow dynamics studies. Your thoughtful advice has been invaluable to this project.

My sincere thanks go also to Prof. José Roberto Guimarães (*Tuca*) and Dr. Joseph (*Joe*) Bear, who generously contributed to this project. Thank you both for your significant contributions to my development.

I would also like to thank Prof. Davi G.F. Cunha, who gave me my first opportunity as an undergraduate researcher in his lab and has guided me from those early days to the present. Your support has been a cornerstone of my academic journey.

I want to express my gratitude to both the Paracelsus and Crick research groups for their support and friendship throughout the development of this thesis. Without our coffee breaks and conversations, this journey would have been far more challenging.

I am deeply thankful to my friends in London, whose companionship during my BEPE made me feel at home. A special thanks to Jean Lipreri for your help navigating visa bureaucracy and for your enduring friendship.

I also appreciate the support from the Unicamp staff, particularly the CPG-IQ team, for their readiness to assist with any questions or analysis requests. My gratitude extends to the QMUL staff for their support during my time there, which made the experience all the more fulfilling.

To my life partner, Gabriela, words cannot fully express my gratitude for your love, patience, and unwavering support throughout this journey. This thesis is as much yours as it is mine, and I look forward to our future adventures together. I love you more than eight.

I would also like to thank SANASA for their support, without which the monitoring and pilot-plant studies would not have been possible. My gratitude extends to the INCTAA research group for their invaluable discussions and support throughout this project.

Finally, I would like to express my sincere appreciation to the funding agencies that made this research possible. Without their financial support, this work would not have come to fruition.

This study was financed in part by the Instituto Nacional de Tecnologias Analíticas Avançadas (INCTAA) (grant: FAPESP #2014/50951-4 and CNPq 465768/2014-8).

This study was financed in part by the Coordenação de Aperfeiçoamento de Pessoal de Nível Superior – Brasil (CAPES) – Finance Code 001.

This study was financed by the São Paulo Research Foundation (FAPESP) grants #2021/08123-0 and #2022/11350-1.

“There is no such thing as teaching without research and research without teaching”¹

Paulo Freire

¹“Não há ensino sem pesquisa e pesquisa sem ensino”, In Pedagogia da Autonomia. São Paulo, Paz e Terra, 1996

RESUMO

O aumento do consumo de água potável, aliado à diminuição da disponibilidade de água doce, gera a necessidade de alternativas para o abastecimento público. Embora o reúso potável direto (RPD) seja viável, sua implementação é desafiadora devido à necessidade de processos avançados de tratamento e à grande variedade de contaminantes. A EPAR Capivari II, em Campinas (SP), Brasil, é uma estação produtora de água de reúso não potável com tecnologia de biorreator de membranas (MBR). Uma planta piloto, com a capacidade de produção de 350 L/h, instalada na EPAR, contendo tecnologias de osmose reversa (OR), fotoperoxidação (UV/H₂O₂) e colunas de carvão ativado granular (CAG), permite combinar as diferentes tecnologias de tratamento visando o RPD. Neste trabalho, a cromatografia líquida bidimensional acoplada à espectrometria de massas sequencial (LC-LC-MS/MS) foi usada para monitorar 12 contaminantes emergentes no esgoto bruto e no efluente pós-MBR, priorizando cinco para estudos posteriores (caféina, hidroclorotiazida, sacarina, sulfametoxazol e sucralose). O processo OR-UV/H₂O₂–CAG apresentou a melhor remoção dos contaminantes priorizados, além de produzir efluente que atende a portaria GM/MS N° 888. Posteriormente, o carvão ativado (CA) da planta piloto (CA1) e outro comercial (CA2) foram caracterizados e avaliados em estudos de bancada (batelada e contínuo). Ambos os CA apresentaram maior capacidade de adsorção para sulfametoxazol e menor para sucralose. Estudos com CAG, em escala de bancada, revelaram que o uso de fluxo ascendente é mais eficaz na remoção de contaminantes devido a não formação de caminhos preferenciais. Em ambos os estudos, o CA2 apresentou maiores remoções devido à sua maior área superficial. A busca por novos materiais para RPD é essencial para a viabilidade do RPD. Este trabalho investigou o CA como suporte para TiO₂ (TiO₂/CA) e polímeros de enxofre porosos (PEP). Diferentes sínteses e precursores de TiO₂ foram testados para a fabricação de TiO₂/CA, com o material sinterizado pelo método sol-gel combinado com isopropóxido de TiO₂ apresentando as melhores remoções dos cinco contaminantes, aumentando a eficiência do TiO₂ em até 10 vezes. Os polímeros de enxofre foram sintetizados por vulcanização inversa utilizando 1,3-diisopropenilbenzeno (DIB) como monômero e cloreto de sódio como template para criação dos poros. Maiores quantidades de DIB levaram a maior adsorção de caféina, enquanto maiores quantidades de enxofre resultaram em maior atividade fotocatalítica, com eficiência acima de 90% para remoção de caféina. Os estudos na planta piloto comprovaram a viabilidade do processo OR–UV/H₂O₂–CAG na remoção de contaminantes, produzindo água potável conforme os padrões regulatórios. O processo de adsorção foi dependente da área superficial do CA, e os novos materiais estudados mostraram-se promissores para uso em RPD.

ABSTRACT

As freshwater availability declines and global water consumption rises, water scarcity has become critical, driving the need for alternative water sources. Direct potable reuse (DPR) offers a promising solution, though it faces challenges such as advanced treatment requirements and identifying marker contaminants. This thesis focuses on the EPAR Capivari II facility in Campinas, São Paulo, Brazil, a non-potable water reuse plant that uses membrane bioreactor (MBR) technology. A pilot plant (350 L/h) was installed at EPAR Capivari II, incorporating reverse osmosis (RO), UV/H₂O₂ photoperoxidation, and granular activated carbon (GAC) columns to test different DPR treatment configurations. The study monitored 12 contaminants of emerging concern (CECs) in raw sewage and post-MBR effluent using bidimensional liquid chromatography coupled with mass spectrometry (LC-LC-MS/MS), prioritizing five for further investigation: caffeine, hydrochlorothiazide, saccharin, sulfamethoxazole, and sucralose. The RO-UV/H₂O₂-GAC process proved to be the most effective in removing these prioritized CECs, producing effluent that met Brazilian potable water standards (GM/MS Ordinance No. 888). This thesis also evaluated the performance of the pilot plant's activated carbon (AC1) and a commercial activated carbon (AC2) in batch and continuous flow studies. Results indicated that both activated carbons had higher adsorption capacities for sulfamethoxazole and lower for sucralose, with the Sips model best fitting the adsorption data. Continuous flow studies showed that upward flow was more effective for contaminant removal, with AC2 outperforming AC1 due to its larger surface area. To enhance DPR efficiency, this thesis also explored the development of new materials, including TiO₂-supported activated carbon (TiO₂/AC) and porous sulfur polymers (PSPs). Various synthesis methods and TiO₂ precursors were tested, with the sol-gel method using titanium isopropoxide yielding the most effective TiO₂/AC material, increasing TiO₂ efficiency up to tenfold compared to commercially available dispersed TiO₂ nanoparticles. Additionally, PSPs were synthesized via inverse vulcanization using 1,3-diisopropenylbenzene (DIB) as a monomer and sodium chloride (NaCl) as a template for pore formation. Higher DIB content resulted in increased caffeine adsorption, while a higher sulfur content enhanced photocatalytic activity, achieving over 90% caffeine removal. In summary, the pilot plant at EPAR Capivari II successfully demonstrated the feasibility of the RO-UV/H₂O₂-GAC process in producing potable water according to regulatory standards. Comparative studies highlighted AC2's superior performance due to its larger surface area. The exploration of TiO₂/AC composites and PSPs underscores the potential of these materials to improve DPR systems' sustainability and effectiveness, emphasizing the ongoing need for innovation and optimization in water treatment technologies.

List of Figures

Figure 1: Global freshwater withdrawals for agricultural, industrial, and domestic uses by aggregated regional groupings (left side). Renewable internal freshwater resources flows refer to internal renewable resources (internal river flows and groundwater from rainfall) (right side). OECD members are defined as countries who were members in 2010, and their membership was carried back in time. BRICS countries are Brazil, Russia, India, China and South Africa. Source: (Diniz et al. 2024a)	20
Figure 2: Detailed schematic of the EPAR Capivari II wastewater treatment plant, with the colors and lines used to guide the eye. Source: Author.....	25
Figure 3: Main characterization techniques used for materials in water treatment. Source: Author.	32
Figure 4: Classification of adsorption isotherms. Green dotted lines represent desorption hysteresis. Type I is characteristic of microporous adsorbents; Type II corresponds to non-porous or macroporous adsorbents; Type III indicates weaker interactions in non-porous or macroporous adsorbents; Type IV is typical of mesoporous adsorbents; Type V represents weaker interactions in micro- or mesoporous adsorbents; and Type VI describes layer-by-layer adsorption on a highly uniform surface. Adapted from Rouquerol et al. (2014)	33
Figure 5: Movement of the mass transfer zone and breakthrough curve over time in a fixed-bed column. Source: Author.....	48
Figure 6: Tracer injection types and their respective concentration curves. A: Pulse injection; B: Step injection. C _{max} is the tracer maximum concentration and C ₀ is the tracer initial concentration. Adapted from (Silva 2006).	53
Figure 7: Flow anomalies in reactors based on the E curve. (A) no anomalies observed; (B) Channeling; (C) Experimental errors; (D) Internal recirculation; and (E) two parallel paths. Adapted from (Zaiat 2005).	55
Figure 8: General scheme for inverse vulcanization polymerization. Source: Author.....	61
Figure 9: Adsorption kinetics of the selected contaminants of emerging concern (CECs) by AC1 (A) and AC2 (B). Initial concentration of 500 µg/L. Source: Author.....	182

List of Tables

Table 1: Principal functional groups and their bands in Fourier Transform Infrared (FTIR) analysis (Tran, Chao, and You 2018).	36
Table 2: Major functional groups affecting adsorbate-adsorbent interaction (Patel et al. 2019).....	46
Table 3: Specific parameters for fixed-bed column adsorption models.	51
Table 4: Properties of activated carbons (AC1 & AC2) determined by nitrogen gas (N ₂) adsorption at 77 K and Boehm titration.....	181
Table 5: Summary of Elovich model parameters for both AC1 and AC2	182
Table 6: Summary of breakthrough curve model parameters for both AC1 and AC2 at different bed heights and downflow mode.	185
Table 7: Summary of breakthrough curve model parameter for both AC1 and AC2 at different flow rates and downflow mode.	186
Table 8: Summary of breakthrough curve model parameters for both AC1 and AC2 at different bed heights and upflow mode.....	188
Table 9: Summary of breakthrough curve model parameters for both AC1 and AC2 under different water composition.....	189

List of Abbreviations and Acronyms

ΔG	Gibbs free energy variation
ΔH	Enthalpy variation
ABNT	Associação Brasileira de Normas Técnicas
AC1	Activated carbon from the pilot-plant of the EPAR Capivari II
AC2	Commercial activated carbon
AES	Auger electron spectroscopy
AFM	Atomic force microscopy
ASTM	American Society for Testing and Materials
C_0	Initial Concentration
C_e	Concentration of the adsorbate at equilibrium
C_{MAX}	Maximum concentration
CEC	Contaminant of emerging concern
DIB	1,3-diisopropenylbenzene
DPR	Direct potable reuse
DWTP	Drinking water treatment plant
E	Adsorption Energy
EBCT	Empty bed column time
EDS	Energy-dispersive X-ray spectroscopy
EMA	European Medicine Agency
FTIR	Fourier transform infrared
g	Redlich-Peterson model exponent
GAC	Granular activated carbon
HRT	Hydraulic retention time
IEP	Isoelectric point
JIS	Japanese Industrial Standards
K_f	Freundlich constant
LC-LC-MS/MS	Bidimensional liquid chromatography coupled with tandem mass spectrometry
LOQ	Limit of quantification
MBR	Membrane bioreactor

MPV	Maximum permissible value
MTZ	Mass transfer zone
<i>n</i>	Freundlich intensity parameter
OECD	Organization for Economic Cooperation and Development
OH·	Hydroxyl radical
PAC	Powder activated carbon
PZC	Point of zero charge
<i>q</i>	Amount adsorbed
Q_{max}^0	Monolayer saturation capacity
R²	Coefficient of determination
RO	Reverse osmosis
RTD	Residence time distribution
SAXS	Small-angle X-ray scattering
SD	Standard deviation
SEM	Scanning electron microscopy
SLR	Surface loading rate
<i>t</i>	Time
<i>t_b</i>	Breakthrough time
TEM	Transmission electron microscopy
Ti(OBu)₄	Titanium butoxide
Ti(OiPr)₄	Titanium isopropoxide
TiCl₄	Titanium tetrachloride
TiO₂	Titanium dioxide
<i>t_s</i>	Saturation time
UHPLC-MS/MS	Ultra-high performance liquid chromatography-tandem mass spectrometry
UV/H₂O₂	Photoperoxidation
WHO	World Health Organization
WWTP	Wastewater treatment plant
XPS	X-ray photoelectron spectroscopy
ε	Polanyi potential
χ²	Chi-square

Table of Contents

Chapter 1. Introduction.....	18
1.1. Water scarcity	19
1.2. Potable reuse.....	21
1.2.1. Prioritization of contaminants of emerging concern	22
1.2.2. EPAR Capivari II and pilot plant	24
1.3. Adsorption: general considerations	26
1.3.1. Adsorption for water treatment	28
1.3.1.1. Activated carbon.....	30
1.3.2. Adsorption modelling: batch studies.....	37
1.3.2.1. Kinetics modelling.....	38
1.3.2.2. Isotherms modelling	41
1.3.2.3. Adsorption mechanism	45
1.3.3. Adsorption modelling: continuous flow studies.....	47
1.3.3.1. Hydrodynamics.....	52
1.4. Advanced materials	56
1.4.1. Activated carbon as support for photocatalysts.....	58
1.4.2. Inverse vulcanization sulfur polymers	60
Chapter 2. Aims and objectives	64
2.1. Aims and objectives	65
Chapter 3. Published Manuscripts	67
3.1. List of published manuscripts.....	68
3.1.1. Adsorption of recalcitrant contaminants of emerging concern onto activated carbon: A laboratory and pilot-scale study.....	69
3.1.2. Adsorption of aqueous phase contaminants of emerging concern by activated carbon: Comparative fixed-bed column study and in situ regeneration methods.....	101
3.1.3. Synthesis and characterization of TiO ₂ -carbon filter materials for water decontamination by adsorption-degradation processes.....	127
3.1.4. Porous sulfur polymers for effective aqueous-phase organic contaminant removal.....	152
Chapter 4. Discussion.....	177
Chapter 5. Final Remarks	197
5.1. Summary of Research Contributions.....	198

5.2.	Implications for Water Treatment Technologies	199
5.3.	Challenges and Future Research Directions	200
5.4.	Broader Impact and Societal Relevance	201
5.5.	Conclusion.....	202
Chapter 6.	References	203
Chapter 7.	Annexes	221

Preface

As global water scarcity escalates due to factors such as population growth, urbanization, and climate change, the urgency for innovative water management and purification solutions has never been greater. Traditional freshwater sources are being depleted, and the demand for potable water is surging, making effective Direct Potable Reuse (DPR) systems increasingly vital. DPR offers a promising strategy to address water scarcity by recycling treated wastewater into potable water, thus conserving valuable freshwater resources and ensuring a sustainable supply. The wastewater treatment plant EPAR Capivari II in Campinas, Brazil, produces high-quality effluent through a membrane bioreactor and features a multiconfiguration pilot plant for DPR investigations, presenting a promising alternative for water supply in Brazil.

In this context, efficient sewage management and purification are crucial for optimizing DPR processes and effectively removing critical contaminants. While activated carbon has been a mainstay in water purification due to its proven adsorption capabilities, this thesis investigated advanced hybrid materials that combine adsorption with photocatalysis. By developing and evaluating these innovative materials, the research aimed to enhance contaminant removal efficiency and improve the overall effectiveness and cost-efficiency of DPR systems. Structured into six chapters, this thesis offers a comprehensive examination of these advanced DPR materials, providing valuable insights into optimizing water purification processes to address the pressing challenge of water scarcity.

Chapter 1 introduces the study, offering a comprehensive review of the literature and theoretical background on DPR, adsorption, and advanced materials. It sets the research context by identifying key gaps. *Chapter 2* frames the thesis objectives. *Chapter 3* presents the four core manuscripts of this research, providing detailed insights and findings. *Chapter 4* integrates these findings into a cohesive narrative, showing how they collectively contribute to advance the understanding of advanced materials in DPR systems. *Chapter 5* summarizes the key findings, their significance, and suggests directions for future research. *Chapter 6* lists all references, and *Chapter 7* contains supplementary materials and additional supporting data.

Together, these chapters reflect a dedicated effort to address the critical need for effective water treatment solutions, offering insights into new materials that could significantly enhance the sustainability and efficiency of DPR systems.

Chapter 1.

Introduction

1.1. Water scarcity

Water is essential for all forms of life, playing a crucial role in maintaining ecological balance, supporting human health, and driving economic activities (Westall and Brack 2018; Al-Nuaim, Alwasiti, and Shnain 2023). It is vital for drinking, sanitation, agriculture, industry, and energy production (Gemedo *et al.* 2021; Shamoona *et al.* 2022). The availability of clean water is directly linked to public health and environmental quality maintenance, as it prevents waterborne diseases and supports hygiene practices (Collier *et al.* 2021; Ferreira *et al.* 2021). Moreover, water is integral to food security and environmental services (D'Odorico *et al.* 2020). Beyond its practical uses, water also plays a significant role in cultural and recreational activities (Cugusi *et al.* 2023), highlighting its multifaceted importance in human societies.

Despite its abundance, water scarcity is a growing global concern affecting millions of people (Rosinger 2023). Over the past 50 years, global freshwater use surged by 121%, while resources dropped by 52.1% (**Figure 1**) (Diniz *et al.* 2024a). Factors such as population growth, urbanization, climate change, and pollution are intensifying water shortages (Scanlon *et al.* 2023). Many regions around the world, particularly arid and semi-arid areas, already face severe water stress (Karimi *et al.* 2024; do Vale *et al.* 2024). This scarcity not only harms daily living conditions but also threatens food security, economic development, and geopolitical stability (Bedasa 2024; Mohapatra 2023). In some cases, the lack of access to clean water also leads to conflicts and forced migrations, exacerbating social and political tensions (Nagabhatla *et al.* 2020). Addressing water scarcity is, therefore, a critical challenge that requires immediate and coordinated action at local, national, and global levels.

One promising solution to water scarcity is the reuse of treated wastewater (Keller, Su, and Jassby 2022; WHO 2017). Reuse water, also known as reclaimed or recycled water, is wastewater that has been treated to remove contaminants and can be used for various purposes such as agriculture, industrial processes, landscape irrigation, and even for drinking (Jeffrey, Yang, and Judd 2022; Lahnsteiner, van Rensburg, and Esterhuizen 2018; Chen *et al.* 2021). This practice not only conserves freshwater resources but also reduces the environmental impact of wastewater discharge (Jodar-Abellan, López-Ortiz, and Melgarejo-Moreno 2019). By recycling water, communities can create a sustainable water supply, reducing dependency on freshwater sources and enhancing resilience against droughts and climate variability (Liu *et al.* 2020). The use of “reuse” water is increasingly

being recognized as a viable strategy to address water scarcity and ensure long-term water security (Liu *et al.* 2020).

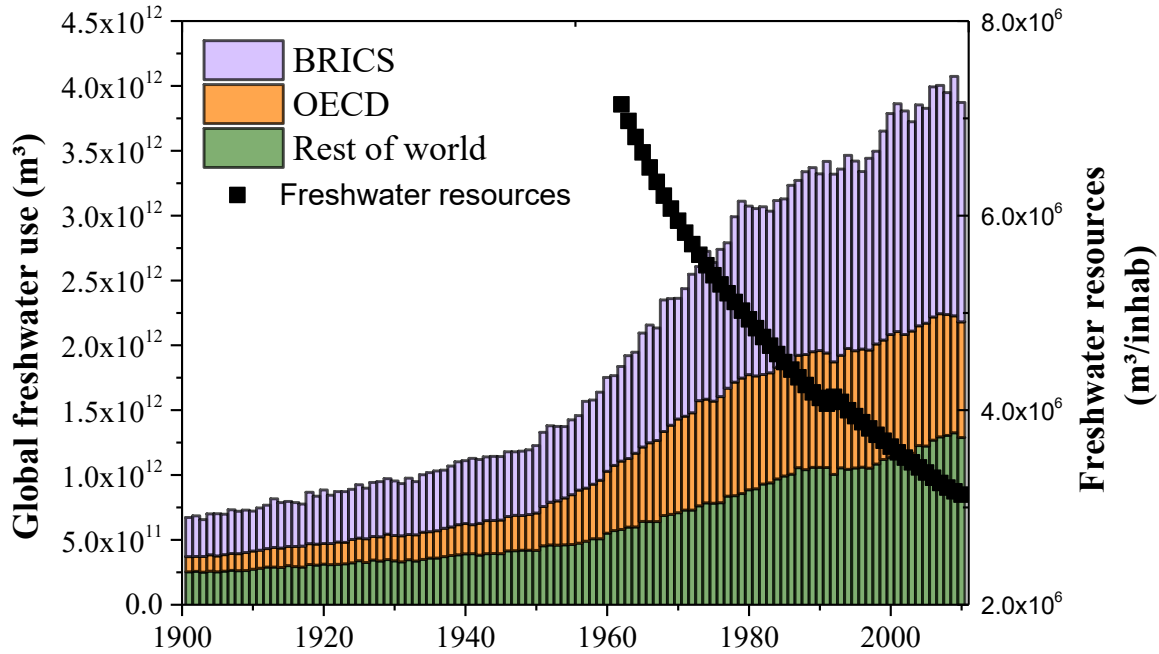


Figure 1: Global freshwater withdrawals for agricultural, industrial, and domestic uses by aggregated regional groupings (left side). Renewable internal freshwater resources flows refer to internal renewable resources (internal river flows and groundwater from rainfall) (right side). OECD members are defined as countries who were members in 2010, and their membership was carried back in time. BRICS countries are Brazil, Russia, India, China and South Africa. Source: (Diniz *et al.* 2024a)

Implementing water reuse practices involves advanced treatment technologies to ensure that the reclaimed water meets safety standards (Jeffrey, Yang, and Judd 2022). These technologies include adsorption, advanced oxidation processes, biological treatment, membrane filtration, ultraviolet disinfection, among others (Jeffrey, Yang, and Judd 2022; WHO 2017). While the initial investment in infrastructure can be high, the long-term benefits of water reuse are significant (Keller, Su, and Jassby 2022). These include reduced pressure on natural water bodies, enhanced water availability, and improved sustainability of water resources. Furthermore, public awareness and acceptance of water reuse are crucial for its success. Education and transparent communication about the safety and benefits of reusing water can help overcome societal resistance and promote the widespread adoption of this sustainable practice (Baawain *et al.* 2020; Kaiser, Ribeiro, and Montagner 2024).

1.2. Potable reuse

The World Health Organization (WHO) classifies potable reuse into three categories:

(i) *unplanned potable reuse*, where treated or untreated wastewater is discharged into rivers, and downstream communities use the same water body as a drinking water source without prior planning; (ii) *indirect potable reuse*, where treated wastewater is intentionally mixed with environmental buffers such as rivers, lakes, reservoirs, or aquifers under controlled conditions before being used as a drinking water source; and (iii) *direct potable reuse* (DPR), where treated wastewater is directly introduced into a drinking water supply system without prior discharge to an environmental buffer (WHO 2017).

Among them, DPR has emerged as a groundbreaking and viable water management strategy, addressing the urgent global water scarcity issue (Soller, Eftim, and Nappier 2018; Liu *et al.* 2020). By treating wastewater to meet or exceed potable water standards and then distributing it directly into the distribution system, DPR maximizes the use of water resources, offering a reliable and sustainable water supply for communities (Reddy *et al.* 2023). Despite its promise, DPR implementation faces challenges and costs due to the complex composition of municipal wastewater, which contains recalcitrant compounds and diverse microbial communities (WHO 2017). Recent efforts have focused on developing safe, robust, and cost-effective DPR processes (Liu *et al.* 2020).

The Guidance for Producing Safe Drinking Water from the WHO emphasizes the importance of reliability, redundancy, robustness, and resilience (the 4Rs criteria) in DPR projects (WHO 2017). Meeting these criteria involves defining quality indicators, including contaminants of emerging concern (CECs), and employing multi-barrier treatment approaches (Jeffrey, Yang, and Judd 2022; WHO 2017). The most used multi-barrier process combines membrane filtration, oxidation, and media filtration (Jeffrey, Yang, and Judd 2022). This combination ensures significant removal of a range of contaminants and enhances the reliability of treatment systems by providing adaptability, security, and time to address potential process failures.

As DPR practices evolve, concerns have arisen regarding the presence and fate of CECs in treated wastewater (Wallmann *et al.* 2021; Villarin and Merel 2020). CECs are a diverse array of chemical and biological substances that are not typically monitored or regulated in the drinking water industry but have the potential to pose risks to human health and the environment (Puri, Gandhi, and

Kumar 2023; Mukhopadhyay, Duttagupta, and Mukherjee 2022). Analyses of sewage samples have revealed a staggering variety of these contaminants, presenting a complex challenge for water resource management and treatment (Porto *et al.* 2019; Pivetta *et al.* 2020; Alves *et al.* 2021). This range includes pharmaceuticals, hormones, microplastics, flame retardants, per- and polyfluoroalkyl substances, and numerous other chemical and biological compounds (Richardson and Kimura 2020). The detection of such a vast number of contaminants highlights the dynamic nature of our society and the constant introduction of new substances into the environment. Therefore, given the extensive number of CECs, prioritization studies are urgently needed.

1.2.1. Prioritization of contaminants of emerging concern

Prioritizing CECs in DPR involves a multifaceted approach that considers human health risks, ecological impacts, and the technical feasibility of removal during treatment. Assessing human health risks requires understanding the toxicological properties of contaminants, their exposure pathways, and potential accumulation in the body (Ritter *et al.* 2002). Ecological risks must also be evaluated to protect sensitive ecosystems affected by treated wastewater discharge (Fawell and Ong 2012). Effective treatment technologies are crucial, necessitating consideration of technical feasibility and cost-effectiveness (Diniz, Cunha, and Rath 2023). Identifying appropriate marker compounds in both raw and treated sewage that can be quantified using current analytical methods is also essential. By integrating these aspects, a comprehensive prioritization framework can guide decision-makers in targeting the most critical CECs, ensuring the production of safe and sustainable drinking water.

Over the past decade, our research group has investigated various classes of CECs, including anesthetics, anthelmintics, antacids, antiallergics, antidiabetics, antihypertensives, antilipidemic, antimicrobials, antipsychotics, artificial sweeteners, corticosteroids, cytotoxic, diuretics, steroidal anti-inflammatory drugs, and stimulants. They conducted monitoring, degradation, leaching, and ecotoxicology studies to identify suitable markers CECs for monitoring purposes (Pivetta *et al.* 2020; Alves *et al.* 2021; Porto *et al.* 2019; Rodrigues-Silva *et al.* 2019; Caianelo *et al.* 2022; Diniz *et al.* 2020; Diniz *et al.* 2022; Diniz, Rath, Rath, Rodrigues-Silva, *et al.* 2021; Porto, Pinheiro, and Rath 2021; Spina *et al.* 2021; Venancio *et al.* 2021; Caianelo *et al.* 2021; Diniz and Rath 2023; Diniz, Rath, and Crick 2023). They have also identified a wide array of CECs in Brazilian wastewater treatment plants (WWTPs), with concentrations ranging from ng/L to µg/L.

Bench-scale experiments revealed that many of these contaminants are resistant to traditional treatment processes and pose toxicity risks to both bacteria and algae.

Key characteristics of a marker compound include its presence in both raw and treated sewage and its easy quantification using available analytical methods. This means the compound should be recalcitrant to or only partially removed during sewage treatment. Pharmaceutical active ingredients that are widely consumed, minimally metabolized, and excreted as the parent compound are preferred for prioritization. However, predicting their concentrations in Brazilian wastewater is challenging due to the lack of official consumption data and regional variations in pharmaceutical use (Marson *et al.* 2022). For prioritizing pharmaceutical active ingredients, our group have used 2018 sales data (number of boxes and market size) from *IQVIA Soluções de Tecnologia do Brasil Ltda.* to estimate daily doses and consumption (kg/year/inhabitant). This worst-case scenario estimation considered the highest quantity of units per package and the highest active ingredient amount (mg) per unit. Predicted concentrations in WWTP influent were then calculated based on the European Medicine Agency (EMA) guidelines (EMA 2006), assuming linear distribution of consumption over the year and population (Pivetta *et al.* 2020). Using this approach, forty-five pharmaceutical active ingredients were initially selected: sulfamethoxazole, ciprofloxacin, azithromycin, cefepime, ampicillin, trimethoprim, penicillin, piperacillin, tetracycline, cloxacillin, levofloxacin, imipenem, amoxicillin, chloramphenicol, cefazolin, fluoxetine, bupropion, escitalopram, clonazepam, carbamazepine, nortriptyline, amitriptyline, sertraline, trazodone, alprazolam, diazepam, hydrochlorothiazide, albendazole, ricobendazole, prednisolone, lidocaine, diclofenac, ibuprofen, acetaminophen, piroxicam, capecitabine, simvastatin, metformin, atenolol, propranolol, captopril, fexofenadine, dexamethasone, ranitidine, and caffeine.

Additionally, artificial sweeteners permitted in Brazil were also tested, including aspartame, saccharin, sucralose, acesulfame, neotame, and cyclamate (Alves *et al.* 2021). Low-calorie sweeteners have attracted significant attention due to their global consumption, with an estimated 28% of the population consuming them daily (Shankar, Ahuja, and Sriram 2013). Most of it are minimally metabolized and excreted unchanged, except for aspartame, which breaks down into phenylalanine, aspartic acid, and methanol (Li *et al.* 2020). Despite their high consumption (Luo *et al.* 2019; Li *et al.* 2021), these compounds are poorly removed by WWTPs (Alves *et al.* 2021) and specific data on Brazilian consumption were lacking.

Therefore, this preliminary work of our group led to the selection of 12 potential candidate compounds (acesulfame, acetaminophen, albendazole, carbamazepine, caffeine, diclofenac, hydrochlorothiazide, propranolol, ricobendazole, saccharin, sucralose, and sulfamethoxazole) based on their presence, persistence, and quantifiability in treated sewage to be further monitored in the raw sewage and the effluent of the EPAR Capivari II (Campinas, Brazil).

1.2.2. EPAR Capivari II and pilot plant

The EPAR Capivari II WWTP in Campinas (Brazil) (-22.956785, -47.221532) produces non-potable reuse water using a membrane bioreactor (MBR) system (**Figure 2**) (SANASA). Prior to entering the bioreactor, sewage undergoes primary treatment, which includes bar screening (15 mm spacing), a rotary drum screen (2 mm apertures), and a sand remover to remove larger debris and solids. The bioreactor is then split into three zones: anaerobic, anoxic, and aerobic, where submerged mixers ensure proper agitation in the non-aerated zones, while fine bubble diffusers and an air blower provide necessary oxygen in the aerated zone. In the anaerobic zone, bacteria break down organic matter in the absence of oxygen. The anoxic zone, which lacks free oxygen but contains nitrates or nitrites, allows denitrifying bacteria to remove nitrogen compounds. The aerobic zone employs mechanical aeration to support several key processes: oxidation of organic matter, nitrification of ammonia, and phosphate uptake. For additional phosphorus removal, the plant is equipped with an aluminum polychloride (also known as PAC) dosing system. These processes reduce biochemical oxygen demand, ammonia, and phosphate levels. The ultrafiltration membrane at the end of the process removes protozoa, bacteria, and suspended solids.

The treated water is used for non-potable applications in Campinas, leading to significant potable water savings of up to 80% for the fire department and 88% for nearby industries. Additionally, the EPAR Capivari II WWTP features a pilot plant dedicated to research and development in DPR, showcasing its potential to help address water scarcity challenges.

The pilot-scale treatment plant at EPAR Capivari II WWTP was initially designed by Hespanhol, Rodrigues, and Mierzwa (2019). It features various treatment units, including activated carbon, biological activated carbon, photoperoxidation, reverse osmosis, and ozonation. According to Diniz, Cunha, and Rath (2023) the current setup operates at a flow rate of 350 L/h. The system includes a multi-channel configuration for testing different treatment combinations of the MBR

effluent: I – photoperoxidation; II – activated carbon; III – reverse osmosis; IV – reverse osmosis + photoperoxidation; V – reverse osmosis + activated carbon; and VI – reverse osmosis + photoperoxidation + activated carbon. For a detailed schematic description of the pilot plant and its components, refer to the section “*Adsorption of recalcitrant contaminants of emerging concern onto activated carbon: A laboratory and pilot-scale study*”.

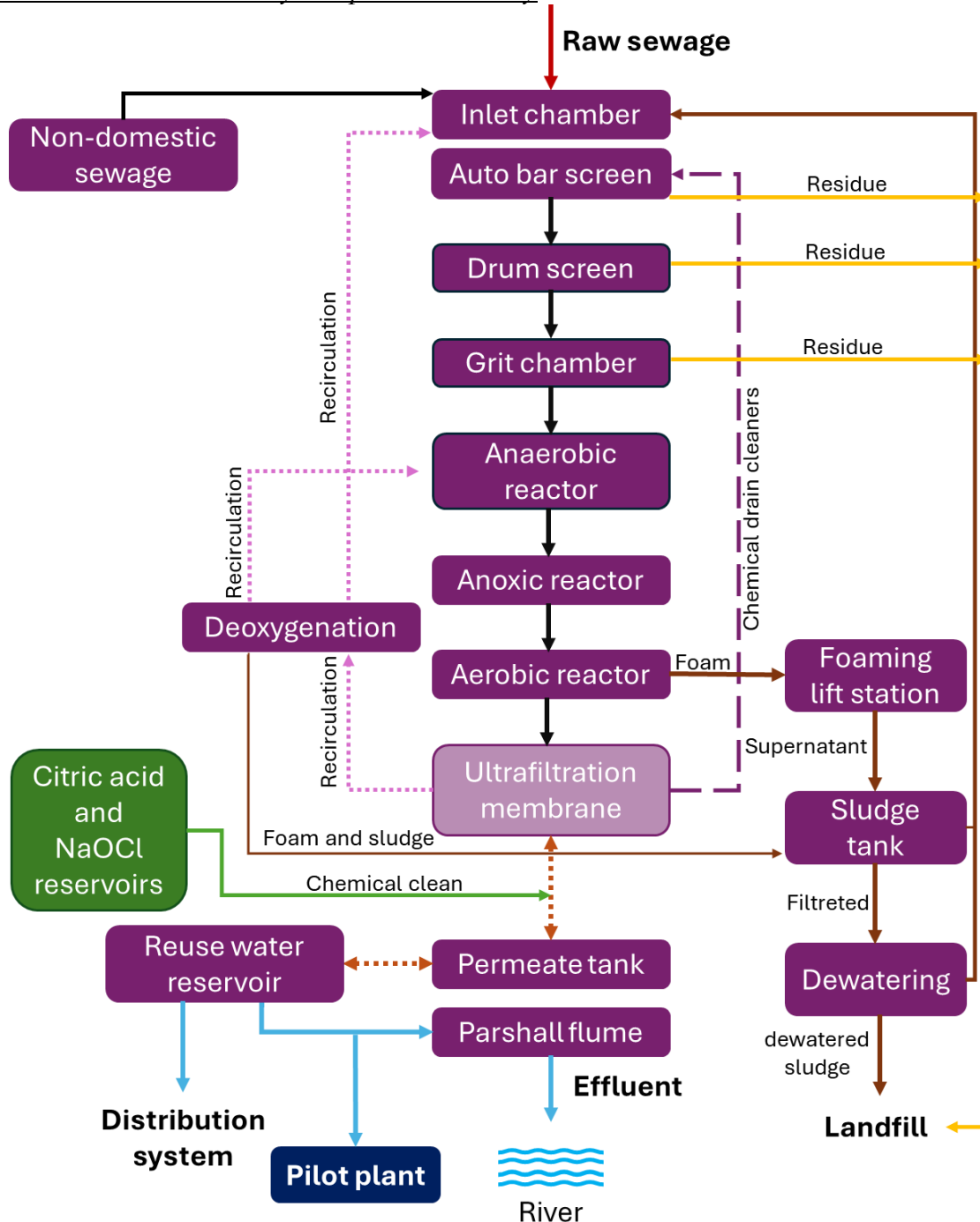


Figure 2: Detailed schematic of the EPAR Capivari II wastewater treatment plant, with the colors and lines used to guide the eye. Source: Author.

1.3. Adsorption: general considerations

Adsorption is a highly effective and versatile technique for water treatment, capable of removing a wide range of pollutants including organic and inorganic compounds, including metals (Diniz, *et al.* 2021; Velarde *et al.* 2023; Müller, Lisboa, and Chalker 2023). Its simplicity in implementation and operation, combined with low energy requirements, makes it an attractive option for treating both industrial and municipal wastewater (Diniz and Rath 2023; Fan *et al.* 2010).

In general, the adsorption process occurs in a system containing a porous solid and a fluid, which can be either a gas or a liquid. During this process, mass transfer takes place from the fluid phase (adsorbate) to the solid phase (adsorbent) (Di Bernardo, Dantas, and Voltan 2017). Two distinct mechanisms can govern this adsorption process: chemical adsorption (chemisorption) and physical adsorption (physisorption). Chemisorption involves the formation of chemical bonds between the adsorbate and adsorbent, forming a single layer through the exchange or sharing of electrons between the chemical elements on the surface of the adsorbate and the adsorbent. On the other hand, physisorption is driven primarily by van der Waals forces and can occur over one or multiple layers (Rouquerol *et al.* 2014).

It is also important to highlight the main steps of the adsorption process in these general considerations. Notably, adsorption occurs in two distinct stages, the combination of which is referred to as sorption (McBain 1909). The primary steps and characteristics of this process are as follows (Di Bernardo, Dantas, and Voltan 2017; Howe *et al.* 2012; Tran *et al.* 2017):

- i) **Transport of adsorbate from the fluid to the boundary layer:** The adsorbate is transported to the boundary layer surrounding the adsorbent particle via external diffusion, driven by a disturbance in the system.
- ii) **Transport through the boundary layer:** The adsorbate is transported through the boundary layer to the surface of the porous solid via molecular diffusion. Increased flow/turbulence in the process accelerates mass transport.
- iii) **Transport of adsorbate through the pores of the porous solid:** This involves the transport of the adsorbate through the active sites, either on the surface (surface diffusion) or within the pores (pore diffusion) of the solid. Driven by molecular diffusion, this process is known as internal diffusion and contributes to the overall sorption process.

- iv) **Adsorption:** This is the process in which the adsorbates form a bond with the active site on the surface of the adsorbent. The bond can either be physical, occurring rapidly or chemical, which usually takes longer to form.
- v) **Absorption:** This process involves the adsorbate entering and settling within the pores of the porous solid.
- vi) **Sorption:** The combined result of both adsorption and absorption processes.

The physisorption process is maintained by weaker adsorbent-adsorbate interactions (permanent dipole interactions and London-Van der Waals forces) and by electrostatic attraction between the adsorbate and functional groups on the adsorbent surface (Hill Jr and Root 2014; Srivastava and Goyal 2010). Physisorption is also characterized by multilayer adsorption; however, it can also occur in monolayers (Ruthven 1984). Chemisorption, on the other hand, occurs due to chemical bonds and depends on the surface area of the adsorbent (Ruthven 1984; Hill Jr and Root 2014; Moreno-Piraján 2011). This process is characterized by the formation of a single layer on the adsorbent surface due to the reduction of adsorbent-adsorbate interaction forces with distance (Hill Jr and Root 2014).

While the physisorption process is considered fully reversible, chemisorption is usually irreversible due to the strength of the chemical bonds (Cooney 1999). Regarding adsorption kinetics, physisorption is almost instantaneous if the activation energy is less than 4.2 kJ/mol (Hill Jr and Root 2014; Lowell *et al.* 2004; Saha and Chowdhury 2011). The low activation energy of the physisorption process is due to the interaction energies between the adsorbent and adsorbate being of the same order of magnitude but higher than the condensation energy (Moreno-Piraján 2011). The rate at which a chemisorption process reaches equilibrium is intrinsically dependent on the activation energy (Jiang and Wen 2011). Unlike physisorption, chemisorption can be fast at high temperatures and slow at low temperatures (Hagen 2015). Interestingly, chemisorption can be instantaneous at low temperatures if the process has no activation energy, known as non-activated chemisorption (Hill Jr and Root 2014). This process occurs when the adsorption sites are instantly occupied by adsorbent-adsorbate interactions and depends on the nature of the chemical bonds (Malet and Munuera 1989).

Both processes are predominantly exothermic (Hagen 2015). However, chemisorption can be endothermic if the dissociation energy of the adsorbate is greater than the energy of the adsorbent-adsorbate chemical bond formation (Hill Jr and Root 2014). Physisorption usually dominates at low temperatures, and its adsorption capacity decreases with increasing temperature

(Hill Jr and Root 2014). In contrast, chemisorption predominates at high temperatures, with its adsorption capacity increasing as the temperature rises (Rouquerol *et al.* 2014). In terms of enthalpy (ΔH) and Gibbs free energy variation (ΔG), the physisorption process has $\Delta H < 40$ kJ/mol (Inglezakis and Pouloupoulos 2006) and $-20 < \Delta G < 0$ kJ/mol. In contrast, chemisorption generally has $40 < \Delta H < 800$ kJ/mol (Inglezakis and Pouloupoulos 2006) and $-400 < \Delta G < -80$ kJ/mol (Antunes *et al.* 2012; Jaerger *et al.* 2015). Finally, using the Dubinin-Radushkevich isotherm, it is possible to calculate the adsorption energy of the system (E), which for physisorption is $E < 8$ kJ/mol, while for chemisorption it is $8 < E < 16$ kJ/mol (ion exchange) or $E > 16$ kJ/mol (Tran, You, and Chao 2016).

1.3.1. Adsorption for water treatment

Currently, various polishing processes are documented in the literature and have been implemented in treatment plants worldwide (Spina *et al.* 2021; Venancio *et al.* 2021; Silva *et al.* 2021; Ensano *et al.* 2019). Each of these processes has its advantages and disadvantages, but since the focus here is on the adsorption process, we will limit our discussion to that. In treatment plants, the adsorption process can occur in two distinct ways. The adsorbent, usually in powdered form, is added to rapid mixing tanks to remove seasonal contaminants - those that do not frequently occur in treatment plants. However, if the occurrence of the contaminants is perennial, meaning consistently present in treatment plants, the use of a stationary adsorbent is recommended. These adsorbents typically have larger particle sizes and are installed as fixed beds (columns), with their lifespan depending on both the properties of the adsorbate and the specific conditions of use (Di Bernardo, Dantas, and Voltan 2017).

A variety of adsorbents are used for the removal of CECs in treatment plants. Despite their differences, the main characteristics required of an effective adsorbent are the same (Sophia and Lima 2018). Since adsorbents can account for up to 70% of the operational costs in a treatment plant, it is important that these materials be low-cost, widely available, and, if possible, regenerable (Sophia and Lima 2018). Additionally, as they are frequently exposed to different aqueous matrices and high pressures, they should also have chemical and mechanical stability. Lastly, the adsorption characteristics of these materials should be optimized to ensure favorable textural and physicochemical properties, and high adsorption capacity. These parameters aim to ensure efficient and optimized treatment plant operations while minimizing operational costs (Sophia and Lima 2018).

Carbon nanotubes are recently developed adsorbents for water treatment applications. These adsorbents are considered promising due to their high surface area, small size, and high porosity (Yu *et al.* 2016). Despite their recent use, some challenges have already been identified, such as difficulty in removal from the aqueous phase, poor dispersion, and small particle size (Sophia and Lima 2018). However, the chemical modification of these adsorbents has shown promising results in the adsorption of CECs. Yu, Ma, and Han (2014) and Yu *et al.* (2016) evaluated the effect of oxygen presence in multi-walled carbon nanotubes on the adsorption of tetracyclines and ciprofloxacin. Interestingly, the authors observed that the maximum adsorption of these CECs was related to the amount of oxygen in the adsorbent. The highest tetracycline adsorptions were observed with 3.2% oxygen (Yu, Ma, and Han 2014), while for ciprofloxacin, these values increased to 4.7% (Yu *et al.* 2016). Another interesting point regarding the adsorption of antibiotics was made by Peng *et al.* (2012). The authors observed that, in addition to hydrophobicity, surface components of nanotubes, such as hydroxyl groups (-OH, which increases the electron-donating characteristics of π bonds) and carbonyl groups (C=O, which increase the electron-accepting characteristics of π bonds), and the structure of the adsorbates are crucial in the adsorption process since the predominant adsorption mechanism is electron exchange. Thus, various authors have reported that oxidation methods are simple ways to functionalize carbon nanotubes and increase their adsorption efficiency (Zhang *et al.* 2011; Yu *et al.* 2014; Wang *et al.* 2015).

Following the line of carbon-based nanomaterials, graphene can also be used for the adsorption of CECs mainly due to its ability to bind with π -displaced electrons of many CECs (Apul *et al.* 2013). The use of graphene for CEC adsorption depends on the presence of functional groups on the adsorbent's surface, hence it is called graphene oxide or reduced graphene oxide (Santhosh *et al.* 2016). The high adsorption capacity of these materials has been attributed to the occurrence of hydrogen bonds, π - π interactions, and simple sp^2 hybrid structures (Sophia and Lima 2018). However, a study relating to graphene functionalization was conducted by Chen, Gao, and Li (2014). The authors observed that pristine graphene, due to a higher amount of π - π interaction sites, had a greater capacity to adsorb sulfamethoxazole compared to graphene-NH₂, graphene-COOH, and graphene-OH, which indicates that hydrophobic interactions play an important role in sulfamethoxazole adsorption.

Zeolites are crystalline aluminosilicates with uniformly distributed micropores that are also used as adsorbents. The porous structure of these materials is created from a three-dimensional structure (Jacobs *et al.* 2001). Briefly, the adsorptive properties of zeolites vary according to the

silica-to-aluminum molar ratio used in their synthesis. Zeolites with low silica content ($\text{Si/Al} < 2$) have high ion exchange capacity, while those with high silica content are effective adsorbents for CECs (Jiang *et al.* 2020). Jiang *et al.* (2020) reported that the highest triclosan adsorption capacities were strongly linked with the volume and surface area of micropores. Additionally, they observed that high silica content resulted in favorable S-type adsorption isotherms for trichlorophenol. The authors also noted that high aluminum concentrations on the zeolite surface could lead to the formation of water molecule clusters, resulting in competition for active sites between water and more polar molecules.

A good example of low-cost, widely available material for use as adsorbents are clays and other minerals. The adsorption of these materials is predominantly influenced by surface charges (Sophia and Lima 2018). For example, studies with amoxicillin and trimethoprim using bentonite and montmorillonite showed better adsorption in acidic pH (Putra *et al.* 2009; Bekci, Seki, and Yurdakoc 2006). Rodriguez-Liebana *et al.* (2016) observed that a high polar pesticide (metalaxyl) was adsorbed more quickly and effectively than fludioxonil due to electrostatic interactions and hydrogen bonds between the adsorbate and adsorbent.

Other adsorbents have also been studied for the removal of CECs, such as those with organometallic structures (Zhuo *et al.* 2017; Song and Jhung 2017) and articulated magnetic resins (Zhu *et al.* 2016). However, activated carbons (including biochars) are the most widely used adsorbents for CEC adsorption (Sophia and Lima 2018; Tran *et al.* 2017). Biochars are stable carbon sources obtained from different biomasses through thermal or hydrothermal processes carried out at high temperatures and low oxygen content (Klinar 2016). Additionally, these adsorbents can be activated to increase their surface area, porosity, functionality, interactions, and other parameters, forming modified biochars (Ahmed *et al.* 2016). The authors explain that due to the high difficulty in distinguishing between activated carbons and modified biochars, the latter can also be named activated carbon.

1.3.1.1. Activated carbon

Adsorption using activated carbon is the most common polishing technique used in Brazilian drinking water treatment plants (Di Bernardo, Dantas, and Voltan 2017). The widespread use of this adsorbent is due to its high availability and low cost, and the ease with which it can be produced from a wide range of raw materials (Cheng *et al.* 2021). While the cost of producing

adsorbents varies among countries and even within a single country, it is noteworthy that, when comparing prices, activated carbon costs around \$0.001 per gram. In contrast, nanotube and graphene-based adsorbents, which rely on nanotechnology, can cost up to \$100,000 per gram (Cheng *et al.* 2021).

Activated carbon is available in two main forms: powdered and granular. Powdered activated carbon (PAC) is commonly used seasonally in suspension and added to raw or pre-oxidized water. The use of PAC typically incurs lower initial costs for the treatment plant, as it does not require the construction of new facilities or regeneration of the activated carbon. On the other hand, granular activated carbon (GAC) is used in fixed-bed columns and installed permanently in treatment plants. The initial financial investment for GAC is higher compared to PAC; however, GAC can be regenerated and has a longer lifespan (Di Bernardo, Dantas, and Voltan 2017).

In a study with different activated carbons, Diniz *et al.* (2022) observed that pore distribution reduced competition for the active site of the activated carbons, allowing for greater adsorption quantities. Araújo *et al.* (2018) observed a high positive linear correlation ($r = 0.980$) between mesopore volume and the adsorption potential of microcystin-LR. Jaria *et al.* (2020), in their study aiming for the removal of six pharmaceuticals, found that specific surface area, micropore area, and micropore volume had the greatest influence on the adsorption process. Additionally, they noted that functionalized activated carbons showed lower adsorption compared to the original adsorbent. Besides physical properties, the chemical properties of the activated carbon also influence adsorption. The presence of acidic and/or basic compounds on the granule surface can enhance or reduce the adsorption of CECs, depending on their physicochemical properties (Quesada *et al.* 2019). Therefore, the production and characterization of activated carbons are essential for estimating their adsorption capacity and gaining insights into the adsorption process (Tran *et al.* 2017; Araújo *et al.* 2018; Tran, Chao, and You 2018). Characterization techniques, ranging from classic methods like BET isotherm to more advanced approaches such as scanning electron microscopy and synchrotron radiation (**Figure 3**), provide valuable information about the structural and surface properties of activated carbons.

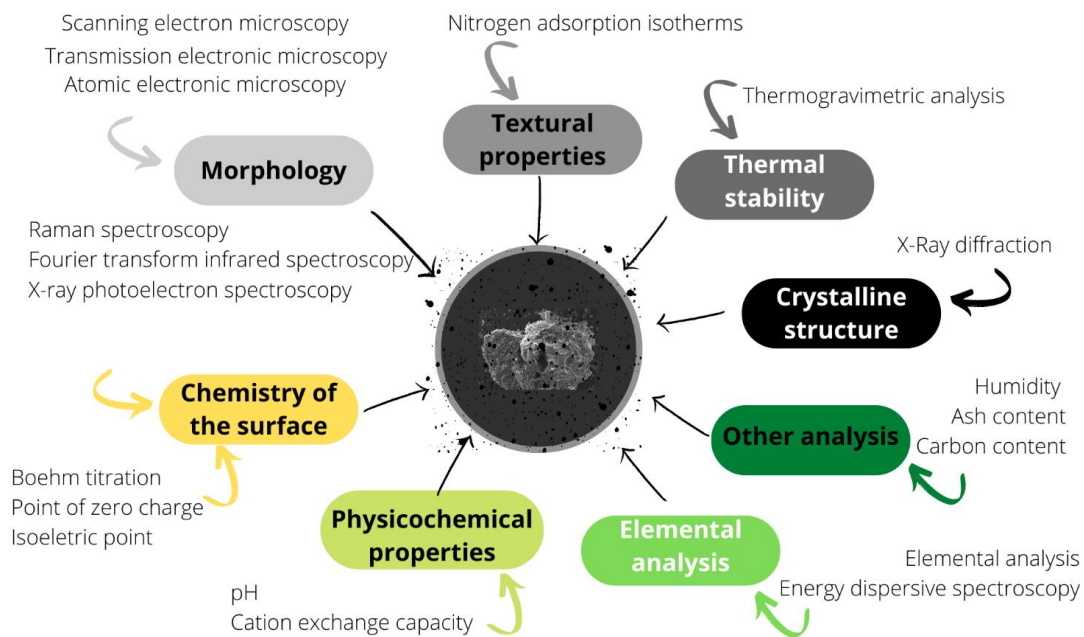


Figure 3: Main characterization techniques used for materials in water treatment. Source: Author.

The texture-related characteristics of activated carbon can be effectively assessed using the BET isotherm model (Brunauer, Emmett, and Teller 1938). This technique involves analyzing nitrogen adsorption at temperatures as low as 77 K, enabling the determination of surface area and pore size distribution (Tran, Chao, and You 2018). Additionally, the BET isotherm produces characteristic curves, classified into nine distinct types (**Figure 4**), which are instrumental in identifying the pore structure of activated carbon.

Type I isotherms are reversible and concave with respect to the relative pressure. These isotherms are associated with microporous adsorbents, where the narrow pressure range needed to reach the plateau indicates uniform pore size, and the nearly horizontal plateau suggests a low surface area. The difference between *Ia* and *Ib* lies in the width of the micropores, with type *Ia* indicating narrower micropores, while type *Ib* indicates wider micropores (Rouquerol *et al.* 2014). Type II isotherms are characteristic of non-porous or essentially macroporous adsorbents, allowing for multimolecular adsorption at high relative pressures. Generally, the inflection at the beginning of the isotherm can estimate the adsorbent's monolayer adsorption capacity. Type *Ila* exhibits a complete

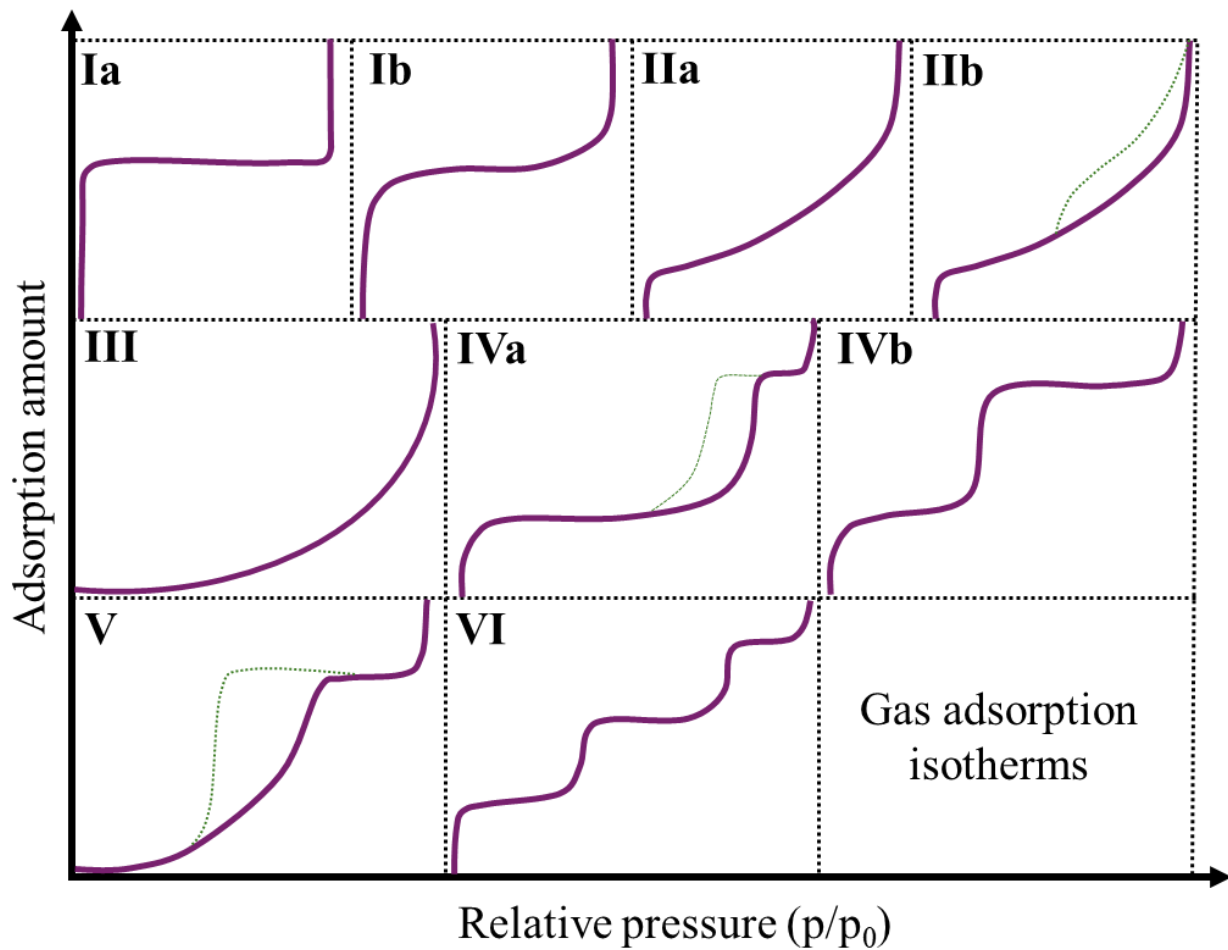


Figure 4: Classification of adsorption isotherms. Green dotted lines represent desorption hysteresis. Type I is characteristic of microporous adsorbents; Type II corresponds to non-porous or macroporous adsorbents; Type III indicates weaker interactions in non-porous or macroporous adsorbents; Type IV is typical of mesoporous adsorbents; Type V represents weaker interactions in micro- or mesoporous adsorbents; and Type VI describes layer-by-layer adsorption on a highly uniform surface. Adapted from Rouquerol *et al.* (2014)

adsorption-desorption isotherm without hysteresis, indicating the absence of capillary condensation effects. In contrast, Type *IIb* features an isotherm with H3 hysteresis, typically associated with plate-like adsorbents (Rouquerol *et al.* 2014). Furthermore, H4 hysteresis is indicative of slit-shaped micropores within the material. The Type *III* isotherm, although infrequently observed, is indicative of weak interactions between the adsorbent and adsorbate, typically found in non-porous or macroporous adsorbents. Type *IV* isotherms are associated with mesoporous adsorbents. The Type *IVa* isotherm is commonly observed and exhibits H1 hysteresis, which is characteristic of porous materials with spherical pores of relatively uniform size. This hysteresis is related to the capillary condensation and desorption within mesopores. The Type *IVb* isotherm, in contrast, is fully reversible and occurs in mesoporous adsorbents with a well-ordered pore structure. The Type *V* isotherm,

similar to Type *III*, also indicates weak adsorbent-adsorbate interactions but is relevant for micro- or mesoporous adsorbents. The associated H2 hysteresis is indicative of the presence of bottle-shaped pores and the associated filling and emptying of these pores. Finally, the Type *VI* isotherm, or stepwise isotherm, reflects a layer-by-layer adsorption process on a highly uniform surface.

Synchrotron small-angle X-ray scattering (SAXS) is another technique for estimating pore size distribution, capable of evaluating pores with diameters in the angstrom range (Zhao *et al.* 2014). The grain size of activated carbon can also be assessed using granulometric curves and the coefficient of uniformity. Generally, commercial GAC has particle sizes between 0.30 and 2.40 mm and a coefficient of uniformity between 1.5 and 2.0 (Di Bernardo, Dantas, and Voltan 2017). In contrast, PAC typically has particle sizes between 0.01 and 0.10 mm, with 90% of the mass being smaller than 0.04 mm (Di Bernardo, Dantas, and Voltan 2017). Other tests related to pore size include iodine number, methylene blue index, phenol index, and molasses number (Araújo 2017).

The thermal stability of activated carbon is evaluated through thermogravimetric analysis, which assesses ash content and moisture levels (lower values indicate higher quality), as well as volatile substance content (Tran, Chao, and You 2018). Morphological and crystallographic analyses are also important for understanding adsorption processes. Morphological analyses can be performed using scanning electron microscopy (SEM), transmission electron microscopy (TEM), and atomic force microscopy (AFM), which provide high-resolution images of material structures. Most current studies on water treatment materials use SEM and TEM. SEM provides surface and three-dimensional analyses, while TEM can determine pore size in addition to morphology.

Physical and physicochemical properties analyses of activated carbon assess various characteristics such as pH, bulk density, ash content, and fixed and volatile carbon. Generally, these analyses follow internationally established protocols, such as standards from the American Society for Testing and Materials (ASTM), Japanese Industrial Standards (JIS), and the Organization for Economic Co-operation & Development (OECD), as well as national standards like those from the Brazilian Association of Technical Standards (ABNT) (Araújo *et al.* 2018; Di Bernardo, Dantas, and Voltan 2017).

Elemental analyses, such as the surface chemical composition of activated carbon, are important for predicting potential chemical reactions between adsorbate and adsorbent. This quantification can be done using energy dispersive spectroscopy (EDS) or Auger electron spectroscopy (AES), allowing the quantification of a wide range of elements (Adamson and Gast

1997; Araújo 2017). Surface characterization is essential for understanding and predicting the mechanisms involved in the adsorption process (Tran, Chao, and You 2018). Various methods can be used for surface characterization, such as point of zero charge (PZC), isoelectric point (IEP), Boehm titration method, Raman spectroscopy, Fourier-transform infrared spectroscopy (FTIR), and X-ray photoelectron spectroscopy (XPS) (Adamson and Gast 1997). It is important to consider some points to avoid ambiguities within these various techniques.

While the PZC defines the conditions where the sum of the internal and external surface charges is zero, the IEP reflects the external surface charge of the material in solution (Menendez *et al.* 1995). The difference between the PZC and IEP values provides insight into the charge distribution on the adsorbent (Onjia and Milonjic 2003). If $PZC/IEP \gg 1$, it indicates that the external surface is more negatively charged compared to the internal part; if $PZC/IEP \approx 1$, the charge distribution is nearly homogeneous (Tran *et al.* 2017). $PZC/IEP = 1$ occurs only when there is no specific adsorption of counter-ions in the solution (Onjia and Milonjic 2003).

Regarding the presence of oxides on the activated carbon surface, the Boehm titration method (Boehm 1994, 2002) has proven to be a powerful tool for quantifying acidic and basic compounds (Tran, Chao, and You 2018). Generally, the acidity of activated carbon surfaces is related to the presence or absence of carboxyl, lactonic, and phenolic hydroxyl groups (Boehm 2002). Differentiation among these groups by titration is due to the strength of the bases used in the adsorption process: NaOH, Na₂CO₃, and NaHCO₃ (Tran, Chao, and You 2018). The number of phenolic groups can be estimated by the difference between moles neutralized by NaOH and Na₂CO₃, the number of lactonic groups by the difference between Na₂CO₃ and NaHCO₃, and the number of carboxyl groups by neutralization with NaHCO₃ (Tran, Chao, and You 2018; Boehm 2002). It is noteworthy that the method is based on a back titration process with HCl and NaOH and was later standardized by Goertzen *et al.* (2010) by introducing a CO₂ expulsion methodology with nitrogen gas.

In line with identifying functional groups on the activated carbon surface, infrared spectroscopy has proven very effective, particularly due to advancements in FTIR (Boehm 2002). The technique is based on infrared radiation incidence on the sample, with part being absorbed and part transmitted, generating a transmittance versus wavelength graph (Bacsik, Mink, and Keresztury 2004). Specific chemical bonds have characteristic bands, and their occurrence can be identified by

a decrease in transmittance. The main bonds occurring in activated carbons and their characteristic wavelengths are shown in **Table 1**.

Table 1: Principal functional groups and their bands in Fourier Transform Infrared (FTIR) analysis (Tran, Chao, and You 2018).

Functional group	Representative groups	Characteristic band (cm ⁻¹)
-OH	Hydroxyls	3000 - 3700
-CH _n -	Methyl or Methylene	2800 - 3000
C≡C	Disubstituted alkynes	2150 – 2450
C=O	Carboxyl or lactones	1650 - 1800
C=C	Aromatic rings	1480 - 1650
C-O	C-O stretching	970 - 1290
C-H	Benzene aromatic rings	730 - 970

XPS determines binding energy by measuring the kinetic energy of core electrons excited by X-rays (Boehm 2002; Adamson and Gast 1997). This allows for the acquisition of a spectrum of Auger electrons² and primary electrons (electrons present in a beam extracted from a known source, accelerated by a potential difference, and focused by a magnetic field (Adamson and Gast 1997). Despite its power, XPS is very sensitive due to the escape depth of photoelectrons reaching only a few atomic layers. The binding energy is influenced by the atom's bonding to more electronegative or electropositive atoms, affecting it positively or negatively, respectively (Boehm 2002). It is recommended that the measurement (*i.e.*, binding energy) be referenced by the C1 signal (Papirer *et al.* 1994). However, it is important to note that the technique requires prior calibration since the sample's charge can influence the kinetic energies (Boehm 2002).

In conclusion, a thorough and well-conducted characterization not only allows for inferences about the adsorption potential of activated carbon but also enables a correct identification of the adsorption mechanism involved in the process.

² The Auger effect occurs when an electron is ejected during an electronic transition without photon emission.

1.3.2. Adsorption modelling: batch studies

Adsorption modelling is essential for understanding the interactions between adsorbates and adsorbents, optimizing process conditions, and predicting adsorption behavior under different scenarios. Several models describe adsorption isotherms, kinetics, and thermodynamics, while studies on pH, ionic strength, desorption, and regeneration further elucidate adsorption mechanisms (Quesada *et al.* 2019). The specific studies and models used depend on the objectives of each investigation, but three main components are typically considered: kinetics, isotherms, and pH effects. The equilibrium study is fundamental to adsorption models and essential for understanding the kinetics and dynamics of the process. In these studies, it is assumed that adsorption capacity and, consequently, residual concentration are functions of contact time, while adsorption dynamics (used in fixed-bed adsorption processes) also consider these parameters as functions of space (Worch 2012).

Building on the understanding of adsorption dynamics, these studies often evaluate two key metrics: the adsorption capacity of the adsorbent, calculated using mathematical models from the amount adsorbed (**Equation 1**), and the percentage removal of the adsorbate (**Equation 2**). While higher removal percentages are associated with greater availability of active sites, this does not always equate to higher adsorption capacities. To prevent inaccurate estimates of adsorption capacity, it is crucial to avoid achieving 100% removal of the adsorbate, as this may overlook the presence of remaining active sites on the adsorbent (Fan *et al.* 2017).

$$q = \frac{C_0 - C_f}{m} V \quad \text{Equation 1}$$

$$\text{Removal (\%)} = \frac{C_0 - C_f}{C_0} * 100 \quad \text{Equation 2}$$

Where: C_0 and C_f are the initial and final concentration of the adsorbate, m is the mass of the adsorbent, and V is the volume of the solution.

Understanding and analyzing the adsorption process often requires the use of various mathematical models, with statistical tools playing a critical role in evaluating their accuracy (Quesada *et al.* 2019; Tran *et al.* 2017). Key statistical metrics used in this evaluation include the Chi-square test (χ^2) (**Equation 3**) and the coefficient of determination (R^2) (**Equation 4**) (Tran *et al.* 2017). Additionally, the standard deviation (SD) of the residuals can be used to assess the validity of kinetic model (**Equation 5**) (Wu, Tseng, and Juang 2009).

$$\chi^2 = \sum \frac{(q_{e,obs} - q_{e,cal})^2}{q_{e,cal}} \quad \text{Equation 3}$$

$$R^2 = 1 - \frac{\sum (q_{e,obs} - q_{e,cal})^2}{\sum (q_{e,obs} - q_{e,med})^2} \quad \text{Equation 4}$$

$$SD (\%) = 100 \left\{ \frac{\sum_N (1 - \frac{q_{e,cal}}{q_{e,obs}})^2}{N} \right\}^{\frac{1}{2}} \quad \text{Equation 5}$$

Where: $q_{e,obs}$ is the observed amount adsorbed (from **Equation 1**), $q_{e,cal}$ is the calculated amount adsorbed (from model parameters), $q_{e,med}$ is the mean of $q_{e,obs}$ e N is the number of data points.

These statistical evaluations are essential for validating adsorption models and ensuring their accuracy in representing experimental data. Precise modeling and analysis are fundamental to optimizing adsorption processes in applications such as water treatment, environmental remediation, and industrial processes.

1.3.2.1. Kinetics modelling

The adsorption of an adsorbate onto an adsorbent can be represented chemically by **Equation 6**. In a reversible adsorption process, where both adsorption and desorption occur simultaneously, the system will eventually reach equilibrium when the rates of adsorption and desorption equalize, indicating no further net removal of the adsorbate (Di Bernardo, Dantas, and Voltan 2017).



Where: A is the adsorbate, B is the adsorbent, and AB is the adsorbate-adsorbent complex.

Understanding **Equation 6** allows for the identification of true equilibrium in the adsorption process, leading to better estimations of adsorption capacity using mathematical models (Tran, Chao, and You 2018). Despite involving complex mechanisms, adsorption kinetics can be simplified using well-known mathematical models (Quesada *et al.* 2019). The primary models utilized to analyze the adsorption of CECs by activated carbon (or any other kind of adsorbent material) are (Tran et al. 2017) the pseudo-first-order (Lagergren 1898; Ho and McKay 1999), pseudo-second-order (Blanchard, Maunaye, and Martin 1984; Ho and McKay 1999), Elovich or

Roginsky-Zoldovich (Roginsky and Zoldovich 1934) and intraparticle diffusion or Weber and Morris (Weber and Morris 1963).

The pseudo-first-order model proposed by Lagergren (1898) can be expressed in both its non-linear (**Equation 7**) and linear forms (**Equation 8**). This model assumes that adsorption occurs at specific active sites without interaction between adsorbates, that the adsorption energy remains constant regardless of the amount adsorbed, that maximum adsorption corresponds to the saturation of adsorption sites on the adsorbent surface, and that the process follows first-order kinetics (Largitte and Pasquier 2016). It is noteworthy that while linear models are available in the literature, their use should be approached with caution to ensure accurate estimation of adsorption capacity (Tran *et al.* 2017).

$$q_i = q_e (1 - e^{-k_1 t}) \quad \text{Equation 7}$$

$$\ln(q_e - q_i) = -k_1 t + \ln(q_e) \quad \text{Equation 8}$$

Where: q_e e q_i are the amounts adsorbed at equilibrium and at time i , respectively, k_1 is the adsorption rate constant, and t is the contact time.

The pseudo-second-order model, originally proposed by Blanchard, Maunaye, and Martin (1984) for the adsorption of inorganic contaminants using natural zeolites as the adsorbent, can also be expressed in both non-linear (**Equation 9**) and various linear forms (**Equation 10, Equation 11, Equation 12, and Equation 13**). The initial adsorption rate can also be estimated using **Equation 14**. While this model shares the same premises as the pseudo-first-order model, it assumes second-order kinetics (Largitte and Pasquier 2016). Although a good fit to the pseudo-second-order model may suggest chemisorption, this mechanism should be validated through analytical techniques like FTIR, Raman spectroscopy, XPS, Boehm titration, and thermodynamic studies (Tran *et al.* 2017). The authors also caution that a good fit to the non-linear model does not necessarily guarantee a good fit to the linear model.

$$q_i = \frac{q_e^2 k_2 t}{1 + k_2 q_e t} \quad \text{Equation 9}$$

$$\frac{t}{q_i} = \left(\frac{1}{q_e}\right) t + \frac{1}{k_2 q_e^2} \quad \text{Equation 10}$$

$$\frac{t}{q_i} = \left(\frac{1}{q_e}\right) + \left(\frac{1}{k_2 q_e^2}\right) \frac{1}{t} \quad \text{Equation 11}$$

$$q_i = -\left(\frac{1}{k_2 q_e^2}\right) \frac{q_i}{t} + q_e \quad \text{Equation 12}$$

$$\frac{q_i}{t} = -(k_2 q_e) q_i + k_2 q_e^2 \quad \text{Equation 13}$$

$$h = k_2 q_e^2 \quad \text{Equation 14}$$

Where: q_e e q_i are the amounts adsorbed at equilibrium and at time i , respectively, k_2 is the adsorption rate constant, t is the contact time, and h is the initial adsorption rate.

The empirical model proposed by Roginsky and Zeldovich (1934), also known as the Elovich model, was originally developed to describe the adsorption of carbon monoxide on manganese dioxide and has since become widely used in cases suggestive of chemisorption (McLintock 1967; Tran *et al.* 2017). The Elovich model can be expressed in its non-linear form (**Equation 15**) or a linear simplification (**Equation 16**) (Chien and Clayton 1980). This model assumes that adsorption occurs at specific active sites, involves interaction between adsorbates and that the adsorption energy increases linearly with the surface coverage of the adsorbent. Additionally, it posits that after the initial exponential adsorption phase, the adsorption process becomes negligible, following a zero-order kinetic process (Largitte and Pasquier 2016).

$$q_i = \frac{1}{\beta} \ln(1 + \alpha \beta t) \quad \text{Equation 15}$$

$$q_i = \frac{1}{\beta} \ln(t) + \frac{1}{\beta} \ln(\alpha \beta) \quad \text{Equation 16}$$

Where: q_i is the amount adsorbed at time i , α is the initial adsorption rate, β is the desorption constant, and t is the contact time.

The intraparticle diffusion model proposed by Weber and Morris (1963) can be expressed linearly by **Equation 17**. Originally developed to describe the adsorption of alkylbenzene sulfonates onto activated carbon, the model divides the adsorption process into two linear phases. In the first part, the constant related to the boundary layer thickness is negligible (Weber and Morris 1963). However, contemporary applications focus on the second phase, as external mass transfer effects cannot be ignored (Largitte and Pasquier 2016).

$$q_i = k_p \sqrt{t} + C$$

Equation 17

Where: q_i is the amount adsorbed at time i , C is the constant related to the boundary layer thickness, and t is the contact time.

Simplistically, the intraparticle diffusion model helps identify adsorption pathways and mechanisms and predicts the rate-limiting step of the process (Tran *et al.* 2017). According to Tran *et al.* (2017), if plotting q_i versus $t^{0.5}$ yields in a linear model passing through the origin (0,0), the entire process is governed by the intraparticle diffusion rate. Conversely, multiple linear regions indicate control by various mechanisms.

Additional kinetic models offer further insights into adsorption. External diffusion can be modeled using Fick's law (Largitte and Pasquier 2016), while internal diffusion is analyzed with models such as the Crank model (Crank 1956), its derivatives (such as the Boyd equation (Boyd, Adamson, and Meyers Jr 1947)), and the Bangham model. The pseudo- n -order model complements traditional models like the pseudo-first and second-order and Elovich models (Ritchie 1977). Complex computational models, such as those proposed by Leyva-Ramos and Geankoplis (1985), can provide a comprehensive understanding of the adsorption process. For more details, see the original publications or the review by Largitte and Pasquier (2016).

1.3.2.2. Isotherms modelling

The study of the equilibrium of the adsorbent-adsorbate system is crucial for understanding the adsorption process (Rouquerol *et al.* 2014). Isotherms, or equilibrium equations, provide crucial data and parameters for both theoretical and practical insights into adsorption (Tran *et al.* 2017). According to Kumar (2006), plotting q versus C_e is vital for a comprehensive understanding of adsorption regions.

In the literature, various adsorption isotherm models for adsorbents are available, and classified into four categories (Tran *et al.* 2017):

- i) Irreversible isotherms or single-parameter isotherms: Henry's isotherm.
- ii) Two-parameter isotherms: Langmuir, Freundlich, Dubinin-Radushkevich, Temkin, Flory-Huggins, and Hill isotherms.

- iii) Three-parameter isotherms: Redlich-Peterson, Sips, Toth, Koble-Corrigan, Kahn, Fritz-Schlunder, Vieth-Sladek, and Radke-Prausnitz isotherms.
- iv) Isotherms with more than three parameters: Weber-van Vliet, Fritz-Schlunder, and Baudu isotherms.

Among these, the Freundlich and Langmuir isotherms are most commonly used due to their applicability, simplicity, and ease of interpretation (Di Bernardo, Dantas, and Voltan 2017). The Dubinin-Radushkevich and Redlich-Peterson models are also widely applied (Tran *et al.* 2017). Quesada *et al.* (2019) also report the extensive use of the Sips, Tempkin, and Toth models for solid-liquid systems, such as the adsorption of CECs. This study focuses on the Freundlich, Langmuir, Dubinin-Radushkevich, Redlich-Peterson, and Sips models, with further details available in Al-Ghouti and Da'ana (2020).

The Langmuir model (Langmuir 1918) assumes a fixed number of adsorption sites on the adsorbent, each with equal energy. Adsorption is considered reversible, occurs in a single layer (no further adsorption at an occupied site), and there is no interaction between adsorbate species (Tran *et al.* 2017). The original Langmuir model is nonlinear (**Equation 18**), but linear forms such as Hanes (1932) (**Equation 19**), Lineweaver and Burk (1934) (**Equation 20**), Eadie (1942) (**Equation 21**), and Scatchard (1949) (**Equation 22**) have been developed for practical use.

$$q_i = \frac{Q_{max}^0 K_L C_e}{1 + K_L C_e} \quad \text{Equation 18}$$

$$\frac{C_e}{q_i} = \left(\frac{1}{Q_{max}^0} \right) C_e + \frac{1}{Q_{max}^0 K_L} \quad \text{Equation 19}$$

$$\frac{1}{q_i} = \left(\frac{1}{Q_{max}^0 K_L} \right) \frac{1}{C_e} + \frac{1}{Q_{max}^0} \quad \text{Equation 20}$$

$$q_i = \left(\frac{-1}{K_L} \right) \frac{q_i}{C_e} + Q_{max}^0 \quad \text{Equation 21}$$

$$\frac{q_i}{C_e} = -K_L q_i + Q_{max}^0 K_L \quad \text{Equation 22}$$

Where: q_i is the amount adsorbed at equilibrium, C_e is the concentration of the adsorbate at equilibrium, K_L is the Langmuir constant related to the adsorbent-adsorbate affinity, and Q_{max}^0 is the monolayer saturation capacity of the adsorbent.

Although the linearization of the Langmuir model is described in the literature, the models should be used cautiously and ideally alongside the non-linear model. The Hanes-Woolf linearization may overestimate the fit because C_e and $\frac{C_e}{q_i}$ are not independent variables. Similarly, the Eadie-Hofstee and Scatchard linearization may underestimate the fit due to their reliance on $\frac{q_i}{C_e}$ and C_e , which are also not independent (Tran *et al.* 2017). Lineweaver-Burk linearization is particularly sensitive to variability in low q_i values due to possible data clustering near the origin (Tran *et al.* 2017).

The Freundlich model (Freundlich 1907) is one of the most used models for adsorption studies (Di Bernardo, Dantas, and Voltan 2017). The Freundlich model can be expressed in both its non-linear form (**Equation 23**) and linear form (**Equation 24**). It is based on five key assumptions: (i) the energies of adsorption and desorption are equal, (ii) the adsorption energy is independent of surface coverage, (iii) the surface contains independent patches, where each patch includes all sites with the same adsorption energy, (iv) the adsorption capacity has a logarithmic dependence on the residual concentration of the adsorbate, and (v) interactions between adsorbate species are possible, allowing for the adsorption of multilayers.

$$q_i = K_F C_e^{\frac{1}{n}} \quad \text{Equation 23}$$

$$\text{Log}(q_i) = \text{Log}(K_F) + \frac{1}{n} \text{Log}(C_e) \quad \text{Equation 24}$$

Where: q_i is the amount adsorbed at equilibrium, C_e is the concentration of the adsorbate at equilibrium, K_F is the Freundlich constant, and n is the Freundlich intensity parameter.

According to Freundlich's theory, the dimensionless parameter n indicates the adsorption intensity or the surface heterogeneity. Specifically, if $n = 1$, the process is linear, if $n < 1$ the process is favorable, and if $n > 10$, the process is unfavorable (Freundlich 1907). Kumar (2006) later suggested that values of n up to 10 indicate favorable adsorption, while values above 10, although theoretically possible, are often impractical. Although K_F e Q_{max}^0 do not represent the same adsorption capacity (*i.e.*, K_F indicates the maximum adsorption capacity only if n tends to infinity (Lu 2008)), these parameters should be of the same order of magnitude (Tran *et al.* 2017). Furthermore, despite being dimensionless, n reflects the strength of the adsorbate-adsorbent interactions, with higher values of n corresponding to stronger binding forces (Di Bernardo, Dantas, and Voltan 2017).

A combination of the Langmuir and Freundlich models was proposed by Sips (1948). Known as the Langmuir-Freundlich isotherm or the Sips isotherm (**Equation 25**), this model addresses the heterogeneity of the adsorption process, overcoming some of the limitations of the Freundlich model (such as high adsorbate concentrations), and predicts behaviors similar to the Langmuir model at high adsorbate concentrations (Perez-Marin *et al.* 2007).

$$q_i = \frac{Q_m (K_s C_e)^n}{(K_s C_e)^n + 1} \quad \text{Equation 25}$$

Where: q_i is the amount adsorbed at equilibrium, Q_m is the system's adsorption capacity, C_e is the concentration of the adsorbate at equilibrium, K_s is the Sips constant, and n is the Sips intensity parameter.

Similar to the Sips model, the Redlich-Peterson model (Redlich and Peterson 1959) integrates features of both the Freundlich and Langmuir models, making it applicable across a wide range of adsorbate concentrations (Tran *et al.* 2017). The model can be expressed in both its non-linear form (**Equation 26**) and its linear form (**Equation 27**). At low concentrations, the Redlich-Peterson model approximates the Langmuir model with the model exponent $g = 1$. At high concentrations, where K_{RP} and α_{RP} are high values and $g = 1$, the model approximates the Freundlich model (Tran *et al.* 2017; Al-Ghouti and Da'ana 2020). When $g = 0$, the model simplifies to a linear isotherm (Henry's Law). If $g > 1$ or $g < 0$, the data cannot be accurately described by the Redlich-Peterson model (Tran *et al.* 2017).

$$q_i = \frac{K_{RP} C_e}{1 + \alpha_{RP} C_e^g} \quad \text{Equation 26}$$

$$\ln \left(K_{RP} \frac{C_e}{q_i} + 1 \right) = g \ln(C_e) + \ln(\alpha_{RP}) \quad \text{Equation 27}$$

Where: q_i is the amount adsorbed at equilibrium, K_{RP} and α_{RP} are the Redlich-Peterson constants, C_e is the concentration of the adsorbate at equilibrium, and g is the model exponent.

The Dubinin-Radushkevich model (Dubinin and Radushkevich 1947) addresses the impact of pore structure on the adsorption process by incorporating a Gaussian distribution of energy across the adsorbent's surface (Al-Ghouti and Da'ana 2020). It assumes multilayer formation driven by van der Waals interactions and helps differentiate between physisorption and chemisorption

through the average adsorption energy (Tran *et al.* 2017; Al-Ghouti and Da'ana 2020). The model can be expressed in both its non-linear form (**Equation 28**) and its linear form (**Equation 29**), while the Polanyi potential (ε) can be determined using **Equation 30** (Hu and Zhang 2019).

$$q_i = q_{DR} e^{-K_{DR}\varepsilon^2} \quad \text{Equation 28}$$

$$\ln(q_i) = -K_{DR}\varepsilon^2 + \ln(q_{DR}) \quad \text{Equation 29}$$

$$\varepsilon = RT \ln\left(1 + \frac{1}{C_e/C_s}\right) \quad \text{Equation 30}$$

Where: q_i is the amount adsorbed at equilibrium, q_{DR} is the adsorption capacity, K_{DR} is the constant related to the energy of sorption, ε is the Polanyi potential, R is the gas constant, T is the temperature of the system, C_e is the concentration of the adsorbate at equilibrium, and C_s is the solubility of the adsorbate in the medium.

From K_{DR} , it is possible to calculate the average adsorption energy (E) using **Equation 31**:

$$E = \frac{1}{\sqrt{2 K_{DR}}} \quad \text{Equation 31}$$

1.3.2.3. Adsorption mechanism

The adsorption of inorganic and organic contaminants onto activated carbon is influenced by the adsorbent's surface functional groups (**Table 2**) (Wu *et al.* 2019) and its physical-chemical properties (Zhang *et al.* 2018). In general, this process is driven by strong interactions between the aromatic ring of the π -donor in activated carbon and the π -protonated adsorbate (Cheng *et al.* 2021). These bonds (π - π) are generally weak, occur between aromatic rings and significantly impact the adsorption of organic contaminants onto carbonaceous materials (Cheng *et al.* 2021; Wang and Wu 2008). These interactions arise from electron transfer between the acceptor and donor groups (Wang and Wu 2008). It is reported that modifications of activated carbon with methanol (CH_3OH) (Jing *et al.* 2014) and potassium hydroxide (Li *et al.* 2018) have increased the efficiency of the materials in removing tetracyclines and ciprofloxacin from water matrices. These modifications reduced the organic content of the adsorbent by altering the density of oxygen-containing functional groups, thereby enhancing π - π interactions between the adsorbent and the adsorbate. Cheng *et al.* (2021) also

noted that increasing the number of π - π interaction sites on the adsorbent's surface can improve its capacity to adsorb various CECs.

Table 2: Major functional groups affecting adsorbate-adsorbent interaction (Patel *et al.* 2019).

Functional group	Structural formula*	Binding atom
Carboxyl	-COOH	O
Esters	-COOR	O
Piperazinyl	-C ₄ H ₆ N ₂	N
Amides	-CONRR'	O, N
Hidroxyl	-OH	O
Amino	RNR'R''	N
Carbonyl	-C=O	O
Silanol	-(SiOH)RR'	O
Thiol	-SH	S
Phenyl	-C ₆ H ₅	Ring
Methyl-substituted Amide	-CONHCH ₃	O, N
Imina	RR'C=NR''	C, N

*R, R', R'' can be H, alkyls, or aromatic groups.

Hydrogen bonds also play a significant role in CEC adsorption. This type of bond is reported as the primary interaction of hormones, such as estradiol, 17 α -ethynyl estradiol, bisphenol, and nonylphenol (Cheng *et al.* 2021). In addition to hydrogen bonding, hydrophobic interactions also contribute significantly to CEC adsorption, driven by nonpolar groups in the adsorbate repelling water molecules (Xie *et al.* 2020). Ion exchange³ serves as a complementary mechanism, involving reversible reactions between liquid and solid-phase ions (Cheng *et al.* 2021). Although CECs are rarely converted to their ionic forms, this adsorption mechanism has been reported as a complementary mechanism (Guo *et al.* 2016; Liu *et al.* 2019).

The PZC of these materials can directly influence the adsorption process. When pH is different from PZC, the adsorbent's surface may gain a positive or negative charge, impacting electrostatic interactions with CECs (Zhao *et al.* 2018). CECs can appear protonated, deprotonated, or amphoteric depending on their pK_a, leading to electrostatic interactions with the adsorbent. Such interactions are considered an interesting mechanism in CEC adsorption (Chen *et al.* 2018; Paunovic

³ Reversible chemical process in which ions from a liquid phase (typically an aqueous solution) are exchanged with ions on a solid phase (usually an adsorbent material)

et al. 2019). For example, sulfonamide antimicrobials are more effectively adsorbed under acidic conditions due to electrostatic interactions (Peiris *et al.* 2017). In contrast, alkaline environments result in better adsorption of tetracyclines (Chen *et al.* 2018). Paunovic *et al.* (2019) reported that KOH-functionalized activated carbon interacts with naproxen through electrostatic forces when deprotonated and protonated.

In addition to the previously discussed mechanisms, most adsorption processes include dispersion and pore filling, followed by intraparticle diffusion (Cheng *et al.* 2021). The intraparticle diffusion model (Weber and Morris 1963), is instrumental in evaluating the significance of this process in contaminant adsorption (Tran *et al.* 2017). Jang *et al.* (2018) identified intraparticle diffusion as the rate-limiting step in the adsorption of tetracyclines by *Pinus taeda* activated carbon. Their study also highlighted that hydrogen bonding and π - π interactions were the primary mechanisms involved in the adsorption process.

Interactions between adsorbates and competition for active sites on activated carbon can significantly impact adsorption, especially when multiple contaminants are present (Varga *et al.* 2019). For instance, ibuprofen showed weaker adsorption in the presence of other non-steroidal anti-inflammatory drugs due to lower binding energy, reduced π - π interactions, and electrostatic repulsion (Jung *et al.* 2015). Diniz *et al.* (2022) found that mesopores in activated carbon reduced competition for active sites between ricobendazole and caffeine, and between carbamazepine and caffeine, thereby promoting intraparticle diffusion. They also noted that carbon with higher surface oxygen content exhibited lower adsorption of more lipophilic contaminants, likely due to the clustering of oxygen and water molecules. Thus, a comprehensive understanding of adsorption mechanisms necessitates integrating insights from various models and empirical studies.

1.3.3. Adsorption modelling: continuous flow studies

Continuous flow adsorption involves passing a contaminated fluid stream through a fixed-bed column containing adsorbent material, allowing for dynamic and steady-state removal of contaminants. The effectiveness of these columns is assessed using breakthrough curves (**Figure 5**), which plot the ratio of outlet to inlet concentration (C/C_0) over time (AWWA 2011).

A breakthrough curve typically features two main components: the mass transfer zone (MTZ) and the breakthrough point. The MTZ represents the depth of the adsorbent required to

transfer the adsorbate from the fluid to the adsorbent (Di Bernardo, Dantas, and Voltan 2017). As shown in **Figure 5**, the MTZ progresses along the column over time, with the adsorbent below the MTZ remaining unused until the entire column is "contaminated". The breakthrough point occurs when the concentration of the adsorbate in the effluent exceeds an acceptable level, usually defined as $C/C_0 = 0.05$ (AWWA 2011). For regulated adsorbates, this point is determined by allowable concentration limits and signals when the adsorbent needs replacement or regeneration (Di Bernardo, Dantas, and Voltan 2017). Continued operation past the breakthrough point leads to saturation, where the effluent concentration equals the inlet concentration ($C/C_0 = 1$) (**Figure 5**).

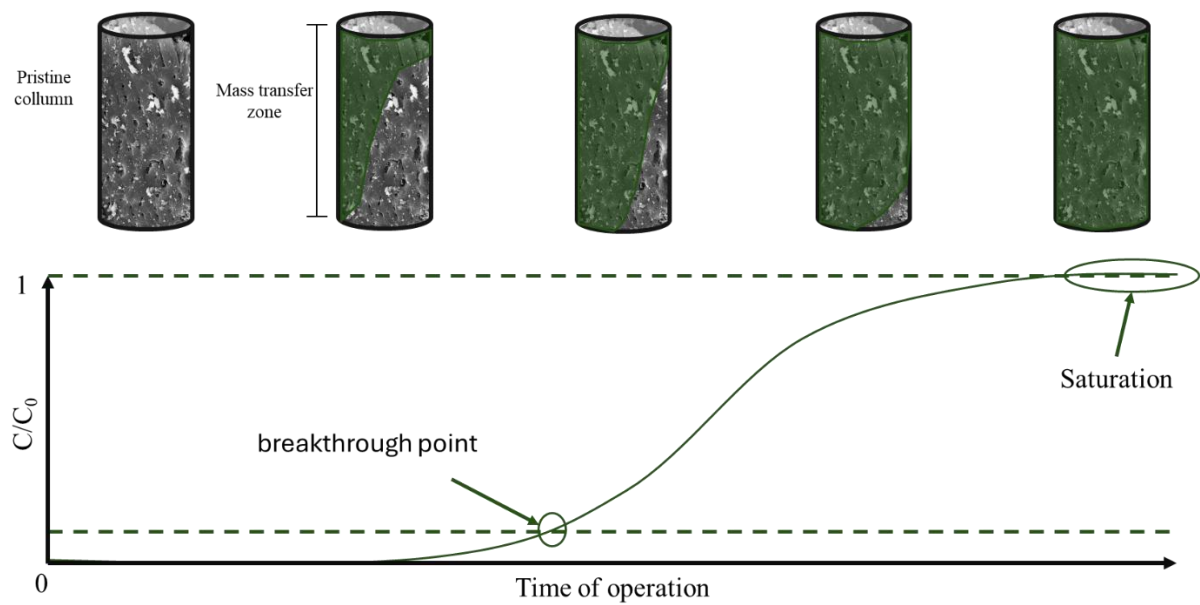


Figure 5: Movement of the mass transfer zone and breakthrough curve over time in a fixed-bed column. Source: Author.

Several factors influence contaminant removal in fixed-bed columns. For instance, the particle size of the adsorbent affects the length of MTZ when intraparticle diffusion controls the adsorption process (AWWA 2011). Smaller particles typically result in a shorter MTZ, enhancing efficiency. However, smaller particles also increase the pressure drop, which can raise energy costs and limit their practicality. Moreover, particle size uniformity is important; coefficients greater than 1.9 may necessitate column expansion for effective backwashing procedures (AWWA 2011).

The Empty Bed Contact Time (EBCT) (**Equation 32**) is another critical parameter in the design of adsorbent columns. It is important to avoid very short EBCTs to prevent premature

breakthroughs, while excessively long EBCTs can lead to higher project costs (AWWA 2011). EBCT, along with related parameters, must be carefully analyzed for effective column design. Ahmed and Hameed (2018) note that the influent flow rate directly impacts column removal efficiency. For example, a study on cephalexin showed that increasing the flow rate from 4.5 to 7.5 mL/min reduced breakthrough time by 71% and decreased the total cephalexin adsorbed from 221.8 to 105.7 mg/g (Nazari *et al.* 2016). Besides flow rate, the bed height is another factor affecting sizing of fixed-bed columns (Ahmed and Hameed 2018). Higher bed heights increase the contact time between the adsorbent and adsorbate, improving adsorption performance. A study with ranitidine and activated carbon indicated that increasing the column height from 1 to 3 cm resulted in a 340% increase of the breakthrough time and a 46.7% improvement in adsorption capacity (Jung *et al.* 2017).

$$EBCT = \frac{V_{ADS}}{Q} = \frac{A h}{Q} \quad \text{Equation 32}$$

Where: V_{ADS} is the volume of the granular adsorbent bed, Q is the influent flow rate, A is the column cross-sectional area, and h is the bed height.

The initial concentration of the adsorbate significantly impacts column removal efficiency (Ahmed and Hameed 2018). Higher initial concentrations enhance the concentration gradient along the MTZ, accelerating the adsorption rate and leading to earlier saturation of the adsorbent bed (Jung *et al.* 2017). Darweesh and Ahmed (2017) observed that, with the same operation time (35 min) and flow rate (1.5 mL/min), higher initial concentrations of levofloxacin increased C/C_0 values.

Although often discussed in the context of fixed-bed columns sizing, the surface loading rate (SLR) does not typically affect column efficiency directly (AWWA 2011). However, SLR (**Equation 33**) is important for system load considerations. High SLRs can lead to increased pressure losses, potentially requiring higher filtration pressures and raising energy costs (Di Bernardo, Dantas, and Voltan 2017).

$$SLR = \frac{Q}{A} \quad \text{Equation 33}$$

Where: Q is the influent flow rate and A is the column cross-sectional area.

Backwashing fixed-bed columns, while not always necessary, can be crucial for managing microbial growth and removing particles that contribute to system pressure loss (AWWA

2011). During backwashing, it is important to prevent particle movement and desorption of adsorbed molecules. Additionally, pre-treating the effluent by reducing turbidity, total organic carbon, and organic matter can help extend the column's lifespan by minimizing competition for the adsorbent's active sites (AWWA 2011).

Breakthrough curves are essential for deriving various parameters related to the adsorbent's capacity (Tan and Hameed 2017). Analyzing these curves involves solving three simultaneous conservation equations: mass balance, energy balance, and momentum balance (Casas *et al.* 2012). However, in liquid-phase studies, temperature effects and pressure drops are generally minimal, simplifying the problem of solving the mass balance differential equation (**Equation 34**) (Tan and Hameed 2017).

$$\frac{dC}{dt} + v \frac{dC}{dz} + \frac{1 - \varepsilon}{\varepsilon} \rho \frac{dq}{dt} = D_L \frac{d^2C}{dz^2} \quad \text{Equation 34}$$

Where: C is the adsorbate concentration, z is the spatial coordinate along the column length, t is the time, v is the interstitial liquid velocity, ε is the bed porosity, Q is the adsorption capacity, ρ is the adsorbent density, and D_L is the axial dispersion coefficient.

Considering $\frac{dq}{dt}$ as a time-dependent variable and assuming a single-layer adsorption model while neglecting axial dispersion (*i.e.*, ideal plug-flow reactor), Thomas (1944) derived an exact solution for **Equation 34**. However, the assumptions made by him often deviate from real-world conditions, leading to the development of various numerical methods over the years. These methods require advanced computational resources and prior knowledge of kinetic and transport parameters (Tan and Hameed 2017). Due to these limitations, simplified models have been developed, with the Bohart-Adams, Thomas, and Yoon-Nelson models being among the most commonly used throughout the 20th century (Ahmed and Hameed 2018). Despite their differences, these models generally follow a nonlinear equation (**Equation 35**) or a linear equation (**Equation 36**) (Chatterjee and Schiewer 2011).

$$\frac{C}{C_0} = \frac{1}{1 + \exp(a - b t)} \quad \text{Equation 35}$$

$$\ln \left(\frac{C_0}{C} - 1 \right) = a - b t \quad \text{Equation 36}$$

Where: a and b are the model parameters, as shown in **Table 3**.

Table 3: Specific parameters for fixed-bed column adsorption models.

Model	a	b
	$\frac{k_{BA} N_0 Z}{v}$	$k_{BA} C_0$
Bohart-Adams	Where: k_{BA} is the Bohart-Adams rate constant, N_0 is the adsorption capacity per volume of adsorbent, Z is the column height, and v is the superficial velocity.	Where: k_{BA} is the Bohart-Adams rate constant and C_0 is the initial concentration of the adsorbate.
	$\frac{k_T q_0 m}{Q}$	$k_T C_0$
Thomas	Where k_T is the Thomas rate constant, q_0 is the adsorption capacity at saturation, m is the mass of adsorbent in the column, and Q is the feed flow rate.	Where k_T is the Thomas rate constant and C_0 is the initial concentration of the adsorbate.
	τk_{YN}	k_{YN}
Yoon-Nelson	Where τ is the time at which $C/C_0 = 0.5$ e k_{YN} is the adsorption rate.	Where k_{YN} is the adsorption rate.

The Bohart-Adams model (Bohart and Adams 1920), originally proposed for gas adsorption on coal, is now widely used for solid-liquid adsorption (Tan and Hameed 2017). It assumes negligible axial dispersion and that the adsorption rate is proportional to the residual adsorption capacity and the concentration of the adsorbate (Smaranda *et al.* 2017). The model is most accurate in the region where $C/C_0 = 0.5$ (Ahmed and Hameed 2018).

The Thomas model (Thomas 1944) assumes that adsorption in a fixed bed follows the Langmuir isotherm and pseudo-second-order kinetics, with negligible axial dispersion (Tan and Hameed 2017). It also presumes that the physical properties of the adsorbent and adsorbate are constant, and that intraparticle diffusion and internal mass transfer resistance are negligible (Sonobe 2018).

The Yoon-Nelson model (Yoon and Nelson 1984a, 1984b) is simpler and does not require detailed information about the adsorbent or fixed-bed column. It assumes that the probability of molecule adsorption decreases as the breakthrough progresses and that this decrease is related to the adsorbate's adsorption probability and fixed-bed breakthrough (Ahmed and Hameed 2018). This model has demonstrated effective results in the adsorption of pharmaceuticals in fixed-bed columns (Cabrera-Lafaurie, Roman, and Hernandez-Maldonado 2015). The Yoon-Nelson maximum adsorption capacity can be determined using **Equation 37**:

$$q_{ads,YN} = \frac{C_0 * Q * \tau}{m_{ads}} \quad \text{Equation 37}$$

Where: $q_{ads,YN}$ is the adsorption capacity of the Yoon-Nelson Model and τ is the time (min) required for 50% adsorbate breakthrough.

In addition to the models already described, breakthrough curves can be used to derive key parameters such as breakthrough time (t_b) (**Equation 38**) and the saturation time (t_s) **Equation 39**). Breakthrough time is the time at which the adsorbate concentration in the effluent exceeds a predefined threshold, typically set as $C/C_0 = 0.05$. Saturation time is the time at which the adsorbent reaches its maximum capacity, and the effluent concentration approaches the inlet concentration ($C/C_0 \approx 1$).

$$t_b = \int_0^{t_{bb}} \left(1 - \frac{C}{C_0}\right) dt \quad \text{Equation 38}$$

$$t_s = \int_0^t \left(1 - \frac{C}{C_0}\right) dt \quad \text{Equation 39}$$

Where: t_b , t_{bb} , t_s and t are the breakthrough time, first sampling point after $C/C_0 > 0.05$, saturation time and experiments duration (min), respectively and C and C_0 are the outlet and inlet concentrations (mg L^{-1}), respectively.

The experimental q value is then obtained from the breakthrough curves by **Equation 40**:

$$q = \frac{Q * C_0}{m_{ads}} * \int_0^t \left(1 - \frac{C}{C_0}\right) dt \quad \text{Equation 40}$$

1.3.3.1. Hydrodynamics

According to Zaiat (2005), mapping the velocity distribution within reactors - such as identifying stagnant zones, preferential pathways, and short-circuiting areas - is essential for understanding internal flow dynamics. However, experimental data collection for these parameters is often challenging and impractical (Zaiat 2005). Therefore, the author suggests that hydrodynamic characterization should instead focus on practical aspects that provide valuable information for reactor design, among which residence time distribution (RTD) curves are particularly significant (Yianatos *et al.* 2017).

RTD curves are typically obtained through stimulus-response tests, where a perturbation (*e.g.*, a tracer) is introduced into the reactor, and its concentration is measured at the effluent. The two classic perturbation methods are pulse injection and step injection (Silva 2006) (**Figure 6**). Pulse injection requires less tracer material but demands that the injection time be negligible compared to the reactor's hydraulic retention time and minimal dispersion at the injection point (Zaiat 2005). Conversely, step injections require more material but are less sensitive to dispersion, injection velocity, and initial tracer concentration (C_0), making it often preferred for fixed-bed column tests (Silva 2006). After injection (at time 0), the tracer concentration is measured at the outlet over time, generating the concentration curve ($C(t)$).

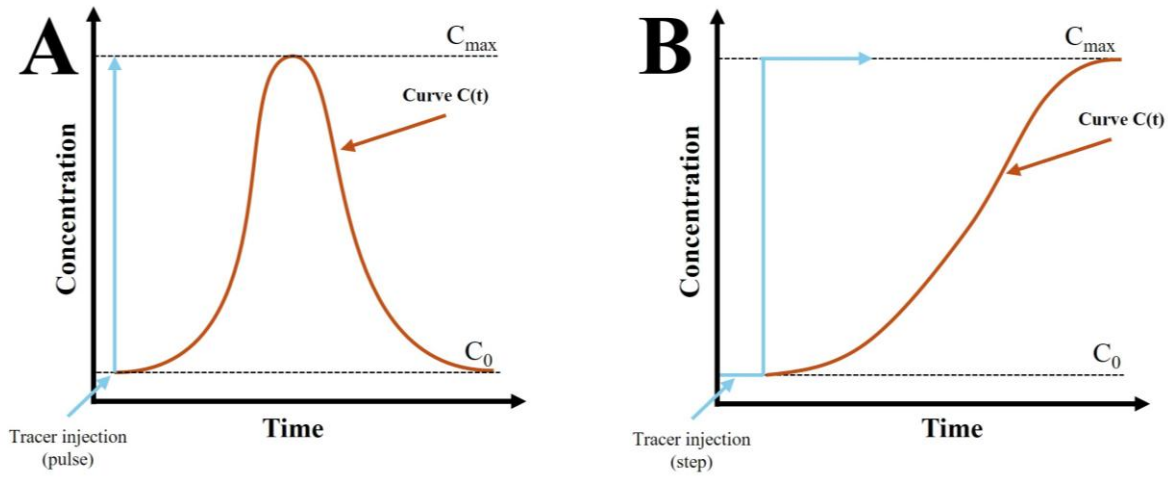


Figure 6: Tracer injection types and their respective concentration curves. A: Pulse injection; B: Step injection. C_{max} is the tracer maximum concentration and C_0 is the tracer initial concentration. Adapted from (Silva 2006).

As this study utilizes the step injection method due to its advantages, a detailed explanation is provided. The normalized concentration curve ($F(t)$) is then derived from the concentration curve ($C(t)$) using **Equation 41**.

$$F = \frac{C}{C_{max}} \quad \text{Equation 41}$$

Where: C e C_{max} represent the tracer concentrations at time t and the maximum concentration, respectively.

To derive the RTD curve ($E(t)$), the concentration of the tracer in the effluent stream from the reactor is related to the concentration in the inlet stream using the convolution integral (**Equation**

42) (Levenspiel 1999). Since the function F is C/C_0 , the RTD can be obtained using either **Equation 43** or **Equation 44**.

$$\frac{C(t)}{C_0} = \int_0^t E(t') dt \quad \text{Equation 42}$$

$$F = \int_0^t E dt \quad \text{Equation 43}$$

$$E = \frac{dF}{dt} \quad \text{Equation 44}$$

Where: $C(t)$ e C_0 are the tracer concentrations at time t in the influent stream, respectively, t is time, F is the normalized concentration curve (Curve $F(t)$), and E is the RTD curve (Curve $E(t)$).

Finally, by considering a time range from 0 to infinity, where the sum of all the tracer injected into the reactor and all the tracer remaining in the reactor until time t_1 equals 1, the amount of tracer exiting the reactor is obtained by **Equation 45**, and the mean hydraulic retention time (HRT) of the reactor is obtained by **Equation 46**.

$$\int_{t_1}^{\infty} E(t)dt = 1 - \int_0^{t_1} E(t)dt \quad \text{Equation 45}$$

$$HRT = \frac{\int_0^{\infty} t E(t)dt}{\int_0^{\infty} E(t)dt} = \int_0^{\infty} t E(t)dt \quad \text{Equation 46}$$

The mean hydraulic retention time derived from the hydrodynamic test is expected to be equal to or close to the value calculated using **Equation 47** (Zaiat 2005). However, a visual analysis of the RTD curve can also reveal reactor anomalies. For instance, an early peak (**Figure 7-B**) may indicate channeling or stagnant regions within the reactor, while a delayed peak (**Figure 7-C**) could suggest experimental errors such as inaccuracies in flow measurement, non-inert tracers, or reactor volume issues. Multiple peaks may indicate internal recirculation (**Figure 7-D**) or flow through two parallel paths (**Figure 7-E**) (Zaiat 2005).

$$\theta_c = \frac{Q}{V} \quad \text{Equation 47}$$

Where: θ_c is the calculated hydraulic retention time, Q is the flow rate, and V is the reactor volume.

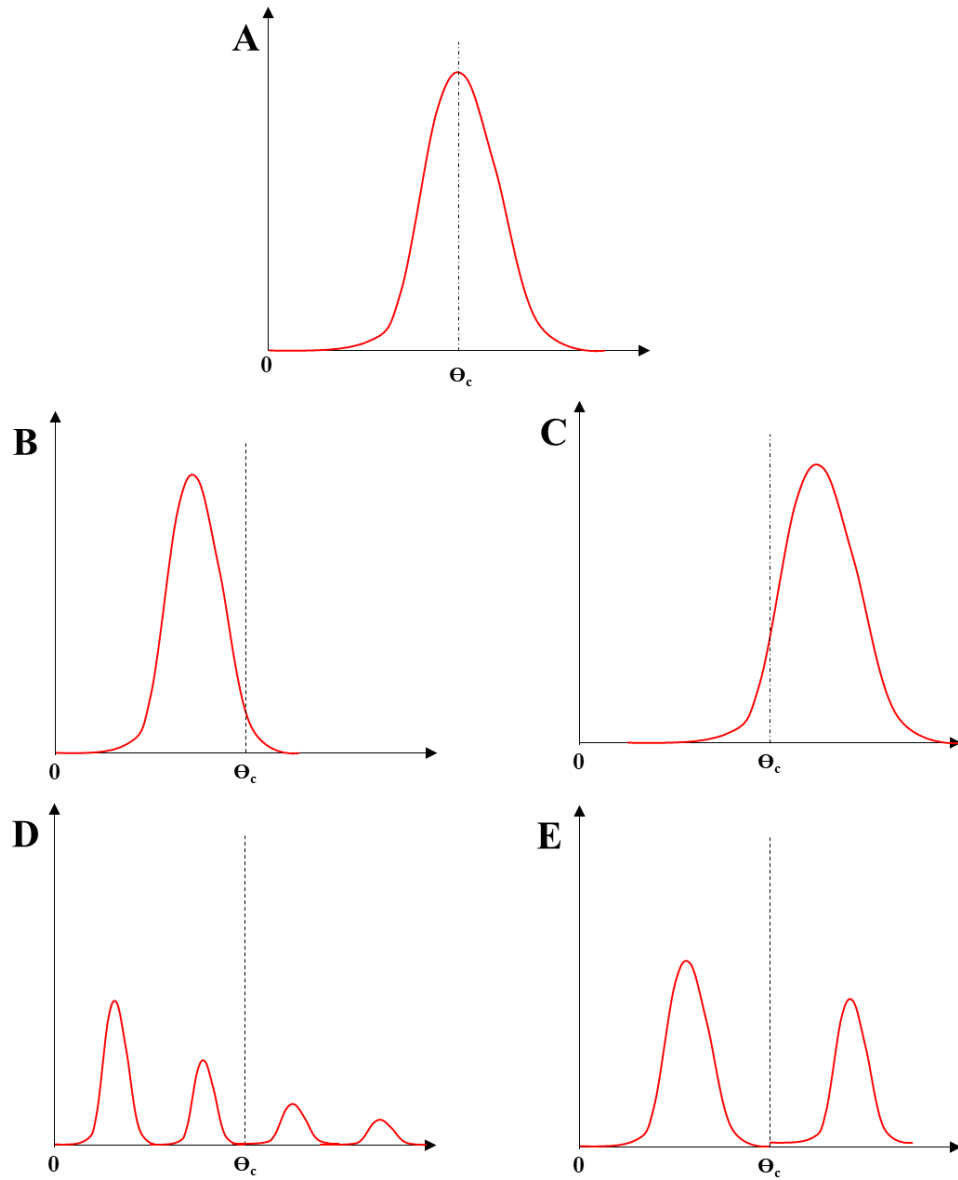


Figure 7: Flow anomalies in reactors based on the E curve. (A) no anomalies observed; (B) Channeling; (C) Experimental errors; (D) Internal recirculation; and (E) two parallel paths. Adapted from (Zaiat 2005).

1.4. Advanced materials

Although potable reuse has its benefits, its global implementation presents several significant challenges (Jeffrey, Yang, and Judd 2022; Liu et al. 2020; Barnes, Krishen, and Hu 2021; Hartley, Tortajada, and Biswas 2019; Bass *et al.* 2022):

- i) The quality of wastewater sources varies significantly, often containing a complex mixture of chemical contaminants, including pharmaceuticals, personal care products, and industrial chemicals. These contaminants can be difficult to remove using conventional treatment methods, necessitating advanced technologies that can effectively address a broad spectrum of pollutants. The challenge is further compounded by the variability in wastewater quality, which can affect the efficiency and reliability of treatment processes.
- ii) The treatment process required for potable reuse is often complex and space-intensive compared to conventional processes. In many urban areas, available space for installing and maintaining these advanced treatment systems is limited, posing a significant challenge. Additionally, these systems can be costly to implement and operate, which can be a barrier for many municipalities, especially in developing regions. The integration of multiple treatment stages, such as advanced oxidation processes, membrane filtration, and biological treatments, requires careful planning and significant investment.
- iii) Public acceptance remains a substantial hurdle. Despite the growing body of evidence supporting the safety and benefits of potable reuse, public perception can lag scientific advancements. Misconceptions about water quality and safety, combined with concerns about the "toilet-to-tap" concept, contribute to resistance. Efforts to improve public acceptance include transparency in water quality reporting, education campaigns, and community engagement to build trust and demonstrate the safety and benefits of potable reuse.

The potential consequences of system failures in potable reuse systems are severe, underscoring the need for robust and reliable infrastructure (WHO 2017). To mitigate risks, it is essential to implement comprehensive monitoring systems that can continuously assess water quality and detect any anomalies. These systems should be capable of identifying potential issues before they

affect the safety of the water supply. Additionally, reliable treatment trains and engineered storage buffers play a crucial role in providing redundancy and time for response in case of system failures. These measures ensure that any detected faults can be addressed promptly, minimizing the risk of contamination.

The complexity of treatment processes required for potable reuse often demands sophisticated technologies and operational expertise. DPR treatment plants, which are designed to treat wastewater to a level that meets drinking water standards, often employ a combination of advanced treatment technologies (Jeffrey, Yang, and Judd 2022; Schimmoller, Kealy, and Foster 2015). These may include membrane bioreactors, reverse osmosis, and advanced oxidation processes. Each of these technologies has its own set of operational requirements and limitations, making the design and management of DPR systems a complex task.

In low-income countries, the high costs associated with these advanced technologies and the complexity of their implementation can be prohibitive (Guo, Englehardt, and Wu 2014; Diniz *et al.* 2024a). Therefore, there is a need for cost-effective solutions that can achieve similar levels of treatment while being feasible for deployment in resource-limited settings.

Innovative materials play a crucial role in addressing the challenges associated with potable reuse (Zodrow *et al.* 2017). Research and development in this field focus on materials that can improve the efficiency of water treatment processes while reducing energy consumption and environmental impact. For instance, advancements in membrane technology and the development of novel adsorbent materials can enhance the performance of treatment systems (Ngo *et al.* 2022; Ayyaru and Ahn 2023; Luhar *et al.* 2021).

Additionally, the use of low-cost and sustainable materials can help reduce the overall cost of treatment processes, making potable reuse more accessible in low-income regions (Huang *et al.* 2021). By improving the efficiency of existing technologies and introducing new materials with enhanced properties, it is possible to reduce both the energy and environmental footprints of urban water systems.

An effective DPR scheme typically integrates conventional WWTPs with advanced units like membrane filtration, advanced oxidation processes, and adsorption systems (WHO 2017). Combining the advanced oxidation process unit with adsorption technologies offers significant advantages, particularly in enhancing the efficiency of oxidizers while reducing the energy demands

associated with these processes (Lim *et al.* 2011; Wang *et al.* 2016). Within these systems, activated carbon plays a crucial role due to its high surface area and exceptional adsorption capacity. Beyond its standalone benefits, activated carbon also serves as an excellent support for photocatalysts, such as titanium dioxide (TiO₂), which further amplifies the degradation of organic contaminants under UV light (Rodriguez-Reinoso and Sepúlveda-Escribano 2009).

The synergy between activated carbon and TiO₂ not only enhances the removal of contaminants through dual mechanisms - adsorption and photocatalysis - but also contributes to a more efficient and sustainable water purification process. This integrated approach is particularly valuable in the context of DPR, where the need for reliable and energy-efficient solutions is paramount (Li Puma *et al.* 2008).

Moreover, recent advancements in materials science have introduced inverse vulcanization sulfur polymers as promising candidates for water purification applications (Chung *et al.* 2013; Berk *et al.* 2023). These polymers, derived from waste sulfur, are not only sustainable but also exhibit a high affinity for binding inorganic contaminants (*e.g.*, mercury) (Müller, Lisboa, and Chalker 2023). Their intrinsic photocatalytic properties further augment their utility in water treatment, providing a dual-function material that addresses both adsorption and advanced oxidation needs (Upton *et al.* 2022).

The integration of these innovative materials - activated carbon, TiO₂, and sulfur polymers - into DPR systems has the potential to significantly improve the performance of water treatment plants. By leveraging the combined adsorption and photocatalytic capabilities of these materials, DPR schemes can achieve higher contaminant removal efficiency, ensuring the provision of safe and clean drinking water. This approach also aligns with the broader goals of sustainability, as it minimizes environmental impact while maximizing the effectiveness of water purification technologies.

1.4.1. Activated carbon as support for photocatalysts

The use of photocatalysts for the removal of contaminants from aqueous matrices has been extensively documented in the literature, showcasing their potential for degrading a wide range of contaminants (Caianelo *et al.* 2022; Zhao *et al.* 2018; Santhosh *et al.* 2016). Photocatalysts generate reactive oxidizing species under light irradiation, which can effectively degrade organic

contaminants. However, the efficiency of these catalysts is highly dependent on their dispersion within the aqueous phase and their proximity to the target contaminants, as the reactive species they generate have limited diffusion capabilities (Mineiro, Catozzo, and Pelizzetti 1992; Juntgen 1986). This poses a significant challenge in ensuring effective contact between the photocatalyst and the pollutants, particularly in continuous-flow systems such as drinking water treatment plants (DWTPs) or WWTPs.

For practical applications in DWTPs and WWTPs, it is crucial that photocatalysts are not only effective but also recoverable from the effluent to prevent secondary pollution and allow for reuse (Adán *et al.* 2018). Among the various support materials used to enhance the recovery and stability of photocatalysts, activated carbon stands out as the most commonly employed. Its popularity is due to its multiple advantageous properties, including its ability to reduce metallic phases (for metallic catalysts), resistance to acidic and basic environments, thermal stability, availability in various physical forms (powder, granules, fibers, pellets), ease of recovery, and lower cost relative to other supports such as alumina and silica (Gerber and Serp 2020).

In the realm of photocatalysis, TiO_2 remains the most widely used catalyst when combined with activated carbon (Li Puma *et al.* 2008). The anchoring of TiO_2 particles onto activated carbon (TiO_2/AC) is achieved through various techniques, including anodization, electrodeposition, sputtering, chemical vapor deposition, sol-gel, aerosol pyrolysis, and hydrothermal synthesis. Each of these methods significantly impacts the efficiency of the resulting TiO_2/AC composites, influencing factors such as surface area, porosity, and photocatalytic activity.

For instance, Peñas-Garzón *et al.* (2020) demonstrated that while the sol-gel process did not alter the band gap of TiO_2 , it led to a decrease in photocatalytic efficiency for the removal of acesulfame, primarily due to a reduction in the specific surface area and porosity of the AC support. Similarly, the calcination process has been shown to play a critical role in determining the crystalline phase of TiO_2 and, consequently, its photocatalytic performance. Briche *et al.* (2020) reported that calcining TiO_2/AC at 400 °C increased the proportion of the anatase phase - known for its superior photocatalytic activity (Caianelo *et al.* 2022) - while Wang *et al.* (2009) found that calcining at 600 °C improved the removal efficiency of methyl orange. However, when the temperature was increased to 700 °C, despite further enhancing the anatase phase, the surface area and porosity of the support material decreased, which limited the accessibility of contaminants to the TiO_2 surface, thereby reducing the overall efficiency.

The quantity of TiO₂ anchored on activated carbon is another critical factor affecting the performance of the composite material. Interestingly, increasing the amount of TiO₂ does not necessarily correlate with improved contaminant removal efficiency. Briche *et al.* (2020) found that excessive TiO₂ loading on activated carbon actually reduced the surface area, porosity, and pore size, leading to a decrease in the adsorption capacity of the material. This finding highlights the importance of balancing the oxidative and adsorptive components within the photocatalyst to achieve optimal performance.

Further illustrating the interplay between adsorption and photocatalysis, Mesones *et al.* (2020) investigated the removal of *Escherichia coli* from simulated surface water using a UV-activated TiO₂/AC reactor. They found that anchoring TiO₂ onto activated carbon altered the zeta potential of the adsorbent, making it less negative (-41.9 mV for activated carbon to -29.2 mV for TiO₂/AC). This change enhanced electrostatic interactions between *E. coli* and TiO₂/AC, resulting in a 100-fold increase in removal efficiency. Additionally, the activation of TiO₂'s photocatalytic properties by UV light led to a more than 200-fold increase in *E. coli* inactivation.

Despite the numerous studies exploring various synthetic methods and titania precursors for creating TiO₂/AC composites, there remains no consensus on the optimal approach for photodegrading organic contaminants. Common titania precursors include titanium tetrachloride (TiCl₄), titanium isopropoxide (Ti(OiPr)₄), and titanium butoxide (Ti(OBu)₄). Among these, TiCl₄ is particularly challenging due to its rapid hydrolysis in air, which complicates its use in synthesizing TiO₂/AC composites (Zhang, Yin, and Sato 2009). While significant advancements have been made over recent decades, further research is needed to determine the optimal synthetic methods and precursor materials for maximizing photocatalytic efficiency. Additionally, the performance of these composites in real-world water matrices, as opposed to controlled laboratory conditions, remains largely uninvestigated and presents an important avenue for future research. Understanding how these materials interact with complex mixtures of contaminants in real water sources will be critical for their successful implementation in water treatment facilities.

1.4.2. Inverse vulcanization sulfur polymers

Inverse vulcanization sulfur polymers represent a significant advancement in the field of material science, offering a novel approach to stabilizing sulfur through its reaction with unsaturated

organic monomers (Chung *et al.* 2013). This innovative process fundamentally differs from traditional vulcanization, where sulfur is used to cross-link polymers. Instead, in inverse vulcanization, organic crosslinkers are employed to stabilize the sulfur itself, transforming it from a brittle substance into a robust, high-performance polymer (Chung *et al.* 2013). The polymerization process begins by heating elemental sulfur above the temperature of 159 °C, which induces homolysis of the sulfur-sulfur (S–S) bonds (**Figure 8**). This homolysis generates thiyl radicals, which subsequently initiate a series of ring-opening reactions, leading to the formation of new S–S bonds between sulfur molecules (Meyer 1976; Kennedy *et al.* 1983). These interactions create an unstable polysulfide chain that, if left unstabilized, would naturally depolymerize back into cyclic sulfur species through a process known as backbiting (Meyer 1976). To prevent this depolymerization, Chung *et al.* (2013) introduced the use of unsaturated crosslinking agents to trap the thiyl radicals, thereby forming a stable, networked polymer.

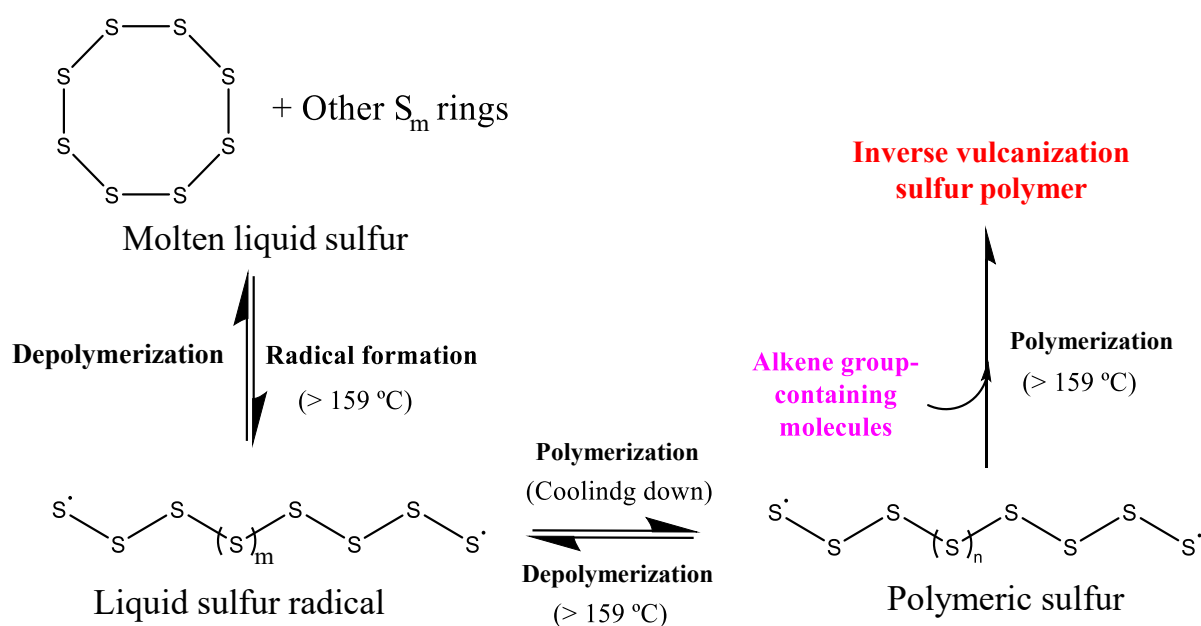


Figure 8: General scheme for inverse vulcanization polymerization. Source: Author.

One of the most compelling aspects of inverse vulcanization is its more sustainable approach. The process is highly atom-efficient, utilizing sulfur and alkenes as both co-monomers and the reaction medium, eliminating the need for external solvents or reagents. This ensures that all starting materials are fully incorporated into the final product, minimizing waste and environmental impact (Worthington, Kucera, and Chalker 2017). Such characteristics not only make inverse

vulcanization an environmentally friendly method but also pave the way for a diverse array of applications for sulfur-based polymers.

Inverse vulcanization sulfur polymers have garnered attention across various fields due to their unique properties and versatility (Yan *et al.* 2020; Upton *et al.* 2022; Hasell *et al.* 2016; Dop, Neill, and Hasell 2021). In the realm of energy storage, these polymers are particularly valuable in lithium-sulfur batteries, where their high sulfur content contributes to enhanced battery performance. The sulfur-rich composition of these polymers allows for higher energy densities and improved cycling stability, making them a promising alternative to conventional battery materials (Gomez *et al.* 2016; Alex, Singha, and Choudhury 2023).

In environmental applications, sulfur polymers have shown exceptional potential in the adsorption of inorganic contaminants. Their strong affinity for metals like mercury and lead makes them highly effective for capturing these contaminants from wastewater, offering a sustainable solution for industrial pollution control (Bear *et al.* 2016; Müller, Lisboa, and Chalker 2023). The high sulfur content in the polymers facilitates the formation of stable metal-sulfur complexes, which can be easily separated from the aqueous phase, ensuring efficient removal of toxic metal.

Beyond inorganic contaminants adsorption, the optical properties of sulfur polymers have led to their use in infrared lenses and other optical devices. The ability to tailor these polymers by altering the organic cross-linkers used in their synthesis allows for the fine-tuning of their optical characteristics, making them suitable for a variety of applications in the field of optics (Kleine *et al.* 2016; Chalker *et al.* 2019; Boyd *et al.* 2019). The versatility of these materials stems from their ability to be tailored for specific needs by altering the organic cross-linkers used in their synthesis (Dale, Hanna, and Hasell 2023).

These sulfur polymers are used in the field of metal adsorption, where these materials demonstrate a strong affinity for various metal ions. The interaction between the high sulfur content in these polymers and metal ions results in the formation of stable complexes, effectively separating these hazardous materials from the water. Studies have confirmed the efficacy of sulfur polymers in adsorbing metals such as mercury, lead, and cadmium, making them a sustainable and cost-effective option for wastewater treatment (Hasell *et al.* 2016; Müller, Lisboa, and Chalker 2023).

In addition to their role in metal adsorption, sulfur polymers also show promise in the removal of organic contaminants from water (Berk *et al.* 2023; Diniz *et al.* 2024a). These polymers

possess intrinsic photocatalytic activity, attributed to their high sulfur content (Upton *et al.* 2022). This photocatalytic capability enables the degradation of organic contaminants under light exposure, further broadening the potential applications of these materials in advanced water treatment technologies. Therefore, these polymers offer an alternative approach to water purification, combining efficiency with environmental sustainability.

Chapter 2.

Aims and objectives

2.1. Aims and objectives

The aim of this thesis is to advance the understanding of new hybrid materials with both adsorptive and photocatalytic properties as alternatives to activated carbon in direct potable reuse (DPR) schemes. The project is organized around the following objectives:

Development of analytical methods for the determination of CECs in water matrices. A bidimensional liquid chromatography coupled with mass spectrometry (LC-LC-MS/MS) for determining CECs in water matrices (raw sewage, treated effluent, water) was developed and validated. The LC-LC-MS/MS method was used to monitor the CECs at the EPAR Capivari II and its pilot plant and for the batch adsorption studies. An UHPLC-MS/MS for determining the five marker CECs in water matrices (raw sewage, treated effluent, water) was developed and validated. The UHPLC-MS/MS was used to determine the CECs in the continuous flow adsorption study and TiO₂/AC studies.

Monitor the CECs at the EPAR Capivari II. The presence of 12 CECs (acesulfame, acetaminophen, albendazole, carbamazepine, caffeine, diclofenac, hydrochlorothiazide, propranolol, ricobendazole, saccharin, sucralose, and sulfamethoxazole) was monitored at the raw sewage and effluent post-MBR of the EPAR Capivari II to select five marker CECs.

Establishment of treatment train at the EPAR Capivari II pilot plant. Reverse osmosis, photoperoxidation, and adsorption (fixed-bed column of granular activated carbon) were assessed individually and in combination to select the best treatment train for the removal of the previously selected five CECs.

Understand factors influencing the adsorption of CECs by activated carbon. The activated carbon installed at the EPAR Capivari II pilot plant, and a commercially available activated carbon were characterized and investigated for the removal of the previously selected five CECs in batch (kinetics and isothermal studies) and continuous flow (influence of bed height, flow rate, and flow mode) studies.

Design of new hybrid materials as an alternative to activated carbon. As adsorption and photodegradation were revealed as essential for producing high-quality water in DPR schemes, combining these properties into a single material has the potential to significantly enhance the cost-

effectiveness and efficiency of DPR systems. To achieve this, two different approaches were investigated:

- (i) **Synthesis of TiO₂ anchored-activated carbon materials.** Four different synthetic procedures (sol-gel, solvothermal, and two microwave-assisted hydrothermal methods) along with two titania precursors (titanium isopropoxide and titanium butoxide) were investigated to anchor TiO₂ onto activated carbon installed at the EPAR Capivari II pilot-plant, aiming to combine adsorption and photodegradation processes with one material. The materials were characterized and investigated the removal of the previously selected five CECs in batch studies. The regeneration of the TiO₂/AC materials was also investigated using two different regeneration methods.
- (ii) **Synthesis of porous sulfur polymers.** To broaden the scope of innovative materials investigated in this study, sulfur polymers were synthesized by inverse vulcanization using petroleum refinery waste and perillyl alcohol, while table salt (NaCl) was introduced as a template to create pores. The materials also aim to combine adsorption and photodegradation processes. The polymers were characterized and used to remove caffeine in adsorption and photocatalysis batch studies.

Chapter 3.

Published Manuscripts

3.1. List of published manuscripts

Herein, we present a list of the published manuscripts that constitute this thesis:

- i) Diniz, V. Cunha, D. G. F., Rath, S. 2023. Adsorption of recalcitrant contaminants of emerging concern onto activated carbon: A laboratory and pilot-scale study. *Journal of Environmental Management*, 325 (A). <https://doi.org/10.1016/j.jenvman.2022.116489>
- ii) Diniz, V. and Rath, S. 2023. Adsorption of aqueous phase contaminants of emerging concern by activated carbon: Comparative fixed-bed column study and *in situ* regeneration methods. *Journal of Hazardous Materials*, 459. <https://doi.org/10.1016/j.jhazmat.2023.132197>
- iii) Diniz, V., Crick, C. R., Rath, S. 2023. Synthesis and characterization of TiO₂-carbon filter materials for water decontamination by adsorption-degradation processes. *Journal of Environmental Management*, 345. <https://doi.org/10.1016/j.jenvman.2023.118979>
- iv) Diniz, V., Bear, J. C., Rath, S., Crick, C. R. 2024. Porous sulfur polymers for effective aqueous-phase organic contaminant removal. *Scientific Reports*, 14. <https://doi.org/10.1038/s41598-024-57856-8>

3.1.1. Adsorption of recalcitrant contaminants of emerging concern onto activated carbon: A laboratory and pilot-scale study.

Vinicius Diniz^{1,*}, Davi Gasparini Fernandes Cunha², Susanne Rath¹

¹ Department of Analytical Chemistry, Institute of Chemistry, University of Campinas, Rua Josué de Castro, Cidade Universitária, Campinas, SP, 13083-970, Brazil

²São Carlos School of Engineering, Department of Hydraulics and Sanitation, University of São Paulo, Avenida Trabalhador São-Carlense, Centro, São Carlos, SP, 13566-590, Brazil

*Author for correspondence: viniciusdiniz994@gmail.com

Abstract

According to the World Health Organization (WHO), the definition of water quality indicators, including contaminants of emerging concern (CECs), associated with the development of multi-barrier approaches for wastewater treatment, are crucial steps towards direct potable reuse of water. The aims of this study were 1) quantifying twelve CECs (including pharmaceutical, stimulant, and artificial sweetener compounds) in both untreated and treated wastewater samples in a Brazilian wastewater treatment plant (WWTP) using bidimensional liquid chromatography coupled with tandem mass spectrometry, allowing the selection of five marker (*i.e.*, priority) CECs; 2) evaluating the adsorption potential of such selected CECs [caffeine, hydrochlorothiazide, saccharin, sucralose (SUC), and sulfamethoxazole (SMX)] onto coconut-shell granular activated carbon (GAC); and 3) investigating the removal of the same CECs by a multi-barrier system (pilot-scale, 350 L h⁻¹) treating the effluent of the WWTP and composed of reverse osmosis (RO), photoperoxidation (UV/H₂O₂), and filtration with GAC. Such technologies were tested separately and in binary or ternary combinations. Eleven and eight CECs were detected and quantified on the untreated and treated wastewater samples of the Brazilian WWTP, respectively. For the treated wastewater, the concentrations ranged from 499 ng L⁻¹ (SMX) to 87,831 ng L⁻¹ (SUC). The adsorption onto AC data fitted the Sips isotherm model, indicating monolayer chemisorption, which was also suggested by the mean adsorption energy values (>16 kJ mol⁻¹). SMX and SUC were the most and the least adsorbed CECs (4.33 and 1.21 mg g⁻¹, respectively). Concerning the pilot-scale treatment plant, the ternary combination (RO+UV/H₂O₂+GAC) removed >99% of the five marker CECs and promoted reductions on water color, turbidity, as well as on nitrogen and phosphorus concentrations. Further studies on water reuse could prioritize the selected marker CECs as quality indicators. While the removal of marker CECs is one of the WHO performance requirements, the RO+UV/H₂O₂+GAC system showed promising results as a first approach to direct potable reuse of water.

Keywords: Advanced wastewater treatment; Granular activated carbon; Emerging contaminants; Pilot-scale; Water reuse.

Abbreviations: α , initial adsorption rate; β , desorption constant; ABZ, Albendazole; AC, Activated Carbon; ACE, Acetaminophen; ACF, Acesulfame; CEC, Contaminant of Emerging Concern; CAF, caffeine; CMZ, Carbamazepine; DCF, Diclofenac; DMF, Dimethylformamide; DPR, Direct Potable Reuse; E, mean adsorption energy; ESI, Electrospray Ionization Source; GAC, Granular Activated Carbon; HTZ, Hydrochlorothiazide; K_{fd} , Film diffusion constant; K_i , diffusion rate; LC-UHPLC-MS/MS, Bidimensional Liquid chromatography coupled to tandem Mass Spectrometry; LOQ, Limit of Quantification; MBR, Membrane Bioreactor; PFO, Pseudo-First Order; PRP, Propranolol; PSO, Pseudo-Second Order; q_{exp} , maximum adsorption capacity; RBZ, Ricobendazole; RO, Reverse Osmosis; SAC, Saccharin; SSA_{BET} , Specific Surface Area; SSE, Sum of Squared Error; SUC, Sucralose; UV, ultraviolet; UV/H₂O₂, photoperoxidation; WHO, World Health Organization; WWTP, Wastewater Treatment Plant.

1. Introduction

Access to water has been absolutely vital for the development of human society over the centuries (Hosseiny *et al.* 2021). While anthropogenic activities and climate change have been altering rainfall patterns and inducing widespread aridification worldwide (Bonfils *et al.* 2020), strategies to alleviate water demands and enhance water security are urgently necessary. The practice of water reuse is fundamental for more efficient water resources management and in response to water scarcity conditions and intense conflicts among different water users (Hespanhol, 2008). Liu *et al.* (2020) identified municipal wastewater systems as being among the most reliable potential sources of water, even for drinking purposes, due to the advances in wastewater treatment technologies.

The World Health Organization (WHO) describes three types of potable water reuse. The first, known as unplanned potable reuse, is the practice of discharging treated or untreated wastewater into rivers and the subsequent unplanned use of the same water body as a drinking water source by downstream communities. The second, indirect potable reuse, involves mixing treated wastewater under controlled conditions with environmental buffers (such as rivers, lakes, reservoirs, and aquifers) that can be used as drinking water sources. Direct potable reuse (DPR) is the direct introduction of treated wastewater into a drinking water supply system without prior discharge to an environmental buffer (WHO 2017). However, due to the complex composition of municipal wastewaters, including recalcitrant compounds and diverse microbial communities, DPR can be challenging and expensive (WHO 2017). There have been growing efforts to develop safe, robust, and cost-effective processes for DPR in recent years (Liu *et al.* 2020). The Guidance for Producing Safe Drinking Water emphasizes that the DPR requires a performance with 4Rs (reliability, redundancy, robustness, and resilience) (WHO 2017). To meet these 4Rs, the WHO reports the importance of the definition of quality indicators, including contaminants of emerging concern (CECs), and the development of multi-barrier treatment approaches (WHO, 2017).

Multi-barrier treatment processes consisting of oxidation or advanced oxidation in combination with separation processes have been used successfully (WHO 2017). For the effective removal of CECs, membranes with tighter pore size distribution (i.e., nanofiltration or reverse osmosis, RO), adsorbent materials such as activated carbon (AC) (Hoslett *et al.* 2018) or advanced oxidative processes are usually necessary to reduce risks of contamination of treated water. For example, the combination of RO and AC can provide a cost-effective and efficient process, especially in wastewater treatment plants (WWTPs) with limited area availability (Hoslett *et al.* 2018).

Adsorption of recalcitrant contaminants of emerging concern onto activated carbon: a laboratory and pilot-scale study

Among the main processes used in treatment plants aiming at DPR of water (WHO 2017), adsorption with AC obtained from different raw materials can result in contrasting adsorption capacities (Diniz *et al.* 2022; Francoeur *et al.* 2021; Khellouf *et al.* 2021). Therefore, since the demand for AC in such plants is growing, it is necessary to evaluate commercially available ACs to further understand adsorption mechanisms and adsorption capacities of these materials (Tran *et al.* 2018; Tran *et al.* 2017). Coconut-shell-based ACs are widely available (production > 300,000 tons per year) (Mourao *et al.* 2011). These adsorbents have been widely applied in adsorption processes since they have a dense structure, low ash content, and high strength (Arena *et al.* 2016; Deng *et al.* 2021; Gonzalez-Garcia 2018; Mourao *et al.* 2011).

Besides selecting appropriate treatment technologies, considering marker CECs is relevant for studies on DPR of water because such compounds can be used to improve the operation control, speed up decision-making, and monitor treatment facilities. CECs are frequently detected in concentrations ranging from ng L⁻¹ to µg L⁻¹ in Brazilian sewage and surface waters (**Table 1**) since conventional WWTPs usually remove them incompletely due to their low biodegradation, photolysis, and sorption onto sludge (Alves *et al.* 2021; Petrovic *et al.* 2003; Pivetta *et al.* 2020). Non-target organisms can be affected by the toxicity of the CECs, such as albendazole (ABZ) and its metabolites (Belew *et al.* 2021), caffeine (CAF) (Diniz *et al.* 2021), and carbamazepine (CMZ) (Diniz *et al.* 2020). Some CECs can be oxidized and produce even more toxic by-products, such as acesulfame (ACF) (Yin *et al.* 2017), hydrochlorothiazide (HTZ) (Mansor & Tay, 2020), and sucralose (SUC) (Calza *et al.* 2013). Antimicrobials, such as sulfamethoxazole (SMX), can induce antimicrobial resistance genes (Zainab *et al.* 2020). Moreover, mixtures of CECs may lead to still largely unknown effects on humans and aquatic biota (Naidu *et al.* 2016; Pereira *et al.* 2015). While international water quality guidelines are available for some CECs (**Table 1**) (NHMRC, 2008; Parida *et al.* 2021), most CECs frequently reported in aquatic ecosystems are not regulated (Seibert *et al.* 2020). The Brazilian legislation still has no threshold limits or guidelines for most CECs on water matrices (Chaves *et al.* 2021).

Table 1: Occurrence of contaminants of emerging concern (CECs) on water matrixes reported by different studies in Brazil and international water quality guidelines for such CECs when available. Depending on the study, either ranges (minimum-maximum) or average concentrations are reported (please see full references for further details).

CECs	Water matrix			Guideline
	Raw sewage	Treated sewage	Surface water	
Acesulfame (ACF)	18 – 115 $\mu\text{g L}^{-1,\text{a}}$	ND – 45 $\mu\text{g L}^{-1,\text{a}}$	ND – 16.3 $\mu\text{g L}^{-1,\text{a}}$	
Acetaminophen (ACE)			ND – 29.1 $\text{ng L}^{-1,\text{b}}$	
			ND – 1,716 $\text{ng L}^{-1,\text{c}}$	175 $\mu\text{g L}^{-1}$
			ND – 0.13 $\mu\text{g L}^{-1,\text{d}}$	
Albendazole (ABZ)	464 – 3,810 $\text{ng L}^{-1,\text{e}}$	129 $\text{ng L}^{-1,\text{e}}$		
Carbamazepine (CMZ)	240 – 3,000 $\text{ng L}^{-1,\text{f}}$	244 – 3,000 $\text{ng L}^{-1,\text{f}}$	ND – 83 $\text{ng L}^{-1,\text{c}}$	
			ND – 3,350 $\text{ng L}^{-1,\text{f}}$	100 $\mu\text{g L}^{-1}$
			ND – 215.4 $\text{ng L}^{-1,\text{g}}$	2 $\mu\text{g L}^{-1,\text{r}}$
Caffeine (CAF)	32.189 $\mu\text{g L}^{-1,\text{i}}$	0.341 $\mu\text{g L}^{-1,\text{i}}$	11 – 26 $\text{ng L}^{-1,\text{h}}$	
			84,4 – 511.3 $\text{ng L}^{-1,\text{b}}$	0.35 $\mu\text{g L}^{-1}$
			ND – 11,642 $\text{ng L}^{-1,\text{c}}$	87 $\mu\text{g L}^{-1}$
Diclofenac (DCF)	0.8 $\mu\text{g L}^{-1,\text{j}}$	0.2 $\mu\text{g L}^{-1,\text{j}}$	ND – 129,585 $\text{ng L}^{-1,\text{g}}$	
			280 – 1,763 $\text{ng L}^{-1,\text{h}}$	
			ND – 19.4 $\text{ng L}^{-1,\text{b}}$	
Hydrochlorothiazide (HTZ)			ND – 463 $\text{ng L}^{-1,\text{c}}$	1.8 $\mu\text{g L}^{-1}$
Propranolol (PRP)			ND – 385.6 $\text{ng L}^{-1,\text{g}}$	
			32 – 79 $\text{ng L}^{-1,\text{h}}$	
Proprietary (PRP)			ND – 77.3 $\text{ng L}^{-1,\text{g}}$	40 $\mu\text{g L}^{-1}$
Ricobendazole (RBZ)	165 – 3,894 $\text{ng L}^{-1,\text{e}}$	144 $\text{ng L}^{-1,\text{e}}$		
Saccharin (SAC)	21 – 65 $\mu\text{g L}^{-1,\text{a}}$	ND – 63 $\mu\text{g L}^{-1,\text{a}}$	ND – 7 $\mu\text{g L}^{-1,\text{a}}$	
Sucralose (SUC)	11 – 42 $\mu\text{g L}^{-1,\text{a}}$	ND – 54 $\mu\text{g L}^{-1,\text{a}}$	ND – 19.5 $\mu\text{g L}^{-1,\text{a}}$	
Sulfamethoxazole (SMX)	0.980 $\mu\text{g L}^{-1,\text{i}}$	0.301 $\mu\text{g L}^{-1,\text{i}}$	ND – 120 $\text{ng L}^{-1,\text{c}}$	
			ND – 604 $\mu\text{g L}^{-1,\text{k}}$	35 $\mu\text{g L}^{-1}$
			ND – 1.8 $\mu\text{g L}^{-1,\text{l}}$	

^aAlves *et al.* (2021); ^bPereira *et al.* (2016); ^cChaves *et al.* (2020); ^dPomepi *et al.* (2021); ^ePorto *et al.* (2019); ^fPivetta *et al.* (2020); ^gCampanha *et al.* (2015); ^hQuadra *et al.* (2021); ⁱBisognin *et al.* (2019); ^jStumpf *et al.* (1999); ^kJank *et al.* (2014); ^lBoger *et al.* (2021). ^mNHMRC (2008); ⁿParida *et al.* (2021). ND – Not detected.

The objectives of this study were: 1) quantifying 12 CECs [ABZ, acetaminophen (ACE), ACF, CAF, CMZ, diclofenac (DCF), HTZ, propranolol (PRP), ricobendazole (RBZ), saccharin (SAC), SMX, and SUC] in untreated and treated wastewater samples in a Brazilian WWTP using a validated analytical method comprising bidimensional liquid chromatography coupled to tandem mass spectrometry (LC-UHPLC-MS/MS), allowing the prioritization of five marker CECs with different physicochemical properties for further studies; 2) evaluating the adsorption potential of such selected CECs (and likely adsorption mechanisms) using a commercially available AC at the

Adsorption of recalcitrant contaminants of emerging concern onto activated carbon: a laboratory and pilot-scale study

laboratory scale; 3) investigating the removal of the same CECs by a multi-barrier system (pilot-scale, 350 L h⁻¹) treating the effluent of the WWTP. The following technologies were tested alone and in binary or ternary combinations: filtration on fixed-bed column of granular activated carbon (GAC) - loaded with the same AC used in the laboratory-scale experiments; photoperoxidation (UV/H₂O₂); and RO. The initial hypothesis was that the combination of the processes would provide effective removal of the five marker CECs, in addition to improving other water quality parameters.

2. Materials and methods

2.1. Chemicals and reagents

Standard stock solutions of each CEC (ACE, ACF, CAF, CMZ, DCF, HTZ, PRP, SAC, SMX, and SUC) (1,000 µg mL⁻¹) were prepared in methanol, except for ABZ and RBZ, which were prepared in dimethylformamide (DMF). All the stock solutions were kept at 4 °C for no longer than six months. Working standard solutions were prepared daily by diluting the stock solutions in ultrapure water obtained from a Milli-Q purification system (Millipore, USA).

Detailed information concerning the chemicals and reagents, as well as the physicochemical parameters of the CECs (Table S1), are provided in the Supplementary Material.

2.2. Apparatus

The analytical determination of the studied CECs was performed using an LC-UHPLC-MS/MS system (Waters, USA) equipped with a fast-switching electrospray ionization source (ESI) and a triple-quadrupole mass detector (Xevo TQD spray, Waters) [see Tetzner *et al.* (2016) for a detailed description of the system].

An XBridge C8 Direct Connect HP column (2.1 × 30 mm, 10 µm; Waters, USA) was used for the LC dimension and an Acquity UPLC[®] CSH C18 column (130 Å, 1.7 µm, 2.1 × 100 mm; Waters, USA) for the UHPLC dimension. MassLynx v. 4.1 software was used for data acquisition and control of the equipment and the TargetLynx software was necessary for data treatment.

The procedure for optimizing the analytical method can be found elsewhere (Porto *et al.*, 2019; Tetzner *et al.*, 2016). Further details of the LC-UHPLC-MS/MS method and the method validation parameters are provided in the Supplementary Material (Tables S2 and S3). The chromatograms are shown in Figure S1.

2.3. WWTP monitoring

Untreated and treated wastewater samples of the WWTP under evaluation (São Paulo State, Southeast Brazil) were collected monthly from September to November of 2021. The WWTP system operated with a membrane bioreactor (MBR), which consists of preliminary treatment, activated sludge, anaerobic chamber, anoxic chamber, aerobic chamber, and ultrafiltration membrane. The WWTP received the sewage of around 182,000 inhabitants, with an average flow of $1,031 \pm 69 \text{ L h}^{-1}$ (Alves *et al.* 2021; Pivetta *et al.* 2020). The collected samples were transferred to sterile 50 mL Falcon tubes and transported (under refrigeration) to the laboratory. Immediately upon arrival, internal standards were added to the samples, followed by filtration through $0.22 \mu\text{m}$ PVDF membranes and storage at 4°C until analysis within a maximum of 48 h after sampling. The analyses were carried out by directly injecting the filtered samples into the LC-UHPLC-MS/MS system.

2.4. Data analysis

Since the removal efficiency data were not normally distributed (Shapiro-Wilk test, $p < 0.05$), the Mann-Whitney U test was used to indicate statistically significant differences between untreated versus treated samples. These analyses were performed using Statistica[®] software. Kinetic and adsorption models were tested using Origin[®] software. The coefficient of determination (R^2) and the sum of squared error (SSE) (Table S4) were used to evaluate the accuracy of the adsorption model fits.

2.5. Laboratory-scale adsorption experiments with AC

2.5.1. AC characterization

The adsorption experiments were carried out with a commercial granular activated carbon (Charbon500, 12×24 mesh; Carbonado, Brazil) produced from coconut shell. In addition to the characterization provided by the manufacturer (ash content: 9.6%; bulk density: 0.54 g cm^{-3} ; iodine number: $854 \text{ mg I}_2 \text{ g}^{-1}$; moisture: 6% w/w), further physicochemical characterization of the AC was performed (details are provided in the Supplementary Material).

2.5.2. Adsorption kinetics and adsorption isotherms

Batch adsorption experiments were carried out according to the recommendations of the American Society for Testing and Materials, protocol D3860/2020 (ASTM, 2020), and the Japanese Industrial Standard (JIS, 2014), using 400 mL of water containing $500 \mu\text{g L}^{-1}$ (100 times higher than

Adsorption of recalcitrant contaminants of emerging concern onto activated carbon: a laboratory and pilot-scale study

the first concentration level of the analytical curve) of the previously selected CECs (in a single mixture), in 500 mL Duran® flasks. The standards had to be prepared in methanol or DMF due to their low solubility in water, with the concentrations of the solvents in the test vessels always lower than 0.5% (v/v) (Fukuhara et al., 2006). The mixtures were shaken at 150 rpm (Hoppen et al., 2019) in an agitation chamber (Marconi, Brazil) at a controlled temperature (25 °C) and protected from light.

For the kinetics study, an AC mass of 30 mg was suspended in water. The pH of the medium was measured at the beginning and end of the experiments. Aliquots (2 mL) were removed at different times (10, 20, 30, 60, 120, 150, 180, 210, 240, 270, and 330 min) and filtered (0.22 µm filter) for the quantification of the residual concentrations of the CECs through LC-UHPLC-MS/MS, as described in section 2.2. All the analyses were performed in duplicates. The stabilities of the CECs (at 500 µg L⁻¹) in the water were assessed using the same procedure but with no addition of AC. The adsorption isotherm studies were carried out using different amounts of AC (20, 30, 40, 60, 90, 120, 140, and 160 mg) suspended in 400 mL of water containing the CECs at a concentration of 500 µg L⁻¹ and throughout the previously determined apparent equilibrium time (270 min). In addition, similar assays were performed using samples of the WWTP effluent (i.e., treated) (Table S5) and different masses of AC (20, 40, 60, 90, 120, 150, 200, and 250 mg).

The kinetics data were fitted using the pseudo-first order (PFO), pseudo-second order (PSO), Elovich, intraparticle diffusion, and liquid film diffusion kinetic models (Table S6). The isotherm data were fitted using the Langmuir, Freundlich, Sips, Redlich-Peterson, and Dubinin-Radushkevich isotherm models (Table S6).

2.5.3. Influence of pH

The influence of pH on the adsorption of the CECs onto the AC was studied in the pH range of 2 to 12, maintaining the ionic strength constant at 0.5 mol L⁻¹ using Britton-Robinson buffer. The concentration of the CECs and the mass of AC were 500 µg L⁻¹ and 30 mg, respectively. The experiments were prepared similarly to the adsorption kinetics assays, with the flasks being shaken during the previously determined apparent equilibrium time (270 min), followed by quantification using LC-UHPLC-MS/MS. As described for the kinetics assays, the stabilities of the CECs at each pH were also evaluated.

2.6. Pilot-scale experiments

2.6.1. Description of the pilot-scale treatment plant

The pilot-scale plant considered in the present study was designed by Hespanhol *et al.* (2019) and is composed of a multichannel system allowing different treatment configurations (GAC, UV/H₂O₂, RO, and their combinations), with a continuous flow of 350 L h⁻¹ (**Figure 1**). The plant was built adjacent to the WWTP and continuously received the effluent of the MBR. A detailed description of the pilot-scale plant operation is provided in the Supplementary Material.

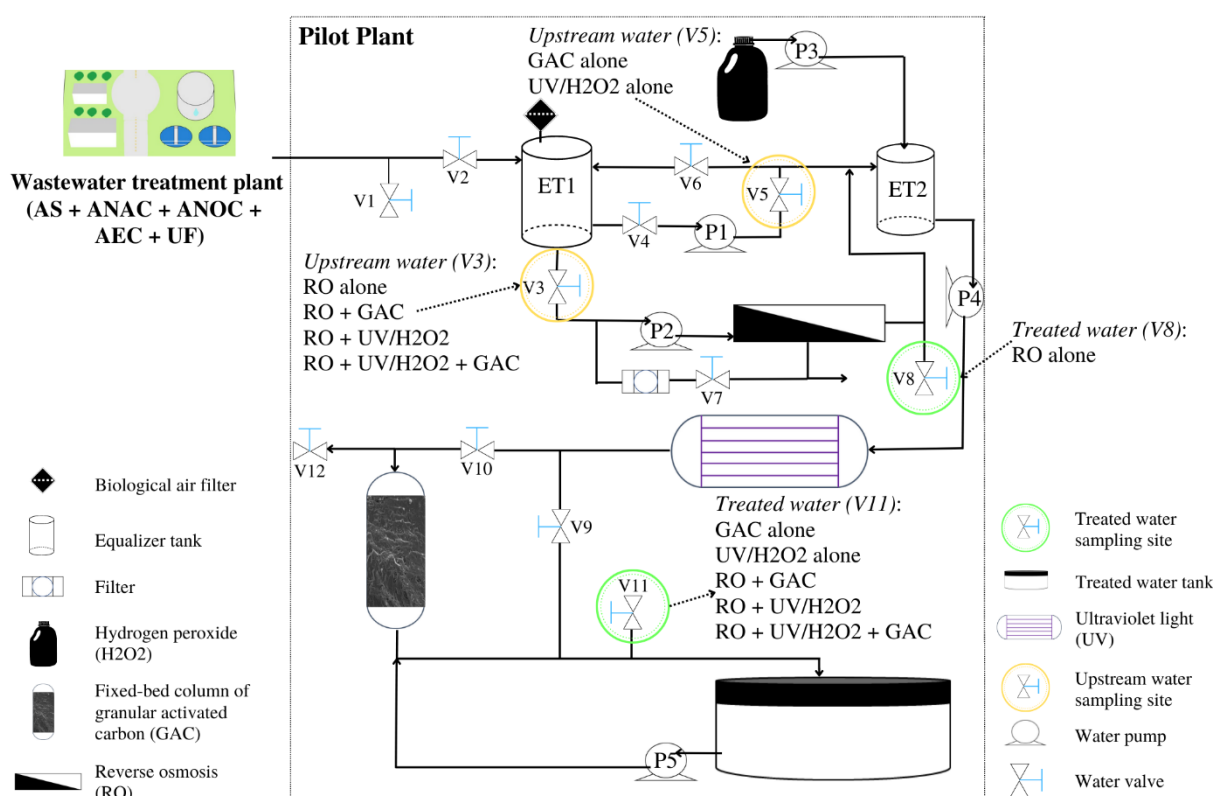


Figure 1: Scheme of the pilot-scale treatment plant. GAC, fixed-bed column of granular activated carbon, AS, activated sludge, ANAC, anaerobic chamber, ANOC, anoxic chamber, AEC, aerobic chamber, UV/H₂O₂, photoperoxidation, RO, reverse osmosis, UF, ultrafiltration, P1, P2, P3, P4, and P5 are water pumps, V1, V2, V3, V4, V5, V6, V7, V8, V9, V10, V11, and V12 are water valves, and ET1 and ET2 are equalizer tanks.

The ultraviolet (UV) reactor (17.5 L) contained 12 UV-C lamps (HNS 55W G13 HO, Osram), providing a UV-C dose of 1,590 mJ cm⁻², with a contact time of 180 s. H₂O₂, at a dose of 6 mg L⁻¹ (based on the value used in the California reuse plant (Bernados 2020)), was pumped into an equalizer tank (80 L) located immediately upstream the UV reactor. The dimensions of the GAC column were 2.2 m (0.5 m of freeboard) × 0.2 m (cross-section of 0.0314 m²) with an empty bed contact time of 10 min (hydraulic retention time of 6.4 min), and the system was operated using a *Adsorption of recalcitrant contaminants of emerging concern onto activated carbon: a laboratory and pilot-scale study*

hydraulic loading rate of 10 m h⁻¹. The RO membrane (LE-4040, DOW FILMTEC) had 34 mil of feed spacer thickness and 7.2 m² of active area.

2.6.2. Pilot-scale plant monitoring

The pilot-scale study was carried out by evaluating each process alone (GAC, UV/ H₂O₂, or RO), as well as using binary or ternary combinations: RO+UV/H₂O₂, RO+GAC, and RO+UV/H₂O₂+GAC. The WWTP effluent upstream the pilot-scale plant, as well as the effluents produced by the different tests at the plant, were sampled once a month, for three months, with no fortification of the effluent. The samples were analyzed as previously described (section 2.2).

Determinations of water color, pH, turbidity, conductivity, biological oxygen demand, chemical oxygen demand, total phosphorus, ammoniacal nitrogen, total Kjeldahl nitrogen, nitrate, and nitrite were also carried out for the WWTP effluent and the ternary process (RO+UV/H₂O₂+GAC) influent, according to the American Public Health Association (APHA 2017). In addition, the effluent of the ternary process (i.e., treated) was screened at two campaigns considering all the parameters of the Brazilian legislation for drinking purposes (GM/MS N° 888, Brazil 2021).

3. Results and discussion

3.1. WWTP monitoring

It is well known that urban and hospital sewage discharges are the primary sources of CECs in surface waters (Alves *et al.* 2021; Pivetta *et al.* 2020). However, studies concerning the presence of CECs in WWTP effluents in Brazil are still scarce (Pivetta *et al.* 2020). In the present study, 12 CECs (Table 1) were monitored in untreated and treated wastewater samples in a Brazilian WWTP, focusing on the possibility of later water reuse. All the CECs were detected in the untreated sewage samples, with the exception of ricobendazole, a metabolite of albendazole (**Figure 2-A**), while eight CECs were observed in treated sewage samples. The MBR technology, which combines a membrane process (ultrafiltration or nanofiltration) and a biological process, is currently one of the most promising developments in wastewater treatment (Judd 2008; Petrovic *et al.* 2003). Sengupta *et al.* (2022) stated that MBR systems can remove CECs by biodegradation (oxidoreductase enzymes), retention (adsorption or size exclusion) on the membrane, and absorption onto the sludge. In the present study, it was not expected that CECs would be removed by size exclusion since ultrafiltration membranes have a low capacity to remove these contaminants due to the high pore size distribution

Adsorption of recalcitrant contaminants of emerging concern onto activated carbon: a laboratory and pilot-scale study

(70 – 1,000 Å) (Kim *et al.* 2019). The MBR process in the studied WWTP was able to reduce the concentrations of ACE, ACF, and DCF to below the limits of quantitation (LOQ) of the analytical method (Table S3). These three compounds are rapidly biodegraded (Castronovo *et al.* 2017; Hasan *et al.* 2021) or absorbed onto sludge due to their Log K_{ow} values (Table S1) (Dolar *et al.* 2012).

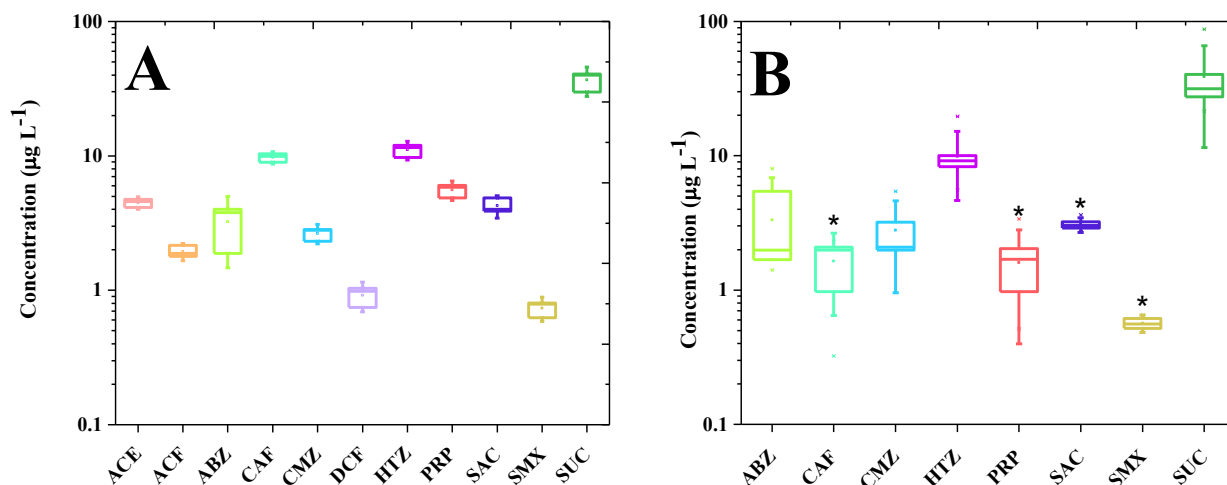


Figure 2: Concentration of the studied contaminants of emerging concern in the untreated (A) and treated (B) samples in the Brazilian wastewater treatment plant. ACE, acetaminophen, ACF, accessulfame, ABZ, albendazole, CAF, caffeine, CMZ, carbamazepine, DCF, diclofenac, HTZ, hydrochlorothiazide, PRP, propranolol, SAC, saccharin, SMX, sulfamethoxazole, and SUC, sucralose. Average values are given by the squares, whereas bottom, center, and top lines of boxplots show the 25th, 50th, and 75th percentiles, respectively. Bottom and top whiskers represent 1.5 time the calculated standard deviation. * indicates significant differences ($p < 0.05$) between untreated and treated samples.

Although residual concentrations were observed, CAF (83.1%), PRP (71.3%), SAC (27.7%), and SMX (48.9%) were effectively removed ($p < 0.05$) by the WWTP (**Figure 2-B**). Kim *et al.* (2014) reported 90%, 16%, and 66% removal percentages of CAF, PRP, and SMX in a Canadian WWTP operating with MBR. SAC was completely removed in the MBR system studied by Alves *et al.* (2021). All these CECs can be biodegraded during the biological treatment (Larcher & Yargeau, 2012; Lin *et al.* 2010; Pang *et al.* 2020); however, it is expected that absorption onto the sludge governs the PRP removal due to its Log K_{ow} value (Table S1) (Lin *et al.* 2010). On the other hand, in the present study, the concentrations of ABZ, CMZ, HTZ, and SUC in the treated sewage were not statistically different from those in the untreated. Particularly HTZ (5,554 to 19,658 ng L⁻¹) and SUC (23,810 to 87,831 ng L⁻¹) were found at the highest concentrations in the treated effluent. These CECs are often inefficiently removed in biological WWTPs or by absorption (Alves *et al.* 2021; Kim *et al.* 2014), probably due to their physicochemical properties, especially the presence of chlorine atoms in the structures, which can hinder biodegradation (Brorström-Lundén *et al.* 2008) and Log K_{ow} (Table

Adsorption of recalcitrant contaminants of emerging concern onto activated carbon: a laboratory and pilot-scale study

S1) (Dolar *et al.* 2012). Likewise, the MBR system is usually not efficient for CMZ removal (Pivetta *et al.* 2020). The initial electrophilic attack by oxygenases from aerobic bacteria can result in an electron deficiency in the presence of electron-withdrawing functional groups, turning CMZ less susceptible to oxidative catabolism (Hai *et al.* 2011). Besides, the hydroxylated metabolite of CMZ can be converted back to CMZ by the action of microorganisms present in WWTP, leading to low removal efficiencies or even CMZ production (Miao *et al.* 2005). Porto *et al.* (2019) observed the presence of ABZ in the effluent of a Brazilian WWTP, emphasizing the importance of additional treatment processes for its removal.

For the assays on the adsorption onto AC, five of the eight CECs detected in the WWTP effluent were selected as marker compounds. These compounds can also be considered in future studies as quality indicators of the overall treatment process, facilitating monitoring strategies. CAF was chosen due to its widespread occurrence in surface waters and extensive use as an indicator of anthropogenic disturbances in water bodies. HTZ and SUC were chosen due to the high concentrations in the WWTP effluent. In addition, both SUC and SAC were selected due to the lack of studies on the adsorption of artificial sweeteners onto AC. Finally, although SMX was detected at low concentrations in the WWTP effluent (499-653 ng L⁻¹), this compound was also selected due to the risk of development of antimicrobial resistance genes in bacteria (Larcher & Yargeau, 2012). Moreover, these five selected CECs present different physicochemical properties, enabling the production of valuable information about their adsorption mechanisms.

3.2. Laboratory-scale assays

3.2.1. AC characterization

The AC presented an average pore diameter of 2.6 nm and a total pore volume of 0.36 cm³ g⁻¹, with 0.27 cm³ g⁻¹ of micropores (≤ 2 nm) and 0.08 cm³ g⁻¹ of mesopores (see Figure S2-A). The N₂ adsorption isotherm for the AC (Specific surface area, SSA_{BET}, of 536.5 m² g⁻¹) (Figure S2-B) was type IV with H4 hysteresis, reflecting the existence of cylindrical pore channels (Rouquerol *et al.* 2014), which was confirmed by scanning electron microscopy images of the morphological structure of the AC (**Figures 3-A and 3-B**). In addition, thermogravimetric analysis corroborated the characterization data provided by the manufacturer. A mass loss of up to 6% occurred in the first minutes of heating (up to 105 °C), followed by high thermal stability up to 500 °C (Figure S3). In the second heating step, from 500 to 900 °C, a 77% mass loss was probably due to the decomposition of the carbonaceous matrix and part of the carbonaceous skeleton. These physical parameters are

Adsorption of recalcitrant contaminants of emerging concern onto activated carbon: a laboratory and pilot-scale study

relevant since an enhanced adsorption process requires the adsorbate to diffuse into the pores of the AC (Tran *et al.* 2017). In addition, although the presence of mesopores leads to a lower SSA_{BET} , it seems to enhance the adsorption in cases with combinations of different CECs (i.e., multi-adsorbate solutions) (Diniz *et al.* 2022), allowing adsorbates to access the internal pores of the AC.

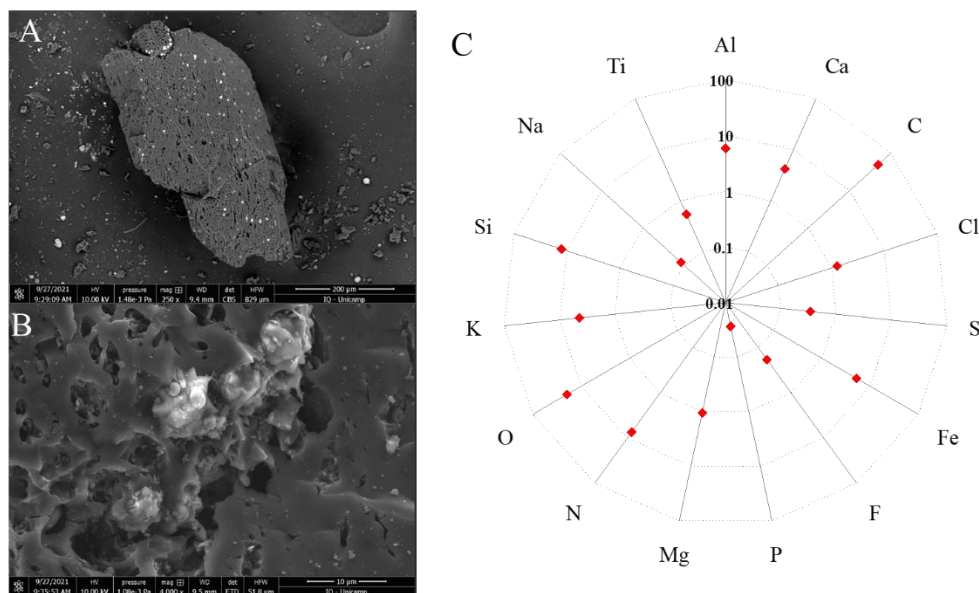


Figure 3: Photomicrographs of activated carbon before the adsorption with (A) 250 and (B) 4000 times of magnification. (C) Energy-dispersive X-ray spectroscopy results of the activated carbon composition.

The AC used in this study was mainly composed of carbon (48.9%), oxygen (19.8%), and silicon (12.7%), but the energy-dispersive X-ray spectroscopy analysis also showed the presence of other elements (Figure 3-C). In the Fourier-transform infrared spectroscopy spectrum (Figure S4-A), a band at approximately 3440 cm^{-1} could be attributed to -OH stretching vibration of carboxylic and phenol groups, and was not related to adsorbed water (Sajjadi *et al.* 2019; Streit *et al.* 2021), since the AC was dried before the analysis. Furthermore, the Boehm titration experiments corroborated the presence of carboxylic and phenol groups. Low-intensity bands at 2920 , 2850 , and 2360 cm^{-1} could be ascribed to C-H stretching, C=C vibration, and CO_2 (Samantara *et al.* 2019; Teng 2015). A band at 1632 cm^{-1} could be attributed to the C=C bonds of aromatic rings and C=O of carbonyls from many functional groups (Lin *et al.* 2012). The Boehm titration experiments also indicated the presence of lactone groups at a concentration of 0.5 mEq g^{-1} . Finally, a band at 1110 cm^{-1} could be explained by the stretching of C-O of phenol and alcohols, as well as the Si-O bond of silicates (Streit *et al.* 2021). The Boehm titration results showed the presence of basic groups on the AC surface, in agreement with the determined pH_{PZC} of 9.2 (Figure S4-B).

Adsorption of recalcitrant contaminants of emerging concern onto activated carbon: a laboratory and pilot-scale study

The Raman spectrum (Figure S4-C) confirmed the graphitic structure and disordered nature of the carbonaceous material (Guan *et al.* 2019; Keppetipola *et al.* 2021). Both peaks observed in the Raman spectrum are commonly found for AC (Guan *et al.* 2019). They are associated with stretching modes of more disordered carbon atoms in planar terminations of the graphite structure (D band at 1330 cm^{-1}) and the stretching mode of the sp^2 hybridized carbon atoms in the rings and chains (G band at 1595 cm^{-1}). In addition, the ratio of the D and G band areas, which provides an indication of the degree of disorder of the AC (Guan *et al.* 2019), with a value of 2.6, reflected a highly amorphous structure and the presence of more active sites available for the adsorption process.

The amorphous nature of the AC was also indicated by the X-ray diffraction spectrum (Figure S4-D), which presented a broad diffraction peak at 24.2° and a low-intensity peak at 44.2° . The first peak could be attributed to the distribution of continuous parallel graphite sheets, while the second was related to the crystallization of the AC by sp^2 hybridization (Guan *et al.* 2019). The microcrystalline structure of the AC used in the present study (Table S7) was in agreement with data reported for other AC materials (Guan *et al.* 2019; Keppetipola *et al.* 2021).

3.2.2. Adsorption kinetics

The adsorption of the selected marker CECs (CAF, HTZ, SAC, SMX, and SUC) onto AC was first performed in water in order to estimate the apparent equilibrium time, the adsorption kinetics, and the adsorption potential. All the compounds were stable in the medium during the time considered for the adsorption process (Figure S5-A), with an apparent equilibrium time of around 270 min in all cases (**Figure 4**). The adsorption capacities (Figure 4) followed the order $\text{SMX} > \text{CAF} > \text{SAC} > \text{HTZ} > \text{SUC}$, with SMX presenting 3.6-fold higher adsorption capacity when compared to SUC. It is commonly reported that in the case of a multi-adsorbate solution, the adsorption is usually governed by the hydrophobicity of the molecules (Dominguez *et al.* 2011; Mansouri *et al.* 2014). However, other studies reported that adsorption involving multi-adsorbate solutions is more complex and depends on many factors (Diniz *et al.* 2022; Liu *et al.* 2015), as observed in the present study.

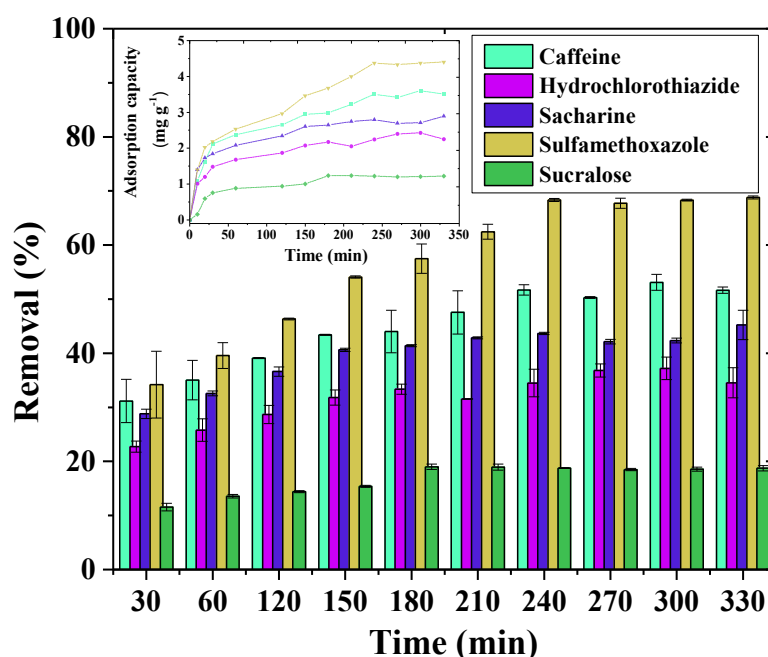


Figure 4: Removal of the marker contaminants of emerging concern selected in the present study versus time and the respective adsorption capacities onto activated carbon versus time (insert graph). (Temperature = 25 °C; Initial concentration = 500 $\mu\text{g L}^{-1}$; Agitation speed = 150 rpm; Amount of activated carbon = 30 mg; Volume of the aqueous solution = 400 mL; pH = 8.4). The whiskers indicate the calculated standard deviation.

Although understanding adsorption mechanisms requires information concerning other aspects such as pH effects, isotherms, and characterization of the AC (Tran *et al.* 2017), kinetic models can provide a first approach to evaluating the potential mechanisms involved in the adsorption process. Here, the kinetic profiles were analyzed using the PFO, PSO, Elovich, intraparticle, and film diffusion models (Figure S6). The first two models (PFO and PSO) provided similar estimations of the adsorption capacity (**Table 2**), despite not resulting in the best fitting parameters. The Elovich model showed a good fit to the adsorption data (**Table 2**), suggesting that chemisorption was the main process involved in the adsorption of the selected molecules (Nwabue & Itumoh, 2020). The values observed for the initial adsorption rate (α) and the desorption constant (β) were indicative of electrostatic interactions in the first minutes of adsorption since β were relatively similar, and α varied among the CECs (**Table 2**) (Park *et al.* 2020). However, in agreement with Park *et al.* (2020), the overall adsorption capacity of the AC for the CECs was also substantially influenced by the different chemical groups (carboxylic and phenolic, lactonic groups) observed on its surface (Figure S4-A).

Table 2: Summary of the kinetic parameters for the adsorption of the studied contaminants of emerging concern onto activated carbon.

Model	Parameter	CAF	HTZ	SAC	SMX	SUC
Experimental	Q_{exp} (mg g ⁻¹)	3.41	2.40	2.70	4.33	1.21
Pseudo-first order	q_{cal} (mg g ⁻¹)	3.24	2.17	2.63	4.05	1.17
	K_1 (min ⁻¹)	0.030	0.039	0.050	0.022	0.026
	R^2	0.936	0.930	0.930	0.899	0.946
	SSE	0.909	0.402	0.549	2.283	0.114
Pseudo-second order	q_{cal} (mg g ⁻¹)	3.67	2.38	2.84	4.67	1.35
	K_2 (g mg ⁻¹ min ⁻¹)	0.010	0.022	0.026	0.006	0.023
	R^2	0.973	0.970	0.975	0.948	0.960
	SSE	0.376	0.171	0.194	1.173	0.085
Elovich	α (mg g ⁻¹ min ⁻¹)	0.308	0.436	1.149	0.261	0.075
	β (mg g ⁻¹)	1.396	2.492	2.385	1.026	3.483
	R^2	0.988	0.987	0.994	0.976	0.949
	SSE	0.169	0.071	0.050	0.483	0.108
Intraparticle Diffusion	K_{i1} (mg g ⁻¹ min ^{-0.5})	0.322	0.220	0.442	0.450	0.137
	K_{i2} (mg g ⁻¹ min ^{-0.5})	0.140	0.077	0.112	0.203	0.049
	K_{i3} (mg g ⁻¹ min ^{-0.5})	0.020	0.028	0.035	0.013	-0.006
	C_i	0.655	0.566	0.856	0.637	0.188
	R^2	0.927	0.902	0.836	0.960	0.875
	SSE	1.037	0.582	1.285	0.902	0.262
Film diffusion	K_{fd} (min ⁻¹)	0.012	0.012	0.02	0.014	0.018
	R^2	0.968	0.907	0.979	0.934	0.948
	SSE	1.579	4.85	1.266	2.497	1.972

CAF: Caffeine; HTZ: Hydrochlorothiazide; SAC: Saccharin; SMX: Sulfamethoxazole; SUC: Sucralose; SSE: Sum of Squared Error.

It is well known that adsorption processes can be divided into three stages: (I) external

Adsorption of recalcitrant contaminants of emerging concern onto activated carbon: a laboratory and pilot-scale study

mass transport, (II) film diffusion, and (III) intraparticle diffusion, with the first often being neglected due to the vigorous shaking employed in batch studies (Wang *et al.* 2015). The film and intraparticle diffusion models can numerically describe the second and third stages, respectively. In addition, these models allow for a better understanding of the rate-controlling steps during the adsorption process (Zeng & Kan 2021). The adsorption kinetics of the CECs exhibited multi-linearities (Figure S6-D). In addition, the fit of the intraparticle diffusion model to the data did not pass through the origin, indicating that two or more steps limited the adsorption process (Wang *et al.* 2015).

The results suggested that the adsorption process was divided into multiple stages, as observed elsewhere for other contaminants (Mashile *et al.* 2018; Zeng & Kan 2021). The diffusion rate decreased over the stages ($K_{i3} < K_{i2} < K_{i1}$) (Table 2), indicating that pore diffusion affected the overall adsorption rate. Furthermore, for the selected CECs, the values of the constant (C) of the intraparticle diffusion model were of the same order of magnitude and higher than zero (Table 2). This observation is indicative that film diffusion also participates in the adsorption process since, according to Park *et al.* (2020) and Zeng & Kan (2021), a similar influence of the diffusion layer film thickness on the adsorption of CECs is expected. However, since the film diffusion constant (K_{fd}) values were lower than C values (**Table 2**), it appeared that film diffusion had a lower effect on the adsorption of the CECs onto the AC than pore diffusion.

3.2.3. Adsorption isotherms

Further understanding of the adsorbent-adsorbate interactions involved assessment using equilibrium isotherms, considering the previously established apparent equilibrium time of 270 min. Five isotherm models were tested (Langmuir, Freundlich, Redlich-Peterson, Sips, and Dubinin-Radsukevich). The shapes of the isotherms were type L2 (Giles *et al.* 1960) for both water and WWTP effluent (Figures S7 and S8), a concave shape indicating favorable adsorption (Giles *et al.* 1960) (*i.e.*, as the active sites of the AC became occupied, there was a low probability of the compound reaching an available active site).

Many studies evaluated the adsorption of CAF and SMX onto AC (Table S8) but with initial concentration up to 1,000 times higher than the present study, which may explain the lower adsorption capacities observed here (**Table 3**). Overall, the best fit to the data was obtained with the Sips model (**Table 3**), which is a three-parameter isotherm that combines the Langmuir and Freundlich models and describes the monolayer adsorption at which one adsorbate molecule can be adsorbed to $1/n$ sites (Foo & Hameed 2010; Wang & Guo 2020). The fitting parameters of all the

Adsorption of recalcitrant contaminants of emerging concern onto activated carbon: a laboratory and pilot-scale study

Table 3: Summary of the isotherm parameters for the adsorption of the studied contaminants of emerging concern onto activated carbon.

Model	Matrix	Parameter	CAF	HTZ	SAC	SMX	SUC
SIPS	Water	k_s	0.010	0.010	0.013	0.022	0.01
	WWTP effluent	(L mg ⁻¹)	0.007	0.005	0.008	0.016	0.005
	Water	q_{cal}	3.95	2.52	2.41	4.42	0.99
	WWTP effluent	(mg g ⁻¹)	2.01	1.38	1.27	3.15	0.68
	Water	n	0.64	0.62	2.94	1.25	1.15
	WWTP effluent		4.12	5.02	4.29	1.42	3.76
	Water	R^2	0.982	0.920	0.943	0.934	0.745
	WWTP effluent		0.935	0.917	0.931	0.988	0.813
	Water	SSE	0.108	0.103	0.324	1.440	0.023
	WWTP effluent		0.260	0.128	0.077	0.120	0.018
Dubinin-Radsukevich	Water	k_{DR}	0.0009	0.0008	0.0016	0.0012	0.0011
	WWTP effluent	(mol ² kJ ⁻²)	0.0026	0.0029	0.0018	0.0015	0.0014
	Water	E	23.4	24.8	17.7	20.0	20.9
	WWTP effluent	(kJ mol ⁻¹)	13.9	13.2	16.5	18.3	18.6
	Water	R^2	0.989	0.923	0.855	0.881	0.845
	WWTP effluent		0.751	0.783	0.747	0.925	0.756
	Water	SSE	0.003	0.010	0.059	0.095	0.004
	WWTP effluent		0.128	0.76	0.069	0.052	0.014

CAF: Caffeine; HTZ: Hydrochlorothiazide; SAC: Saccharin; SMX: Sulfamethoxazole; SUC: Sucralose; ; SSE: Sum of Squared Error; WWTP: Wastewater treatment plant.

models are presented in Tables S9 and S10 for water and WWTP effluent, respectively. The maximum adsorption capacities (q_{exp}) determined from the Sips model were indicative of lower q_{exp} for the contact of the AC with the WWTP effluent when compared with water. These lowest q_{exp} values could be explained by competition for the active sites of the adsorbent by other compounds present in the WWTP effluent (*e.g.*, dissolved organic matter) (Zadaka *et al.* 2009). In comparison to the assays with water, the assay with the WWTP effluent resulted in adsorption capacity decreases of 28.7% (SMX), 31.3% (SUC), 45.2% (HTZ), 47.3% (SAC), and 49.1% (CAF), despite the use of higher adsorbent amounts. Rao *et al.* (2021) observed a reduction of up to 50% in the adsorption capacity for CAF due to the matrix effects when surface water was used instead of ultrapure water. Similarly, Nguyen *et al.* (2020) investigated the effects of different water matrices (seawater, wastewater, tap water, and distilled water) on the adsorption of ACE. As expected, the highest adsorption was observed using the purest matrix (distilled water). In summary, the findings of the present research together with those from earlier studies indicate that although the adsorption is negatively affected by the effluent complexity of the matrix, it is still possible to remove different

Adsorption of recalcitrant contaminants of emerging concern onto activated carbon: a laboratory and pilot-scale study

classes of CECs through adsorption onto AC, with differences in the removal efficiencies, as expected. Likewise, due to different concentrations of the CECs expected in real effluents, the competition by active sites of the AC may vary and should be further investigated.

3.2.4. Insights into the adsorption mechanisms

In addition to fitting the adsorption data to kinetic and isotherm models, studying the influence of the pH of the medium on the adsorption provided interesting insights for elucidating the mechanisms involved in the adsorption process. The pH affects both the speciation of the chemical compounds and the surface properties of the adsorbent (Rhoden *et al.* 2021). The acid-base speciation of the target CECs in water is pH-dependent, so the distribution of the species at each pH value was calculated using the pK_a values (**Figure 5**). AC can be positively or negatively charged, depending on whether the pH is lower or higher than the pH_{PZC} (Frohlich *et al.* 2018). As previously reported (Diniz *et al.* 2022), the adsorption processes were not governed by hydrophobicity alone, despite a trend towards higher adsorption capacity as the $\log K_{ow}$ value increased (Figure S9). The deviations from linearity observed in Equations 1 (water) and 2 (WWTP effluent) could be explained by other forces acting in the adsorption process, such as electrostatic interactions.

$$q_{cal} = \text{Log}K_{ow}1.1(\pm 0.7) + 2.7(\pm 0.5) \quad R^2 = 0.413 \text{ and } SSE = 4.358 \quad (1)$$

$$q_{cal} = \text{Log}K_{ow}0.7(\pm 0.5) + 1.6(\pm 0.4) \quad R^2 = 0.412 \text{ and } SSE = 2.075 \quad (2)$$

Overall, the results suggested that electrostatic interactions and hydrogen bonds influenced the adsorption process. The presence of -OH groups on the AC surface, the good fit to the Elovich model, and the mean adsorption energy (E) higher than 16 kJ mol^{-1} were reliable indicators of hydrogen bonding (Beltrame *et al.* 2018). In addition, the good fit to the Sips isotherms indicated a monolayer chemisorption process related to the surface bonding (Wang & Guo 2020). In addition, as observed in Figure 5, under a commonly expected pH range in WWTP (*i.e.*, 5.5-8), only a slight variation in the removal of the CECs was observed. Therefore, a pH adjustment to optimize the adsorption would not be cost-effective.

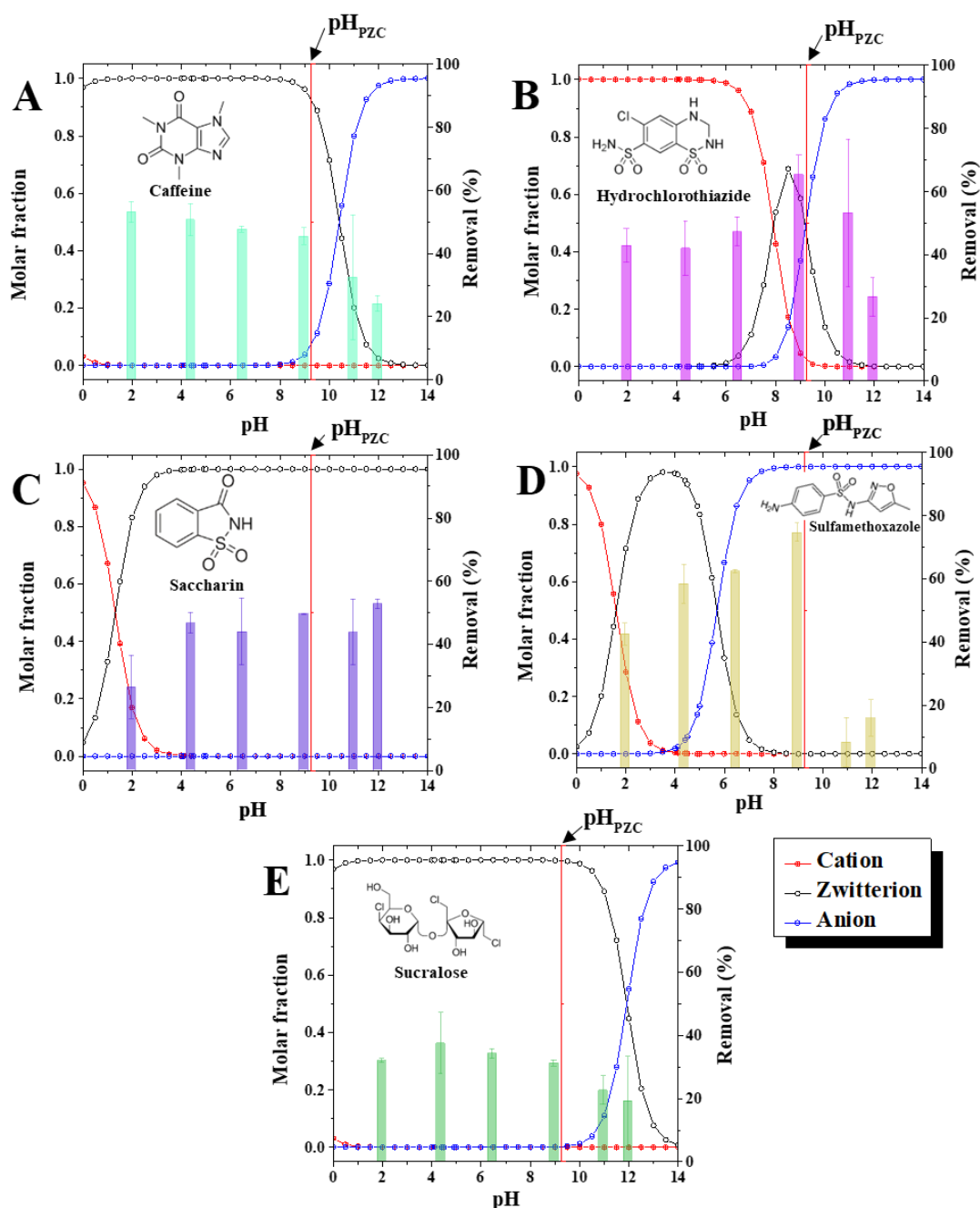


Figure 5: Effect of pH on the removal of the marker contaminants of emerging concern selected in the present study using Britton-Robinson buffer. (Temperature = 25 °C; Initial concentration = 500 $\mu\text{g L}^{-1}$; Agitation speed = 150 rpm; Amount of the activated carbon = 30 mg; Volume of solution = 400 mL; Ionic Strength = 0.5 mol L^{-1} ; contact time = 270 min). The whiskers indicate the calculated standard deviation.

CAF was more adsorbed in its neutral form ($pH < 9.0$) (**Figure 5-A**), indicating that hydrophobic interactions (C=C bonds) play an important role in the adsorption of this CEC. CAF can also interact with the carbonyl groups present on the AC by a nucleophilic addition reaction (Keerthanan *et al.* 2020). However, at $pH > pK_a$ and pH_{PZC} , CAF adsorption decreased probably due

to electrostatic repulsion forces between the anionic form of CAF and the negatively charged surface of AC. The same pattern was observed for HTZ, as it was less adsorbed when the molecule and AC had the same charge (**Figure 5-B**). The highest adsorption was observed when HTZ was predominantly in its neutral form. Rhoden *et al.* (2021) stated that HTZ could be adsorbed onto AC through π - π interactions and hydrogen bonds. The present results (**Figure 5-B**) corroborate these findings since the mean adsorption energy (E) was higher than 16 kJ mol^{-1} (Table 3), indicating hydrogen bonding. In turn, the adsorption of SMX is enhanced when the molecule is in the anionic form (Figure 5-D), probably due to electrostatic attraction forces between the SMX molecule and the positively charged surface of AC. Nonetheless, the E values of 20 kJ mol^{-1} (Table 3) indicate that neutral SMX were adsorbed onto AC via π - π interaction and hydrogen bonds. The study of Zheng *et al.* (2013) corroborates this expectation since the authors stated that SMX could form hydrogen bonds with carboxylic and phenolic groups on the surface of AC. Besides, the same authors pointed out that the strong π -acceptor characteristic of the SMX molecule can lead to π - π interactions with the AC.

To the best of our knowledge, no studies investigating the adsorption mechanisms of SAC and SUC onto AC have been published in the literature. These CECs were more adsorbed in their neutral form and less adsorbed when both the respective molecule and the AC had the same charge (**Figure 5-C** and **Figure 5-E** for SAC and SUC, respectively). The E values (**Table 3**) indicate that hydrogen bonds were related to the adsorption of SAC and SUC, with phenolic groups being the most important H-donor sites for the adsorption. A sharp decrease in the adsorption should be observed at pH of 3–4 due to the deprotonation of carboxylic groups if these functional groups instead of phenolic ones had governed the adsorption process (Yang *et al.* 2022).

3.3. Pilot-scale experiments

The pilot-scale unit continuously received treated effluent by the Brazilian WWTP and could test different advanced treatment (*i.e.*, polishing) processes, including RO, UV/H₂O₂, and GAC, and their binary or ternary combinations. As stated by WHO (2017), in addition to removing of microorganisms, heavy metals, and nutrients, a WWTP focused on DPR of water should be able to remove different classes of CECs, because their presence in sewage has been increasing in recent decades. Therefore, as a contribution for DPR in Brazil, this study evaluated the removal of five selected marker CECs (CAF, HTZ, SAC, SMX, and SUC) by different processes in the pilot-scale treatment plant.

Since the effluent was not fortified, the initial concentrations of the CECs were in the following order: SUC > HTZ > SAC > CAF > SMX (Table S11). In the first step, each process was evaluated independently. In general, the removal efficiencies of the processes followed the order: RO > GAC > UV/H₂O₂ (**Figure 6**). However, irrespective of the process, SMX was removed to below the LOQ, which could have been due to its low concentration the influent to the pilot-scale plant. SMX was the highest adsorbed CEC by the GAC (**Figure 6**), as observed in the laboratory-scale studies. SUC and HTZ were higher adsorbed than CAF (**Figure 6**), although adsorption of CAF (**Tables 2 and 3**) was higher in the laboratory-scale studies. The higher concentrations of SUC and HTZ in the effluent (Table S11) compared to CAF possibly influenced the competition for the active sites of the AC. It is known that the characteristics of the water matrix influence the removal

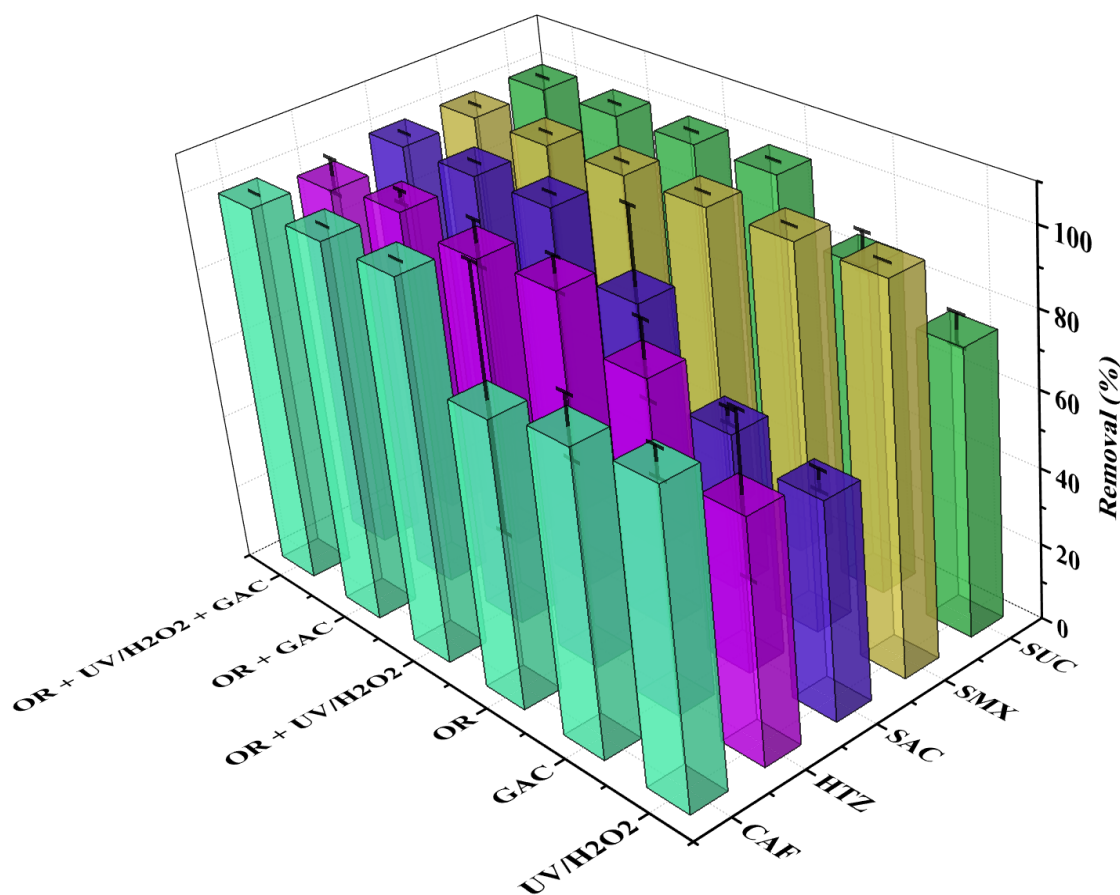


Figure 6: Removal of the marker contaminants of emerging concern selected in the present study by photoperoxidation (UV/H₂O₂), Fixed-bed column of granular activated carbon (GAC), reverse osmosis (RO), reverse osmosis + photoperoxidation (RO + UV/H₂O₂), reverse osmosis + fixed-bed column of granular activated carbon (RO + GAC), and reverse osmosis + photoperoxidation + fixed-bed column of granular activated carbon (RO + UV/H₂O₂ + GAC) in the pilot-scale treatment plant (continuous flow rate = 350 L h⁻¹ and room temperature). The whiskers indicate the calculated standard deviation.

efficiencies achieved using the UV/H₂O₂ and GAC processes. Venancio et al. (2021) observed a reduction of up to 40% in the removal of thiabendazole by UV/H₂O₂ due to constituents of the water matrix that scavenged hydroxyl radicals. As observed in the present study, adsorption using GAC was also influenced by the water matrix due to competition for active sites. It is likely that the constituents (dissolved organic matter) of the WWTP effluent (Table S5) impaired the efficiencies of both the UV/H₂O₂ and GAC processes. In turn, the effectiveness of RO in removing CECs is less influenced by the water matrix (Lopera *et al.* 2019). In the present work, the use of RO alone removed between 75 and 99.9% of the studied CECs.

With the aim of enhancing the removal efficiencies, an evaluation was made of the combination of RO, which provided high removal efficiencies, with GAC or UV/H₂O₂, resulting in percentages >99% (Figure 6). At last, since WHO (2017) recommends a multi-barrier approach in DPR schemes, the ternary combination (RO+UV/H₂O₂+GAC) was investigated and provided reductions in nutrient concentrations (nitrogen and phosphorus), color, conductivity, turbidity, and chemical oxygen demand (Table S5) in addition to reducing CECs to below the LOQ (Table S3). Analysis of the effluent of the RO+UV/H₂O₂+GAC combination showed the water met the Brazilian legislation for drinking purposes (Brazil 2021), except for the pH, which was lower and would therefore require adjustment. To the best of our knowledge, this was the first study in Brazil to define five CECs as possible quality indicators and investigate their removal by employing a multi-barrier system. While the RO+UV/H₂O₂+GAC combination showed promising results under the objective of DPR of water, further investigations, including evaluation of the adjustment of pH, and the formation of disinfection by production after chlorination, should be carried out to verify full compliance with national guidelines.

4. Conclusions

Efforts oriented to the promotion of DPR of water require the definition of appropriate water quality indicators that go beyond the more traditional set of water quality parameters. Among the twelve CECs initially screened in the present study, five (CAF, HTZ, SAC, SMX, and SUC) were selected as possible indicators due to their occurrence on the MBR effluent and contrasting physicochemical characteristics. This prioritization is particularly important in developing countries with limited sanitation infrastructure to allow more affordable monitoring strategies and guide the respective decision-making processes.

In the laboratory-scale adsorption studies performed with a commercial AC, the electrostatic interactions influenced the adsorption process, with the adsorption being reduced when CEC and AC have the same charge. However, the adsorption was mainly governed by chemisorption (π - π interaction and hydrogen bonds, E values $> 16 \text{ kJ mol}^{-1}$) and pore diffusion (C values higher than K_{fd} values). It is important to emphasize that a pH adjustment would not be necessary to enhance adsorption, as maximum or close to maximum adsorption capacity was observed at pH ranges close to those frequently observed for real effluents. In addition, different adsorption capacities were observed for each CEC in the laboratory-scale experiments, with SMX and SUC being the most and least adsorbed compounds, respectively. On the other hand, SUC removal was the second highest removed CEC by GAC in the pilot-scale studies, while SAC was the lowest one. This result shows that the initial concentration directly influences the competition for the active sites of the AC. Future studies can assess competition for active sites considering different initial concentrations of CECs and investigate the life cycle of the AC, such as regeneration and desorption studies and disposal of the AC.

In the pilot-scale studies, RO higher removed the CECs compared to GAC and UV/H₂O₂. The binary combinations of RO with GAC or UV/H₂O₂ provided $>99\%$ elimination of the marker CECs, as well as the ternary combination (RO+UV/H₂O₂+GAC). The RO+UV/H₂O₂+GAC system also reduced nutrients (nitrogen and phosphorus), color, conductivity, turbidity, and chemical oxygen demand. Further investigations about the cost analysis of the RO+UV/H₂O₂+GAC combination should be performed, as well as the investigation of the life cycle of the AC, considering its regeneration or replacement. In addition, although the results reported here indicated that this system preliminarily met most of the parameters of the Brazilian legislation for drinking purposes, further studies should consider more samples over time to confirm the full compliance with the standard limits for potable water parameters and the 4Rs performance of the whole system.

5. Acknowledgements

The authors are grateful for the financial support provided by the Brazilian agencies FAPESP (INCTAA, grant #2014/50951-4) and CNPq (grants #465768/2014-8, #310844/2020-7 and #304584/2021-5). Scholarships were awarded to V.D. (CAPES, grant #88887.619586/2021-00; FAPESP, grant #2021/08123-0). The authors also thank SANASA (Sociedade de Abastecimento de Água e Saneamento, Campinas, São Paulo, Brazil) for collaboration in this study.

6. References

Adsorption of recalcitrant contaminants of emerging concern onto activated carbon: a laboratory and pilot-scale study

- Alves, P. D. C., Rodrigues-Silva, C., Ribeiro, A. R., & Rath, S. (2021). Removal of low-calorie sweeteners at five Brazilian wastewater treatment plants and their occurrence in surface water. *Journal of Environmental Management*, 289. <https://doi.org/10.1016/j.jenvman.2021.112561>
- APHA. (2017). *Standard methods for the examination of water and wastewater* (23 ed.).
- Arena, N., Lee, J., & Clift, R. (2016). Life Cycle Assessment of activated carbon production from coconut shells. *Journal of Cleaner Production*, 125, 68-77. <https://doi.org/10.1016/j.jclepro.2016.03.073>
- ASTM. (2020). D3860-98: Standard Practice for Determination of Adsorptive Capacity of Activated Carbon by Aqueous Phase Isotherm Technique. In.
- Belew, S., Suleman, S., Wynendaele, E., Duchateau, L., & De Spiegeleer, B. (2021). Environmental risk assessment of the anthelmintic albendazole in Eastern Africa, based on a systematic review. *Environmental Pollution*, 269. <https://doi.org/10.1016/j.envpol.2020.116106>
- Beltrame, K. K., Cazetta, A. L., de Souza, P. S. C., Spessato, L., Silva, T. L., & Almeida, V. C. (2018). Adsorption of caffeine on mesoporous activated carbon fibers prepared from pineapple plant leaves. *Ecotoxicology and Environmental Safety*, 147, 64-71. <https://doi.org/10.1016/j.ecoenv.2017.08.034>
- Bernados, B. (2020). Ultraviolet advanced oxidation for indirect and direct potable reuse in California. *AWWA Water Science*, 2(5). <https://doi.org/https://doi.org/10.1002/aws2.1192>
- Bisognin, R. P., Wolff, D. B., Carissimi, E., Prestes, O. D., Zanella, R. (2019). Occurrence and fate of pharmaceuticals in effluent and sludge from a wastewater treatment plant in Brazil. *Environment Technology*, 42. <https://doi.org/10.1080/09593330.2019.1701561>
- Boger, B., Surek, M., Volhena, R. O., Fachi, M. M., Junkert, A. M., Santos, J. M. M. F., Domingos, E. L., Cobre, A. F., Momade, D. R., Pontarolo, R. (2021). Occurrence of antibiotics and antibiotic resistant bacteria in subtropical urban rivers in Brazil. *Journal of Hazardous Materials*, 402. <https://doi.org/10.1016/j.jhazmat.2020.123448>
- Bonfils, C. J. W., Santer, B. D., Fyfe, J. C., Marvel, K., Phillips, T. J., & Zimmerman, S. R. H. (2020). Human influence on joint changes in temperature, rainfall and continental aridity. *Nature Climate Change*, 10(8), 726-+. <https://doi.org/10.1038/s41558-020-0821-1>
- Brasil. Ministério da Saúde, 2021. Anexo XX da Portaria de Consolidação nº 5/2017, alterado pela Portaria GM/MS nº 888 de 2021. *Diário Oficial da República Federativa do Brasil*, Brasília.
- Brorström-Lundén, E., Svenson, A., Viktor, T., & Woldegiorgis, A. (2008). Measurements of sucralose in the Swedish screening program 2007: PART I; sucralose in surface waters and STP samples. In: *Swedish Environmental Protection Agency*.
- Calza, P., Sakkas, V. A., Medana, C., Vlachou, A. D., Dal Bello, F., & Albanis, T. A. (2013). Chemometric assessment and investigation of mechanism involved in photo-Fenton and TiO₂ photocatalytic degradation of the artificial sweetener sucralose in aqueous media. *Applied Catalysis B-Environmental*, 129, 71-79. <https://doi.org/10.1016/j.apcatb.2012.08.043>
- Castronovo, S., Wick, A., Scheurer, M., Nodler, K., Schulz, M., & Ternes, T. A. (2017). Biodegradation of the artificial sweetener acesulfame in biological wastewater treatment and sandfilters. *Water Research*, 110, 342-353. <https://doi.org/10.1016/j.watres.2016.11.041>
- Chaves, M. J. S., Barbosa, S. C., Malinowski, M. M., Volpato, D., Castro, I. B., Franco, T. C. R. S., Primel, E. G. (2020). Pharmaceuticals and personal care products in a Brazilian wetland of international importance: Occurrence and environmental risk assessment, 734. <https://doi.org/10.1016/j.scitotenv.2020.139374>
- Chaves, M. D. S., Barbosa, S. C., & Primel, E. G. (2021). Emerging contaminants in Brazilian aquatic environment: identifying targets of potential concern based on occurrence and

ecological risk. *Environmental Science and Pollution Research*, 28(47), 67528-67543. <https://doi.org/10.1007/s11356-021-15245-y>

Deng, Z. H., Sun, S. X., Li, H. J., Pan, D., Patil, R. R., Guo, Z. H., & Seok, I. (2021). Modification of coconut shell-based activated carbon and purification of wastewater. *Advanced Composites and Hybrid Materials*, 4(1), 65-73. <https://doi.org/10.1007/s42114-021-00205-4>

Diniz, V., Rath, G., Rath, S., Araujo, L. S., & Cunha, D. G. F. (2022). Competitive kinetics of adsorption onto activated carbon for emerging contaminants with contrasting physicochemical properties. *Environmental Science and Pollution Research*, 29(28), 42185-42200. <https://doi.org/10.1007/s11356-021-16043-2>

Diniz, V., Rath, G., Rath, S., Rodrigues-Silva, C., Guimaraes, J. R., & Cunha, D. G. F. (2021). Long-term ecotoxicological effects of ciprofloxacin in combination with caffeine on the microalga *Raphidocelis subcapitata*. *Toxicology Reports*, 8, 429-435. <https://doi.org/10.1016/j.toxrep.2021.02.020>

Diniz, V., Reyes, G. M., Rath, S., & Cunha, D. G. F. (2020). Caffeine reduces the toxicity of albendazole and carbamazepine to the microalgae *Raphidocelis subcapitata* (Sphaeropleales, Chlorophyta). *International Review of Hydrobiology*, 105(5-6), 151-161. <https://doi.org/10.1002/iroh.201902024>

Dolar, D., Gros, M., Rodriguez-Mozaz, S., Moreno, J., Comas, J., Rodriguez-Roda, I., & Barcelo, D. (2012). Removal of emerging contaminants from municipal wastewater with an integrated membrane system, MBR-RO. *Journal of Hazardous Materials*, 239, 64-69. <https://doi.org/10.1016/j.jhazmat.2012.03.029>

Dominguez, J. R., González, T., Palo, P., & Cuerda-Correa, E. M. (2011). Removal of common pharmaceuticals present in surface waters by Amberlite XAD-7 acrylic-ester-resin: Influence of pH and presence of other drugs. *Desalination*, 269, 8. <https://doi.org/10.1016/j.desal.2010.10.065>

Foo, K. Y., & Hameed, B. H. (2010). Insights into the modeling of adsorption isotherm systems. *Chemical Engineering Journal*, 156(1), 2-10. <https://doi.org/10.1016/j.cej.2009.09.013>

Francoeur, M., Ferino-Perez, A., Yacou, C., Jean-Marius, C., Emmanuel, E., Cheremond, Y., Jauregui-Haza, U., & Gaspard, S. (2021). Activated carbon synthesized from *Sargassum* (sp) for adsorption of caffeine: Understanding the adsorption mechanism using molecular modeling. *Journal of Environmental Chemical Engineering*, 9(1). <https://doi.org/10.1016/j.jece.2020.104795>

Frohlich, A. C., Dos Reis, G. S., Pavan, F. A., Lima, E. C., Foletto, E. L., & Dotto, G. L. (2018). Improvement of activated carbon characteristics by sonication and its application for pharmaceutical contaminant adsorption. *Environ Sci Pollut Res Int*, 25(25), 24713-24725. <https://doi.org/10.1007/s11356-018-2525-x>

Fukuhara, T., Iwasaki, S., Kawashima, M., Shinohara, O., & Abe, I. (2006). Absorbability of estrone and 17beta-estradiol in water onto activated carbon. *Water Research*, 40(2), 241-248. <https://doi.org/10.1016/j.watres.2005.10.042>

Giles, C. H., Macewan, T. H., Nakhwa, S. N., & Smith, D. (1960). Studies in Adsorption .11. A System of Classification of Solution Adsorption Isotherms, and Its Use in Diagnosis of Adsorption Mechanisms and in Measurement of Specific Surface Areas of Solids. *Journal of the Chemical Society(Oct)*, 3973-3993. <https://doi.org/10.1039/jr9600003973>

Gonzalez-Garcia, P. (2018). Activated carbon from lignocellulosics precursors: A review of the synthesis methods, characterization techniques and applications. *Renewable & Sustainable Energy Reviews*, 82, 1393-1414. <https://doi.org/10.1016/j.rser.2017.04.117>

Guan, Z., Guan, Z., Li, Z., Liu, J., & Yu, K. (2019). Characterization and Preparation of Nanoporous Carbon Derived from Hemp Stems as Anode for Lithium-Ion Batteries. *Nanoscale Research Letters*, 14. <https://doi.org/10.1186/s11671-019-3161-1>

Adsorption of recalcitrant contaminants of emerging concern onto activated carbon: a laboratory and pilot-scale study

- Hai, F. I., Li, X. Q., Price, W. E., & Nghiem, L. D. (2011). Removal of carbamazepine and sulfamethoxazole by MBR under anoxic and aerobic conditions. *Bioresource Technology*, 102(22), 10386-10390. <https://doi.org/10.1016/j.biortech.2011.09.019>
- Hasan, M., Alfredo, K., Murthy, S., & Riffat, R. (2021). Biodegradation of salicylic acid, acetaminophen and ibuprofen by bacteria collected from a full-scale drinking water biofilter. *Journal of Environmental Management*, 295. <https://doi.org/10.1016/j.jenvman.2021.113071>
- Hespanhol, I. (2008). A New Paradigm for Water Resource Management. *Estudos Avançados*, 22(63), 27. <https://doi.org/10.1590/S0103-40142008000200009>
- Hespanhol, I., Rodrigues, R., & Mierzwa, J. C. (2019). Direct potable water reuse – Technical feasibility study using a pilot plant. *Revista DAE*, 67(217), 13. <https://doi.org/10.4322/dae.2019.026>
- Hoppen, M. I., Carvalho, K. Q., Ferreira, R. C., Passig, F. H., Pereira, I. C., Rizzo-Domingues, R. C. P., Lenzi, M. K., & Bottini, R. C. R. (2019). Adsorption and desorption of acetylsalicylic acid onto activated carbon of babassu coconut mesocarp. *Journal of Environmental Chemical Engineering*, 7(1). <https://doi.org/10.1016/j.jece.2018.102862>
- Hoslett, J., Massara, T. M., Malamis, S., Ahmad, D., van den Boogaert, I., Katsou, E., Ahmad, B., Ghazal, H., Simons, S., Wrobel, L., & Jouhara, H. (2018). Surface water filtration using granular media and membranes: A review. *Science of the Total Environment*, 639, 1268-1282. <https://doi.org/10.1016/j.scitotenv.2018.05.247>
- Hosseiny, S. H., Bozorg-Haddad, O., & Bocchiola, D. (2021). Water, culture, civilization, and history. In O. Bozorg-Haddad (Ed.), *Economical, Political, and Social Issues in Water Resources* (pp. 189-216). <https://doi.org/10.1016/B978-0-323-90567-1.00010-3>
- Jank, L., Hoff, R. B., Costa, F. J., Pizzolato, T. M. (2014). Simultaneous determination of eight antibiotics from distinct classes in surface and wastewater samples by solid-phase extraction and high-performance liquid chromatography–electrospray ionisation mass spectrometry. *International Journal of Environmental Analytical Chemistry*, 94. <https://doi.org/10.1080/03067319.2014.914184>
- JIS. (2014). K1474: Test methods for activated carbon. In. Tokyo.
- Judd, S. (2008). The status of membrane bioreactor technology. *Trends in Biotechnology*, 26(2), 109-116. <https://doi.org/10.1016/j.tibtech.2007.11.005>
- Keppetipola, N. M., Dissanayabe, M., Dissanayabe, P., Karunarathne, B., Dourges, M. A., Talaga, D., Servant, L., Olivier, C., Toupance, T., S., U., Tennakone, K., Kumara, G. R., & Cojocar, L. (2021). Graphite-type activated carbon from coconut shell: a natural source for eco-friendly non-volatile storage devices. *RSC Advances*, 11. <https://doi.org/10.1039/d0ra09182k>
- Khellouf, M., Chemini, R., Salem, Z., Khodja, M., Zeriri, D., & Jada, A. (2021). A new activated carbon prepared from cypress cones and its application in the COD reduction and colour removal from industrial textile effluent. *Environment Development and Sustainability*, 23(5), 7756-7771. <https://doi.org/10.1007/s10668-020-00944-2>
- Kim, M., Guerra, P., Shah, A., Parsa, M., Alaei, M., & Smyth, S. A. (2014). Removal of pharmaceuticals and personal care products in a membrane bioreactor wastewater treatment plant. *Water Science and Technology*, 69(11), 2221-2229. <https://doi.org/10.2166/wst.2014.145>
- Kim, S., Park, C. M., Jang, A., Jang, M., Hernandez-Maldonado, A. J., Yu, M., Heo, J., & Yoon, Y. (2019). Removal of selected pharmaceuticals in an ultrafiltration-activated biochar hybrid system. *Journal of Membrane Science*, 570, 77-84. <https://doi.org/10.1016/j.memsci.2018.10.036>
- Larcher, S., & Yargeau, V. (2012). Biodegradation of sulfamethoxazole: current knowledge and perspectives. *Applied Microbiology and Biotechnology*, 96(2), 309-318. <https://doi.org/10.1007/s00253-012-4326-3>

- Lin, A. Y. C., Lin, C. A., Tung, H. H., & Chary, N. S. (2010). Potential for biodegradation and sorption of acetaminophen, caffeine, propranolol and acebutolol in lab-scale aqueous environments. *Journal of Hazardous Materials*, 183(1-3), 242-250. <https://doi.org/10.1016/j.jhazmat.2010.07.017>
- Lin, Q. H., Cheng, H., & Chen, G. Y. (2012). Preparation and characterization of carbonaceous adsorbents from sewage sludge using a pilot-scale microwave heating equipment. *Journal of Analytical and Applied Pyrolysis*, 93, 7. <https://doi.org/https://doi.org/10.1016/j.jaap.2011.10.006>
- Liu, H., Zhang, J., Nho, H. H., Gio, W., Wu, H., Guo, Z., Cheng, C., & Zhang, C. (2015). Effect on physical and chemical characteristics of activated carbon on adsorption of trimethoprim: mechanisms study. *Royal Soc Chem Adv*, 5, 8. <https://doi.org/10.1039/c5ra17968h>
- Liu, L., Lopez, E., Duenas-Osorio, L., Stadler, L., Xie, Y. F., Alvarez, P. J. J., & Li, Q. L. (2020). The importance of system configuration for distributed direct potable water reuse. *Nature Sustainability*, 3(7), 548-555. <https://doi.org/10.1038/s41893-020-0518-5>
- Lopera, A. E. C., Ruiz, S. G., & Alonso, J. M. Q. (2019). Removal of emerging contaminants from wastewater using reverse osmosis for its subsequent reuse: Pilot plant. *Journal of Water Process Engineering*, 29. <https://doi.org/10.1016/j.jwpe.2019.100800>
- Mansor, N. A., & Tay, K. S. (2020). Potential toxic effects of chlorination and UV/chlorination in the treatment of hydrochlorothiazide in the water. *Science of the Total Environment*, 714. <https://doi.org/10.1016/j.scitotenv.2020.136745>
- Mansouri, H., Carmona, R. J., Gomis-Berenguer, A., Souissi-Najar, S., Ouederni, A., & Ania, C. O. (2014). Competitive adsorption of ibuprofen and amoxicillin combination from aqueous solution on activated carbons. *J Colloid Interface Sci*, 449, 9. <https://doi.org/10.1016/j.jcis.2014.12.020>
- Mashile, P. P., Mpupa, A., & Nomngongo, P. N. (2018). Adsorptive removal of microcystin-LR from surface and wastewater using tyre-based powdered activated carbon: Kinetics and isotherms. *Toxicon*, 145, 7. <https://doi.org/https://doi.org/10.1016/j.toxicon.2018.02.044>
- Miao, X. S., Yang, J. J., & Metcalfe, C. D. (2005). Carbamazepine and its metabolites in wastewater and in biosolids in a municipal wastewater treatment plant. *Environmental Science & Technology*, 39(19), 7469-7475. <https://doi.org/10.1021/es050261e>
- Mourao, P. A. M., Laginhas, C., Custodio, F., Nabais, J. M. V., Carrott, P. J. M., & Carrott, M. M. L. R. (2011). Influence of oxidation, process on the adsorption capacity of activated carbons from lignocellulosic precursors. *Fuel Processing Technology*, 92(2), 241-246. <https://doi.org/10.1016/j.fuproc.2010.04.013>
- Naidu, R., Espana, V. A. A., Liu, Y., & Jit, J. (2016). Emerging contaminants in the environment: Risk-based analysis for better management. *Chemosphere*, 154, 350-357. <https://doi.org/10.1016/j.chemosphere.2016.03.068>
- Nguyen, D. T., Tran, H. N., Juang, R. S., Dat, N. D., Tomul, F., Ivanets, A., Woo, S. H., Hosseini-Bandegharai, A., Nguyen, V. P., & Chao, H. P. (2020). Adsorption process and mechanism of acetaminophen onto commercial activated carbon. *Journal of Environmental Chemical Engineering*, 8(6). <https://doi.org/10.1016/j.jece.2020.104408>
- NHMRC. (2008). Australian Guidelines for Water Recycling: Augmentation of Drinking Water Supplies,. In.
- Nwabue, F. I., & Itumoh, E. J. (2020). Adsorption isotherm and kinetic modeling of a novel procedure for physical modification of silica gel using aqueous solutions of 4,4'-(1,2-ethanediyldinitrilo)bis-(2-pentanone) for preconcentration of Ni(II) ion. *Sep Sci Technol*, 55(16), 14. <https://doi.org/10.1080/01496395.2019.1659821>

Pang, L. N., Borthwick, A. G. L., & Chatzisyseon, E. (2020). Determination, occurrence, and treatment of saccharin in water: A review. *Journal of Cleaner Production*, 270. <https://doi.org/10.1016/j.jclepro.2020.122337>

Parida, V. K., Saidulu, D., Majumder, A., Srivastava, A., Gupta, B., & Gupta, A. K. (2021). Emerging contaminants in wastewater: A critical review on occurrence, existing legislations, risk assessment, and sustainable treatment alternatives. *Journal of Environmental Chemical Engineering*, 9(5). <https://doi.org/10.1016/j.jece.2021.105966>

Park, J., Kang, J., Jung, S., Choi, J., Lee, S., Yargeau, V., & Kim, S. (2020). Investigating Microcystin-LR adsorption mechanisms on mesoporous carbon, mesoporous silica, and their amino-functionalized form: surface chemistry, pore structures, and molecular characteristics. *Chemosphere*, 247. <https://doi.org/10.1016/j.chemosphere.2020.125811>

Pereira, C. D. S., Maranhão, L. A., Cortez, F. S., Pusceddu, F. H., Santos, A. R., Ribeiro, D. A., Cesar, A., Guimaraes, L. L. (2016). Occurrence of pharmaceuticals and cocaine in a Brazilian coastal zone. *Science of the Total Environment*, <https://doi.org/10.1016/j.scitotenv.2016.01.051>

Pereira, L. C., de Souza, A. O., Bernardes, M. F. F., Pazin, M., Tasso, M. J., Pereira, P. H., & Dorta, D. J. (2015). A perspective on the potential risks of emerging contaminants to human and environmental health. *Environmental Science and Pollution Research*, 22(18), 13800-13823. <https://doi.org/10.1007/s11356-015-4896-6>

Petrovic, M., Gonzalez, S., & Barcelo, D. (2003). Analysis and removal of emerging contaminants in wastewater and drinking water. *Trac-Trends in Analytical Chemistry*, 22(10), 685-696. [https://doi.org/10.1016/S0165-9936\(03\)01105-1](https://doi.org/10.1016/S0165-9936(03)01105-1)

Pivetta, R. C., Rodrigues-Silva, C., Ribeiro, A. R., & Rath, S. (2020). Tracking the occurrence of psychotropic pharmaceuticals in Brazilian wastewater treatment plants and surface water, with assessment of environmental risks. *Science of the Total Environment*, 727. <https://doi.org/10.1016/j.scitotenv.2020.138661>

Pompei, C. M. E., Campos, L. C., Silva, B. F., Fogo, J. C., Vieira, E. M. (2019). Occurrence of PPCPs in a Brazilian water reservoir and their removal efficiency by ecological filtration. *Chemosphere*, 226. <https://doi.org/10.1016/j.chemosphere.2019.03.122>

Porto, R. S., Rodrigues-Silva, C., Schneider, J., & Rath, S. (2019). Benzimidazoles in wastewater: Analytical method development, monitoring and degradation by photolysis and ozonation. *Journal of Environmental Management*, 232, 729-737. <https://doi.org/10.1016/j.jenvman.2018.11.121>

Rao, A., Kumar, A., Dhodapkar, R., & Pal, S. (2021). Adsorption of five emerging contaminants on activated carbon from aqueous medium: kinetic characteristics and computational modeling for plausible mechanism. *Environmental Science and Pollution Research*, 28(17), 21347-21358. <https://doi.org/10.1007/s11356-020-12014-1>

Rhoden, C. R. B., Bruckmann, F. S., Salles, T. R., Junior, C. G. K., & Mortari, S. R. (2021). Study from the influence of magnetite onto removal of hydrochlorothiazide from aqueous solutions applying magnetic graphene oxide. *Journal of Water Process Engineering*, 43. <https://doi.org/10.1016/j.jwpe.2021.102262>

Rouquerol, F., Rouquerol, J., Sing, K., Llewellyn, P., & Maurin, G. (2014). *Adsorption by Powders and Porous Solids Principles, Methodology and Applications* (Second ed.). Elsevier.

Sajjadi, S. A., Meknati, A., Lima, E. C., Dotto, G. L., Mendoza-Castillo, D. I., Anastopoulos, I., Alakhra, F., Unuabonah, E. I., Singh, P., & Hosseini-Bandegharai, A. (2019). A novel route for preparation of chemically activated carbon from pistachio wood for highly efficient Pb(II) sorption. *Journal of Environmental Management*, 236, 34-44. <https://doi.org/10.1016/j.jenvman.2019.01.087>

Samantara, A. K., Ratha, S., & Raj, S. (2019). Functionalized Graphene Nanocomposites in Air Filtration Applications. In M. Jawaid, R. Bouhfid, & A. K. Qaiss (Eds.), *Functionalized Graphene Nanocomposites and their Derivatives* (pp. 65-89). <https://doi.org/10.1016/C2017-0-00309-9>

Seibert, D., Zorzo, C. F., Borba, F. H., de Souza, R. M., Quesada, H. B., Bergamasco, R., Baptista, A. T., & Inticher, J. J. (2020). Occurrence, statutory guideline values and removal of contaminants of emerging concern by Electrochemical Advanced Oxidation Processes: A review. *Science of the Total Environment*, 748. <https://doi.org/10.1016/j.scitotenv.2020.141527>

Sengupta, A., Jebur, M., Kamaz, M., & Wickramasinghe, S. R. (2022). Removal of Emerging Contaminants from Wastewater Streams Using Membrane Bioreactors: A Review. *Membranes*, 12(1). <https://doi.org/10.3390/membranes12010060>

Streit, A. F. M., Collazzo, G. C., Druzian, S. P., Verdi, R. S., Foletto, E. L., Oliveira, L. F. S., & Dotto, G. L. (2021). Adsorption of ibuprofen, ketoprofen, and paracetamol onto activated carbon prepared from effluent treatment plant sludge of the beverage industry. *Chemosphere*, 262, 128322. <https://doi.org/10.1016/j.chemosphere.2020.128322>

Stumpf, M., Ternes, T. A., Wilken, R., Rodrigues, S. V., Baumann, W. (1999). Polar drug residues in sewage and natural waters in the state of Rio de Janeiro, Brazil. *Science of the Total Environment*, 225. [https://doi.org/10.1016/S0048-9697\(98\)00339-8](https://doi.org/10.1016/S0048-9697(98)00339-8)

Teng, W. W., Z.; Fan, J.; Zhang, W.; Zhao, D. (2015). Amino-functionalized ordered mesoporous carbon for the separation of toxic microcystin-LR. *Journal of Material Chemistry A.*, 9. <https://doi.org/https://doi.org/10.1039/C5TA05320J>

Tetzner, N. F., Maniero, M. G., Rodrigues-Silva, C., & Rath, S. (2016). On-line solid phase extraction-ultra high performance liquid chromatography-tandem mass spectrometry as a powerful technique for the determination of sulfonamide residues in soils. *Journal of Chromatography A*, 1452, 89-97. <https://doi.org/10.1016/j.chroma.2016.05.034>

Tran, H. N., Chao, H. P., & You, S. J. (2018). Activated carbons from golden shower upon different chemical activation methods: Synthesis and characterizations. *Adsorption Science & Technology*, 36(1-2), 95-113. <https://doi.org/10.1177/0263617416684837>

Tran, H. N., You, S. J., Hosseini-Bandegharaei, A., & Chao, H. P. (2017). Mistakes and inconsistencies regarding adsorption of contaminants from aqueous solutions: A critical review. *Water Research*, 120, 88-116. <https://doi.org/10.1016/j.watres.2017.04.014>

Venancio, W. A. L., Rodrigues-Silva, C., Spina, M., Diniz, V., & Guimaraes, J. R. (2020). Degradation of benzimidazoles by photoperoxidation: metabolites detection and ecotoxicity assessment using *Raphidocelis subcapitata* microalgae and *Vibrio fischeri*. *Environmental Science and Pollution Research*. <https://doi.org/10.1007/s11356-020-11294-x>

Wang, F., Sun, W., Pan, W., & Xu, N. (2015). Adsorption of sulfamethoxazole and 17 β -estradiol by carbon nanotubes/CoFe₂O₄ composites. *Chemical Engineering Journal*, 274, 13. <https://doi.org/https://doi.org/10.1016/j.cej.2015.03.113>

Wang, J. L., & Guo, X. (2020). Adsorption isotherm models: Classification, physical meaning, application and solving method. *Chemosphere*, 258. <https://doi.org/10.1016/j.chemosphere.2020.127279>

WHO. (2017). Guidance for producing safe drinking-water. In (pp. 152).

Yang, X. J., Liu, Z., Chen, H. Q., Feng, Q. G., & Wang, D. B. (2022). An excellent adsorption performance of acesulfame and saccharin from water on porous carbon derived from zinc-based MOFs: The role of surface chemistry and hierarchical pore structure. *Journal of Environmental Chemical Engineering*, 10(1). <https://doi.org/10.1016/j.jece.2021.107114>

Yin, K., Li, F., Wang, Y., He, Q. Y., Deng, Y. X., Chen, S., & Liu, C. B. (2017). Oxidative transformation of artificial sweetener acesulfame by permanganate: Reaction kinetics, transformation

Adsorption of recalcitrant contaminants of emerging concern onto activated carbon: a laboratory and pilot-scale study

products and pathways, and ecotoxicity. *Journal of Hazardous Materials*, 330, 52-60. <https://doi.org/10.1016/j.jhazmat.2017.02.012>

Zadaka, D., Nir, S., Radian, A., & Mishael, Y. G. (2009). Atrazine removal from water by polycation-clay composites: Effect of dissolved organic matter and comparison to activated carbon. *Water Research*, 43(3), 677-683. <https://doi.org/10.1016/j.watres.2008.10.050>

Zainab, S. M., Junaid, M., Xu, N., & Malik, R. N. (2020). Antibiotics and antibiotic resistant genes (ARGs) in groundwater: A global review on dissemination, sources, interactions, environmental and human health risks. *Water Research*, 187. <https://doi.org/10.1016/j.watres.2020.116455>

Zeng, S., & Kan, E. (2021). Adsorption and regeneration on iron-activated biochar for removal of microcystin-LR. *Chemosphere*, 273. <https://doi.org/https://doi.org/10.1016/j.chemosphere.2021.129649>

Zheng, H., Wang, Z. Y., Zhao, J., Herbert, S., & Xing, B. S. (2013). Sorption of antibiotic sulfamethoxazole varies with biochars produced at different temperatures. *Environmental Pollution*, 181, 60-67. <https://doi.org/10.1016/j.envpol.2013.05.056>

3.1.2. Adsorption of aqueous phase contaminants of emerging concern by activated carbon: Comparative fixed-bed column study and in situ regeneration methods

Vinicius Diniz^{1,*}, Susanne Rath¹

¹ Department of Analytical Chemistry, Institute of Chemistry, University of Campinas, Rua Josué de Castro, s/n, Cidade Universitária, Campinas, SP, 13083-970, Brazil

*Author for correspondence: viniciusdiniz994@gmail.com

Abstract

This work investigated the adsorption of five model contaminants of emerging concern (CECs) that are released daily in domestic effluents (caffeine, hydrochlorothiazide, saccharin, sulfamethoxazole and sucralose) onto two activated carbons (ACs), in fixed-bed column experiments with different aqueous matrices (ultrapure water, wastewater treatment plant (WWTP) effluent and WWTP effluent pretreated by reverse osmosis and photoperoxidation (reuse water)). The ACs were chemically similar, but AC1 had smaller particles (0.7 – 1.7 mm) and lower surface area ($551 \text{ m}^2 \text{ g}^{-1}$) than AC2 (1.2 – 2.4 mm and $716 \text{ m}^2 \text{ g}^{-1}$). AC1 had a higher adsorption capacity (q_{ads}) for the CECs in the downflow mode. Overall, the q_{ads} values of the CECs followed the order: caffeine > sulfamethoxazole > hydrochlorothiazide = saccharin > sucralose. In the downflow mode, preferential pathways reduced the hydraulic retention time (HRT) of the fixed-bed column loaded with AC, which reduced the useful lifetime of column and the adsorption capacity. Nevertheless, the adsorption capacity and useful lifetime of the fixed-bed columns remained similar in the upflow mode (no preferential pathways were observed) regardless of the AC used. Since the HRTs were also found to be similar, it was evident that the crucial factor influencing the adsorption of the CECs was the HRT, which played a pivotal role in the overall process becoming evident. Compared to ultrapure water, use of the WWTP effluent reduced q_{ads} for all the CECs by up to 4.1 times, while reuse water reduced q_{ads} by up to 1.2 times. The AC1 could be *in-situ* regenerated using ethanol, with a global efficiency of 97.2%. The results showed the importance of pretreatment techniques and optimization of the operational parameters, such as HRT, for enhancing the useful lifetime and q_{ads} of fixed-bed columns.

Keywords: Emerging contaminants; column plant; particle size; regeneration; reuse water.

1. Introduction

Various classes of contaminants of emerging concern (CECs) are daily released into environmental matrices. Among these classes, artificial sweeteners (Alves *et al.* 2021) and pharmaceuticals such as antimicrobials (Langbehn *et al.* 2021), diuretics (Borowska *et al.* 2016) and stimulants (Buerge *et al.* 2003), have been widely detected. Most of these compounds are highly resistant to biological degradation and photolysis, resulting in persistence in water matrices and low removal efficiencies when conventional technologies such as activated sludge and biological filters are used (Nazari *et al.* 2016; Peteffi *et al.* 2018; Alves *et al.* 2021, Di Marcantonio *et al.* 2023). Others, such as caffeine (CAF), despite the high efficiency of removal by biological treatment, are still present in high concentrations in the final effluent (Diniz *et al.* 2023; Di Marcantonio *et al.* 2023). Furthermore, conventional drinking water treatment plants (employing coagulation, flocculation, sedimentation, dissolved air flotation, rapid sand filtration and disinfection) also present low ability to remove CECs (Malta *et al.* 2022; Rodriguez-Narvaez *et al.* 2017). Therefore, advanced treatment techniques such as oxidation, membrane filtration, electrocoagulation and adsorption have been proposed for the removal of CECs from the aqueous phase (Malta *et al.* 2022; Ahmed and Hameed, 2018).

Among these techniques, activated carbon (AC) is able to effectively remove organic contaminants and small molecules from aqueous solution, due to its high surface area, well-developed porosity and high adsorption capacity (Koshigoe *et al.* 2023; Nazari *et al.* 2016). However, it still needs to be fully understood the adsorption of different types of CECs by AC. In addition, AC is inexpensive and environmentally friendly, since it can be produced from high carbon content materials that would otherwise be discarded (Fan *et al.* 2010). In treatment plants, adsorption can be performed in batch or continuous modes (Ahmed and Hameed 2018), with the latter being most widely used (WHO 2017), due to its simple operation, effectiveness and capacity to treat large volumes of effluents containing CECs, without the need for adsorbent substitution (de Franco *et al.* 2017; Lemus *et al.* 2017). In addition, since the AC is loaded into fixed-bed columns in the continuous mode, an additional step is not required in treatment plants to separate the AC from the aqueous phase. Lastly, it can be easily scaled up from the laboratory scale to real applications, using kinetic data obtained from breakthrough curves (Hussein and Ahmed 2016; Lemus *et al.* 2017).

There are several published reports concerning the effects of fixed-bed column operating conditions (flow rate, bed height and inlet concentration) on the adsorption capacity, breakthrough

time and mass transfer zone (MTZ). In general, the higher the flow rate, the shorter the breakthrough time since this parameter affects the contact between adsorbate and adsorbent. Nazari *et al.* (2016) observed a 2.5-fold reduction of the breakthrough time (with concentration ratio $C/C_0 = 0.05$) when the flow rate was increased from 4.5 to 7.5 mL min⁻¹, using cephalexin as the adsorbate (initial concentration (C_0) = 100 mg L⁻¹) and a fixed-bed column of walnut shell-based AC (bed height = 2 cm). On the other hand, the higher the bed height, the longer the breakthrough time since a greater amount of AC is available. A study with atenolol ($C_0 = 100 \mu\text{g L}^{-1}$; flow rate = 1.5 mL min⁻¹) found a 13-fold increase in the breakthrough time when the bed height was increased from 1 to 3 cm. Lastly, as expected, when the inlet concentration of the contaminant is increased, a shorter breakthrough time is observed, since there is more adsorbate in the solution. However, although the effects of inlet concentration have been widely reported in fixed-bed column studies, these studies have only theoretical applications once this parameter is not inherent to the treatment plant but depends on the population characteristics.

Although there have been many investigations of the adsorption of CECs using fixed-bed columns loaded with AC, there is still a lack of information concerning the effects of adsorbent particle size, flow mode (upflow or downflow), adsorption using real effluents, the presence of multiple CECs in the aqueous phase and techniques for AC regeneration (Ahmed and Hameed 2018). Therefore, the present study aimed to investigate: (1) the effects of fixed-bed AC column operating parameters, including bed height, flow mode, flow rate and particle size, on the adsorption of five model CECs (caffeine (CAF), hydrochlorothiazide (HTZ), saccharin (SAC), sulfamethoxazole (SMX) and sucralose (SUC)), which were defined as fingerprints for anthropogenic contamination in our previous study (Diniz *et al.* 2023); (2) adsorption of the CECs using three aqueous matrices with different compositions (ultrapure water, wastewater treatment plant effluent and final effluent wastewater treatment plant + reverse osmosis + photoperoxidation); and (3) the adsorption capacity after 3 cycles of adsorption/regeneration using different *in-situ* regenerant solutions.

2. Materials and methods

2.1. Chemicals and reagents

Analytical standards of CAF (99.0%), HTZ (99.7%), SAC (99.6%), SMX ($\geq 99.0\%$) and SUC (99.4%) were purchased from Sigma-Aldrich (USA). Physicochemical properties of the CECs are shown in Table S1. The internal standards caffeine-d3, sucralose-d6 and sulfadimethoxine-d3 were purchased from Sigma-Aldrich (USA).

Dimethylformamide (DMF), ammonium acetate (HPLC grade) and methanol (MeOH) (HPLC grade) were obtained from Labsynth (Brazil), Merck (USA) and J.T. Baker (USA), respectively. Potassium chloride, sodium bicarbonate, sodium carbonate, sodium hydroxide, acetic acid and boric acid (all of analytical grade), as well as hydrochloric acid (35%) and phosphoric acid (85%), were purchased from Synth (Brazil).

Stock standard solutions of the CECs ($1000 \mu\text{g mL}^{-1}$) were prepared in methanol. All the stock solutions were kept at -4°C for no longer than 6 months. Working standard solutions were prepared daily by dilution of the stock solutions in ultrapure water obtained from a Milli-Q purification system (Millipore, USA).

2.2. Fixed-bed column studies

2.2.1. Analysis and AC characterization

The analytical measurements of the contaminants were performed using an UHPLC-MS/MS system (Waters, USA). A fast-switching electrospray ionization source (ESI) was used for ionization of the analytes and a triple-quadrupole mass detector (Xevo TQD spray, Waters) was used for detection and quantification.

An Acquity UPLC[®] CSH C18 column (130 \AA , $1.7 \mu\text{m}$, $2.1 \text{ mm} \times 100 \text{ mm}$; Waters, USA) was used for the chromatographic separation. MassLynx v. 4.1 software was employed for data acquisition and control of the equipment. The procedure employed to optimize the analytical method can be found elsewhere (Alves *et al.* 2021; Porto *et al.* 2019). A detailed description of the UHPLC-MS/MS method and the parameters assessed is provided in the Supplementary Material (Tables S2 and S3). Characteristic chromatograms are shown in Figure S1.

The activated carbon produced from coconut shell, here denoted AC1 (Charbon 500, $0.7 \times 1.7 \text{ mm}$ (12 x 24 mesh); Carbonado, Brazil), was characterized in our previous study (Diniz *et al.* 2023). The characterization of the activated carbon denoted AC2, produced from plant material ($1.2 \times 2.4 \text{ mm}$ (8 x 16 mesh); Synth, Brazil), is described in the Supplementary Material (Text T1).

2.2.2. Fixed-bed column experiments

Laboratory-scale fixed-bed column experiments were performed using polypropylene columns with internal diameter of 14.5 mm . The column length was adjusted for each experiment and ultrapure water (hereafter called water) was obtained from the Milli-Q purification system. The

column bed was supported and covered with 180 mg of glass wool to ensure a good liquid distribution (Liao *et al.* 2013). An IPC high precision multichannel dispenser (Ismatec, USA) was used to control the flow rate at the column inlet and outlet. The experiments were performed using different bed heights (1.5, 2.5 and 3.5 cm), influent flow rates (5, 8 and 11 mL min⁻¹), influent flow modes (downflow and upflow) and particle size (AC1 and AC2). The nominal inlet concentration of the CECs was set at 2 mg L⁻¹, with precise measurement by UHPLC-MS/MS at the beginning and end of each experiment, for quality control. The sample pH was measured at the beginning of each experiment and was not adjusted. It was observed that the pH varied by less than 0.4 units during the experiments. Control experiments showed that adsorption of the CECs onto the glass wool or the column wall was negligible during the operation time. At regular time intervals, 2 mL aliquots of the column effluent were collected, filtered (0.22 µm filter) and analyzed by UHPLC-MS/MS.

2.2.3. Water composition

Comparison of the effectiveness of the fixed-bed columns using two other water compositions was performed in downflow mode, with a bed height of 3.5 cm, influent flow rate of 5 mL min⁻¹ and analyte inlet concentrations of 2 mg L⁻¹ or 0.1 mg L⁻¹. For the lower concentration experiments, the LC-UHPLC-MS/MS method described in a previous study of our groups was employed for the quantification of the CECs (Diniz *et al.* 2023). The first water sample (denoted WWTP effluent) was the effluent from a wastewater treatment system that operates with a membrane bioreactor and received the sewage from a population of around 182,000 inhabitants, with an average flow rate of $24,767 \pm 1,648$ L d⁻¹ (Alves *et al.* 2021; Pivetta *et al.* 2020). The second water sample (here called reuse water) was the effluent from a pilot-scale plant system (350 L h⁻¹) that received the effluent of the membrane bioreactor system and applied reverse osmosis and photoperoxidation treatment processes. The physicochemical characterization of the water samples is described in the Supplementary Material (Table S4).

2.2.3.1. Tracer analysis

Investigation of the residence time distribution enables determination of the mean hydraulic retention time (HRT) of a fixed-bed column. For these experiments, a saline tracer (NaCl, 5 g L⁻¹) was selected, because it would not interact with the AC and its presence could be easily detected by monitoring changes in the conductivity of the liquid phase. For each experimental condition (Section 2.2.2), the saline solution was continuously injected and the conductivity of the liquid phase at the fixed-bed column outlet was measured *in situ*, using a conductance flow cell

(Rohwedder and Pasquini 1991; Pasquini and Faria 1987), until no changes in conductivity were observed during at least 60 s (**Figure 1A**). In addition, the Empty Bed Column Time (EBCT) and the dead volume were determined in hydrodynamic experiments performed for each test configuration, but without the AC bed.

The HRT was estimated using the moments modeling method (Stephenson and Sheridan 2021). After the experiments, the F curve (normalized conductivity *versus* time, **Figure 1B**) was plotted after normalizing the conductivity values using **Equation 1**:

$$F(t) = \frac{C_t}{C_{max}} \quad (\text{Equation 1})$$

where, C_t and C_{max} are the conductivity at time t and the maximum conductivity observed, respectively.

In the next step, it was possible to obtain the E curve, also known as the residence time distribution function (**Figure 1C**), using **Equation 2**:

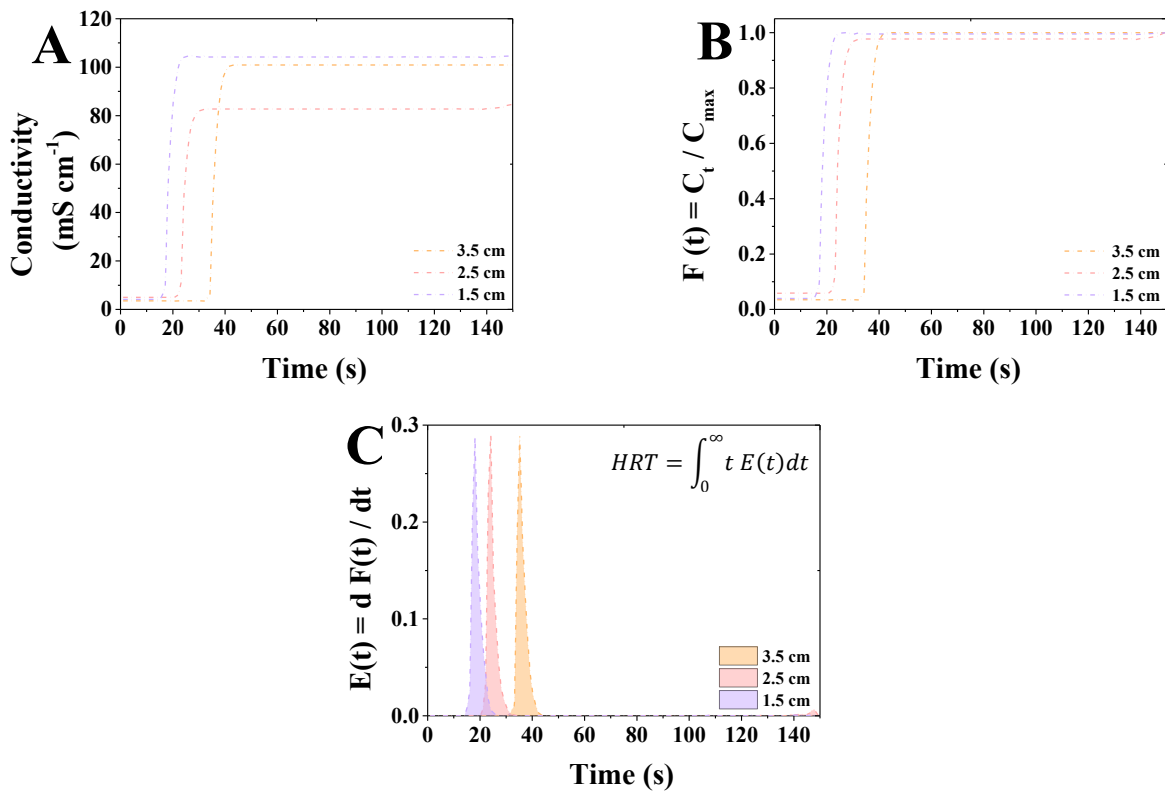


Figure 1: Examples of the step-by-step calculation of the moments modeling method for the estimation of hydraulic retention time (HRT) of the fixed-bed columns operated at different bed heights and upflow mode (flow rate = 5 mL min⁻¹). (A) Real conductivity versus time. (B) Normalized conductivity (F curve) versus time. (C) Residence time distribution curve (E curve) versus time.

$$E(t) = \frac{dF(t)}{dt} \quad (\text{Equation 2})$$

Lastly, considering that the sum of the NaCl that passed through the fixed-bed column and the NaCl that remained inside the column until a hypothetical time was equal to 1, it was possible to estimate the HRT (**Figure 1C**) using **Equation 3**:

$$HRT = \frac{\int_0^\infty t E(t) dt}{\int_0^\infty E(t) dt} = \int_0^\infty t E(t) dt \quad (\text{Equation 3})$$

where, t is the time (s). All the calculations were performed using Origin[®] and Excel365[®] software.

2.2.4. Mathematical modeling

Effluent inlet concentrations ranging from 2% to 100% ($C/C_0 = 0.02-1.00$) were used for the breakthrough curve (BTC) modeling. The breakthrough time (t_b) and the saturation time (t_s), corresponding to the time for 5% adsorbate breakthrough in the effluent and to the time required to achieve 100% of the inlet concentration, respectively, were determined from all the BTC curves. The t_b and t_s values were obtained using **Equations 4** and **5**, respectively:

$$t_b = \int_0^{t_{bb}} \left(1 - \frac{C}{C_0}\right) dt \quad (\text{Equation 4})$$

$$t_s = \int_0^t \left(1 - \frac{C}{C_0}\right) dt \quad (\text{Equation 5})$$

where, t_b , t_{bb} , t_s and t are the breakthrough time, first sampling point after $C/C_0 > 0.05$, saturation time and experiments duration (min), respectively and C and C_0 are the outlet and inlet concentrations (mg L^{-1}), respectively.

The mass transfer zone (MTZ, cm) was estimated using **Equation 6**:

$$MTZ = \left(1 - \frac{t_b}{t_s}\right) H \quad (\text{Equation 6})$$

where, H is the bed height (cm).

The experimental maximum adsorption capacity (q_{ads} , mg g^{-1}), obtained from the BTC, was calculated using **Equation 7**:

$$q_{ads} = \frac{Q \cdot C_0}{m_{ads}} * \int_0^t \left(1 - \frac{C}{C_0}\right) dt \quad (\text{Equation 7})$$

where, Q is the flow rate (L min^{-1}) and m_{ads} is the mass of AC (g).

Knowing the effect of the column operational parameters, the scale-up of a fixed-bed column is possible. The theoretical BTCs were modeled using the Thomas, Yoon-Nelson and Bohart-Adams models, allowing prediction of the behaviors of the fixed-bed columns. According to Chatterjee and Schiewer (2011), these three models can be summarized in one nonlinear general equation (**Equation 8**):

$$\frac{c}{c_0} = \frac{1}{1 + \exp(a - b \cdot t_i)} \quad (\text{Equation 8})$$

where, a and b are the parameters of the models (Table S5) and t_i is the time of the experiment (min).

It is also possible to determine the Yoon-Nelson maximum adsorption capacity ($q_{\text{ads,YN}}$, mg g^{-1}), using **Equation 9**:

$$q_{\text{ads,YN}} = \frac{c_0 \cdot Q \cdot \tau}{m_{\text{ads}}} \quad (\text{Equation 9})$$

where, $q_{\text{ads,YN}}$ is the adsorption capacity of the Yoon-Nelson Model and τ is the time (min) required for 50% adsorbate breakthrough.

The determination coefficient (R^2) and the sum of squared errors (SSE) (Table S6) were used to evaluate the fitting accuracy of the theoretical BTC models. The calculations were performed using Origin[®] and Excel365[®] software.

2.3. In situ regeneration of AC

Since the two ACs showed similar chemical characteristics, AC1 was chosen for the regeneration experiments. The tests were performed using a bed height of 1.5 cm, influent flow rate of 5 mL min^{-1} , inlet concentration of 2 mg L^{-1} , downflow mode and five different regenerant solutions: solution 1, ethanol:water (10:90, v/v); solution 2, ethanol:water (50:50, v/v); solution 3, ethanol; solution 4, water adjusted to pH 2 with HCl; and solution 5, water adjusted to pH 10 with NaOH. Ethanol was used instead of methanol, due to its lower toxicity (Larasati *et al.* 2021). After each adsorption cycle, the regeneration solutions were percolated through the fixed-bed column for 30 min, at a flow rate of 5 mL min^{-1} . Immediately after the regeneration procedure, water was percolated through the column for 30 min at 5 mL min^{-1} , for solutions 1, 2 and 3, or until the effluent pH returned to the initial value, for solutions 4 and 5.

3. Results and discussion

3.1. AC characterization

Knowledge of the origin and the physicochemical property of the AC is essential for understanding the potential of the material for use as an adsorbent in a fixed-bed column. In the present work, two AC adsorbents from different manufacturers were assessed, both produced from coconut shell, but with some distinct physicochemical properties. The two adsorbents (AC1 and AC2) were loaded into columns to evaluate the removal of the five model CECs from the aqueous phase. AC1 had been previously characterized in an earlier study (Diniz et al., 2023) and was selected due to its high adsorption capacity for the selected CECs. AC2 was chosen due to its granulometric characteristics, since it presented a larger particle size, compared to AC1, together with higher specific surface area (1.3x), higher total pore volume (1.5x) and higher total micropore volume (1.4x). However, the two ACs presented similar N₂ adsorption isotherm shapes (type IV, with H4 hysteresis loop) and average pore diameter. Details of the characterization of AC2 can be found in the Supplementary Material (Table S7).

The Raman spectrum of the AC2 showed both D band (around 1330 cm⁻¹) and G band (around 1595 cm⁻¹), indicating a highly amorphous structure. The amorphous nature was confirmed by the X-ray diffraction spectrum, which presented two broad diffraction peaks (23.7° and 43.4°). The AC1 has a very similar amorphous structure, as shown in the previous work of our group (Diniz et al., 2023). Regarding the chemical groups on the surface of the AC2 adsorbent, the FTIR spectra (Figure S2) showed the following characteristic bands: 3440 cm⁻¹ (-OH stretching vibration of carboxylic and phenol groups), 2850 cm⁻¹ (C-H stretching), 2920 cm⁻¹ (C=C vibration), 1632 cm⁻¹ (vibrations of aromatic ring C=C and carbonyl C=O) and 1110 cm⁻¹ (C-O stretching of phenols and alcohols). The FTIR spectrum of AC2 was similar to that of AC1 (see Diniz et al., 2023), considering the main characteristic bands. Furthermore, AC2 had 0.42, 0.59, 0.31 and 1.51 mEq g⁻¹ of carboxylic, phenolic, lactonic, and alkaline groups on the surface, which is similar to those reported for AC1 (see Diniz et al. (2023)). AC1 and AC2 also presented similar point of zero charge and crystallinity (Table S7, Figure S2). Batch adsorption experiments were carried out with AC2 using CAF, HTZ, SAC, SMZ and SUC as adsorbates. The experiments were performed using the same methodology described by Diniz *et al.* (2023) when assessing the adsorption capacity of AC1 by the same CECs by batch experiments. The results (Table S8) demonstrated that AC2 exhibited an adsorption capacity approximately 1.7-fold higher than AC1, which aligns with the observed 1.3-fold greater surface area

of AC2 compared to AC1. The mean adsorption energies for the adsorption of the CECs were similar ($>16 \text{ kJ mol}^{-1}$). These findings highlight the correlation between surface area and adsorption capacity, indicating that the enhanced performance of AC2 can be attributed to its larger surface area. These results were interesting, since one of the hypotheses adopted in this work was that the particle size of the AC would influence the overall adsorption process in a fixed-bed column.

3.2. Fixed-bed column experiments

The primary focus of the present work was the study of the downflow mode, which is the same flow mode utilized at the pilot-scale treatment plant of EPAR Capivari II. The investigations of downflow mode will allow further direct comparison and a better understanding of the performance and behavior of the fixed-bed AC column that will operate in the pilot-scale treatment plant. However, to compare the effects of flow modes on the adsorption of CECs, additional experiments were conducted at different bed heights in the upflow mode.

The studies assessing the impact of different bed heights, flow rates and flow modes selected a concentration of 2 mg L^{-1} of CECs to facilitate monitoring and reduce result uncertainty. Nonetheless, a lower concentration of CECs (0.1 mg L^{-1}) was employed when dealing with the WWTP effluent and reuse water. This concentration is similar to the levels measured in our previous study at the same WWTP (Diniz *et al.* 2023).

3.2.1. Tracer analysis

The quantity of adsorbate removed onto an adsorbent is dependent on the contact time, with longer times leading to increased adsorption, until an equilibrium state is reached. In general, estimation of the HRT in a fixed-bed column employs calculations, rather than the use of saline tracers (Feizi *et al.* 2021). Therefore, in this work, the moments modelling method was employed to estimate the HRT of each experimental configuration (see Section 2.2.2.2). An example of the curves of the moments modeling method for the estimation of the HRT for the different bed heights of the fixed-bed columns operated at upflow mode and flow rate of 5 mL min^{-1} is shown in Figure 1. It should be noted that the HRT calculations included consideration of the dead volumes (Figure S3), corresponding to the tubes and connections. It was found that for both adsorbents, the HRT increased when a greater amount of adsorbent was used in the column (Table 1). In addition, for both ACs, a decrease of the HRT was observed when the flow rate was increased from 5 to 11 mL min^{-1} (Table 1).

Table 1. Hydraulic retention time for each experimental configuration.

Flow mode	Bed height (cm)	Flow rate (mL min ⁻¹)	Hydraulic retention time (s) (AC1 / AC2)
Downflow	1.5	5	18.5 / 8.3
	2.5	5	20.4 / 12.1
	3.5	5	23.6 / 18.9
	3.5	8	19.2 / 12.1
	3.5	11	16.9 / 5.5
Upflow	1.5	5	18.3 / 18.5
	2.5	5	24.5 / 25.9
	3.5	5	32.3 / 34.6

Due to the larger granulometric size of AC2, compared to AC1, it was expected that the HRT would be higher for this adsorbent. However, in the downflow mode, the highest HRT was observed for AC1 (**Table 1**). A possible explanation was the existence of preferential pathways (shown in Figure S4) in the columns loaded with AC2. In turn, in the upflow mode, the HRTs for AC2 and AC1 were similar, as well as no preferential pathways were observed in the columns loaded with AC2 (Figure S4).

3.2.2. Effect of different bed heights on the breakthrough curve (BTC) using downflow mode

The adsorption of CECs in a fixed-bed column is largely dependent on the bed height (Ahmed and Hameed 2018), which in turn is dependent on the quantity of AC loaded in the column. **Figure 2** shows the BTCs for adsorption of the five CECs onto AC1 and AC2, at three different bed heights (1.5, 2.5 and 3.5 cm). For all the CECs and both ACs, the t_b and t_s values increased with increasing of the bed height. When the bed height was increased from 1.5 to 3.5 cm, the t_s values for HTZ increased 2.5-fold (AC1) and 3.4-fold (AC2) (Table S9). Increases were also observed for the t_b values. For SUC, t_b increased 7-fold (AC1) and 9-fold (AC2), when the bed height was increased by 2 cm (from 1.5 to 3.5 cm). There was a direct dependence of the MTZ value on the bed height (Table S9), with higher MTZ values resulting in broader BTC curves (**Figure 2**), revealing non-ideal mass transport since all the active sites of the AC were not being saturated simultaneously (Fernández-Andrade *et al.* 2022).

The effects of the different bed heights on the BTCs were in agreement with the findings of Liao *et al.* (2013), who studied the adsorption of tetracycline and chloramphenicol onto bamboo charcoal adsorbents ($Q = 6.6 \text{ mL min}^{-1}$ and $C_0 = 50 \text{ mg L}^{-1}$). In addition, since increase of the bed

height resulted in greater availability of active sites of the adsorbent, higher τ values (50% adsorbate breakthrough in the effluent) were expected, as observed for SUC and HTZ, where 2.9-fold and 3.6-fold higher values were obtained for adsorption using AC1 and AC2, respectively (Table S9).

On the other hand, although a higher amount of AC loaded in the fixed-bed columns increased the contact time for both ACs (Table 1), no increases in q_{ads} values were observed (Table

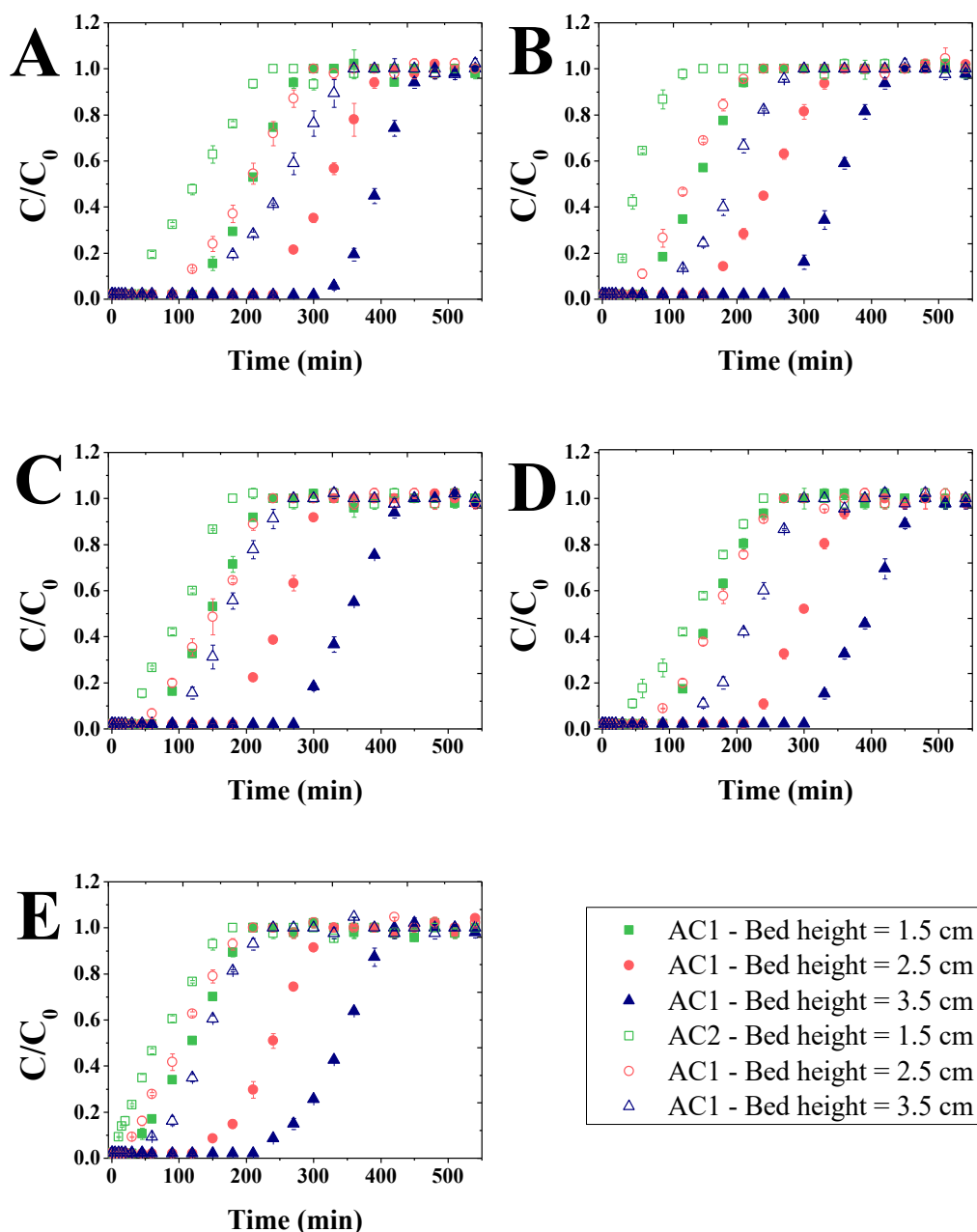


Figure 2. Breakthrough curves for adsorption of CAF (A), HTZ (B), SAC (C), SMX (D), and SUC (E) onto AC1 and AC2 at different bed heights (flow rate = 5 mL min^{-1} , $C_0 = 2 \text{ mg L}^{-1}$, and downflow mode).

S9). Wang *et al.* (2010) explained that although there may be an increase in the availability of active sites, this does not necessarily mean that they are accessible to the adsorbates, which means that the surface area of the ACs does not play a crucial role in the adsorption of the CECs. Therefore, the increase in the amount of CEC adsorbed was due only to the mass of AC loaded in the columns. Although the CECs competed for the available active sites, the effects of variation in the bed height were similar to those observed in studies with single CEC solutions (Nazari *et al.* 2016; Sancho *et al.* 2012).

3.2.3. Effect of flow rate on the breakthrough curve

The flow rate is the main parameter that determines the time of contact between the adsorbate and the absorbent, which is crucial for removing CECs from aqueous solution (Ahmed and Hameed, 2018). The hydrodynamic studies (Section 3.2.1) confirmed that the slower the flow rate, the longer the time of contact between adsorbate and absorbent (Table 1). Figure 3 shows the typical S-shaped BTCs for adsorption of the CECs onto AC1 and AC2, at different flow rates. It was observed that when the flow rate was increased, the t_b , t_s and τ values were reduced (Table S9), associated with faster percolation of the CECs through the fixed-bed columns and occupation of the available active sites. In a study of the adsorption of cephalexin onto walnut shell AC, Nazari *et al.* (2016) found that t_b decreased 3.5-fold when the flow rate was increased from 4.5 to 7.5 mL min⁻¹ (bed height = 2 cm and $C_0 = 100$ mg L⁻¹). Reductions of t_s of 2.6-fold and 1.9-fold were observed for the adsorption of tetracycline and chloramphenicol, respectively, when the flow rate was increased from 3.3 to 10.0 mL min⁻¹ (bed height = 4 cm and $C_0 = 50$ mg L⁻¹) (Nazari *et al.* 2016). These results were consistent with the present findings, since reductions in the t_s , t_b and τ values ranging from 3.0-fold to 43.9-fold were observed for adsorption of the CECs onto the two ACs, when the flow rate was increased from 5 to 11 mL min⁻¹.

As expected, the time of contact between the ACs and the CECs decreased with increasing flow rate (Table 1), which limited the adsorption, with lower q_{ads} values observed for all the CECs (Table S9). Unlike the effects observed in the study with different bed heights, alteration of the flow rate affected each CEC differently. The greatest effect was observed for SUC, where q_{ads} decreased 10.4-fold and 14.0-fold for adsorption onto AC1 and AC2, respectively, when the flow rate was increased from 5 to 11 mL min⁻¹. The q_{ads} values for adsorption of CAF onto AC1 and AC2 decreased 1.3-fold and 5.0-fold, respectively, for the same increase in flow rate. It was expected that CAF would present the highest affinity for the AC, with rapid adsorption, since it had the highest q_{ads} value. On

the other hand, the results suggested that SUC required a longer time of contact with the AC to be adsorbed, resulting in the greatest reductions of q_{ads} when the flow rate was increased. To the best of our knowledge, studies evaluating the adsorption of artificial sweeteners onto AC using fixed-bed columns are still scarce. However, Diniz *et al.* (2023) reported that adsorption onto AC (in batch studies) was faster for CAF, compared to SUC, in agreement with the present findings.

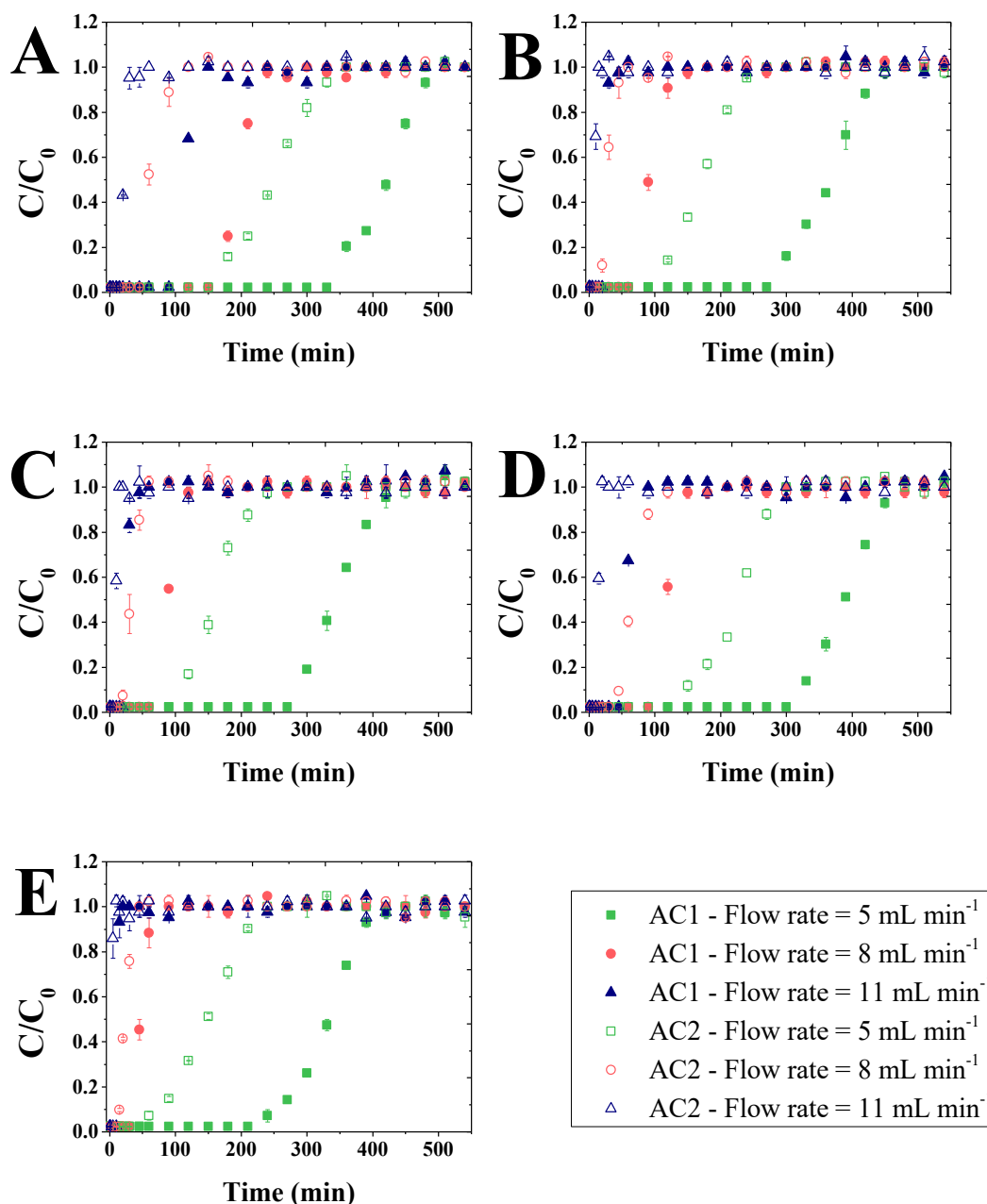


Figure 3. Breakthrough curves for adsorption of CAF (A), HTZ (B), SAC (C), SMX (D), and SUC (E) onto AC1 and AC2, at different flow rates (bed height = 3.5 cm, $C_0 = 2 \text{ mg L}^{-1}$, and downflow mode).

3.2.4. Effect of particle size and flow mode on the breakthrough curve

Determination of the appropriate time of contact between the adsorbent and the adsorbate is essential for optimizing the removal of adsorbates from the aqueous phase (Ahmed and Hameed 2018). In a fixed-bed column, the contact time is governed by the void volume and the porosity of the AC, in addition to operational parameters (bed height and flow rate), with the former depending on the AC particle size. In the present study, the contact time was estimated using an experimental approach with a saline tracer, instead of theoretical calculations (see Section 3.2.1). As shown in Figures 1 and 2, the useful lifetime of the fixed-bed column operated in downflow mode was longer for AC1 than AC2, resulting in higher t_b , τ and q_{ads} values for all the CECs (Table S9), despite the fact that AC2 had the highest specific surface area. In addition, a smaller particle size led to a smaller MTZ value, since the MTZ value increased as the Reynolds number (R_e , **Equation 10**) increased (Hand *et al.* 1984). Therefore, as only the AC particle size varied between the experiments, R_e was higher using AC2 than AC1, resulting in higher MTZ values.

$$R_e = \frac{\rho_{water} v d}{\mu} \quad (\text{Equation 10})$$

where, R_e is the Reynolds number, ρ_{water} is the water density, v velocity of the fluid, d is the particle size and μ is the water viscosity.

On the other hand, when the adsorption was carried out in upflow mode, increases in the t_b , τ and q_{ads} values for all the CECs were obtained using AC2 (Table S10), as also shown from the BTCs (**Figure 4**). These results were in agreement with the HRT experiments (**Table 1**), since higher HRT should lead to higher adsorption. In addition, the contact time was longer in the upflow mode than in the downflow mode (Table 1), which resulted in higher q_{ads} for both ACs. The increases of q_{ads} were more pronounced for AC2 than for AC1, with up to 3.0-fold higher values, irrespective of the bed height. These results indicated that in the upflow mode, particle size did not affect the adsorption since no preferential pathways were observed. Although AC2 had a 1.3 higher surface area than AC1, the adsorption parameters were also similar, which indicates that the HRT ruled the adsorption since the values for both ACs were similar (Table 1).

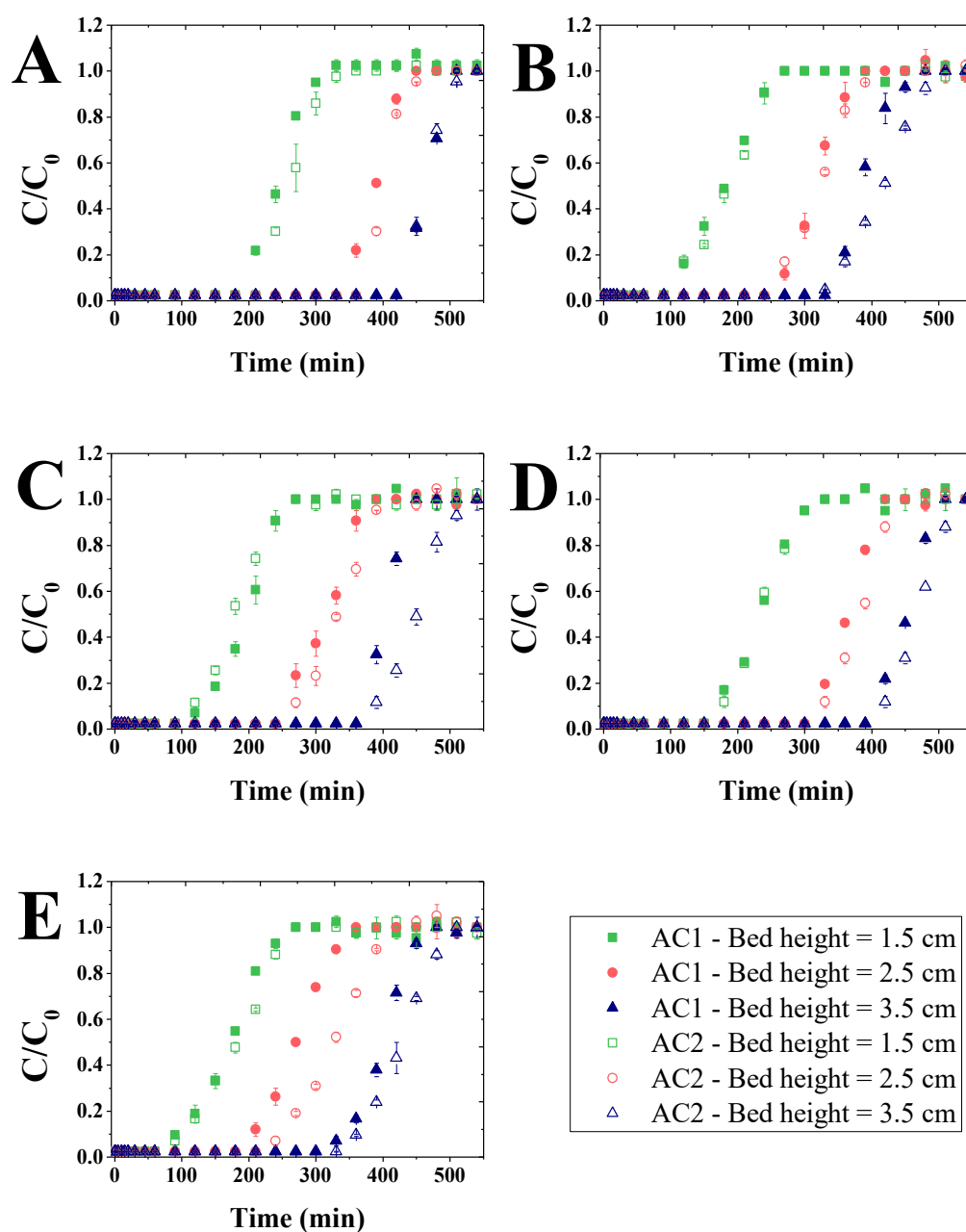


Figure 4. Breakthrough curves for adsorption of CAF (A), HTZ (B), SAC (C), SMX (D), and SUC (E) onto AC1 and AC2, at different bed heights (flow rate = 5 mL min⁻¹, $C_0 = 2$ mg L⁻¹, and upflow mode).

3.2.5. Effect of water composition on the breakthrough curve

The use of aqueous phases with greater compositional complexity than pure water is expected to be associated with lower adsorption of CECs (Sgroi *et al.* 2018), as found in our previous work, where reductions of q_{ads} ranging from 28.7% to 49.1% were observed for batch adsorption studies with the same CECs using WWTP effluent as water matrix (Diniz *et al.* 2023). In the present study, q_{ads} reductions of 56.5% and 63.3%, for AC1 and AC2, respectively, were observed (**Figure**

5, Table S11). In addition to impairing the q_{ads} values, the WWTP effluent also led to up to 90% reductions in the t_b and t_s values (Figure S5 for BTC shapes). In addition, the MTZ values were up to 3.2-fold higher in the adsorption studies using the WWTP effluent, compared to the use of water, indicating less efficient mass transport, probably due to the presence of organic matter, salts and other CECs in the solution.

The competition between organic matter and the CECs for the active sites of the AC can impair the removal of the CECs (Ling *et al.* 2020). As fixed-bed columns find applications in reuse water treatment plants, it becomes paramount to grasp the impact of varying water compositions on the adsorption potential of CECs. This understanding is crucial in developing the most efficient treatment protocol. By gaining insights into how different water compositions influence adsorption, we can better define and implement an optimized treatment strategy for effectively removing CECs

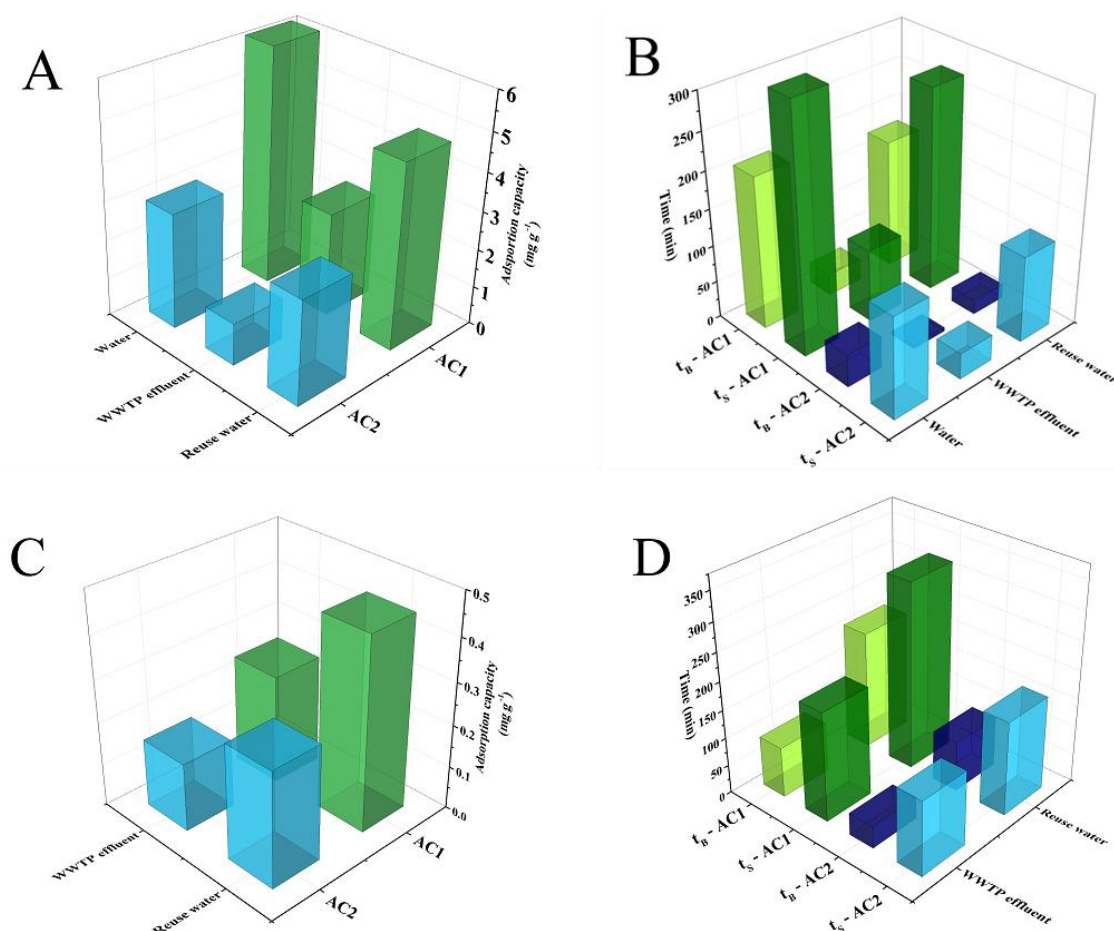


Figure 5. Adsorption capacity (sum of the adsorption capacities of the CECs) according to water composition (A and C). Breakthrough time (t_b) and saturation time (t_s) for the lowest adsorbed CEC (sucralose) (B and D). A and B: $C_0 = 2 \text{ mg L}^{-1}$ (see Table S11 for detailed values and Figure S5 for characteristic BTC shapes). C and D: $C_0 = 0.1 \text{ mg L}^{-1}$ (see Table S12 for detailed values and Figure S5 characteristic BTC shapes).

from the water, ensuring a sustainable and safe water reuse system. Therefore, effluent pretreatment can be a good alternative for increasing the useful lifetime and also the removal efficiency of fixed-bed columns loaded with AC. Reverse osmosis can reduce the organic matter and salts in wastewater by up to 99.9% (Lee *et al.* 2020), while photoperoxidation can decrease the levels of other CECs, as well as residual organic matter (Spina *et al.* 2021). In the present study, the WWTP effluent was pretreated with reverse osmosis and photoperoxidation (reuse water), then the results were compared to those experiments with WWTP effluent. When the experiments were performed with reuse water, an increase of up to 145.5% in the q_{ads} values was observed compared to the experiments with WWTP effluent. Meanwhile, the t_b and t_s values increased by up to 498.3% and 232.4%, respectively.

Diniz *et al.* (2023) reported $\mu\text{g L}^{-1}$ levels of CAF, HTZ, SAC, SMX and SUC in the effluent of a Brazilian WWTP that operates with an ultrafiltration membrane bioreactor. Therefore, studies considering that range of CECs concentration (C_0 of $100 \mu\text{g L}^{-1}$) was performed with the WWTP effluent and reuse water. The results also showed an increase in the q_{ads} , t_b and t_s values when reuse water was compared to WWTP effluent (Figure 5 and S6 and Table S12), which indicates that even at lower concentration levels, the pretreatment of the effluent can enhance the fixed-bed AC columns properties. For example, the q_{ads} values increased 76.6% and 68.5% for AC1 and AC2, respectively. The t_b and t_s values increased by 133.2% and 70.2%, respectively. Compared to the experiments at 2 mg L^{-1} , the t_b and t_s were 357.7% and 42.3%, respectively, longer at experiments with $100 \mu\text{g L}^{-1}$. However, the q_{ads} were 10.4 and 10.0 times lower in the experiments with $100 \mu\text{g L}^{-1}$ compared to those with 2 mg L^{-1} . At lower concentrations, the probability of a molecule reaching the active site of the AC is lower. Although q_{ads} , t_b and t_s values differed, the BTC shapes (Figures S5 and S6) were similar for all the CECs, indicating that the adsorption pattern remained similar even at different concentration levels. The present findings indicated that installing membrane filtration and oxidation processes after the biological treatment can enhance the useful lifetime and the adsorption potential of fixed-bed AC columns regardless of the inlet concentration.

3.3. In situ regeneration experiments

AC is considered a cost-effective material for the removal of organic contaminants from water. However, over time, AC gradually becomes saturated, due to occupation of the active sites by contaminants. At this point, the operation is no longer feasible, so the AC must be discarded (such as in a landfill) and replaced, or be regenerated (Larasati *et al.* 2021). Among the regeneration methods, chemical regeneration has several advantages, such as ease of operation, reduced downtime for

transporting the carbon, low effect on the adsorbent shape, and the possibility of recovering both the adsorbate and the regenerant solution (Guo *et al.* 2011; Cooney *et al.* 1983). Despite being widely studied between 1970 and 1990, there are still gaps in knowledge concerning *in-situ* regeneration, with the need to achieve more accurate representation of full-scale processes (Larasati *et al.* 2021). In addition, *in-situ* regeneration methods prevent fixed-bed columns from being dismantled for regeneration to be carried out elsewhere, reducing the costs related to the disposal of saturated AC. Therefore, in this study, evaluation was made of the use of five different solutions: water with pH adjustment (pH 2 and 10) or ethanol:water in different proportions (100:0; 10:90 and 50:50 v/v) for *in-situ* regeneration of the AC.

The results showed that the increase of the ethanol proportion favored the regeneration of the AC (**Figure 6**) (solution 3, ethanol > solution 2, ethanol:water 50:50 v/v > solution 1, ethanol:water 10:90 v/v), with a regeneration efficiency (RE) of 97.2% achieved with solution 3. It is also noteworthy that 150 mL of ethanol recovered the adsorption capacity of the AC bed after purifying 5,940 mL of solution contaminated with CECs, which indicates a 40x reduction in the volume of contaminated solution for disposal or treatment. Ethanol is also a well-known organic solvent that leads to efficient oxidation (Fiori *et al.* 2022). Therefore, the concentrated CECs could be degraded by electro-oxidation (Fiori *et al.* 2022), avoiding the disposal of the contaminated solution.

It is well-known that water is a weak regenerant, since most organic compounds have greater affinity for AC than for water (Pahl *et al.* 1973). Organic solvents (such as ethanol) can physically displace and solubilize CECs, consequently, enhancing their desorption and enabling regeneration of the AC (Martin and Ng 1985). Since most CECs interact with AC by electrostatic forces (Diniz *et al.* 2022; Rao *et al.* 2021; Gil *et al.* 2019), the pH of the regenerant solution should also affect RE. In this study, the pH 10 aqueous regenerant solution showed a 2.3-fold higher RE, compared to the pH 2 regenerant solution (Figure 6). At pH 10, most of the model CECs selected in this work are in their anionic form (Table S1), while the AC is negatively charged, leading to electrostatic repulsion of the adsorbate compounds. At pH 2, most of the CECs are in the zwitterionic form (Table S1), which reduced their electrostatic repulsion from the AC. In the previous study of our group (Diniz *et al.* 2023), it was observed that although electrostatic interactions influenced the adsorption of CAF, HTZ, SAC, SMX and SUC onto AC1 in batch studies, the adsorption was governed by chemisorption. These results corroborated the present findings, since the organic regenerant solution provided 1.7-fold higher RE, compared to the pH 10 regenerant solution.

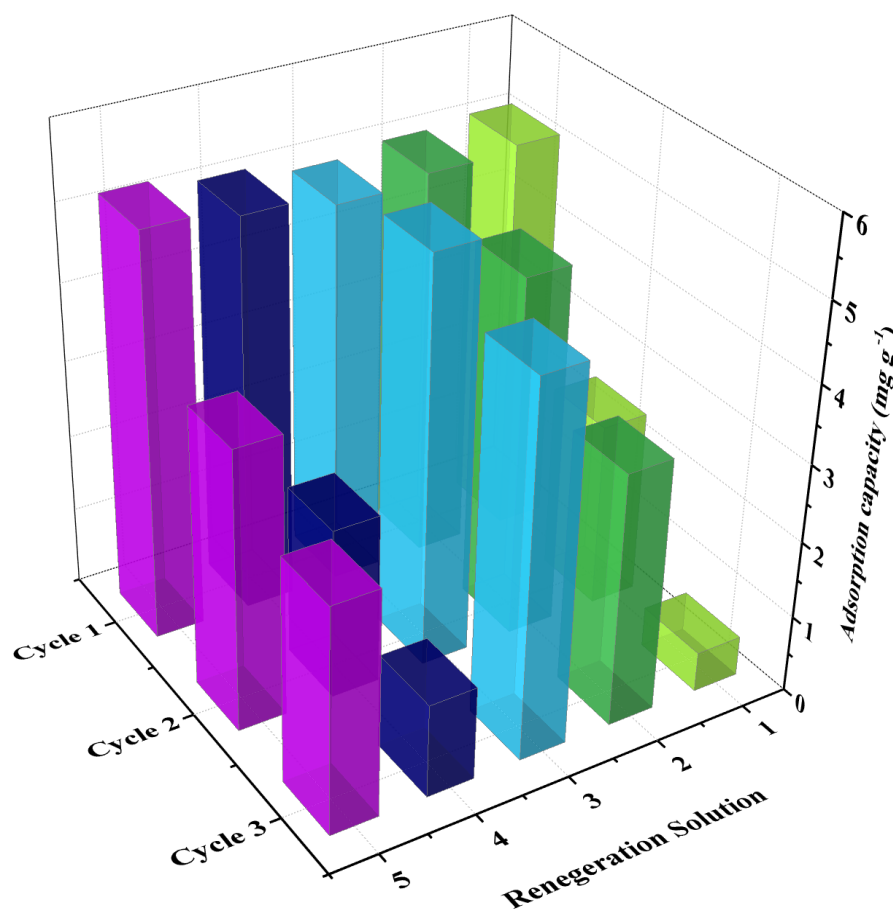


Figure 6. Evolution of adsorption capacity (sum of the adsorption capacities for the different CECs; see Table S13 for detailed values) according to the number of adsorption/regeneration cycles performed. Regenerant solutions: (1) ethanol:water, 10:90 v/v; (2) ethanol:water, 50:50 v/v; (3) ethanol; (4) water at pH 2; (5) water at pH 10.

Most studies evaluating the regeneration of AC with chemical solvents consider only one adsorbate, while real situations involve complex mixtures. In this study, the RE value differed for each CEC (Table S13), although RE could be higher for the overall process. For example, the adsorption capacity for SMX was 1.4-fold higher in the third cycle, compared to the first cycle, using ethanol (solution 3) as the regenerant solution, while the adsorption capacity for SUC decreased by 63.4% (Table S13). This could be explained by the higher adsorption potential for SMX, compared to SUC, as observed in the fixed-bed column studies (Section 3.2). Therefore, although the total adsorption capacity could be regenerated, or even enhanced, the removal of SUC was impaired. Hence, further *in-situ* regeneration studies should consider complex mixtures and the composition of

the aqueous matrix. SUC could be used as a marker compound for operational quality control since it is widely reported in WWTPs and has recalcitrant characteristics in adsorptive processes.

4. Conclusions

Research aiming at the development of advanced techniques to remove CECs from the aqueous phase is essential since these compounds are continuously released into the environment and are present in the composition of many aquatic matrices. Therefore, based on the results of the present study, the following conclusions can be drawn:

- Both ACs effectively removed CAF, HTZ, SAC, SMX and SUC in continuous flow mode. The removal order was equal for both ACs and was the following: CAF > SMX > HTZ = SAC > SUC.
- Increasing the bed height resulted in a longer useful lifetime of the fixed-bed columns and higher MTZ values, indicating deviations from ideal mass transport.
- Higher flow rates led to a shorter useful lifetime of the fixed-bed columns.
- In the downflow mode, the fixed-bed column loaded with AC2 showed preferential pathways, which reduced the HRT and, consequently, the useful lifetime and adsorption capacity of the column despite AC2 having a higher surface area than AC1.
- In the upflow, both ACs had similar adsorption parameters and HRTs, indicating that HRT played a crucial role in the adsorption of the CECs.
- The pretreatment (reverse osmosis + photoperoxidation) of the final effluent of the WWTP increased the adsorption capacity of the CECs and the useful lifetime of the fixed-bed column regardless of the inlet concentration.
- Among the regenerant solution tested, the in-situ regeneration with ethanol was capable of recovering the total adsorption capacity of the fixed-bed columns even after 3 cycles of adsorption/regeneration. However, the adsorption capacity of SUC decreased by 63.4%, indicating that the effectiveness of the regeneration varied among the adsorbates.

Further studies should investigate modifications on the surface of the AC, or the use of other innovative materials, to achieve satisfactory SUC removal. In addition to removing CECs, further studies should evaluate other water quality parameters to optimize its application in reuse water treatment plants. However, the results of the present work showed that upflow mode would be recommended for WWTPs since it depends mainly on the HRT. For those WWTPs that would

implement downflow mode, special attention must be given to forming preferential pathways due to the particle size of ACs. Further studies considering the variability of CECs should be performed regarding the regeneration of the fixed-bed column.

5. Acknowledgements

The authors are grateful for the financial support provided by the Brazilian public agencies São Paulo Research Foundation (FAPESP, INCTAA #2014/50951-4) and CNPq (INCTAA #465768/2014-8 and #304584/2021-5). A scholarship was awarded to V.D. by FAPESP (#2021/08123-0). The authors also thank SANASA (Sociedade de Abastecimento de Água e Saneamento, Campinas, São Paulo, Brazil) for collaboration in this study.

6. References

- Ahmed, M.J., Hameed, B.H., 2018. Removal of emerging pharmaceutical contaminants by adsorption in a fixed-bed column: A review. *Ecotoxicology and Environmental Safety* 149, 257-266. <https://doi.org/10.1016/j.ecoenv.2017.12.012>.
- Alves, P.D.C., Rodrigues-Silva, C., Ribeiro, A.R., Rath, S., 2021. Removal of low-calorie sweeteners at five Brazilian wastewater treatment plants and their occurrence in surface water. *Journal of Environmental Management* 289. <https://doi.org/10.1016/j.jenvman.2021.112561>.
- Borowska, E., Bourgin, M., Hollender, J., Kienle, C., McArdell, C.S., von Gunten, U., 2016. Oxidation of cetirizine, fexofenadine and hydrochlorothiazide during ozonation: Kinetics and formation of transformation products. *Water Research* 94, 350-362. <https://doi.org/10.1016/j.watres.2016.02.020>.
- Buerge, I.J., Poiger, T., Muller, M.D., Buser, H.R., 2003. Caffeine, an anthropogenic marker for wastewater contamination of surface waters. *Environmental Science & Technology* 37(4), 691-700. <https://doi.org/10.1021/es020125z>.
- Chatterjee, A., Schiewer, S., 2011. Biosorption of Cadmium(II) Ions by Citrus Peels in a Packed Bed Column: Effect of Process Parameters and Comparison of Different Breakthrough Curve Models. *Clean-Soil Air Water* 39(9), 874-881. <https://doi.org/10.1002/clen.201000482>.
- de Franco, M.A.E., de Carvalho, C.B., Bonetto, M.M., Soares, R.D., Feris, L.A., 2017. Removal of amoxicillin from water by adsorption onto activated carbon in batch process and fixed bed column: Kinetics, isotherms, experimental design and breakthrough curves modelling. *Journal of Cleaner Production* 161, 947-956. <https://doi.org/10.1016/j.jclepro.2017.05.197>.
- Cooney, D.O., Nagerl, A., Hines, A.L. 1983. Solvent regeneration of activated carbon. *Water Research* 14(4), 403-410. [https://doi.org/10.1016/0043-1354\(83\)90136-7](https://doi.org/10.1016/0043-1354(83)90136-7)
- Di Marcantonio, C., Chiavola, A., Gioia, V., Leoni, S., Cecchini, G., Frugis, A., Ceci, C., Spizziri, M., Boni, M.R. 2023. A step forward on site-specific environmental risk assessment and insight into the main influencing factors of CECs removal from wastewater. *Journal of Environmental Management* 325. <https://doi.org/10.1016/j.jenvman.2022.116541>
- Diniz, V., Cunha, D.G.F., Rath, S. 2023. Adsorption of recalcitrant contaminants of emerging concern onto activated carbon: A laboratory and pilot-scale study. *Journal of Environmental Management* 325 (Part A). <https://doi.org/10.1016/j.jenvman.2022.116489>
- Diniz, V., Rath, G., Rath, S., Araujo, L.S., Cunha, D.G.F. 2022. Competitive kinetics of adsorption onto activated carbon for emerging contaminants with contrasting physicochemical

properties. *Environmental Science and Pollution Research* 29, 42185-42200. <https://doi.org/10.1007/s11356-021-16043-2>

Fan, Y., Wang, B., Yuan, S.H., Wu, X.H., Chen, J., Wang, L.L., 2010. Adsorptive removal of chloramphenicol from wastewater by NaOH modified bamboo charcoal. *Bioresource Technology* 101(19), 7661-7664. <https://doi.org/10.1016/j.biortech.2010.04.046>.

Feizi, F., Sarmah, A.K., Rangisivek, R. 2021. Adsorption of pharmaceuticals in a fixed-bed column using tyre-based activated carbon: Experimental investigations and numerical modelling. *Journal of Hazardous Materials* 417. <https://doi.org/10.1016/j.jhazmat.2021.126010>

Fernandez-Andrade, K.J., González-Vargas, M.C., Rodríguez-Rico, I.L., Ruiz-Reyes, E., Quiroz-Fernández, L.S., Baquerizo, R.S., Rodríguez-Díaz, J.M., 2022. Evaluation of mass transfer in packed column for competitive adsorption of Tartrazine and brilliant blue FCF: A statistical analysis. *Results in Engineering* 14, <https://doi.org/10.1016/j.rineng.2022.100449>

Fiori, I., Santacruz, W., Dionision D., Motheo, A.J. 2022. Electro-oxidation of tetracycline in ethanol-water mixture using DSA-Cl₂ anode and stimulating/monitoring the formation of organic radicals. *Chemosphere* 308. <https://doi.org/10.1016/j.chemosphere.2022.136487>

Gil, A., Taoufik, N., Garcia, A.M., Korili, S.A. 2019. Comparative removal of emerging contaminants from aqueous solution by adsorption on an activated carbon. *Environmental Technology* 40(23), 3017-3030. <https://doi.org/10.1080/09593330.2018.1464066>

Guo, D., Shi, Q., He, B., Yuan, X. 2011. Different solvents for the regeneration of the exhausted activated carbon used in the treatment of coking wastewater. *Journal of Hazardous Materials* 186 (2-3), 1788-1793. <https://doi.org/10.1016/j.jhazmat.2010.12.068>

Hand, D.W., Crittenden, D.W., Crittenden, J.C., Thacker, W.E., 1984. Simplified Models for Design of Fixed-Bed Adsorption Systems. *Journal of Environmental Engineering* 110(2), 440-456. [https://doi.org/10.1061/\(ASCE\)0733-9372\(1984\)110:2\(440\)\)](https://doi.org/10.1061/(ASCE)0733-9372(1984)110:2(440))).

Hussein, M.S., Ahmed, M.J., 2016. Fixed bed and batch adsorption of benzene and toluene from aromatic hydrocarbons on 5A molecular sieve zeolite. *Materials Chemistry and Physics* 181, 512-517. <https://doi.org/10.1016/j.matchemphys.2016.06.088>.

Koshigoe, A.S.H., Diniz, V., Rodrigues-Silva, C., Cunha, D.G.F. 2023. Effect of three commercial algacides on cyanobacteria and microcystin-LR: implications for drinking water treatment using activated carbon. *Environmental Science and Pollution Research* 30, 16003–16016. <https://doi.org/10.1007/s11356-022-23281-5>

Langbehn, R.K., R.K., Michels, C., Soares, H.M., 2021. Antibiotics in wastewater: From its occurrence to the biological removal by environmentally conscious technologie. *Environmental Pollution* 215. <https://doi.org/10.1016/j.envpol.2021.116603>.

Larasati, A., Fowler, G.D., Graha, N.J.D. 2021. Insights into chemical regeneration of activated carbon for water treatment 9(4). <https://doi.org/10.1016/j.jece.2021.105555>

Lee, H.J., Halali, M.A., Baker, T., Sarathy, S., de Lannoy, C.F., 2020. A comparative study of RO membrane scale inhibitors in wastewater reclamation: Antiscalants versus pH adjustment. *Separation and Purification Technology* 240. <https://doi.org/10.1016/j.seppur.2020.116549>.

Lemus, J., Moya, C., Gilarranz, M.A., Rodriguez, J.J., Palomar, J., 2017. Fixed-bed adsorption of ionic liquids onto activated carbon from aqueous phase. *Journal of Environmental Chemical Engineering* 5(6), 5347-5351. <https://doi.org/10.1016/j.jece.2017.10.014>.

Liao, P., Zhan, Z.Y., Dai, J., Wu, X.H., Zhang, W.B., Wang, K., Yuan, S.H., 2013. Adsorption of tetracycline and chloramphenicol in aqueous solutions by bamboo charcoal: A batch and fixed-bed column study. *Chemical Engineering Journal* 228, 496-505. <https://doi.org/10.1016/j.cej.2013.04.118>.

- Ling, Y., Alzate-Sanchez, D.M., Klemes, M.J., Dichtel, W.R., Helbling, D.E., 2020. Evaluating the effects of water matrix constituents on micropollutant removal by activated carbon and beta-cyclodextrin polymer adsorbents. *Water Research* 173. <https://doi.org/10.1016/j.watres.2020.115551>.
- Malta, J.F., Nardocci, A.C., Razzolini, M.T.P., Diniz, V. Cunha, D.G.F. 2022. Exposure to microcystin-LR in tropical reservoirs for water supply poses high risks for children and adults. *Environmental Monitoring and Assessment* 194, 253. <https://doi.org/10.1007/s10661-022-09875-z>
- Margin, R.J., Ng, W.J. 1985. Chemical regeneration of exhausted activated carbon—II. *Water Research* 19(12), 1527-1535. [https://doi.org/10.1016/0043-1354\(85\)90398-7](https://doi.org/10.1016/0043-1354(85)90398-7)
- Nazari, G., Abolghasemi, H., Esmaili, M., Pouya, E.S., 2016. Aqueous phase adsorption of cephalixin by walnut shell-based activated carbon: A fixed-bed column study. *Applied Surface Science* 375, 144-153. <https://doi.org/10.1016/j.apsusc.2016.03.096>.
- Pahl, R.H., Mayhan, K.G., Bertrand, G.L. 1973. Organic desorption from carbon—II. The effect of solvent in the desorption of phenol from wet carbon. *Water Research* 7(9), 1309-1322. [https://doi.org/10.1016/0043-1354\(73\)90008-0](https://doi.org/10.1016/0043-1354(73)90008-0)
- Pasquini, C., Faria, L.C. 1987. Flow-injection determination of ammonia in Kjeldahl digests by gas diffusion and conductometry, *Analytic Chimica Acta*, 193, 19-27. [https://doi.org/10.1016/S0003-2670\(00\)86134-6](https://doi.org/10.1016/S0003-2670(00)86134-6)
- Peteffi, G.P., Fleck, J.D., Kael, I.M., Girardi, V., Bundchen, R., Krajewski, D.M., Demoliner, M., Silva, F.P., da Rosa, D.C., Antunes, M.V., Linden, R., 2018. Caffeine levels as a predictor of Human mastadenovirus presence in surface waters-a case study in the Sinos River basin-Brazil. *Environmental Science and Pollution Research* 25(16), 15774-15784. <https://doi.org/10.1007/s11356-018-1649-3>.
- Pivetta, R.C., Rodrigues-Silva, C., Ribeiro, A.R., Rath, S., 2020. Tracking the occurrence of psychotropic pharmaceuticals in Brazilian wastewater treatment plants and surface water, with assessment of environmental risks. *Science of the Total Environment* 727. <https://doi.org/10.1016/j.scitotenv.2020.138661>.
- Porto, R.S., Rodrigues-Silva, C., Schneider, J., Rath, S., 2019. Benzimidazoles in wastewater: Analytical method development, monitoring and degradation by photolysis and ozonation. *Journal of Environmental Management* 232, 729-737. <https://doi.org/10.1016/j.jenvman.2018.11.121>.
- Rao, A., Kumar, A., Dhodapkar, R., Pal, S. 2021. Adsorption of five emerging contaminants on activated carbon from aqueous medium: kinetic characteristics and computational modeling for plausible mechanism. *Environmental Science and Pollution Research* 28, 21347-21358. <https://doi.org/10.1007/s11356-020-12014-1>
- Rodriguez-Narvaez, O.M., Peralta-Hernandez, J.M., Goonetilleke, A., Bandala, E.R., 2017. Treatment technologies for emerging contaminants in water: A review. *Chemical Engineering Journal* 323, 361-380. <https://doi.org/10.1016/j.cej.2017.04.106>.
- Rohwedder, J.R.R., Pasquini, C. 1991. Differential conductimetry in flow injection. Determination of ammonia in Kjeldahl digests. *Analyst* 116, 841-845. <https://doi.org/10.1039/AN9911600841>
- Sancho, J.L.S., Rodriguez, A.R., Torrellas, S.A., Rodriguez, J.G., 2012. Removal of an emerging pharmaceutical compound by adsorption in fixed bed column. *Desalination and Water Treatment* 45(1-3), 305-314. <https://doi.org/10.1080/19443994.2012.692062>.
- Sgroi, M., Anumol, T., Roccato, P., Vagliasindi, F.G.A., Snyder, S.A., 2018. Modeling emerging contaminants breakthrough in packed bed adsorption columns by UV absorbance and fluorescing components of dissolved organic matter. *Water Research* 145, 667-677. <https://doi.org/10.1016/j.watres.2018.09.018>.

Spina, M., Venancio, W., Rodrigues-Silva, C., Pivetta, R.C., Diniz, V., Rath, S., Guimaraes, J.R., 2021. Degradation of antidepressant pharmaceuticals by photoperoxidation in diverse water composition: a highlight in the evaluation of acute and chronic toxicity. *Environmental Science and Pollution Research*. <https://doi.org/10.1007/s11356-020-11657-4>.

Stephenson, R., Sheridan, C., 2021. Review of experimental procedures and modelling techniques for flow behaviour and their relation to residence time in constructed wetlands. *Journal of Water Process Engineering* 41. <https://doi.org/10.1016/j.jwpe.2021.102044>

Wang, Z.Y., Yu, X.D., Pan, B., Xing, B.S., 2010. Norfloxacin Sorption and Its Thermodynamics on Surface-Modified Carbon Nanotubes. *Environmental Science & Technology* 44(3), 978-984. <https://doi.org/10.1021/es902775u>.

WHO, 2017. Potable reuse: Guidance for producing safe drinking-water. p. 152.

3.1.3. Synthesis and characterization of TiO₂-carbon filter materials for water decontamination by adsorption-degradation processes

Vinicius Diniz^{1,2*}, Colin R Crick², Susanne Rath¹

¹ Department of Analytical Chemistry, Institute of Chemistry, University of Campinas. Address: Rua Josué de Castro s/n. Zip Code 13083-970. Cidade Universitária, Campinas, SP, Brasil.

² School of Engineering and Materials Science, Queen Mary University of London, Mile End Road, E1 4NS, London, UK.

*Author for correspondence: viniciusdiniz994@gmail.com

Abstract

Wastewater treatment is becoming ever more challenging due to the increasing levels of molecular pollutants that are challenging for existing approaches. Innovative materials are required to help produce potable water from heavily contaminated water sources. One such material is titanium dioxide-activated carbon (TiO_2/AC) heterostructures, which combine the photocatalytic properties of TiO_2 with the adsorption properties of the ACs. To date, studies on TiO_2/AC heterostructures for real-world water purification have yet to be performed. This study aimed to address this gap by comparing the effectiveness of titanium isopropoxide ($\text{Ti}(\text{OiPr})_4$) and titanium butoxide ($\text{Ti}(\text{OBu})_4$) for synthesizing TiO_2/AC heterostructures using four different methods (sol-gel, solvothermal, and microwave-assisted hydrothermal methods [x2]). The prepared heterostructures were compared with commercial TiO_2 materials for their ability to degrade five small molecule contaminants (caffeine, hydrochlorothiazide, saccharin, sulfamethoxazole, and sucralose). Hydrochlorothiazide and sulfamethoxazole were demonstrated to be rapidly degraded by UV-C irradiation within 15 min. Caffeine, saccharin, and sucralose were less susceptible to UV degradation. All the elaborated TiO_2/AC heterostructures consisted of pure anatase phase, with $\text{Ti}(\text{OBu})_4$ syntheses generating larger average crystal sizes and lower surface areas. Sol-gel preparations produced the most effective TiO_2/AC heterostructures due to their high surface area. Compared with the commercial TiO_2 , the heterostructures enhanced the photocatalytic activity of TiO_2 by up to 10.0 times. Also, the heterostructures remained effective at environmentally relevant conditions (i.e., concentration of the contaminant and water matrices). The reuse of the materials was tested and showed no reduction in efficiency after four removal/regeneration cycles. Overall, this study presents novel TiO_2/AC heterostructures with increased photocatalytic efficiency that can serve as an efficient material for removing contaminants at large scales (e.g., water treatment plants).

Keywords: Adsorption, Photocatalysis; Sol-gel; Solvothermal; Titania alkoxide, Water treatment

1. Introduction

The World Health Organization (WHO) states that potable reuse is a realistic and practical drinking water source to accommodate the projected 33% population increase between 2014 and 2050 (1). Nonetheless, potable reuse comes with several challenges, including (i) poor-quality wastewater sources containing a wide range of chemical contaminants, (ii) the requirement of complex treatment processes within limited spatial constraints, (iii) reduced public acceptance, and (iv) the severe consequences of potential failures. Although the acceptance of potable reuse (challenge (i)) remains low (2), an increase has been observed in the last few years (3, 4). Challenge (iv) can be addressed by integrating monitoring control, reliable treatment trains, and engineered storage buffers, allowing water suppliers the time to detect and respond to faults (1). Challenges (ii) and (iii) are interrelated and must be addressed conjointly. In this way, various schemes for potable reuse treatment plants (PRTPs) have been proposed in the literature or have been employed in real-scale treatment plants (5). However, in low-income countries, these schemes often entail complex engineering buildings and high-costs. Therefore, innovative solutions in materials science are needed to address these challenges, minimizing the energy and environmental footprint of cities and ensuring a resilient and safe water supply (6).

A typical PRTP consists of a conventional wastewater treatment plant, a membrane filtration unit, an advanced oxidation process (AOP) unit, and an adsorption unit (1). While incorporating a membrane filtration unit in PRTPs is almost mandatory to ensure process robustness (7, 8), combining the AOP and adsorption units can enhance the oxidation properties of oxidizers (9) and reduce the energy consumption of PRTPs (10). Although heterogeneous photocatalysis is considered a due process for water treatment (11), a sufficient contact time between the contaminant and the photocatalyst (typically titanium dioxide (TiO_2)) is required for optimum photocatalysis efficiency. This is due to the limited migration of oxidant species from the active centers of the photocatalyst, resulting in virtual surface-bound reactions (12). In contrast, using activated carbon (AC) as a support for photocatalysts increases the photodegradation rate by allowing increased contaminants exposure to the photocatalyst through adsorption. Additionally, this approach provides an effective way to recover the photocatalyst from the water matrix (13). Moreover, ACs are low-cost materials with high surface area and are a good way of valorizing carbonaceous waste (14).

Different synthesis methods for preparing TiO₂/AC heterostructures have been proposed in the scientific literature (14-16), and it is clear that the properties of these materials depend on the chosen synthesis method. Generally, sol-gel methods require high-temperature activation to yield a photoactive anatase phase (which has the highest bandgap of 3.5 eV (11) among TiO₂ crystalline phases (17)); solvothermal methods employ low-temperature activation; and microwave-assisted methods allow faster synthesis due to their they rapid heating rates (18), which can be combined with hydrothermal methods that are environmentally friendly methods for synthesizing TiO₂ nanoparticles (16, 19). Regarding titania precursor, titanium tetrachloride (TiCl₄), titanium isopropoxide (Ti(OiPr)₄), and titanium butoxide (Ti(OBu)₄) are commonly used alkoxides as titanium sources, but TiCl₄ hydrolyzes rapidly due to high moisture activity of the air (20). To the best of our knowledge, a detailed comparative study of the performance of TiO₂/AC heterostructures elaborated by different synthesis methods and using different titania precursors have yet to be performed for the photodegradation of organic contaminants. Also, the adsorption-degradation performance of these materials in real water matrices is yet to be investigated (21). In this work, (i) four different synthesis methods (one sol-gel, one solvothermal, and two microwave-assisted hydrothermal methods) using two different titania precursors (Ti(OBu)₄ and Ti(OiPr)₄) were tested for elaborating TiO₂/AC heterostructures using a commercially available AC as support for the TiO₂ photocatalyst; (ii) the resulting materials were fully characterized and tested for the photodegradation of organic contaminants of great interest (caffeine (CAF), hydrochlorothiazide (HTZ), saccharin (SAC), sulfamethoxazole (SMX), and sucralose (SUC)), previously defined in a study by our group (7) under relevant environmental conditions; (iii) the results were compared with commercially available TiO₂ photocatalysts (P25 and PC500); (iv) degradation products of individual organic contaminants were screened; (v) the reusability of the heterostructures was investigated employing different regeneration methods (UV-C + water and UV-C).

2. Experimental section

2.1. Materials

The granular AC (Charbon500, 12 × 24 mesh) was purchased from Carbonado, Brazil. Titanium tetrabutoxide (Ti(OBu)₄; ≥97%) and titanium isopropoxide (Ti(OiPr)₄; ≥97%) were used as titania precursors, both were supplied by Sigma Aldrich (USA). Titanium (IV) oxide (TiO₂) Aeroxide® P25 (average particle size of 30 nm, 80% wt. anatase and 20% wt.

rutile crystalline phases) and CristalACTiV™ PC-500 (average particle size of 8 nm, ~99% wt. anatase crystalline phase, 100% anatase on its surface) were purchased from Evonik (Germany) and Tronox (USA), respectively. CAF (99%), Caffeine-d3 (99.0%), HTZ (99.7%), SAC (99.6%), SMX ($\geq 99.0\%$), and SUC (99.4%) were purchased from Sigma-Aldrich (USA). Methanol, ethanol, isopropanol, and formic acid (analytical standard) were purchased from J.T. Baker (USA), Labsynth (Brazil), and Merck (USA), respectively. Polytetrafluoroethylene (PTFE) was purchased from Sigma-Aldrich (USA). Ultrapure water was obtained from a Milli-Q purification system (Millipore, USA). UV-A light (8 W power “Nards BLB T5”, $\lambda_{\text{max}} = 320$ nm), UV-C light (16 W power, Philips TUV G16T5, $\lambda_{\text{max}} = 254$ nm), and UV-C light (8 W power, Philips TUV G8T5, $\lambda_{\text{max}} = 254$ nm) were used throughout the studies. The photonic fluxes of 0.54 J s^{-1} for the UV-A light and 1.59 J s^{-1} and 130 J s^{-1} for the 8W and 16 W UV-C light, respectively, were determined in previous studies of our group (22-24).

2.2. Photodegradation of the organic contaminants

2.2.1. Studies using commercial TiO_2

The experiments were conducted using an apparatus previously described by our group (11). Briefly, the system consists of: (i) a 1.0 L jacketed cylindrical glass vessel ($h = 39$ cm, $d_{\text{internal}} = 10$ cm); (ii) a peristaltic pump promoting fluid recirculation for temperature control (always set as 25°C); and an inner concentric quartz tube with sealed base housing the UV lamp. All the experiments were conducted using ultrapure water (resistivity $< 18.2 \text{ M}\Omega \text{ cm}$) with a natural pH (of 6.8).

For all photodegradation experiments, the initial concentration of CAF, HTZ, SAC, SMX, and SUC was set as 2 mg L^{-1} , but the actual concentration was measured at the beginning of each experiment for quality control. The removal of the contaminants was assessed using different reaction conditions: i) adsorption (presence of catalyst (P25 or PC500) and no light); (ii) direct photolysis (no catalyst and presence of UV light (UV-A (8W), UV-C (8W or 16W))); (iii) hydrolysis (no light and no catalyst); and (iv) photocatalysis (presence of catalyst and light). The process was investigated by changing the photocatalyst loading (10, 25, and 50 mg L^{-1}), catalyst type (P25 or PC500), and initial concentration of contaminants (250, 500, 1,000, and $2,000 \mu\text{g L}^{-1}$). All experiments were performed in duplicates.

Analytical determination of contaminants was performed using ultra-high performance liquid chromatography coupled to tandem mass spectrometry (UHPLC-MS/MS)

(Waters, USA). An electrospray ionization source and a triple-quadrupole mass detector (Xevo TQD spray, Waters) were used for the ionization of the analytes and detection and quantification, respectively. An ACQUITY UPLC® CSH C18 column (130 Å, 1.7 µm, 2.1 mm x 100 mm; Waters, USA) was used for chromatographic separation, which was performed using isocratic elution mode (40:60, water with 0.1% of formic acid:methanol,) at 0.3 mL min⁻¹, with an injection volume of 10 µL. Software MassLynx v. 4.1 was used for data acquisition. Characteristic chromatograms are shown in Figure S1.

2.2.2. Degradation products

For the investigation of degradation products, each contaminant (initial concentration of 10 mg L⁻¹) was subject to UV-light irradiation (UV-C, 8 W) in the presence of 25 mg L⁻¹ of PC500 for 60 min. At different intervals (0, 1, 5, 10, 15, 20, 30, 45, and 60 min), volumes of 800 µL were sampled from the reaction medium, spiked with an internal standard (CAF-d₃, 200 µL), and then filtered using 0.2 µm PTFE syringeless filters.

The intermediate products were identified by liquid chromatography coupled to high-resolution mass spectrometry. The electrospray ionization source, operating in both positive and negative modes, was used for ionizing the target analytes. An Orbitrap Thermo Q-Exactive (Thermo Scientific) was used as a mass analyzer. Experimental data were collected in the *m/z* range from 50 to 1000, employing a full scan analysis of 0.1 s and a collision energy of 30 eV. The mobile phase was the same as employed in the analytical determination of the model contaminants.

2.3. Synthesis of TiO₂/AC heterostructures

Four different synthesis methods (Table 1) were investigated for the elaboration of the TiO₂/AC heterostructures. In all synthesis methods, 10% (m/m) of TiO₂ was anchored in the AC, aiming for a balance between photocatalytic and adsorption processes (25, 26).

2.3.1. Sol-gel method

For the sol-gel synthesis, 3.4 mL of Ti(OiPr)₄ or 3.9 mL of Ti(Obu)₄ were added to isopropanol (QSP) to a final volume of 50 mL while undergoing vigorous stirring. The solutions were stirred continuously for 60 min or until the whitish color disappeared (15). Then, 2 mL of nitric acid (1 mol L⁻¹) was added, and the solutions were subjected to 30 min of sonication. The resulting gels were mixed with 8 g of AC using an overhead stirrer for 1 h. The

final solution was then dried at 80 °C for 60 min and calcined at 400 °C for 4 h. Depending on the titania precursor used, the elaborated materials were labeled as shown in **Table 1**.

Table 1: Summary of the synthesis method, titania precursor and labeled code of the TiO₂/AC heterostructures.

Synthesis method	Titania precursor	Code
Sol-gel	Titanium isopropoxide (Ti(OiPr) ₄)	SGIP
	Titanium butoxide (Ti(Obu) ₄)	SGIB
Solvothermal	Titanium isopropoxide (Ti(OiPr) ₄)	STIP
	Titanium butoxide (Ti(Obu) ₄)	STIB
Microwave assisted hydrothermal I	Titanium isopropoxide (Ti(OiPr) ₄)	MWIP-I
	Titanium butoxide (Ti(Obu) ₄)	MWIB-I
Microwave assisted hydrothermal II	Titanium isopropoxide (Ti(OiPr) ₄)	MWIP-II
	Titanium butoxide (Ti(Obu) ₄)	MWIB-II

2.3.2. Solvothermal method

For the solvothermal synthesis, a suspension of 2 g of AC in 45 mL of ethanol (A1), a solution consisting 0.8 mL of Ti(OiPr)₄ or 1.0 mL of Ti(Obu)₄ in 15 mL of ethanol (B1), and a solution consisting 3 mL of ultrapure water in 15 mL of ethanol (C1) were prepared. Then, solution B1 was added to solution A1 under continuous stirring, followed by gradual dropwise addition of solution C1 to facilitate the hydrolysis of the titania precursor. The resulting mixtures were stirred for 5 min, transferred to a crucible, and heated at 160 °C for 3 h. The resulting solid was separated by centrifugation (3,300 RCF, 10 min) and washed once with ethanol and three times with ultrapure water. Depending on the titania precursor used, the elaborated materials were labeled as shown in Table 1.

2.3.3. Microwave-assisted hydrothermal methods

2.3.3.1. Microwave-assisted hydrothermal method I

For the microwave-assisted hydrothermal method I, 500 mg of AC were suspended in 30 mL of ethanol and added to a solution containing 0.2 mL of Ti(OiPr)₄ in 9.8 mL of ethanol or 0.25 mL of Ti(Obu)₄ in 9.75 mL of ethanol, all while undergoing continuous stirring. Then, a solution consisting of 0.65 mL of ultrapure water in 9.45 mL of ethanol was gradually dropwise incorporated, with continuous stirring maintained for 5 min. The final mixtures were then transferred into a 100 mL Teflon-lined reactor (Ethos 1, Milestone, Italy), which was placed inside an SK-15 Microwave Digestion Rotor (Milestone, Italy). The synthesis was performed setting 80 °C as a constant temperature (600 W) for 30 min. The resulting materials

were finally separated and washed as described in section 2.3.2. Depending on the titania precursor used, the elaborated materials were labeled as shown in Table 1.

2.3.3.2. Microwave-assisted hydrothermal method II

For the microwave-assisted hydrothermal method II, 4 g of AC were mixed with 1.7 mL of $\text{Ti}(\text{OiPr})_4$ or 1.9 mL of $\text{Ti}(\text{OBu})_4$, alongside water (23.3 mL for $\text{Ti}(\text{OiPr})_4$ and 23.1 mL for $\text{Ti}(\text{OBu})_4$), all while maintaining continuous stirring for 2 h at room temperature. The final mixtures were then transferred into a 100 mL Teflon-lined reactor (Ethos 1, Milestone, Italy), which was placed inside an SK-15 Microwave Digestion Rotor (Milestone, Italy) for further synthesis, conducted under the same conditions outlined in section 2.3.2.1. Depending on the titania precursor used, the elaborated materials were labeled as MWIP-II ($\text{Ti}(\text{OiPr})_4$) and MWIB-II ($\text{Ti}(\text{OBu})_4$).

2.4. Characterization of the TiO_2/AC heterostructures

The TiO_2/AC heterostructures were characterized by adsorption/desorption isotherms of nitrogen at 77 K, using a mercury porosimeter PoreMaster (Quantachrome) and surface area analyzer NOVA 4200e (Quantachrome). Previously to the analysis, the materials were degassed at 150 °C under a vacuum chamber for 24 h. The structural, morphological, and chemical composition were conducted using scanning electron microscopy (SEM) and energy-dispersive X-ray spectroscopy (EDX) on a field-emission scanning microscope (Jeol J6360 LV). Thermogravimetric analyses were carried out in a TGA-2950 (TA instruments) with a heating ratio of 10 °C min⁻¹ under an inert atmosphere. The determination of the mass of TiO_2 anchored to the AC was performed by weighing the materials before and after the synthesis. Controls were employed (AC without titania precursor) in each synthesis method.

X-ray diffraction (XRD) spectra of the materials were acquired using an XRD-7000 (SHIMADZU) diffractometer utilizing a copper anode ($\text{K}\alpha$ radiation). The Raman Confocal Raman spectroscopy studies were carried out with a 785 nm laser (1 to 500 mW, Cobalt, mode 08-011) operating with a 100 μm spot. Control and data acquisition were managed through the computational program Solis (Andor/Oxifor Andor Solis 64-bit). Prior to Raman analysis, pellets were prepared by mixing the materials (300 mg) with PTFE powder having a particle size of 1 μm (300 mg) and subsequently pressing the mixture for 5 minutes at a pressure of 5 kN.

2.5. Photocatalytic performance of the TiO₂/AC heterostructures

The photocatalytic activity of each TiO₂/AC heterostructure was evaluated for the photodegradation of CAF, HTZ, SAC, SMX, and SUC under UV-C (Philips TUV G16T5, $\lambda_{\text{max}} = 254 \text{ nm}$, 8 W) irradiation. The photodegradations were conducted using a procedure previously described by our group (11). In a typical experiment, the concentration of the photocatalyst was set as 25 mg L⁻¹, and the concentration of each contaminant was theoretically fixed as 2 mg L⁻¹. All the experiments were conducted using ultrapure water (resistivity < 18.2 M Ω cm) with a natural pH (of 6.8). Finally, the photocatalytic experiments were carried out for 1 h under UV light irradiation. Each experiment was performed in duplicate. At different irradiation intervals, samples were collected, as described in section 2.2.1. The quantification of the model contaminants was performed by UHPLC-MS/MS as previously described.

SGIP was also tested under environmentally relevant conditions (contaminants concentration and reclaimed water). For detailed information on the reclaimed water composition and LC-UHPLC-MS/MS analytical method employed in these analyses, see the previous study of our group (7).

2.5.1. Regeneration measurements

The regeneration of the SGIP heterostructure was investigated by two different methods, each involving four cycles of removal/regeneration. Briefly, following each cycle, the material was isolated from the solution through filtration. Then, regeneration was performed either by stirring it for 30 min in 100 mL of ultrapure water while simultaneously being exposed to UV-C irradiation or solely by subjecting it to UV-C irradiation without any stirring or ultrapure water. The regenerated materials were then dried at 60 °C for 60 min, and a new photodegradation cycle was started in the same manner as described in section 2.5.

3. Results and discussion

3.1. Studies using commercial TiO₂

The investigation into the hydrolysis of contaminants without UV irradiation or photocatalyst revealed negligible effects within 60 min (Figure S2 A). Besides, although PC500 has a 3.5x higher specific surface area (SSA) than P25, the adsorption of the contaminants on both materials was similar (around 10%) and reached an apparent equilibrium after 15 min of stirring (Figure S2 B and C).

On the other hand, UV-C promoted higher photolysis of the contaminants than UV-A. For example, no photolysis was observed under UV-A irradiation for any contaminants for 60 min. Conversely, UV-C (8 W) almost totally photodegraded HTZ and SMX after 15 min of irradiation (Figure S2 D and E). UV-A lights emit lower energy than UV-C lights due to their longer wavelengths, affecting their ability to degrade organic pollutants. In addition, for all contaminants tested, the UV-C emission wavelength (254 nm) did overlap with their typical absorption spectra, resulting in photolysis. No variance was observed when comparing UV-C light wattages (8 W vs. 16 W) (Figure S2), prompting the choice of the more energy-efficient 8 W UV-C light for subsequent studies.

The content of anatase is positively correlated with the photocatalytic activity of a photocatalyst, but synergistic effects due to the presence of different polymorphs might increase photodegradation properties (27). Therefore, a comparison of P25 (80% anatase and 20% rutile) and PC500 (100% anatase) was performed while considering variations in photocatalyst loading and initial concentration of the contaminants. For both P25 and PC500, HTZ and SMX were almost instantaneously photodegraded regardless of the photocatalyst loading or initial concentration of the contaminant (Figures S3 and S4, respectively). The type or loading of photocatalyst also had negligible impacts on the photodegradation of CAF, achieving nearly 100% photodegradation within 20 min of irradiation. However, the lower the initial concentration of CAF, the faster the concentration of CAF went below the limit of quantification ($10 \mu\text{g L}^{-1}$) (Figure S5).

On the other hand, it was observed that PC500 induced a faster photodegradation of SAC (Figure S6) and SUC (**Figure 1**), but photocatalyst loadings higher than 25 mg L^{-1} did not increase the photodegradation rate. Also, for SAC and SUC, lower initial concentrations correlated with accelerated photodegradation rates, with PC500 consistently inducing the highest degradation rate for both compounds. These results corroborate those of Caianelo et al. (11), who observed that PC500 led to a higher photodegradation of the antimicrobial gatifloxacin (initial concentration of 0.5 mg L^{-1}) than P25.

It is reported in the literature that two major factors impact the efficiency of TiO_2 -photocatalysts: (i) the adsorption of contaminant on the surface of the photocatalyst and (ii) the presence of active surface species that can oxidize molecules (28). Therefore, the adsorption of CAF, SAC, and SUC onto P25 and PC500 would directly influence the removal efficacy of these contaminants by the TiO_2 nanoparticles. Within the pH range used in the present study

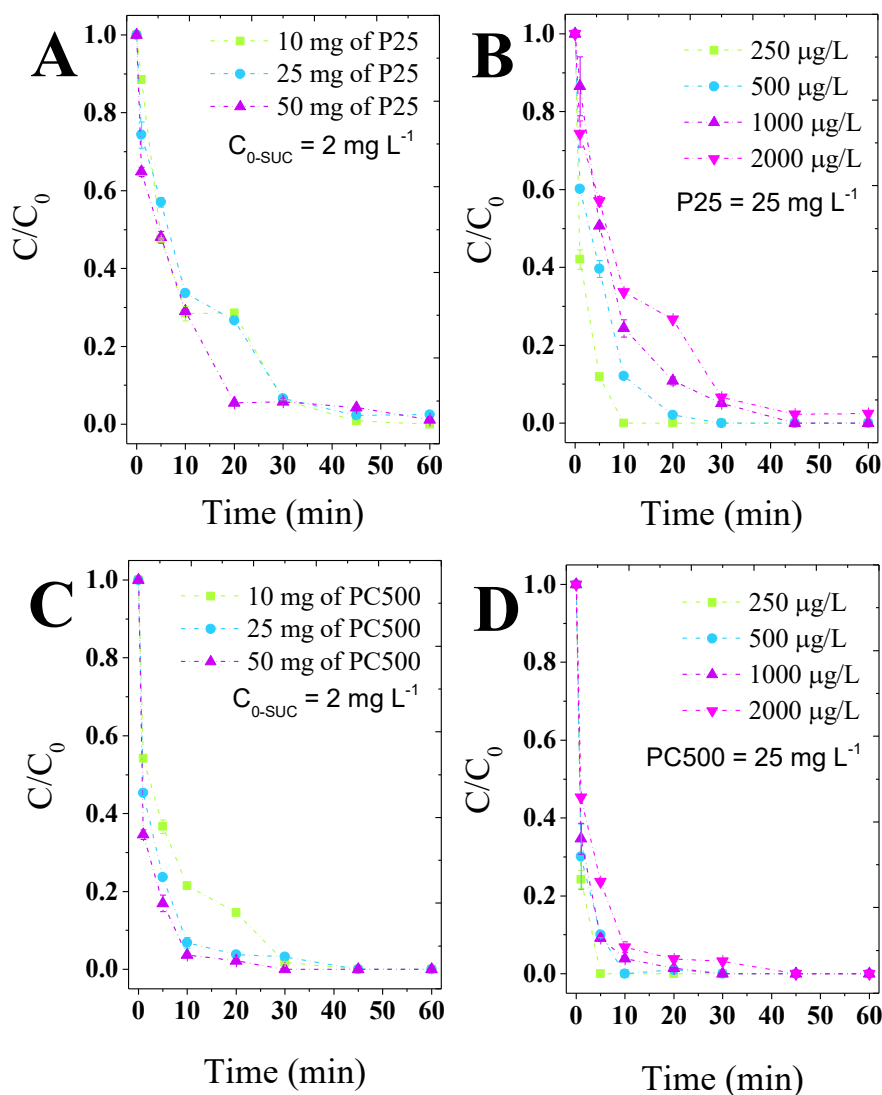


Figure 1: Photodegradation of sucralose by photocatalysis using $\text{TiO}_2\text{-P25}$ (A and B) and $\text{TiO}_2\text{-PC500}$ (C and D). $C_{0\text{-SUC}}$: initial concentration of sucralose.

(i.e., 6.8), it is anticipated that hydrogen bonds (7) between CAF, SAC, and SUC and water molecules on the adsorbed TiO_2 surface are expected to govern the adsorption (28). CAF exhibited the highest adsorption on both TiO_2 (Figure S2), which corroborates the previous findings (7) that have compared the adsorption of these three contaminants by activated carbon. The highest adsorption of CAF aligns with the higher degradation of this contaminant by PC25 and PC500 compared to SAC and SUC (Figure 1, S5, and S6). On the other hand, although SUC exhibited higher adsorption compared to saccharin (Figure S2), their removal was similar (Figure 1 and S6), probably due to low degradation of sucralose by HO^\cdot radicals (29).

Although TiO_2 led to almost 100% photodegradation of the contaminants, it is well-reported that degradation products can also be generated (11). In the present study, the most

common degradation products of CAF (30-32), HTZ (33-35), SAC (36), SMX (37-41), and SUC (36, 42, 43) were scanned using high-resolution mass spectrometry. Those identified with an error lower than 5 ppm (44) have been compiled in Table S1. Briefly, three degradation products of CAF were still present in the solution after 60 min of irradiation (e.g., $C_7H_{10}N_4O_3$, $C_5H_6N_2O_3$, and $C_3H_6N_2O_2$) (Figure S7-A, B, and C), being $C_3H_6N_2O_2$ the one with the highest relative area ($\text{area}_{\text{degradation product}}/\text{area}_{\text{internal standard}}$) among them. Regarding SAC and SMX, only one degradation product of each compound was identified in the solution after 60 min of irradiation ($C_7H_7NO_6S$ (Figure S7-D) and $C_4H_8N_2O_3$ (Figure S7-E), respectively). No-degradation products of HTZ were identified after 20 min of irradiation, and no degradation products of SUC were identified after 45 min. Further studies should investigate the mineralization of these contaminants by heterogeneous photocatalysis.

Photocatalysts have been extensively investigated for the photodegradation of various contaminants on a laboratory scale (11, 45). However, the application of TiO_2 -based photocatalysis on real-world scales still faces significant challenges, such as low adsorption of organic pollutants, difficult recovery of the photocatalyst from effluents, potential aggregation at the nanoscale, and the formation of undesired degradation products (46). Anchoring TiO_2 photocatalysts onto support materials has emerged as a promising strategy to overcome these limitations (47). Therefore, the present study investigated different synthetic methods for anchoring TiO_2 onto AC.

3.2. Characterization of TiO_2 /AC heterostructures

Table 2 summarizes the TiO_2 content of the different elaborated heterostructures, showing values in line with the expected nominal content across different synthetic methods. All the XRD spectra of the heterostructures had the characteristic peaks of the anatase phase (2θ of 25.2° , 37.7° , and 47.9° (48)) (Figure S8). On the other hand, peaks at 2θ of 27.2° and 37.7° attributed to the rutile phase were only observed in the P25 photocatalyst, which was anticipated from the specifications of the manufacturer. The lack of a rutile crystalline phase on the heterostructures can be attributed to the temperature-controlled methods employed in the present study, which avoids further crystallization of anatase into rutile (49). The average crystal size (D, **Table 2**) was calculated from Scherrer's equation applied to the most intense peak of anatase. The crystal sizes of TiO_2 in sol-gel heterostructures (SGIP and SGIB) were smaller compared to the other synthesis methods. Besides, $Ti(OBu)_4$ induced the formation of larger crystal sizes than $Ti(OiPr)_4$, probably because of the faster hydrolyzation of this alkoxide

upon contact with water (14). It was also noteworthy that S_{BET} values were negatively correlated with the D values ($R^2 = 0.856$) (**Table 2**). Therefore, the heterostructures synthesized

Table 2: TiO_2 content, average crystal size (D), and surface area (S_{BET}) of the TiO_2/AC heterostructures.

Labeled Code	% TiO_2	D (nm) ^a	S_{BET} (m ² /g)
SGIP	13.4	11.8	830.2
SGIB	13.2	12.3	743.4
STIP	13.6	13.3	569.0
STIB	13.3	15.4	481.1
MWIP-I	14.8	14.0	498.8
MWIB-I	13.2	17.1	435.8
MWIP-II	11.9	18.9	364.7
MWIB-II	9.0	21.1	269.8

^a From (101) anatase diffraction peak.

using $\text{Ti}(\text{OBu})_4$ as the titania precursor had the lowest S_{BET} .

The formation of high-size agglomerates in the syntheses using $\text{Ti}(\text{OBu})_4$ can be observed in the high-magnification SEM micrographs (**Figures 2A and 2B**). The micrographs also reveal that the synthesized photocatalysts consist of spherical TiO_2 nanoparticles distributed on the AC surface. EDS elemental mapping confirmed the presence of carbon, oxygen, and titanium on the AC surface while uncovering a non-homogeneous distribution of TiO_2 (Figure S9). **Figures 2C and 2D** show the heterogeneous distribution of TiO_2 on the heterostructures elaborated via the sol-gel method. Although heterogeneous distribution was expected due to the AC content exceeding 13% (13), this distribution prevents complete pore filling by TiO_2 nanoparticles, which might be beneficial for the adsorption of the contaminants.

Raman spectra of the heterostructures were registered in the range of 0–2000 cm^{-1} (**Figure 3**). Characteristic bands of the pristine AC (i.e., used as received from the supplier) were observed around 1310 cm^{-1} (G band) and 1560 cm^{-1} (D band) in all heterostructures. In addition, a well-resolved TiO_2 Raman peak was observed at 145 cm^{-1} for all the heterostructures, attributed to the primary anatase vibration mode. Three other bands were observed at 396, 510, and 642 cm^{-1} , indicating the presence of anatase species crystallites (50). The bands observed at 291 and 732 cm^{-1} are related to the PTFE (Figure S10 shows a pristine PTFE spectrum).

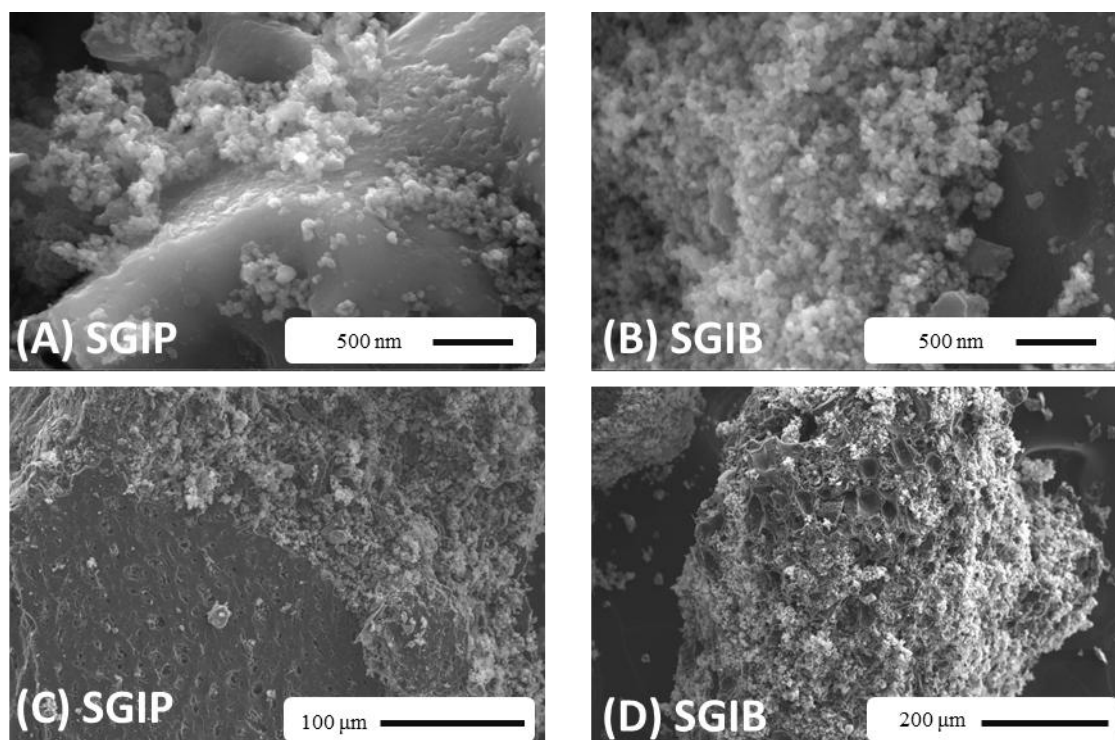


Figure 2: High-magnification SEM micrographs of (A) SGIP and (B) SGIB TiO_2/AC heterostructures. Low-magnification SEM micrographs of (C) SGIP and (D) SGIB TiO_2/AC heterostructures. Scale bars are shown

TGA analysis revealed that the stability of the heterostructures was not correlated with the titania precursor but rather with the synthetic method or content of TiO_2 (**Figure 4**). To the best of our knowledge, this is the first study to conduct a TGA analysis of TiO_2/AC heterostructures elaborated through different synthetic methods. The results indicated that the stability of the heterostructures depends on the heating temperature employed during the synthesis. Specifically, higher temperatures correspond to increased stability in the heterostructure. These results corroborate those reported by Arutanti et al. (51) regarding the stability of TiO_2/AC heterostructures synthesized at different temperatures. Furthermore, as both microwave-assisted hydrothermal methods were carried out at the same temperature, it was expected that both would have the same stability. However, it was also observed that microwave-assisted hydrothermal method II resulted in heterostructures with a lower content of TiO_2 than microwave-assisted hydrothermal method I (**Table 2**), which could explain the lower thermal stability of these heterostructures.

3.3. Photocatalytic performance of the TiO₂/AC heterostructures

The TiO₂/AC heterostructures are interesting materials for water treatment, combining the adsorption properties of the AC and the photodegradation properties of the TiO₂. In this study, pristine AC and eight TiO₂/AC heterostructures synthesized by different methods were compared. HTZ and SMX were removed to < 10 µg L⁻¹ within 30 and 5 min of irradiation,

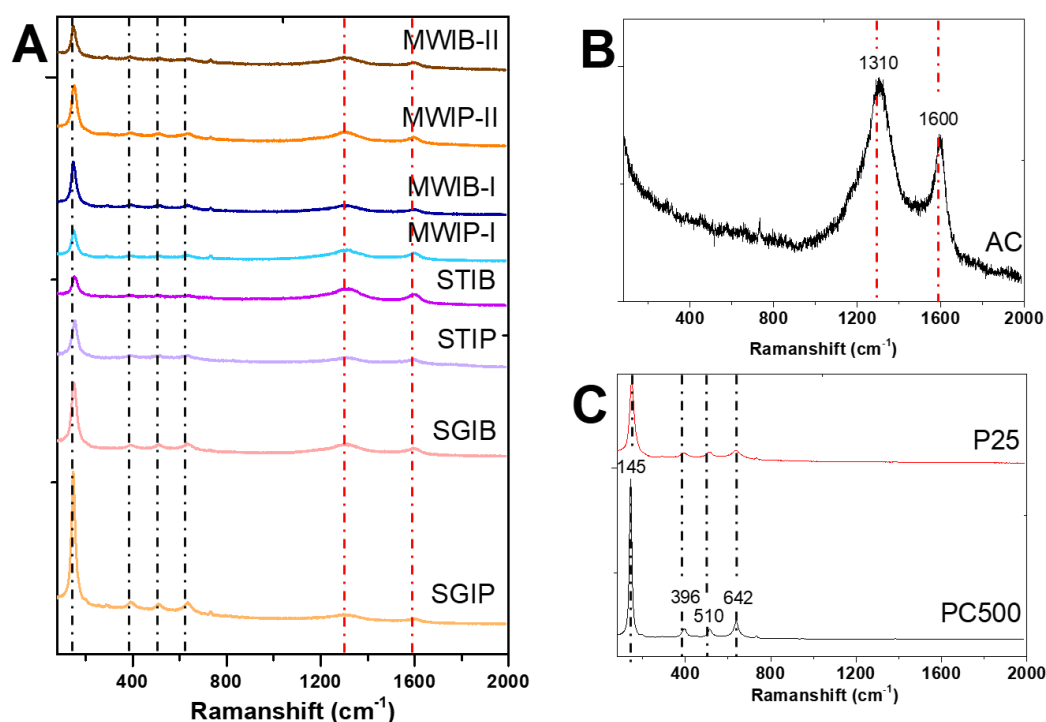


Figure 3: Raman shift patterns of the (A) TiO₂/AC heterostructures; (B) pristine AC; and (C) pristine P25 and PC500. The dotted black lines are related to TiO₂ bands, and the dotted red lines are related to AC bands.

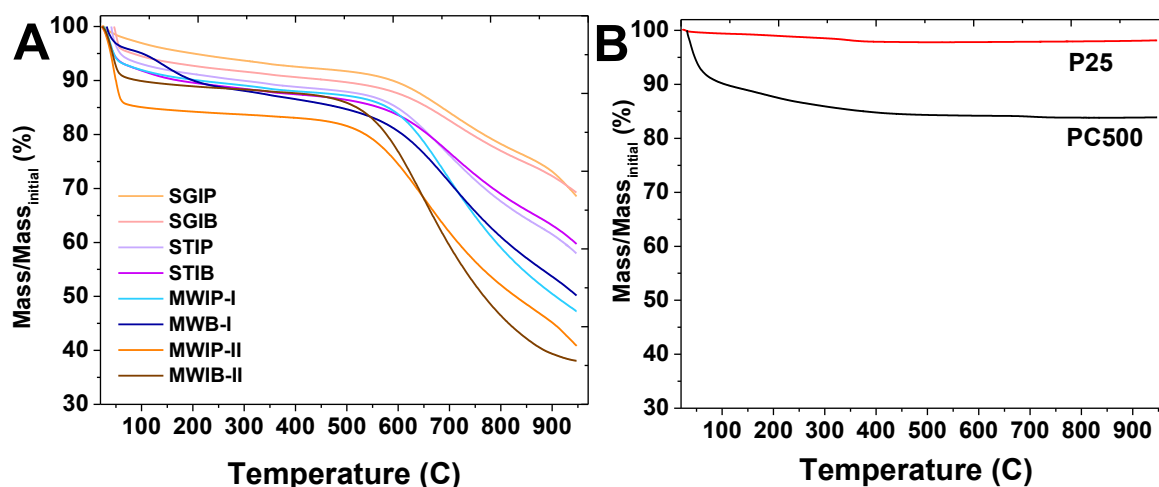


Figure 4: TGA thermograms (A) of the TiO₂/AC heterostructures and (B) pristine P25 and PC500.

respectively, regardless of the TiO₂/AC heterostructures used (Figure S11 and Table S2). On the other hand, **Figure 5** shows the removal of CAF, SAC, and SUC upon the irradiation time with all the TiO₂/AC heterostructures and the pristine AC. The AC employed in this study can remove these contaminants by adsorption (7, 52), and in the experiments conducted, this adsorption was complemented by partial degradation through photolysis (Figure S2). As a result of this synergistic interaction, an overall removal rate of approximately 60% was achieved.

SGIP was the most effective TiO₂/AC heterostructure in removing CAF, SAC, and SUC from the aqueous solution. When compared to pristine AC, SGIP increased the first-order

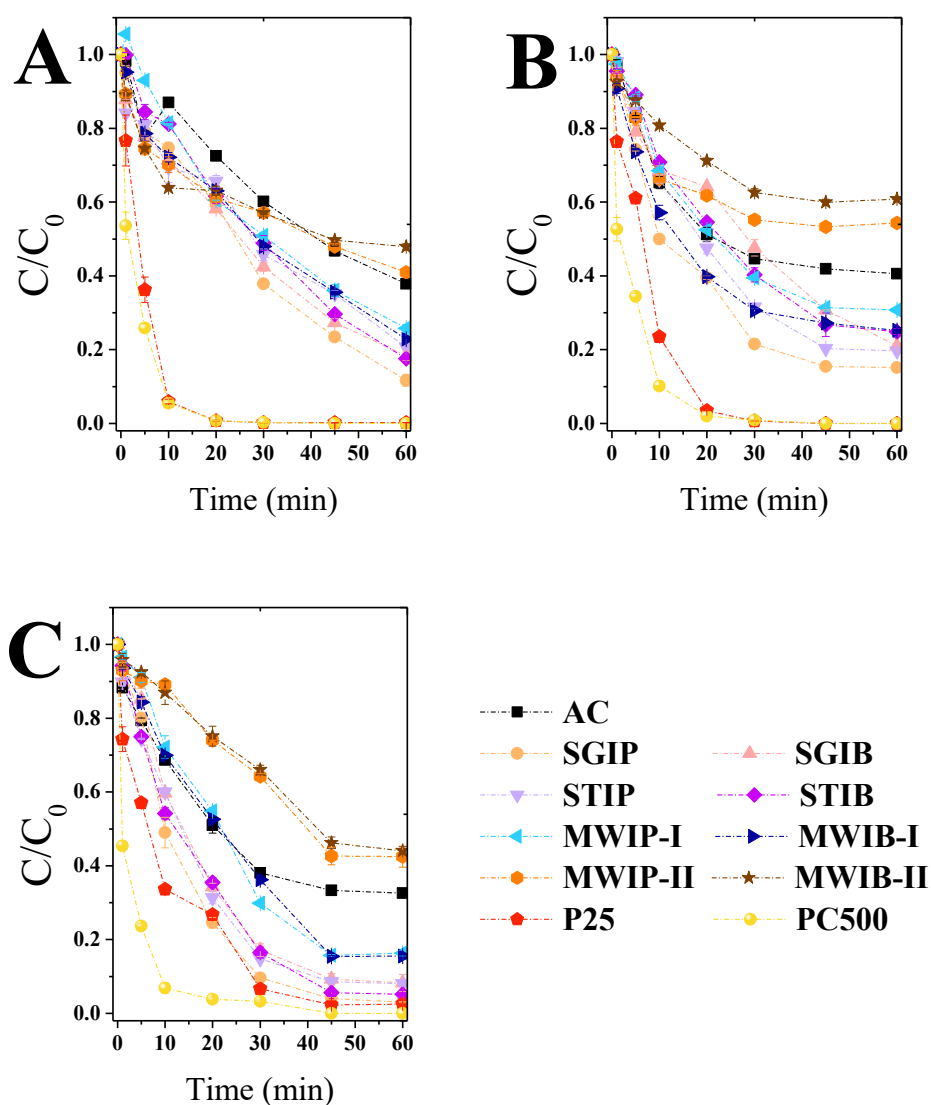


Figure 5: Removal of caffeine (A), saccharin (B), and sucralose (C) by the TiO₂/AC heterostructures, pristine AC under UV-C, TiO₂-P25, and TiO₂-PC500 (8 W) irradiation. Initial concentration of the contaminants = 2 mg L⁻¹ and TiO₂/AC heterostructure = 25 mg L⁻¹.

kinetic constant (k) by 1.9, 2.2, and 2.4 times for CAF, SAC, and SUC, respectively (**Figure 6**). When compared to pristine AC, an overall increase in the k values was also observed for SGIB, STIP, STIB, MWIP-I, and MWIB-I heterostructures. However, for MWIP-II and MWIB-II heterostructures, a decrease in k values was observed (**Figure 6**). These latter heterostructures exhibited the lowest S_{BET} values and the least TiO_2 content anchored onto AC among all the elaborated heterostructures (**Table 2**), which explains the low removals even compared to pristine AC (**Figure 5**). Higher S_{BET} values allow greater interactions between contaminants and TiO_2 (13), implying that low S_{BET} values resulted in poor removal rates. These findings are corroborated by Penas-Garzon et al. (14), who reported that the heterostructure with the lowest S_{BET} value exhibited the lowest removal rate.

To the best of our knowledge, this is the first study investigating the effects of titania precursors on the synthesis of TiO_2/AC heterostructures. The overall findings suggested using $\text{Ti}(\text{OiPr})_4$ to obtain the best heterostructures when the sol-gel method and microwave-assisted hydrothermal method II were applied (**Table 2**). On the other hand, $\text{Ti}(\text{OBu})_4$ was the most effective choice for synthesizing heterostructures via microwave-assisted hydrothermal method I (**Figure 6**). Similar results were observed in cases where the solvothermal method

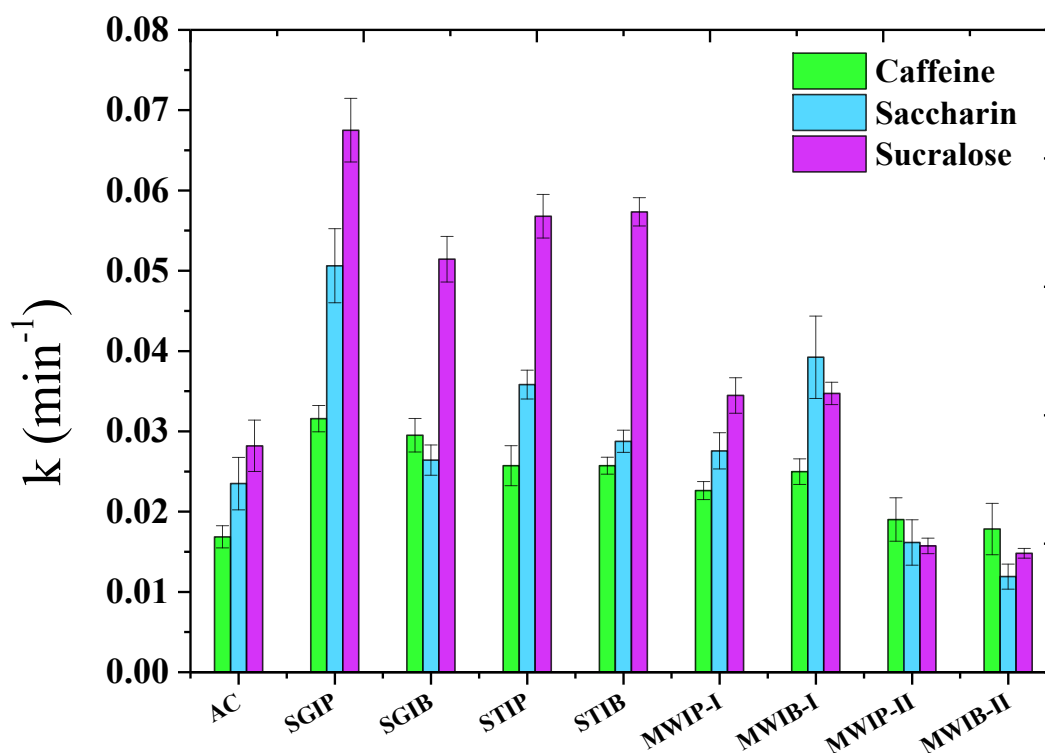


Figure 6: Values of the first-order kinetic constant (k , min^{-1}) of caffeine, saccharin, and sucralose removal under UV-C irradiation light using TiO_2/AC heterostructures and pristine AC.

was employed. For all the methods of syntheses tested in the present study, the initial step involves the hydrolysis of the alkoxide bond of the chosen titania precursor (here $\text{Ti}(\text{OiPr})_4$ or $\text{Ti}(\text{OBu})_4$), leading to the formation of a hydroxyl group (Figure S12). Then, two of these generated molecules having orthogonal hydroxyl groups react to form Ti-O-Ti *via* water condensation (53). Compared to $\text{Ti}(\text{OiPr})_4$, $\text{Ti}(\text{OBu})_4$ exhibits faster hydrolyzation, facilitating the formation of high-size agglomerates of titanium oxyhydroxides (14), which consequently resulted in low S_{BET} values, as can be observed in **Table 2**. Therefore, for both synthesis methods entailing extended hydrolysis time (sol-gel and microwave-assisted hydrothermal method II), the best results were achieved using $\text{Ti}(\text{OiPr})_4$. In the case of microwave-assisted hydrothermal method I, $\text{Ti}(\text{OBu})_4$ resulted in the best heterostructure (**Figure 6**), probably due to its shorter hydrolysis time. However, for the solvothermal method, although employing only 5 min of stirring time, the lower S_{BET} value of the heterostructure synthesized using $\text{Ti}(\text{OBu})_4$ when compared to $\text{Ti}(\text{OiPr})_4$ could explain the similar k values observed (**Figure 6**).

As observed in section 3.1, HTZ and SMX were rapidly removed regardless of TiO_2/AC heterostructure used (Figure S13 shows the removal evolution employing SGIP as a photocatalyst). A previous study (7) found that the adsorption rate of these contaminants by the same pristine AC followed the order $\text{SAC} = \text{SUC} > \text{CAF}$. In the present study, CAF also exhibited the lowest k values (**Figure 7A**). For instance, when comparing SAC and SUC, the k values associated with the SGIP heterostructure were 1.6 and 2.2 times higher than those for CAF. On the hand, the k values for P25 in the present study followed the order $\text{SUC} > \text{SAC} > \text{CAF}$, which indicates that the adsorption process contributed to removal of the contaminants. However, the adsorption capacity of these contaminants by the AC followed the order $\text{CAF} > \text{SAC} > \text{SUC}$ (see Diniz et.(7)), which contrast with to removal capacity of the TiO_2/AC heterostructures (**Figure 7B**). These results indicate that although the adsorption process partially contributed to the removal of the contaminants, the photocatalytic process governed the removal efficiency of contaminants by the TiO_2/AC heterostructures. Also, when compared to TiO_2 nanoparticles, it appears that TiO_2/AC heterostructures showed a lower efficiency in removing the contaminants (**Figure 5**). However, when the removal capacity is normalized by the mass of TiO_2 , it is evident an increase in the photocatalytic efficiency (**Figure 7B**). For example, SGIP increased the photocatalytic efficiency of TiO_2 by up to 10.0 times (**Figure 7A**), probably due to the prolonged contact time between the contaminant and the TiO_2 nanoparticles.

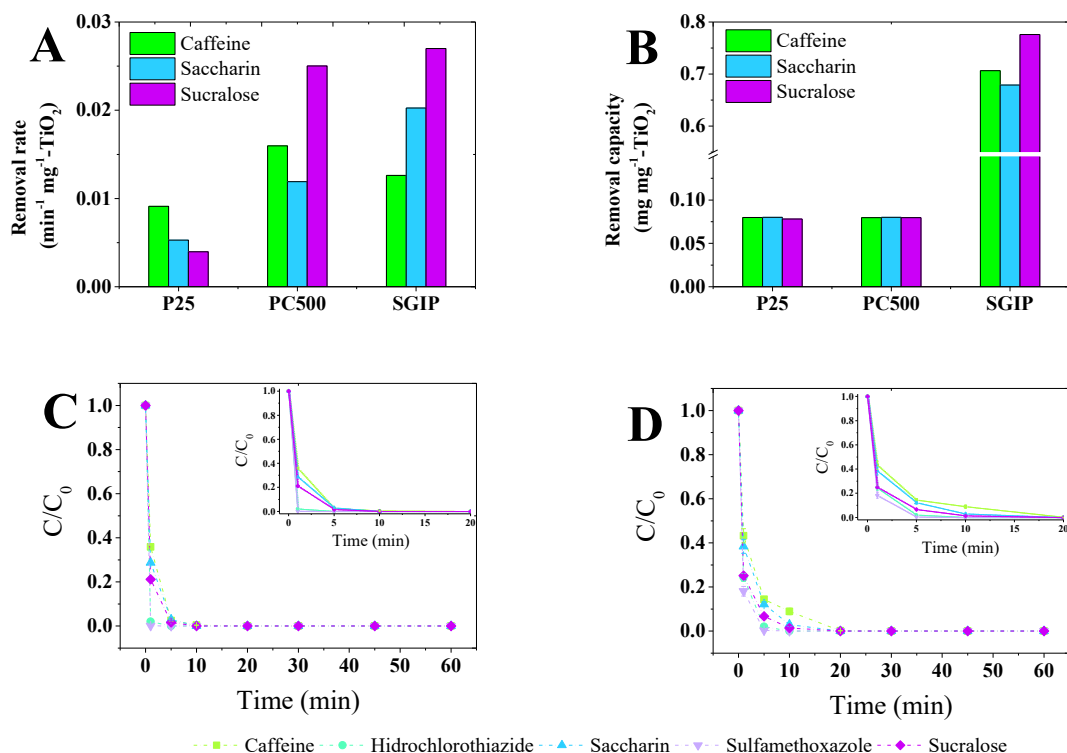


Figure 7. (A) Normalized values of the first-order model kinetic model (k , min⁻¹) and (B) removal capacity (mg mg⁻¹) by means of TiO₂ mass for caffeine, saccharin, and sucralose removal by P25, PC500, and SGIP. Initial concentration of the contaminants = 2 mg L⁻¹ and photocatalyst = 25 mg L⁻¹. Removal of the contaminants by the SGIP heterostructure under UV-C (8 W) irradiation in (B) ultrapure water and (C) reclaimed water. The inset graphs show a zoom-in of the first 20 min of the removal process. Initial concentration of the contaminants = 0.1 mg L⁻¹ and TiO₂/AC heterostructure = 25 mg L⁻¹.

The performance of the SGIP heterostructure was further assessed under conditions more representative of wastewater compositions (7). The results confirmed the capability of the material to remove the contaminants even in more complex water matrices compared to ultrapure water. However, achieving the same removal efficiency demanded extended irradiation periods (20 min) (**Figure 7C** and **7D**). These findings underscore the applicability of the elaborated heterostructure for mitigating organic contaminants in real-world scenarios, reinforcing its potential for practical environmental remediation applications. Further studies should investigate the residual organic carbon of the solution after the treatment with TiO₂/AC heterostructures.

3.3.1. Regeneration performance

To evaluate the reusability of the TiO₂/AC heterostructures, regeneration studies were performed with the SGIP heterostructure. The results (depicted in **Figure 8** in terms of k values) demonstrated that after 4 cycles of usage, the k values remained almost unchanged

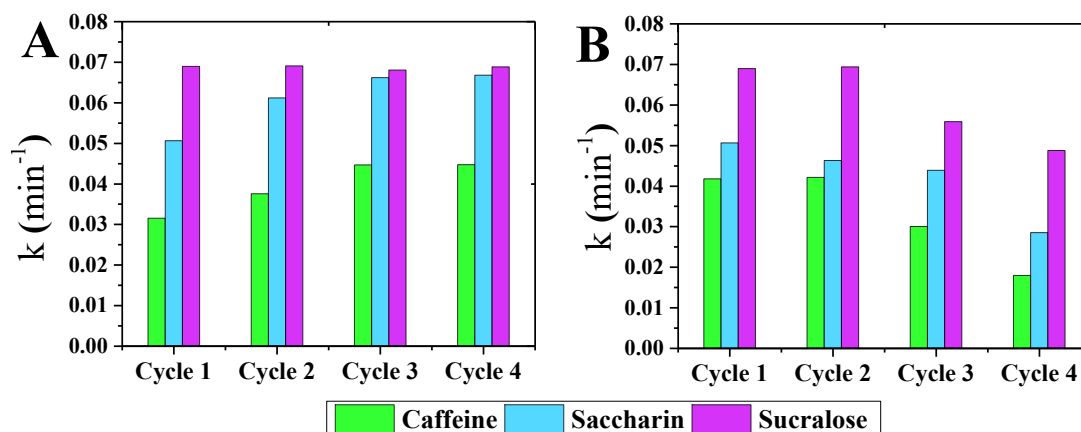


Figure 8: Removal rate of the contaminants after 4 cycles using (A) water and UV-C irradiation and (B) UV-C irradiation as regeneration procedures. Initial concentration of the contaminants = 2 mg L⁻¹ and SGIP = 25 mg L⁻¹.

when the regeneration was performed in ultrapure water along with UV-C irradiation. On the other hand, a reduction in the k values was observed after the second cycle when only UV-C irradiation was employed. Two reasons can usually explain the gradual efficiency decline over successive treatment cycles: (i) deficient contaminant-TiO₂ contact: the oxidant species generated by TiO₂ are unable to reach the contaminants due to the location of the adsorbed contaminants compared to the position of the TiO₂ centers or (ii) contaminant accumulation: the contaminants are being accumulated on the TiO₂ over several treatment cycles, reducing the probability of reaction with the oxidant species (26). While both factors could contribute to the reductions in the efficiency of the heterostructure, it is more feasible that the position of the contaminants on the AC surface (reason (i)) governed the regeneration process. This is supported by the observation that when the heterostructures were stirred with water, no significant decreases in efficiency were observed, which suggests that the accessibility of contaminants to the TiO₂ active sites was crucial in governing the regeneration process.

4. Conclusions

This study describes the preparation of TiO₂/AC heterostructures using various synthetic methods and different titania precursors to remove organic contaminants (CAF, HTZ, SAC, SMX, and SUC). Therefore, based on the results of the present study, the following conclusions can be drawn:

- To the best of our knowledge, this is the first study comparing the effects of different titania precursors (Ti(OiPr)₄ and Ti(Obu)₄) in the synthesis of

TiO₂/AC heterostructures. The choice of the precursor was found to impact the structural and performance characteristics of the resulting materials;

- All elaborated heterostructures consisted of only anatase as the crystalline phase of TiO₂, and the thermal stability of the heterostructures was correlated with the synthetic method and the TiO₂ content;
- Heterostructures synthesized via the sol-gel method exhibited the highest S_{BET}, leading to the highest first-order kinetic constant (k) values for the removal of the contaminants;
- The heterostructures synthesized with Ti(OBu)₄ had the largest average crystal size, as this alkoxide undergoes faster hydrolysis than Ti(OiPr)₄, leading to the formation of high-size agglomerates of titanium oxyhydroxides and resulting in lower S_{BET} values;
- The elaborated heterostructures increased the photocatalytic efficiency of TiO₂ by up to 10.0 times, providing increased contact time between the contaminant and the oxidant species of the photocatalytic particle;
- At relevant environmental conditions (concentration of the contaminants and water matrices), SGIP remained effective in removing the contaminants, showcasing their ability to remove contaminants even in complex water matrices effectively;
- Regeneration studies of the SGIP heterostructure revealed that the efficiency remained almost unchanged after four cycles when regeneration was performed by stirring with ultrapure water under UV-C irradiation. This indicated the importance of the stirring process in allowing the TiO₂ oxidant species to access the contaminants during regeneration.

The present study opens up new ways for future research on TiO₂/AC heterostructures and provides viable solutions for reducing the environmental impact and energy consumption associated with water treatment, thereby ensuring a sustainable and reliable water supply. Furthermore, this study addressed a crucial research gap by demonstrating how the two most used titania precursors affect the efficiency of the resulting material. Further investigations could focus on scaling up the synthesis method, quantifying degradation products/mineralization, and evaluating residual toxicity. The results confirm that TiO₂/AC heterostructures are an effective material that synergistically combines the beneficial properties of both AC and TiO₂.

Synthesis and characterization of TiO₂-carbon filter materials for water decontamination by adsorption-degradation processes

5. Acknowledgements

The authors are grateful for the financial support provided by the Brazilian public agencies São Paulo Research Foundation (FAPESP) (INCTAA, #FAPESP #2014/50951-4 and CNPq #465768/2014-8) and CNPq (#304584/2021-5). Scholarships were awarded to V.D (FAPESP #2021/08123-0 and #2022/11350-1).

6. References

1. WHO. Potable reuse: guidance for producing safe drinking-water 2017. 138 p.
2. Barnes JL, Krishen AS, Hu HF. Untapped Knowledge about Water Reuse: the Roles of Direct and Indirect Educational Messaging. *Water Resour Manag.* 2021;35(8):2601-15.
3. Faria DC, Naval LP. Wastewater reuse: Perception and social acceptance. *Water Environ J.* 2022;36(3):433-47.
4. Hartley K, Tortajada C, Biswas AK. A formal model concerning policy strategies to build public acceptance of potable water reuse. *J Environ Manage.* 2019;250.
5. Schimmoller LJ, Kealy MJ, Foster SK. Triple bottom line costs for multiple potable reuse treatment schemes. *Environ Sci-Wat Res.* 2015;1(5):644-58.
6. Zodrow KR, Li QL, Buono RM, Chen W, Daigger G, Duenas-Osorio L, et al. Advanced Materials, Technologies, and Complex Systems Analyses: Emerging Opportunities to Enhance Urban Water Security. *Environ Sci Technol.* 2017;51(18):10274-81.
7. Diniz V, Cunha DGF, Rath S. Adsorption of recalcitrant contaminants of emerging concern onto activated carbon: A laboratory and pilot-scale study. *J Environ Manage.* 2023;325.
8. Lopera AEC, Ruiz SG, Alonso JMQ. Removal of emerging contaminants from wastewater using reverse osmosis for its subsequent reuse: Pilot plant. *J Water Process Eng.* 2019;29.
9. Lim TT, Yap PS, Srinivasan M, Fane AG. TiO₂/AC Composites for Synergistic Adsorption-Photocatalysis Processes: Present Challenges and Further Developments for Water Treatment and Reclamation. *Crit Rev Env Sci Tec.* 2011;41(13):1173-230.
10. Wang J, Sun YB, Feng JW, Xin L, Ma JZ. Degradation of triclocarban in water by dielectric barrier discharge plasma combined with TiO₂/activated carbon fibers: Effect of operating parameters and byproducts identification. *Chem Eng J.* 2016;300:36-46.
11. Caianelo M, Espindola JC, Diniz V, Spina M, Rodrigues-Silva C, Guimaraes JR. Gatifloxacin photocatalytic degradation in different water matrices: Antimicrobial activity and acute toxicity reduction. *J Photoch Photobio A.* 2022;430.
12. Gerber IC, Serp P. A Theory/Experience Description of Support Effects in Carbon-Supported Catalysts. *Chem Rev.* 2020;120(2):1250-349.
13. Li Puma GL, Bono A, Krishnaiah D, Collin JG. Preparation of titanium dioxide photocatalyst loaded onto activated carbon support using chemical vapor deposition: A review paper. *J Hazard Mater.* 2008;157(2-3):209-19.
14. Penas-Garzon M, Gomez-Aviles A, Belver C, Rodriguez JJ, Bedia J. Degradation pathways of emerging contaminants using TiO₂-activated carbon heterostructures in aqueous solution under simulated solar light. *Chem Eng J.* 2020;392.
15. Taoufik N, Elmchaouri A, Anouar F, Korili SA, Gil A. Improvement of the adsorption properties of an activated carbon coated by titanium dioxide for the removal of emerging contaminants. *J Water Process Eng.* 2019;31.

- 16.Orha C, Pode R, Manea F, Lazau C, Bandas C. Titanium dioxide-modified activated carbon for advanced drinking water treatment. *Process Saf Environ.* 2017;108:26-33.
- 17.Kaplan R, Erjavec B, Drazic G, Grdadolnik J, Pintar A. Simple synthesis of anatase/rutile/brookite TiO₂ nanocomposite with superior mineralization potential for photocatalytic degradation of water pollutants. *Appl Catal B-Environ.* 2016;181:465-74.
- 18.Awfa D, Ateia M, Fujii M, Johnson MS, Yoshimura C. Photodegradation of pharmaceuticals and personal care products in water treatment using carbonaceous-TiO₂ composites: A critical review of recent literature. *Water Res.* 2018;142:26-45.
- 19.Liu SX, Chen XY, Chen X. A TiO₂/AC composite photocatalyst with high activity and easy separation prepared by a hydrothermal method. *J Hazard Mater.* 2007;143(1-2):257-63.
- 20.Zhang PL, Yin S, Sato T. Synthesis of high-activity TiO₂ photocatalyst via environmentally friendly and novel microwave assisted hydrothermal process. *Appl Catal B-Environ.* 2009;89(1-2):118-22.
- 21.Song JS, M.; Xia, L.; Dai, J.; Luo, L.; Wang, H.; Wang, H.; Shu, L.; Jiang, F. The comparative study on inhibitory effect of natural organic matters on the TiO₂ and activated carbon/TiO₂ composites for the removal of 17 α -ethinylestradiol. *Chemosphere.* 2023;333.
- 22.Venancio WAL, Rodrigues-Silva C, Spina M, Diniz V, Guimaraes JR. Degradation of benzimidazoles by photoperoxidation: metabolites detection and ecotoxicity assessment using *Raphidocelis subcapitata* microalgae and *Vibrio fischeri*. *Environ Sci Pollut R.* 2021;28(19):23742-52.
- 23.Venancio WAL, Rodrigues-Silva C, Maniero MG, Guimaraes JR. Photocatalytic removal of fluoroquinolones and their antimicrobial activity from water matrices at trace levels: a comparison of commercial TiO₂ catalysts. *Water Sci Technol.* 2018;78(8):1668-78.
- 24.Caianelo M, Rodrigues-Silva C, Maniero MG, Guimaraes JR. Antimicrobial activity against Gram-positive and Gram-negative bacteria during gatifloxacin degradation by hydroxyl radicals. *Environ Sci Pollut R.* 2017;24(7):6288-98.
- 25.Briche S, Derqaoui M, Belaiche M, El Mouchtari E, Wong-Wah-Chung P, Rafqah S. Nanocomposite material from TiO₂ and activated carbon for the removal of pharmaceutical product sulfamethazine by combined adsorption/photocatalysis in aqueous media. *Environ Sci Pollut R.* 2020;27(20):25523-34.
- 26.Chekem CT, Goetz V, Richardson Y, Plantard G, Blin J. Modelling of adsorption/photodegradation phenomena on AC-TiO₂ composite catalysts for water treatment detoxification. *Catal Today.* 2019;328:183-8.
- 27.Bouanimba N, Laid N, Zouaghi R, Sehili T. A Comparative Study of the Activity of TiO₂ Degussa P25 and Millennium PCs in the Photocatalytic Degradation of Bromothymol Blue. *Int J Chem React Eng.* 2018;16(4).
- 28.Verbruggen SW, Masschaele K, Moortgat E, Korany TE, Hauchecorne B, Martens JA, et al. Factors driving the activity of commercial titanium dioxide powders towards gas phase photocatalytic oxidation of acetaldehyde. *Catal Sci Technol.* 2012;2(11):2311-8.
- 29.Lester Y, Ferrer I, Thurman EM, Linden KG. Demonstrating sucralose as a monitor of full-scale UV/AOP treatment of trace organic compounds. *J Hazard Mater.* 2014;280:104-10.
- 30.Manoli K, Nakhla G, Ray AK, Sharma VK. Oxidation of Caffeine by Acid-activated Ferrate(VI): Effect of Ions and Natural Organic Matter. *Aiche J.* 2017;63(11):4998-5006.
- 31.Chuang LC, Luo CH, Huang SW, Wu YC, Huang YC. Photocatalytic Degradation Mechanism and Kinetics of Caffeine in Aqueous Suspension of Nano-TiO₂. *Adv Mater Res-Switz.* 2011;214:97-102.

Synthesis and characterization of TiO₂-carbon filter materials for water decontamination by adsorption-degradation processes

32. Dalmazio I, Santos LS, Lopes RP, Eberlin MN, Augusti R. Advanced oxidation of caffeine in water: On-line and real-time monitoring by electrospray ionization mass spectrometry. *Environ Sci Technol*. 2005;39(16):5982-8.
33. Naghizadeh M, Aghapour AA, Khorsandi H. The degradation and mineralization of hydrochlorothiazide (HCTZ) using catalytic ozonation process (COP) with Al₂O₃/granular activated carbon composite. *React Kinet Mech Cat*. 2022;135(4):1875-89.
34. Fernandez-Perales M, Sanchez-Polo M, Rozalen M, Lopez-Ramon MV, Mota AJ, Rivera-Utrilla J. Degradation of the diuretic hydrochlorothiazide by UV/Solar radiation assisted oxidation processes. *J Environ Manage*. 2020;257.
35. Monteil H, Oturan N, Pechaud Y, Oturan MA. Efficient removal of diuretic hydrochlorothiazide from water by electro-Fenton process using BDD anode: a kinetic and degradation pathway study. *Environ Chem*. 2019;16(8):613-21.
36. Davididou K, McRitchie C, Antonopoulou M, Konstantinou I, Chatzisyseon E. Photocatalytic degradation of saccharin under UV-LED and blacklight irradiation. *J Chem Technol Biot*. 2018;93(1):269-76.
37. Noroozi R, Gholami M, Farzadkia M, Kalantary RR. Synthesis of new hybrid composite based on TiO₂ for photo-catalytic degradation of sulfamethoxazole and pharmaceutical wastewater, optimization, performance, and reaction mechanism studies. *Environ Sci Pollut R*. 2022;29(37):56403-18.
38. Gong H, Chu W. Determination and toxicity evaluation of the generated products in sulfamethoxazole degradation by UV/CoFe₂O₄/TiO₂. *J Hazard Mater*. 2016;314:197-203.
39. Ioannidou E, Frontistis Z, Antonopoulou M, Venieri D, Konstantinou I, Kondarides DI, et al. Solar photocatalytic degradation of sulfamethoxazole over tungsten - Modified TiO₂. *Chem Eng J*. 2017;318:143-52.
40. Abellan MN, Bayarri B, Gimenez J, Costa J. Photocatalytic degradation of sulfamethoxazole in aqueous suspension of TiO₂. *Appl Catal B-Environ*. 2007;74(3-4):233-41.
41. Hu LH, Flanders PM, Miller PL, Strathmann TJ. Oxidation of sulfamethoxazole and related antimicrobial agents by TiO₂ photocatalysis. *Water Res*. 2007;41(12):2612-26.
42. Xu Y, Lin ZY, Wang Y, Zhang H. The UV/peroxymonosulfate process for the mineralization of artificial sweetener sucralose. *Chem Eng J*. 2017;317:561-9.
43. de Oliveira DN, de Menezes M, Catharino RR. Thermal degradation of sucralose: a combination of analytical methods to determine stability and chlorinated byproducts. *Sci Rep-Uk*. 2015;5.
44. Jimenez-Salcedo M, Monge M, Tena MT. Study of intermediate by-products and mechanism of the photocatalytic degradation of ciprofloxacin in water using graphitized carbon nitride nanosheets. *Chemosphere*. 2020;247.
45. Perez-Lucas G, El Aatik A, Aliste M, Navarro G, Fenoll J, Navarro S. Removal of Contaminants of Emerging Concern from a Wastewater Effluent by Solar-Driven Heterogeneous Photocatalysis: A Case Study of Pharmaceuticals. *Water Air Soil Poll*. 2023;234(1).
46. Balakrishnan A, Appunni S, Gopalram K. Immobilized TiO₂/chitosan beads for photocatalytic degradation of 2,4-dichlorophenoxyacetic acid. *Int J Biol Macromol*. 2020;161:282-91.
47. Balakrishnan A, Appunni S, Chinthala M, Vo DVN. Biopolymer-supported TiO₂ as a sustainable photocatalyst for wastewater treatment: a review. *Environ Chem Lett*. 2022;20(5):3071-98.
48. Song XL, Li YY, Wei ZD, Ye SY, Dionysiou DD. Synthesis of BiVO₄/P25 composites for the photocatalytic degradation of ethylene under visible light. *Chem Eng J*. 2017;314:443-52.

49.Hanaor DAH, Sorrell CC. Review of the anatase to rutile phase transformation. J Mater Sci. 2011;46(4):855-74.

50.Yu Y, Yu JC, Yu JG, Kwok YC, Che YK, Zhao JC, et al. Enhancement of photocatalytic activity of mesoporous TiO₂ by using carbon nanotubes. Appl Catal a-Gen. 2005;289(2):186-96.

51.Arutanti O, Sari AL, Kartikowati CW, Sari AA, Arif AF. Design and Application of Homogeneous-structured TiO₂/Activated Carbon Nanocomposite for Adsorption-Photocatalytic Degradation of MO. Water Air Soil Poll. 2022;233(4).

52.Diniz V, Rath S. Adsorption of aqueous phase contaminants of emerging concern by activated carbon: comparative fixed-bed column study and in situ regeneration methods. J Hazard Mater. 2023.

53.Nawaratna G, Lacey R, Fernando SD. Effect of hydrocarbon tail-groups of transition metal alkoxide based amphiphilic catalysts on transesterification. Catal Sci Technol. 2012;2(2):364-72.

1

2

3.1.4. Porous sulfur polymers for effective aqueous-phase organic contaminant removal

Vinicius Diniz^{1,2}, Joseph C. Bear³, Susanne Rath² and Colin R. Crick^{1*}

¹School of Engineering and Materials Sciences, Queen Mary University of London, London, E1 4NS, UK.

²Institute of Chemistry, University of Campinas, 13083-970 Campinas, Brazil.

³School of Life Sciences, Pharmacy and Chemistry, Kingston University, Penrhyn Road, Kingston-upon-Thames, KT1 2EE, UK.

*Authors for correspondence: *c.crick@qmul.ac.uk*

Abstract

Sulfur polymers produced through 'inverse vulcanization' exhibit various attributes, such as photocatalytic activity and a high capacity to adsorb heavy metals. Nevertheless, there is a lack of research investigating the use of sulfur polymers as materials for the removal of organic contaminants. In this work, porous sulfur polymers (PSPs) were synthesized from elemental sulfur and 1,3-diisopropenylbenzene, with porosity introduced via salt templating. The result is a material that can strongly absorb and chemically neutralize a model organic contaminant (caffeine). PSPs show adsorption up to 5 times higher than a leading adsorption material (activated carbon). Furthermore, either the adsorption or degradation processes can govern the removal efficiency depending on the synthesis parameters of PSPs. This is the first-ever report demonstrating sulfur polymers as effective materials for removing emerging contaminants from water. The versatile synthesis of sulfur polymers offers variation, which means that there is much more to explore in this exciting research area.

Keywords: Adsorption; Caffeine; Inverse vulcanization; Photocatalysis; Porous materials.

1. Introduction

Over the past 50 years, global freshwater use surged by 121%, while resources dropped by 52.1% (Figure S1)¹. The United Nations 2030 Agenda outlines seventeen goals, including making cities resilient, ensuring water access, and fostering sustainable industries. Direct potable reuse (DPR) and, in coastal areas, seawater desalination emerging as promising alternatives to deal with water scarcity due to their capability of reducing vulnerability by increasing resilience, diversity, adaptability and sustainability of drinking-water supplies, developing new and preferably more climate independent water resources in close proximity to major population centres². However, seawater desalination is restricted to coastal areas², which means that DPR is an interesting alternative to produce large volumes of drinking-water from wastewater in both coastal and inland locations³. According to the World Health Organization, a DPR scheme requires performance with four Rs (reliability, redundancy, robustness, and resilience)², which means the implementation of multi-barrier (membrane filtration, advanced oxidation, and media filtration units) water treatment processes, which can be costly compared to conventional treatment processes, such activated sludge or coagulation and flocculation over the years, as can be seen in Figure S2⁴.

Elemental sulfur (S₈) is a by-product of the hydrodesulfurization process used to remove sulfur-containing compounds from petroleum during refinement, and is estimated to be produced at more than 60 million tons each year⁵. Given the relative abundance and affordability of sulfur, and provides a highly promising area to explore new approaches and techniques for creating innovative functional materials⁶. One such technique is “inverse vulcanization”, which is a solvent-free process introduced by Chung *et al.* in 2013⁵. By incorporating unsaturated organic monomers with elemental sulfur, this process enables the production of polymers with high sulfur content, usually at elevated temperatures⁷. The added monomer stabilizes sulfur chains using crosslinking, forming a hyperbranched network, which imparts stability against depolymerization and results in the creation of durable and functional materials^{6,8}.

“Inverse vulcanization” sulfur polymers have a wide range of applications in different fields such as optical, optoelectronic, superhydrophobic materials, and photochemical materials, along with pharmaceutical preparations based on biopolymers, proton-conducting electrolytes, cathodes in lithium-sulfur batteries, and electromembrane processes⁸⁻¹¹. Amongst these applications, the use of porous sulfur polymers for the gas phase adsorption of heavy metals, such as mercury, has already been proposed^{6,12,13}. Additionally, Upton *et al.*⁸ reported photoactive properties of sulfur-

containing polymers when irradiated by UV-C lamps (254 nm), as well as antibacterial properties. Although these materials have been used in a range of fields, (*e.g.* antifouling, or heavy metal removal) to the best of our knowledge, no studies have been performed to evaluate the potential of these polymers to be used for removing organic contaminants from aqueous matrices, such as emerging contaminants (pharmaceuticals, personal care products, and endocrine disruptors). Caffeine was chosen as the representative compound for our removal studies. This selection was based on the reported presence of caffeine in water bodies, with concentrations ranging from ng L^{-1} to $\mu\text{g L}^{-1}$, as documented in previous studies¹⁴⁻¹⁶ and its use as tracer for anthropogenic contamination¹⁷. Furthermore, the effectiveness of caffeine removal by wastewater treatment plants and drinking water treatment plants can differ significantly based on the technologies employed, leading to persistently high concentrations in the effluent, as noted in previous research^{14,18}.

Although the potable water generation process is established¹⁹, challenges persist in enhancing efficiency, cost-effectiveness, and sustainability, speeding up future innovations²⁰. Among the different materials that have been proposed in the literature, “inverse vulcanization” sulfur polymers are inexpensive and relatively easy to synthesize^{13,21}, and with the use of table salt as a template to create pores have been used for the adsorption of mercury and other heavy metals^{6,12,22} from both air and water phase and gas selectivity¹³. In the present study, we demonstrate that porous sulfur-containing polymers (PSPs) (here, synthesized *via* “inverse vulcanization”, using 1,3-diisopropenylbenzene (DIB)) can also be used for aqueous phase-adsorption and degradation of organic contaminants, adding a new potential application of these materials. Further, the properties of the PSPs produced simply by the removal of the template, such as effective adsorption and photocatalysis, are dependent on the ratio of sulfur and DIB from which they are formed.

2. Materials and methods

2.1. Chemicals and reagents

Elemental sulfur (S_8 , sublimed powder, reagent grade, $\geq 99.5\%$) was purchased from Honeywell Lab (UK). 1,3-Diisopropenylbenzene (stabilized with TBC, $>97\%$) was purchased from TCI Limited. Caffeine (99.0%) was purchased from Sigma-Aldrich (UK). Deuterated chloroform (D , 99.8%) was purchased from Cambridge Isotopes Laboratories (UK). “A pinch of table salt” [Brand Name] as the source of NaCl was obtained from a Co-op (London, UK). Ethanol (p.a), hydrochloric acid (35%) and sodium hydroxide (p.a.) were purchased from Fischer Chemical (UK).

2.2. Synthesis of porous sulfur polymers

A general schematic diagram for the preparation of PSPs is shown in **Figure 1**. Briefly, elemental sulfur was heated to ca. 170–190 °C under continuous magnetic stirring. The chosen temperature range has been carefully determined to facilitate the opening of elemental sulfur rings⁸, while simultaneously preventing the degradation or breakdown of the elemental sulfur molecules. Once completely molten (indicated by a change in appearance from a pale-yellow powder to a yellow/orange liquid), DIB was gradually added dropwise. In the experiments, the elemental sulfur:DIB monomer mass ratio was varied from 40:60 to 90:10. DIB content higher than 40% led to non-rigid, sticky PSPs. Conversely, 100% sulfur PSPs are brittle⁶. The mixtures were stirred at 1500 rpm for 5–10 minutes until the reaction was nearly complete. Subsequently, the still-liquid pre-polymer was transferred into a silicone mould containing different amounts of table salt (ground using a pestle and mortar, with ratios of 1:4 to 3:2 (mass of table salt/mass of sulfur)). The mixture was thoroughly blended with a glass rod and left to cure at 140 °C for 4 hours. For the template removal, the PSPs were stirred with ultrapure water overnight, filtered and then dried. The PSPs were named according to the amount of DIB, sulfur and table salt used. For example, the PSP synthesized with 40%[DIB]:60%[S₈]:1.000g[NaCl] is named PSP_{40:60:1.000}.

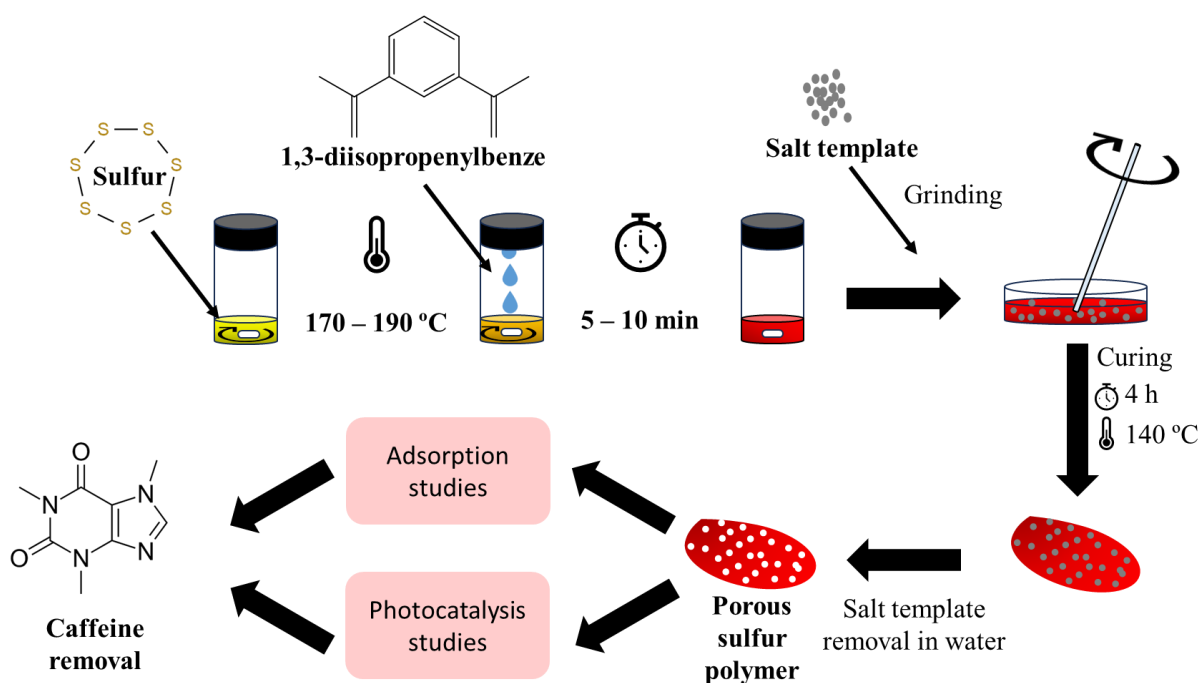


Figure 1: General schematic diagram for the preparation and application of the porous sulfur polymers

2.3. Characterization of porous sulfur polymers

The characterization of PSPs encompassed a series of analytical techniques. Nitrogen adsorption/desorption isotherms were acquired at 77 K using a surface area analyzer (NOVA 4200e, Quantachrome). Prior to analysis, the materials underwent a 24-hour degassing process under vacuum at 35 °C. Scanning Electron Microscopy (SEM) imaging and Energy-Dispersive X-ray Spectroscopy (EDS) were performed using an FEI Inspect F system with an operational acceleration voltage of 10–20 kV. To enhance electrical conductivity within the SEM, samples were sputter-coated with a thin layer of gold using an Automatic Sputter Coater. Fourier transformed infrared (FTIR) spectra were recorded using a Bruker Tensor 27 instrument over the wavenumber range of 500 to 4000 cm^{-1} . Nuclear magnetic resonance analysis utilized a Bruker Advance DRX (400 MHz) spectrometer, with deuterated chloroform as the solvent and tetramethylsilane as the internal standard. All NMR experiments were conducted at room temperature. Differential scanning calorimetry measurements were carried out using a TA Instruments Discovery Series DSC 25. A heat-cool-heat method was employed, with heating and cooling rates set at 10 °C min^{-1} , spanning from -20 to 150 °C. Powder X-ray diffraction (patterns were collected in reflection mode using a Panalytical X'Pert PRO MPD equipped with a high throughput screening XYZ stage, X-ray focusing mirror, and PIXcel detector. Cu $K\alpha$ radiation was utilized, and data were collected over a range of 5–70° using loose powder samples on thin Mylar film within aluminium well plates. Thermogravimetric analysis (was conducted under an inert atmosphere on a TA Instruments TGA 5500. Heating was carried out at a heating rate of 10 °C min^{-1} , from room temperature to 600 °C. The investigation of the point of zero charge of the PSPs was determined according to Diniz *et al.*¹⁴. Briefly, a 300 mL solution containing 0.01 mol L^{-1} NaCl was evenly distributed into 10 mL glass vials (10 mL per vial). The pH of each vial was carefully adjusted with HCl or NaOH within the range of 0.5 to 11.5. Subsequently, 50 mg of PSPs were introduced into each vial. These mixtures were then maintained at a temperature of 25 °C for 48 hours to assess the resultant pH values.

2.4. Removal experiments

2.4.1. Adsorption studies

The batch adsorption experiments were conducted following the guidelines of the American Society for Testing and Materials (ASTM) protocol D3860/2020. A total of 400 mL of water, containing 7.5 mg L^{-1} of caffeine, was used in a 500 mL Beaker. To prepare the standards, low concentrations of methanol (< 0.5% v/v) were employed due to the low solubility of caffeine¹⁴.

The studies were performed at the mg L^{-1} concentration range to facilitate monitoring and reduce any uncertainty in the results obtained^{18,23-26}.

For the adsorption studies, 100 mg of the PSPs was suspended in water containing 7.5 mg L^{-1} of caffeine and stirred using a hot plate (300 rpm) and a magnetic stirrer bar (25 mm x 7 mm). The solution was kept at 25°C during the experiments. At different time intervals, 2 mL aliquots were collected and filtered through a $0.22 \mu\text{m}$ filter for quantifying the residual concentrations of the caffeine by UV-Vis, using a Perkin Elmer Lambda 35 UV-vis spectrometer at 273 nm. All analyses were performed in duplicates. To evaluate the stabilities of caffeine (at 7.5 mg L^{-1}) in water, the same procedure was followed, but without the addition of the PSPs, and no degradation was observed.

To better understand the adsorption mechanisms, thermodynamic studies were carried out at 35°C and 45°C , alongside studies at different pH and ionic strengths. The thermodynamic studies mirrored those at 25°C , and control samples were employed at each temperature to confirm caffeine stability. The influence of pH on the adsorption of caffeine onto the PSPs was studied in the pH range of 1–10, maintaining the ionic strength constant at 0.5 mol L^{-1} ¹⁴. The concentration of caffeine and PSPs were 7.5 mg L^{-1} and 250 mg L^{-1} , respectively. The experiments were prepared similarly to the adsorption kinetics assays, with the flasks being shaken during the previously determined apparent equilibration time (120 min), followed by quantification using UV-Vis. As previously reported by Diniz *et al.*¹⁴, caffeine is chemically stable under the entire range of pH studied. The influence of ionic strength was studied considering the range of NaCl concentration of $0.01 - 10 \text{ g L}^{-1}$. The procedure was the same as used for the pH studies.

The adsorption isotherm studies were carried out using different amounts of PSP_{40:60:1.000} suspended in 400 mL of water containing the caffeine at a concentration of 7.5 mg L^{-1} and throughout the previously determined apparent equilibration time (120 min).

2.4.2. Photocatalysis studies

Photocatalytic activity of all the PSPs was tested by using the Cole-Parmer Handheld UV Lamp of 6 W. For the photocatalytic degradation of caffeine under 254 nm, 25 mg of PSP was dispersed in 100 mL of caffeine solution (7.5 mg L^{-1}). Then 500 μL of ethanol was added to the solution to reduce the surface tension and increase the dispersion of the PSPs²⁷. The mixture was kept in the dark for the first 60 min, then irradiated and after several times (65, 70, 80, 90, 105, 120,

3. Results and discussion

3.1. Characterization

Chung *et al.*⁵ first synthesized poly(sulfur-co-1,3-diisopropenylbenzene) copolymers in 2013. Their approach involved ring-opening polymerization at temperatures above 170 °C, converting S₈ rings into sulfur diradicals chains. A cross-linking agent was slowly added at room temperature, leading to color change from yellow to red and increased viscosity. The main structure (**Figure 2A**) of the copolymer poly(sulfur-co-1,3-diisopropenylbenzene) is predominantly composed of thiocumyl fragments, serving as the major building blocks. These are then accompanied by smaller segments consisting of either thiopropyl fragments or bis-thiopropyl fragments. Furthermore, the end groups of the poly(sulfur-co-1,3-diisopropenylbenzene) can be deduced to be either –SSH sulfanes or exposed isopropenyl moieties²⁸.

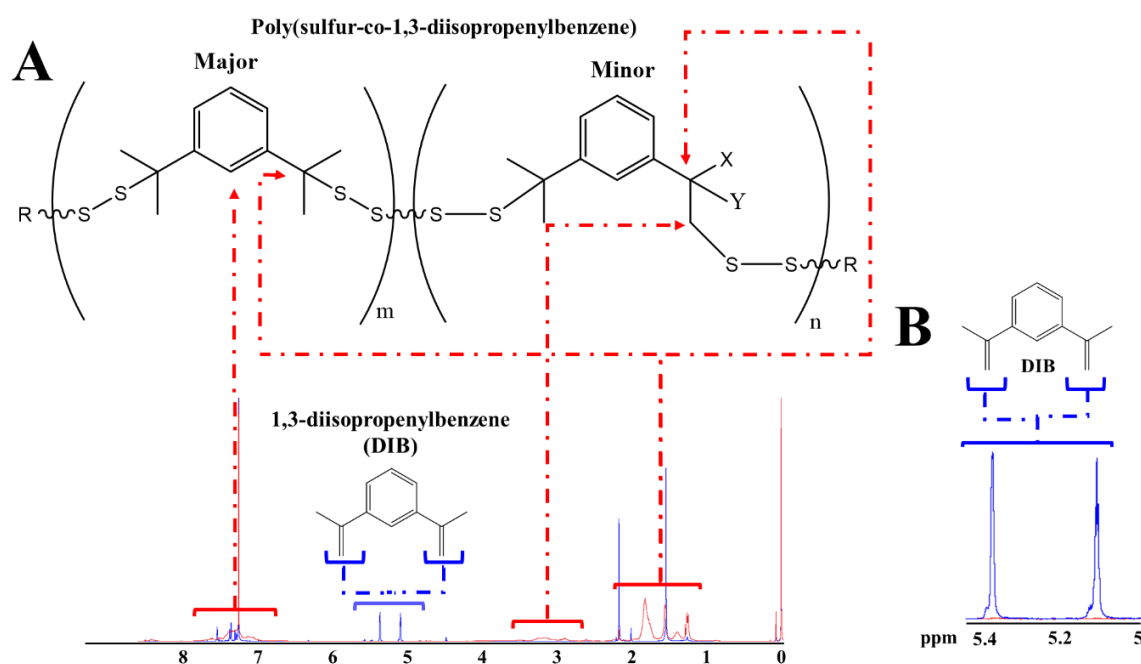


Figure 2: (A and B) Full and zoom-in of ^1H -NMR spectrum of PSP_{40:60:1.000} (red) and 1,3-diisopropenylbenze (DIB) (blue) in CDCl_3 after water treatment, respectively. R: $-\text{SH}$, $\text{Ph}-\text{C}(\text{CH}_3)=\text{CH}_2$; X: CH_3 , $-\text{Sn}$; Y: CH_3 , H. The poly(sulfur-co-1,3-diisopropenylbenzene) was adapted from Bao et al.²⁸. PSP_{X:Y:Z} = X%[DIB]:Y%[S₈]:Zg[NaCl].

Figures 2 and 3 display the ^1H -NMR and FTIR (see Figure S3 for full range FTIR) spectra of $\text{PSP}_{40:60:1.000}$. Due to overlapping with the deuterated solvent signal (CDCl_3 : proton signal at $\delta = 7.26$ ppm), this spectrum can only be used qualitatively²⁹. The extent of DIB consumption can be confirmed by the disappearance of methylene proton signals ($\delta = 5.10$ - 5.40 ppm) in the $\text{PSP}_{40:60:1.000}$ (**Figure 2B**). This is also supported by the disappearance of the 900 cm^{-1} band in the FTIR spectrum, indicating substantial consumption of double bonds during the crosslinking process³⁰ (**Figure 3A**). The detailed spectrum of methyl protons at $\delta = 1.0$ - 2.2 ppm indicated the formation of true copolymers through sulfur copolymerization (**Figure 2A**). This complexity emerges due to the random polymerization, resulting in a final product with a heterogeneous composition consisting of polymers of varying sizes⁵. The peaks at $\delta = 6.80$ - 7.80 ppm (**Figure 2A**) are related to the presence of the aromatic rings of the DIB in the polymers²⁹. Further, resonances between $\delta = 2.9$ - 3.4 ppm (**Figure 2A**), corresponding to methylene peaks in the $\text{PSP}_{40:60:1.000}$ backbone, were observed. These peaks are linked to sulfur comonomer units, which is also supported by the appearance of a 692 cm^{-1} band in the FTIR spectra, indicating C-S bond formation (**Figure 3B**)³¹. The PZC for the PSPs was also carried out (Figure S4), revealing an inherent correlation with the DIB content. Notably, an increase in DIB content corresponded to an elevated PZC value. For instance, $\text{PSP}_{10:90:1.000}$ exhibited a PZC of 9.1, while $\text{PSP}_{40:60:1.000}$ displayed a PZC of approximately 10.5.

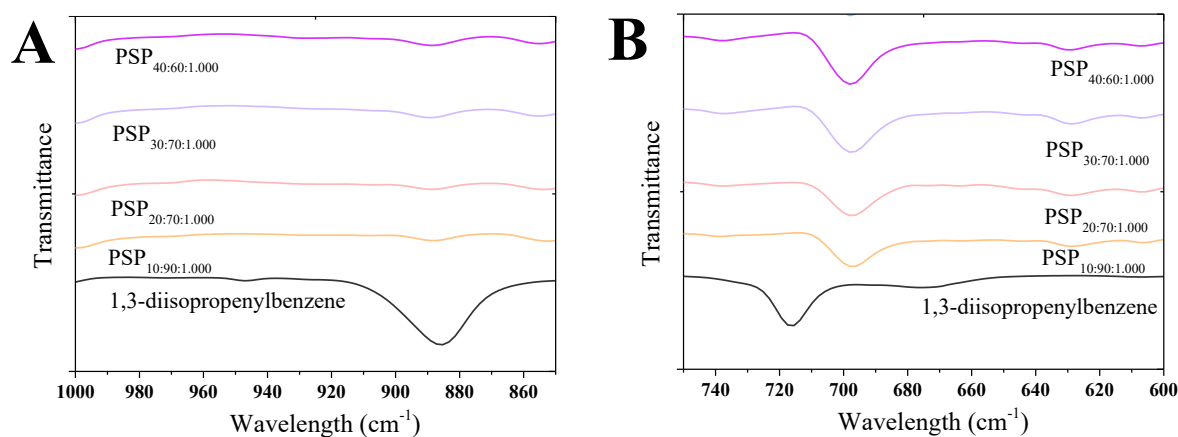


Figure 3: (A and B) FTIR spectra of the porous sulfur polymer (PSP) synthesized considering different sulfur/DIB ratios and 1.000 g of table salt after water treatment. $\text{PSP}_{X:Y:Z} = X\%[\text{DIB}]:Y\%[\text{S}_8]:Z\text{g}[\text{NaCl}]$.

The DSC curves offer insights into the sulfur conversion process and the glass transition of PSPs (Figure S5). Elemental sulfur exhibits a melting transition temperature of around $119\text{ }^\circ\text{C}$, attributed to the melting of monoclinic sulfur⁶. PSPs with over 10% wt. DIB showcase an absence of melting transition of sulfur, underscoring the amorphous nature of the co-polymers, which

reinforces the structural characteristics observed in the NMR data. Furthermore, the glass transition temperature (T_g) within the PSP series increased proportionally with elevated DIB content. Notably, PSP_{20:80:1.000} exhibits a minimum T_g of approximately -5.4 °C, while PSP_{40:60:1.000} displays a maximum of about 14.9 °C. This T_g elevation stems from the higher DIB content leading to shorter sulfur–sulfur chain lengths in the copolymers. Consequently, chain mobility is constrained, resulting in the higher T_g values observed. The thermogram of PSP_{10:90:1.000} unveils residual monoclinic sulfur due to its elevated sulfur content relative to DIB. This excess sulfur diminishes the T_g value to -17.6 °C. These findings align with those of Chung *et al.* (3), who observed similar trends during the synthesis of sulfur polymers through the “inverse vulcanization” process.

The thermal stability assessment of PSPs was conducted *via* TGA. **Figure 4A** illustrates TGA thermograms for pure sulfur as well as PSPs with varying weight percentages of sulfur and DIB. The graph depicts that the degradation of pure sulfur commences at approximately 190 °C, with complete weight loss (100%) observed around 283 °C. However, the PSPs exhibited a higher decomposition temperature than pure sulfur. Additionally, the PSPs had a residue at 600 °C, and this residual content increased with a rise in DIB content within the composition.

PXRD patterns for pure sulfur, sodium chloride (NaCl), and PSPs after water treatment are presented in **Figure 4B**. In the case of pure sulfur, characteristic diffraction peaks were discernible at $2\theta = 23^\circ, 27^\circ, 28^\circ, 53^\circ$, and 56° . However, these peaks were absent following the copolymerization reaction in polymers containing over 10% DIB content, which was already observed in the DSC thermograms. This absence suggests a transformation from crystalline monoclinic sulfur to a highly

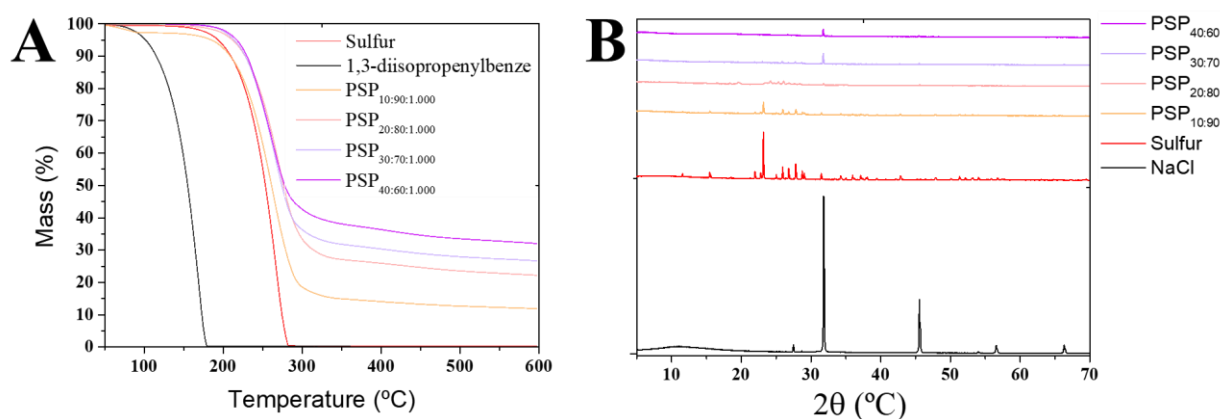


Figure 4: (A) Thermogravimetric thermograms and (B) Powder X-ray Diffraction spectra of the porous sulfur polymer (PSP) synthesized considering different sulfur/DIB ratios and 1.000 g of table salt after water treatment. $PSP_{X:Y:Z} = X\%[DIB]:Y\%[S_8]:Zg[NaCl]$.

cross-linked amorphous copolymer structure. The diffraction peaks originating from pure table salt (NaCl at $2\theta = 31^\circ$, 46° , 56° , and 66°) remained observable in PSPs after water treatment. This persistence indicates the presence of residual table salt even after the water washing treatment.

SEM images of PSP_{40:60:1.000} before water treatment reveal a rugged and non-porous surface (**Figure 5A**), comprising approximately 42.2% sulfur and 57.2% table salt (Table S1). Moreover, the SEM image indicates an even distribution of table salt and sulfur throughout the

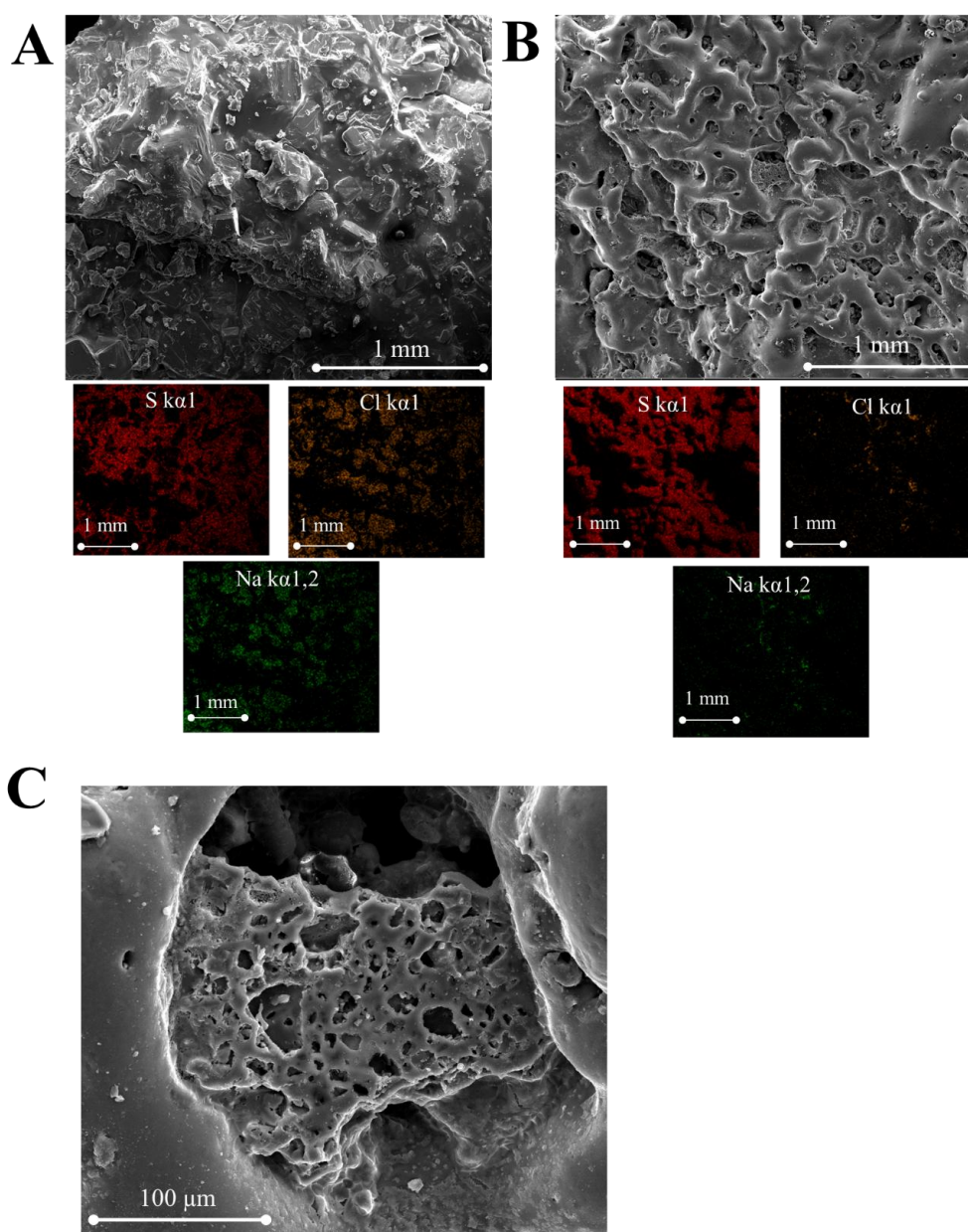


Figure 5: SEM image of PSP_{40:60:1.000} (A) before water treatment (insight image shows the Na, Cl, and S elemental mapping) and (B) after treatment with water (insight image shows the EDS of the sample). (C) High magnification image of the PSP_{40:60:1.000} after water treatment. PSP_{X:Y:Z} = X%[DIB]·Y%[S₈]·Zg[NaCl].

sample. Elemental mapping (specifically of Na, Cl, and S) provides validation that the crystal-like formations originate from the table salt surface. After water treatment, these salts were dissolved in water, prompting the development of a porous structure (**Figure 5B**). The residual table salt content after treatment amounted to around 10.8% (Table S1), consistent with PXRD data. The non-uniform distribution of pore sizes can be ascribed to the irregular structure of NaCl crystals. **Figure 5C** illustrates the presence of pores of varying dimensions, adopting a mixed cellular configuration characterized by partially open and partially closed cell arrangements.

The link between the adsorption capacity of porous materials and their surface area is well-established^{14,18,32-34}. Therefore, the surface area of the PSPs was examined using BET isotherms (Figure S6), and the corresponding data is detailed in Table S2. Notably, PSPs with a lower monomer content (PSP_{10:90:1.000}) exhibited a higher surface area, primarily attributed to reduced volume shrinkage owing to a lower cross-linking density⁶. On the other hand, PSPs containing a higher proportion of DIB (PSP_{40:60:1.000}) demonstrated lower surface area due to the heightened volume shrinkage linked with more pronounced cross-linking⁶.

To explore the impact of varying table salt quantities on the PSPs, PSP_{40:60} was synthesized using four different table salt amounts (0.250, 0.500, 1.000, and 1.500 g). The table salt was not observed to affect the structure of polymers, which can be seen in the FTIR spectra (Figure S7). In addition, no changes in the DSC curves were observed, with T_g remaining around 14.9 °C (Figure S8). On the other hand, the BET isotherm results revealed a proportional increase in surface area with higher table salt quantities, and an optimal table salt amount of 1.000 g was identified (Table S2). However, in the case of PSP_{40:60:1.500}, a significant decrease in surface area was observed, attributable to the presence of a high content of residual table salt within the PSP even following water treatment. The higher residual of table salt can be confirmed by PXRD, TGA thermogram and elemental mapping (Figures S8 and S9).

3.2. Removal experiments

3.2.1. Adsorption studies

3.2.1.1. Kinetics studies and isotherm studies

The adsorption of caffeine onto the PSPs was first performed to estimate the apparent equilibrium time, the adsorption kinetics, and the adsorption potential. The apparent equilibrium time was around 120 min regardless of the PSP (Figure S10). For a more in-depth understanding of the

kinetic characteristics of the adsorption process of caffeine by the PSPs, the pseudo-first order, pseudo-second order, Elovich, intraparticle diffusion, and film diffusion (see supplementary information for equations) models were used to fit the experimental data (Figure S9) and the relevant data parameters were listed in **Table 1**.

The fitting coefficient of the pseudo-second-order model (R^2) was larger than that of the pseudo-first-order model, and the standard deviation (SD) of the pseudo-second-order model was lower than the pseudo-first-order model. Additionally, the theoretical adsorption capacity (q_{ads}) values calculated by the pseudo-second-order model were also closer to the experimental values (Q_{ads}) (**Table 1**). The pseudo-second-order model is better suited to describe the adsorption kinetics of caffeine onto the PSP, which also suggests that the adsorption process was governed by chemical adsorption³⁵. The good fitting coefficients of the Elovich model are also an indicator of a chemisorption process^{14,36,37}. Furthermore, achieving a good fit to the Elovich model holds significant recognition as evidence of sorption site heterogeneity³⁸. This heterogeneity denotes the presence of diverse surface types, including micro- and mesopores, which in turn engender multiple sorption steps. These steps encompass phenomena like "monolayer–multilayer" adsorption, capillary condensation, and the filling of pores of varying sizes³⁹.

The process of adsorption is commonly delineated into three consecutive stages: (I) external mass transport, (II) film diffusion, and (III) intraparticle diffusion. In batch studies, the initial stage is often overlooked due to the vigorous agitation employed¹⁴. Proficiency in numerically characterizing the second and third stages is demonstrated by the film and intraparticle diffusion models, respectively. These models not only provide insights into the rate-controlling phases of adsorption⁴⁰ but also uncover multi-linear adsorption kinetics. Importantly, it was notable that the fit of the intraparticle diffusion model does not originate from the origin, signifying the participation of two or more steps in constraining the adsorption process^{14,41}.

The findings suggest the segmentation of the adsorption process into several stages, aligning with observations made for other contaminants^{40,42}. The intraparticle's diffusion rate progressively diminished across these stages ($K_{i1} > K_{i2} > K_{i3}$) (Table 1), underscoring the influence of pore diffusion on the overall adsorption pace. In addition, as the film diffusion constants (K_{fd}) were lower than the corresponding intraparticle's constant (C) values (Table 1), film diffusion had a lower impact on the adsorption of caffeine onto PSPs than pore diffusion.

Table 1: Kinetics adsorption parameters of caffeine onto porous sulfur polymers (PSPs)

Model	Parameter	PSP _{10:90:1.000}	PSP _{20:80:1.000}	PSP _{30:70:1.000}	PSP _{40:60:1.000}	PSP _{40:60:0.250}	PSP _{40:60:0.500}	PSP _{40:60:1.500}
Experimental	Q _{ads} (mg g ⁻¹)	9.81	10.56	13.50	21.73	7.33	13.20	9.45
Pseudo-first order	q _{ads} (mg g ⁻¹)	8.77	9.70	12.44	20.11	6.72	12.64	9.29
	K ₁ (min ⁻¹)	0.1521	0.0669	0.0575	0.0714	0.0683	0.0615	0.0573
	R ²	0.937	0.955	0.953	0.963	0.974	0.965	0.983
	SD	0.754	0.740	0.978	1.411	0.414	0.866	0.444
Pseudo-second order	q _{ads} (mg g ⁻¹)	9.43	10.89	14.07	22.53	7.58	14.28	10.54
	K ₂ (g mg ⁻¹ min ⁻¹)	0.024	0.008	0.005	0.004	0.011	0.005	0.007
	R ²	0.978	0.977	0.982	0.985	0.960	0.978	0.993
	SD	0.606	0.536	0.606	0.894	0.514	0.684	0.276
Elovich	α (mg g ⁻¹ min ⁻¹)	27.20	2.62	2.51	5.83	1.50	2.74	1.758
	β (mg g ⁻¹)	0.848	0.502	0.368	0.245	0.690	0.367	0.484
	R ²	0.994	0.974	0.982	0.976	0.913	0.965	0.977
	SD	0.234	0.562	0.609	1.128	0.760	0.862	0.519
Intraparticle diffusion	K _{i1} (mg g ⁻¹ min ^{-0.5})	1.667	1.146	1.857	3.269	1.183	1.777	1.401
	K _{i2} (mg g ⁻¹ min ^{-0.5})	0.354	0.455	0.960	1.113	0.428	0.442	0.659
	K _{i3} (mg g ⁻¹ min ^{-0.5})	-0.100	-0.080	-0.053	-0.326	0.050	0.128	0.000
	C _i	3.34	2.26	2.55	4.86	1.52	2.71	1.87
	R ²	0.732	0.850	0.875	0.837	0.752	0.843	0.856
	SD	1.560	1.358	1.597	2.950	1.28	1.839	1.292
Film diffusion	K _{fd} (min ⁻¹)	0.348	0.030	0.037	0.039	0.039	0.037	0.046
	R ²	0.526	0.615	0.911	0.950	0.844	0.972	0.985
	SD	0.577	0.510	0.217	0.249	0.306	0.240	0.181

PSP_{X:Y:Z} = X%[DIB]:Y%[S₈]:Zg[NaCl].

To gain a more comprehensive comprehension of the interactions between the adsorbent and the adsorbate, equilibrium isotherms were evaluated for PSP_{40:60:1.000}, leveraging the previously established apparent equilibrium time of 120 minutes. Four distinct isotherm models (see supplementary information for equations): Langmuir, Freundlich, Redlich-Peterson, and Sips. The isotherms exhibited a type L2 shape ⁴³ (**Figure 6**), signifying a concave curvature, which indicates a favorable adsorption scenario ⁴³. This curvature suggests that as active sites on the surface of the adsorbent material became occupied, the likelihood of the compound encountering an available active site diminished, further substantiating the notion of adsorption favorability.

The Sips model provided the best fitting for the adsorption of caffeine onto PSP_{40:60:1.000} since R^2 and SD values were higher and lower, respectively, than the values obtained by the other three models. In this context, at low adsorbate concentrations, the Sips model takes on the characteristics of the Freundlich isotherm. However, as the adsorbate concentration increases, it transitions into the Langmuir isotherm. This phenomenon elucidates the distribution of adsorption energies across the heterogeneous surface of the adsorbent ⁴⁴. Therefore, the Sips combines the multilayer adsorption of the Freundlich model with the monolayer adsorption of the Langmuir model, evidencing a "monolayer-multilayer" adsorption onto a heterogeneous surface of the adsorbent. The

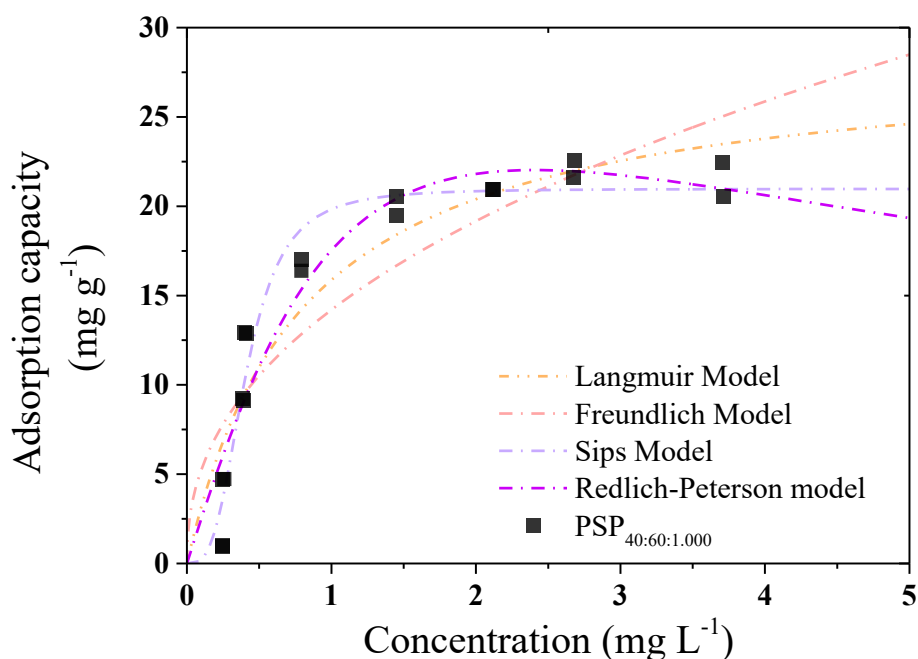


Figure 6: Effect of initial PSP_{40:60:1.000} loading on the adsorption of caffeine. PSP_{X:Y:Z} = X%[DIB]:Y%[S₈]:Zg[NaCl].

isotherm results agree with the good fitting of the Elovich model already observed. In addition, the q_{ads} value (20.97 mg g^{-1}) obtained by the Sips models was very similar to the experimental one (**Table 2**).

Activated carbon is a porous material well-known for removing organic contaminants and small molecules from aqueous solution due to its high surface area, well-developed porosity and high adsorption capacity^{18,45}. In this work, the adsorption of caffeine by a commercially available activated carbon was performed and compared to the results from the adsorption of caffeine onto the PSPs. The q_{ads} values were normalized by the surface area of the adsorbent (**Equation 1**). The results indicated that the adsorption per square meter (m^2) onto the PSPs was at least 2.1 times higher when compared to the activated carbon (Table S3). This observation underscores the more efficient nature of the adsorption process facilitated by the PSPs. Furthermore, when evaluating the results in the context of similar studies available in scientific literature, the superiority of PSPs remains evident even when confronted with higher initial concentrations of caffeine that inherently favor the adsorption process (Table S3).

$$q_{\text{norm}} = \frac{Q_{\text{ads}}}{SA} \quad \text{Equation 1}$$

Where q_{norm} is the normalized adsorption capacity (mg m^{-2}) and SA is the surface area ($\text{m}^2 \text{ g}^{-1}$).

It is also important to note that although increasing the DIB content leads to materials with lower surface area, the normalized adsorption increases. This observation indicates that the

Table 2: Equilibrium adsorption parameters of caffeine onto PSP_{40:60:1.000}

Model	Parameter	PSP _{40:60:1.000}	Model	Parameter	PSP _{40:60:1.000}
Langmuir	$K_L (\text{L mg}^{-1})$	1.25	Redlich-Peterson	$K_{RP} (\text{L mg}^{-1})$	25.43
	$q_{\text{ads}} (\text{mg g}^{-1})$	28.54		$\alpha_{RP} ((\text{mg g}^{-1})^g)$	0.45
	R^2	0.871		g	1.56
	SD	2.83		R^2	0.908
Freundlich			Sips	SD	2.47
	$K_F ((\text{mg/g})/(\text{mg/L})^n)$	14.20		$K_s (\text{L mg}^{-1})$	2.46
	n	2.31		$q_{\text{ads}} (\text{mg g}^{-1})$	20.97
	R^2	0.779		n	3.17
	SD	3.70		R^2	0.955
				SD	1.72

$$\text{PSP}_{X:Y:Z} = X\%[\text{DIB}]:Y\%[\text{S8}]:Z\%[\text{NaCl}].$$

monomer plays a crucial role in the adsorption of caffeine (Table S3). Adsorption experiments using another emerging contaminant (saccharin) with the PSPs synthesized with different content of monomers (PSP_{10:90:1.000}, PSP_{20:80:1.000}, PSP_{30:70:1.000}, PSP_{40:60:1.000}) were also carried out to confirm the effects of DIB on the adsorption properties of the material. The results also showed that the higher the content of the DIB, the higher the normalized adsorption capacity (Figure S11). To further understand the mechanisms involved in this process, adsorption studies at different pH, ionic strength, and temperature were carried out using the PSP that provided the best adsorption results (*i.e.*, PSP_{40:60:1.000}).

3.2.1.2. Adsorption mechanism

One of the key variables in the adsorption process is the pH of the medium, which in turn modulates the surface charge and functional groups of the adsorbent and the charge speciation of the chemical compounds^{18,46}. Caffeine occurs predominantly in zwitterion form at pH below 9 and in negative form at pH higher than 11 (**Figure 7A**). According to the adsorption results, the q_{ads} values were similar in the range of pH studied, which indicates that electrostatic forces did not govern the

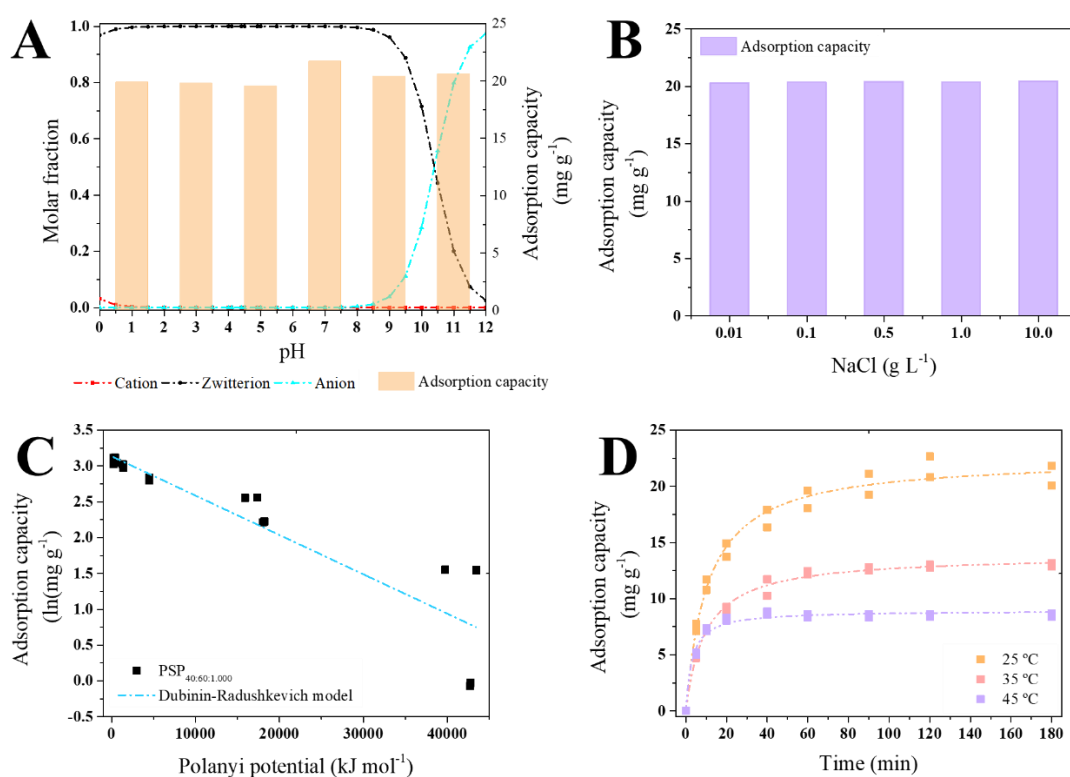


Figure 7: (A) Influence of pH, (B) ionic strength, (C) Fitting to the Dubinin-Radushkevich model, AND (D) temperature in caffeine (CAF) adsorption onto PSP_{40:60:1.000}, and. PSP_{X:Y:Z} = X%[DIB]:Y%[S₈]:Zg[NaCl].

adsorption of caffeine onto PSP_{40:60:1.000}⁴⁷, which was further confirmed by the studies carried at different ionic strengths (**Figure 7B**).

The Dubinin-Radushkevich model exhibited an R^2 value of 0.845 (**Figure 7C**). This model may provide interesting insights into the adsorption of caffeine onto PSP_{40:60:1.000}. The model constant value (K_{DR}) enables the estimation of the mean adsorption energy (E), which is defined as the free energy transfer of 1 mol of solute from infinity to the surface of the adsorbent⁴⁸. The magnitude of the E value offers insight into the adsorption mechanism: E values ranging from 4 to 8 kJ mol⁻¹ imply weak bonds such as van der Waals interactions or physisorption, E values from 2 to 40 kJ mol⁻¹ signify hydrogen bonding, and E values above 60 kJ mol⁻¹ correspond to chemisorption involving valence bond forces of chemical bonds⁴⁹⁻⁵¹.

In the case of the caffeine adsorption onto PSP_{40:60:1.000}, the calculated E value was 95.40 kJ mol⁻¹, suggesting the prevalence of chemisorption. This outcome aligns with expectations, considering the adsorption was unaffected by pH and ionic strength (**Figure 7**). Additionally, the q_{ads} value of the Dubinin-Radushkevich model was 23.00 mg g⁻¹, which was similar to the experimental result (**Table 2**).

However, to confirm whether or not the adsorption of caffeine onto PSP_{40:60:1.000} belongs to chemical adsorption or physical adsorption, the activation energy (E_a) of the reaction was also explored by kinetics thermodynamic studies (**Figure 7D**)⁵². The adsorption E_a of caffeine onto PSP_{40:60:1.000} was determined using the PSO rate constant K_2 at different temperatures (**Figure 7D**) and the Arrhenius equation, as previously described by Wang *et al.*³⁵.

The fitting results of the experimental data are shown in Figure S12. The calculated E_a (*i.e.*, 87.2 kJ mol⁻¹) also confirmed that the adsorption of caffeine onto PSP_{40:60:1.000} is an activated chemical adsorption process. The value was similar to the adsorption energy obtained by Zanella *et al.*⁵³ in the adsorption of caffeine by activated biochar derived from macrophytes. Therefore, the adsorption of caffeine onto PSP_{40:60:1.000} belongs to a "monolayer-multilayer" chemisorption as already predicted by the good fitting on pseudo-second order, Elovich, and Sips models.

In addition to the determination of E_a values, kinetics thermodynamic studies can be used to calculate the standard enthalpy ($\Delta H^\#$), and entropy of activation ($\Delta S^\#$) by the Eyring equation. The free energy of activation ($\Delta G^\#$) was also obtained by the $\Delta H^\#$ and $\Delta S^\#$ values.

The fitting of the experimental data (Figure S13) resulted in a $\Delta H^\#$ of 83.7 kJ mol⁻¹ and $\Delta S^\#$ of - 43.15 J mol⁻¹. These values are indicative of an exothermic process with an associative mechanism, which means that adsorbate does not cleave bonds but forms a complex compound during the chemisorption process^{48,54}. The large positive values of $\Delta G^\#$ (70.8, 70.4, and 70.0 kJ mol⁻¹) values indicate that energy (e.g., agitation) was required in the adsorption reaction to convert reactants into products⁴⁸.

The adsorption of organic contaminants such as caffeine usually occurs by combining several mechanisms^{14,55}. However, it has been reported that hydrophobic interactions significantly contribute to the adsorption of caffeine onto porous materials since the highest q_{ads} values are frequently reported for neutral caffeine species¹⁴. In the present study, it was observed that increasing the content of DIB, which also increased the content of benzene rings in the PSPs, led to higher adsorption of caffeine. Caffeine can form complexes with benzene rings due to aromatic molecule associations mainly in the 7-nitrogen region, acting as an electron acceptor in these complexes⁵⁶. In addition, the amide group of caffeine molecule can form NH/ π geometries of face-on type with benzene rings with energies higher than 40 kJ mol⁻¹⁵⁷ and therefore benzene rings can interact strongly with amide groups wing to their higher π - π stack bonding energies and hydrogen bonding^{58,59}. However, due to the high free adsorption energy, it is expected that caffeine molecules had integrated into the PSPs structure, as Dittmann *et al.*⁶⁰ observed in their studies with carbamazepine and activated carbons. Nevertheless, further studies should be conducted to investigate the adsorption mechanisms of caffeine and other organic pollutants into PSPs and also the effects of using other monomers on the adsorption properties.

3.2.2. Photocatalysis studies

The light absorbance of the PSPs was investigated using UV-Vis spectroscopy (Figure S14). All PSPs exhibited an extended light absorption range compared to pure S₈ and DIB. To be specific, the PSPs absorbed light across a broad spectrum, ranging from visible (475 nm) to UV (250 nm) regions. In contrast, pure S₈ absorbed light from 350 nm and downwards. Therefore, the photocatalytic properties of the PSPs were tested for the degradation of caffeine. For equilibrium to be reached, the solutions were left in the dark for 60 minutes, during which the PSPs with higher DIB content exhibited greater adsorption capabilities (**Figure 8A**), as expected. Conversely, the higher sulfur-content polymers showed higher photocatalytic activity (Figure 8B). PSP_{10:90:1.000} showcased a degradation capacity of 12.8 mg g⁻¹, which was 1.9 times higher than PSP_{40:60:1.000}.

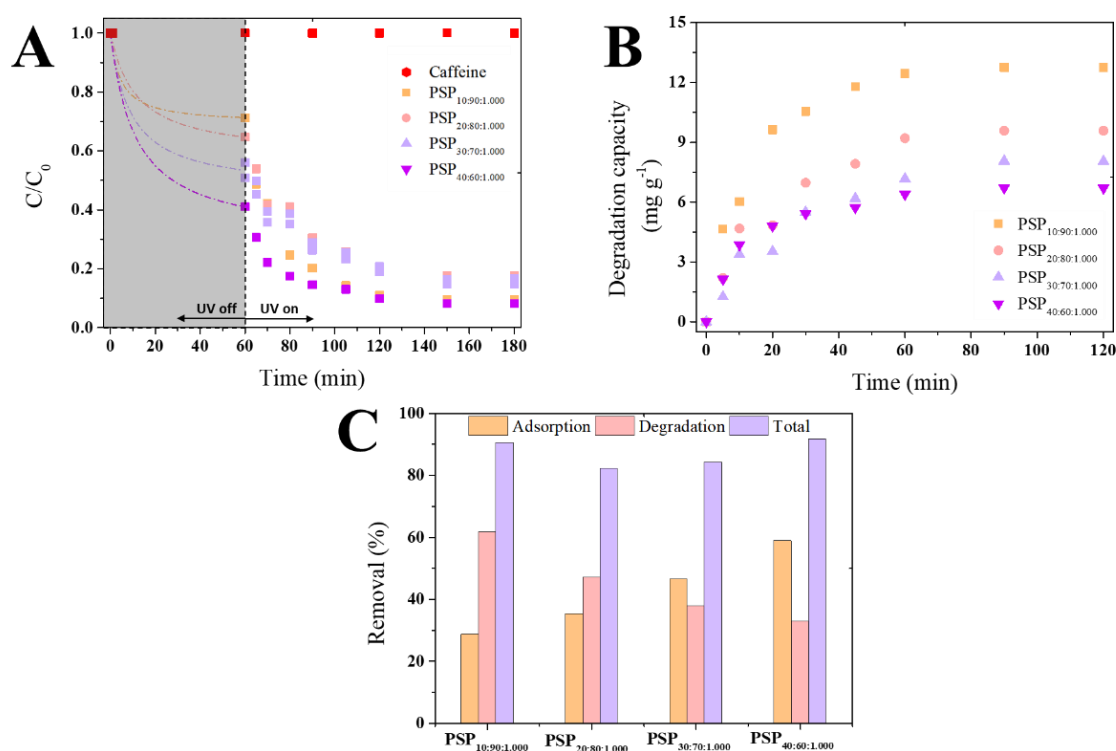


Figure 8: (A) Removal of caffeine by porous sulfur polymers (PSPs) considering 60 min of adsorption and 120 min of irradiation (254 nm). The dash-dot lines indicate the simulated pseudo-second adsorption process. (B) Normalized degradation capacity of the PSPs. (C) Estimation of the contribution of adsorption and degradation to caffeine removal by PSPs. $PSP_{X:Y:Z} = X\%[DIB]:Y\%[S_8]:Zg[NaCl]$.

While previous research has proven the photocatalytic activity of sulfur by doping metal and non-metal^{61,62}, and some studies also showed that high-sulfur content polymers have a potential photocatalytic activity^{8,27,63}, this study pioneers the investigation of the ability of the PSPs to remove emerging contaminants, such as caffeine, through a dual-action mechanism (adsorption and photocatalysis). The PSPs achieved up to 92% of caffeine removal when both adsorption and photocatalysis were combined. Whereas almost no adsorption occurs after 60 min (<10%) (Figure S10), it can be observed that the removal of caffeine by higher sulfur content PSPs was governed by the photocatalytic activity, while PSPs with higher DIB content leaned towards the adsorption process (Figure 8C). As an illustration, in the case of PSP_{10:90:1.000}, approximately 28.7% of the caffeine removal can be attributed to the adsorption mechanism, while 61.8% is ascribed to the photocatalysis activity. Conversely, in the case of PSP_{40:60:1.000}, the adsorption mechanism accounts for 58.9% of caffeine removal, whereas photocatalysis is responsible for 32.8% of caffeine removal. As a first report, this exciting achievement opens a new field of investigation, and further studies can explore modifications on the polymers and the removal of other emerging contaminants.

4. Conclusions

The present study reports the synthesis of PSPs by “inverse vulcanization” using DIB as monomers and introducing porosity via salt templating that can remove caffeine by dual-action mechanism (adsorption and photocatalysis). The adsorption studies revealed a strong correlation between DIB content in the PSPs and their adsorption capacity, with higher DIB content PSPs displaying greater adsorption abilities. The thermodynamic analysis yielded E_a values of 87.2 kJ mol^{-1} , $\Delta H^\#$ of 83.7 kJ mol^{-1} and $\Delta S^\#$ of $-43.15 \text{ J mol}^{-1}$, indicating an exothermic chemisorption process that results in the formation of complexes between the benzene ring of the polymers and 7-nitrogen region of caffeine. The PSPs also showed extended light absorption spectra ranging from 475 nm into the UV region. This broad spectrum enabled photocatalytic activity that correlated with sulfur content in the PSPs, with higher sulfur content PSPs demonstrating superior photocatalytic potential. Notably, all the PSPs showed a dual-action mechanism that resulted in the removal of caffeine by up to 92%. However, it was demonstrated that for PSPs with higher sulfur content, the removal was governed by a degradation mechanism. Meanwhile, for those with higher DIB content, adsorption was the primary removal mechanism. The present study highlights the potential of utilizing PSPs to address the issue of sulfur waste responsibly, showcasing their capacity to generate value-added products through the dual-action mechanism of removing organic contaminants. The versatile synthesis of sulfur polymers offers variation, which means that there is much more to explore in this exciting research area.

5. Acknowledgements

The authors are grateful for the scholarship provided by the São Paulo State Research Foundation (FAPESP) to V.D. #2022/11350-1). In addition, CRC would like to thank the EPSRC for its research funding.

6. References

- 1 *Our World in Data*, <<https://ourworldindata.org/>> (2023).
- 2 WHO. Potable reuse: guidance for producing safe drinking-water. (2017).
- 3 UNESCO. (United Nations Educational, Scientific and Cultural Organization, Paris, 2017).
- 4 Guo, T. J., Englehardt, J. & Wu, T. T. Review of cost versus scale: water and wastewater treatment and reuse processes. *Water Sci Technol* **69**, 223-234 (2014). <https://doi.org/10.2166/wst.2013.734>
- 5 Chung, W. J. *et al.* The use of elemental sulfur as an alternative feedstock for polymeric materials. *Nat Chem* **5**, 518-524 (2013). <https://doi.org/10.1038/nchem.1624>

- 6 Abraham, A. M., Kumar, S. V. & Alhassan, S. M. Porous sulphur copolymer for gas-phase mercury removal and thermal insulation. *Chem Eng J* **332**, 1-7 (2018). <https://doi.org/10.1016/j.cej.2017.09.069>
- 7 Salman, M. K., Karabay, B., Karabay, L. C. & Cihaner, A. Elemental sulfur-based polymeric materials: Synthesis and characterization. *J Appl Polym Sci* **133** (2016). <https://doi.org/10.1002/app.43655>
- 8 Upton, R. L. *et al.* Investigating the viability of sulfur polymers for the fabrication of photoactive, antimicrobial, water repellent coatings. *J Mater Chem B* **10**, 4153-4162 (2022). <https://doi.org/10.1039/d2tb00319h>
- 9 Tarasova, N. P., Zanin, A. A., Krivoborodov, E. G. & Mezhuev, Y. O. Elemental sulphur in the synthesis of sulphur-containing polymers: reaction mechanisms and green prospects. *Rsc Adv* **11**, 9008-9020 (2021). <https://doi.org/10.1039/d0ra10507d>
- 10 Alex, A., Singha, N. K. & Choudhury, S. Exploring inverse vulcanization in lithium-sulfur batteries. *Curr Opin Electroche* **39** (2023). <https://doi.org/10.1016/j.coelec.2023.101271>
- 11 Zhang, B. W. *et al.* Inverse vulcanised sulfur polymer nanoparticles prepared by antisolvent precipitation. *J Mater Chem A* **10**, 13704-13710 (2022). <https://doi.org/10.1039/d2ta01653b>
- 12 Hasell, T., Parker, D. J., Jones, H. A., McAllister, T. & Howdle, S. M. Porous inverse vulcanised polymers for mercury capture. *Chem Commun* **52**, 5383-5386 (2016). <https://doi.org/10.1039/c6cc00938g>
- 13 Bear, J. C., McGettrick, J. D., Parkin, I. P., Dunnill, C. W. & Hasell, T. Porous carbons from inverse vulcanised polymers. *Micropor Mesopor Mat* **232**, 189-195 (2016). <https://doi.org/10.1016/j.micromeso.2016.06.021>
- 14 Diniz, V., Cunha, D. G. F. & Rath, S. Adsorption of recalcitrant contaminants of emerging concern onto activated carbon: A laboratory and pilot-scale study. *Journal of Environmental Management* **325** (2023). <https://doi.org/10.1016/j.jenvman.2022.116489>
- 15 Diniz, V., Reyes, G. M., Rath, S. & Cunha, D. G. F. Caffeine reduces the toxicity of albendazole and carbamazepine to the microalgae *Raphidocelis subcapitata* (Sphaeropleales, Chlorophyta). *Int Rev Hydrobiol* **105**, 151-161 (2020). <https://doi.org/10.1002/iroh.201902024>
- 16 Rigueto, C. V. T. *et al.* Alternative techniques for caffeine removal from wastewater: An overview of opportunities and challenges. *J Water Process Eng* **35** (2020). <https://doi.org/10.1016/j.jwpe.2020.101231>
- 17 Stamatis, N. K. & Konstantinou, I. K. Occurrence and removal of emerging pharmaceutical, personal care compounds and caffeine tracer in municipal sewage treatment plant in Western Greece. *J Environ Sci Heal B* **48**, 800-813 (2013). <https://doi.org/10.1080/03601234.2013.781359>
- 18 Diniz, V. & Rath, S. Adsorption of aqueous phase contaminants of emerging concern by activated carbon: comparative fixed-bed column study and in situ regeneration methods. *J Hazard Mater* (2023). <https://doi.org/10.1016/j.jhazmat.2023.132197>
- 19 Jeffrey, P., Yang, Z. & Judd, S. J. The status of potable water reuse implementation. *Water Res* **214** (2022). <https://doi.org/10.1016/j.watres.2022.118198>
- 20 Warsinger, D. M. *et al.* A review of polymeric membranes and processes for potable water reuse. *Prog Polym Sci* **81**, 209-237 (2018). <https://doi.org/10.1016/j.progpolymsci.2018.01.004>
- 21 Gomez, I. *et al.* Inverse vulcanization of sulfur with divinylbenzene: Stable and easy processable cathode material for lithium-sulfur batteries. *J Power Sources* **329**, 72-78 (2016). <https://doi.org/10.1016/j.jpowsour.2016.08.046>

- 22 Crockett, M. P. *et al.* Sulfur-Limonene Polysulfide: A Material Synthesized Entirely from Industrial By-Products and Its Use in Removing Toxic Metals from Water and Soil. *Angew Chem Int Edit* **55**, 1714-1718 (2016). <https://doi.org/10.1002/anie.201508708>
- 23 Mengesha, D. N., Abebe, M. W., Appiah-Ntiamoah, R. & Kim, H. Ground coffee waste-derived carbon for adsorptive removal of caffeine: Effect of surface chemistry and porous structure. *Sci Total Environ* **818** (2022). <https://doi.org/10.1016/j.scitotenv.2021.151669>
- 24 Oliveira, E. N. *et al.* Highly effective adsorption of caffeine by a novel activated carbon prepared from coconut leaf. *Environ Sci Pollut R* (2022). <https://doi.org/10.1007/s11356-022-18788-w>
- 25 Salam, J. A. *et al.* Mono- and Multicomponent Biosorption of Caffeine and Salicylic Acid onto Processed Cape Gooseberry Husk Agri-Food Waste. *Acs Omega* **8**, 20697-20707 (2023). <https://doi.org/10.1021/acsomega.3c01254>
- 26 de Oliveira, J. T., Costa, L. R. D., Agnol, G. D. & Feris, L. A. Experimental design and data prediction by Bayesian statistics for adsorption of tetracycline in a GAC fixed-bed column. *Sep Purif Technol* **319** (2023). <https://doi.org/10.1016/j.seppur.2023.124097>
- 27 Berk, H. *et al.* Synthesis, characterization and application of high sulfur content polymeric materials from fatty acids. *React Funct Polym* **187** (2023). <https://doi.org/10.1016/j.reactfunctpolym.2023.105581>
- 28 Bao, J. H. *et al.* On the Mechanism of the Inverse Vulcanization of Elemental Sulfur: Structural Characterization of Poly(sulfur-random-(1,3-diisopropenylbenzene)). *J Am Chem Soc* **145**, 12386-12397 (2023). <https://doi.org/10.1021/jacs.3c03604>
- 29 Deng, Z. L., Hoefling, A., Theato, P. & Lienkamp, K. Surface Properties and Antimicrobial Activity of Poly(sulfur-co-1,3-diisopropenylbenzene) Copolymers. *Macromol Chem Phys* **219** (2018). <https://doi.org/10.1002/macp.201700497>
- 30 Almeida, C. *et al.* Electrochemical activity of sulfur networks synthesized through RAFT polymerization. *J Appl Polym Sci* **133** (2016). <https://doi.org/10.1002/app.43993>
- 31 Rafie, A., Pereira, R., Shamsabadi, A. A. & Kalra, V. In Operando FTIR Study on the Effect of Sulfur Chain Length in Sulfur Copolymer-Based Li-S Batteries. *J Phys Chem C* (2022). <https://doi.org/10.1021/acs.jpcc.1c09124>
- 32 Alsulaili, A. D., Refaie, A. A. & Garcia, H. A. Adsorption capacity of activated carbon derived from date seeds: Characterization, optimization, kinetic and equilibrium studies. *Chemosphere* **313** (2023). <https://doi.org/10.1016/j.chemosphere.2022.137554>
- 33 Nielsen, L. & Bandosz, T. J. Analysis of the competitive adsorption of pharmaceuticals on waste derived materials. *Chem Eng J* **287**, 139-147 (2016). <https://doi.org/10.1016/j.cej.2015.11.016>
- 34 Zhao, J. L. *et al.* A comparative evaluation of coal specific surface area by CO₂ and N₂ adsorption and its influence on CH₄ adsorption capacity at different pore sizes. *Fuel* **183**, 420-431 (2016). <https://doi.org/10.1016/j.fuel.2016.06.076>
- 35 Wang, H., Wang, S., Wang, S. X., Fu, L. K. & Zhang, L. B. Efficient metal-organic framework adsorbents for removal of harmful heavy metal Pb(II) from solution: Activation energy and interaction mechanism. *J Environ Chem Eng* **11** (2023). <https://doi.org/10.1016/j.jece.2023.109335>
- 36 Nwabue, F. I. & Itumoh, E. J. Adsorption isotherm and kinetic modeling of a novel procedure for physical modification of silica gel using aqueous solutions of 4,4'-(1,2-ethanediylidinitrilo)bis-(2-pentanone) for preconcentration of Ni(II) ion. *Sep Sci Technol* **55**, 2919-2932 (2020). <https://doi.org/10.1080/01496395.2019.1659821>

- 37 Khnifira, M. *et al.* Adsorption characteristics of dopamine by activated carbon: Experimental and theoretical approach. *J Mol Struct* **1278** (2023). <https://doi.org/10.1016/j.molstruc.2023.134964>
- 38 Rassaei, F. Kinetics, isotherms, thermodynamic adsorption, and desorption studies of chromium in two types of calcareous soils. *Arabian Journal of Geosciences* **16** (2023). <https://doi.org/10.1007/s12517-023-11291-7>
- 39 Dalby, O. P. L., Abbott, S., Matubayasi, N. & Shimizu, S. Cooperative Sorption on Heterogeneous Surfaces. *Langmuir* **38**, 13084-13092 (2022). <https://doi.org/10.1021/acs.langmuir.2c01750>
- 40 Zeng, S., Choi, Y. K. & Kan, E. Iron-activated bermudagrass-derived biochar for adsorption of aqueous sulfamethoxazole: Effects of iron impregnation ratio on biochar properties, adsorption, and regeneration. *Sci Total Environ* **750**, 141691 (2021). <https://doi.org/10.1016/j.scitotenv.2020.141691>
- 41 Wang, J. L. & Guo, X. Adsorption kinetic models: Physical meanings, applications, and solving methods. *J Hazard Mater* **390** (2020). <https://doi.org/10.1016/j.jhazmat.2020.122156>
- 42 Mashile, P. P., Mpupa, A. & Nomngongo, P. N. Adsorptive removal of microcystin-LR from surface and wastewater using tyre-based powdered activated carbon: Kinetics and isotherms. *Toxicon* **145**, 25-31 (2018). <https://doi.org/10.1016/j.toxicon.2018.02.044>
- 43 Giles, C. H., Macewan, T. H., Nakhwa, S. N. & Smith, D. Studies in adsorption .11. A system of classification of solution adsorption isotherms, and its use in diagnosis of adsorption mechanisms and in measurement of specific surface areas of solids. *J. Chem. Soc.*, 3973-3993 (1960). <https://doi.org/10.1039/jr9600003973>
- 44 Rajahmundry, G. K., Garlapati, C., Kumar, P. S., Alwi, R. S. & Vo, D. V. N. Statistical analysis of adsorption isotherm models and its appropriate selection. *Chemosphere* **276** (2021). <https://doi.org/10.1016/j.chemosphere.2021.130176>
- 45 Nazari, G., Abolghasemi, H., Esmaili, M. & Pouya, E. S. Aqueous phase adsorption of cephalixin by walnut shell-based activated carbon: A fixed-bed column study. *Appl Surf Sci* **375**, 144-153 (2016). <https://doi.org/10.1016/j.apsusc.2016.03.096>
- 46 Rhoden, C. R. B., Bruckmann, F. D., Salles, T. D., Kaufmann, C. G. & Mortari, S. R. Study from the influence of magnetite onto removal of hydrochlorothiazide from aqueous solutions applying magnetic graphene oxide. *J Water Process Eng* **43** (2021). <https://doi.org/10.1016/j.jwpe.2021.102262>
- 47 Nguyen, D. T. *et al.* Adsorption process and mechanism of acetaminophen onto commercial activated carbon. *J Environ Chem Eng* **8** (2020). <https://doi.org/10.1016/j.jece.2020.104408>
- 48 Chowdhury, S., Mishra, R., Saha, P. & Kushwaha, P. Adsorption thermodynamics, kinetics and isosteric heat of adsorption of malachite green onto chemically modified rice husk. *Desalination* **265**, 159-168 (2011). <https://doi.org/10.1016/j.desal.2010.07.047>
- 49 Beltrame, K. K. *et al.* Adsorption of caffeine on mesoporous activated carbon fibers prepared from pineapple plant leaves. *Ecotox Environ Safe* **147**, 64-71 (2018). <https://doi.org/10.1016/j.ecoenv.2017.08.034>
- 50 Song, Y. R. *et al.* Preparation of silicon-doped ferrihydrite for adsorption of lead and cadmium: Property and mechanism. *Chinese Chem Lett* **32**, 3169-3174 (2021). <https://doi.org/10.1016/j.ccllet.2021.03.001>
- 51 Tseng, R. L., Tran, H. N. & Juang, R. S. Revisiting temperature effect on the kinetics of liquid-phase adsorption by the Elovich equation: A simple tool for checking data reliability. *J Taiwan Inst Chem E* **136** (2022). <https://doi.org/10.1016/j.jtice.2022.104403>

- 52 Hu, Q. L. & Zhang, Z. Y. Application of Dubinin-Radushkevich isotherm model at the solid/solution interface: A theoretical analysis. *J Mol Liq* **277**, 646-648 (2019). <https://doi.org/10.1016/j.molliq.2019.01.005>
- 53 Zanella, H. G. *et al.* Caffeine adsorption on activated biochar derived from macrophytes (Eichornia crassipes). *J Mol Liq* **340** (2021). <https://doi.org/10.1016/j.molliq.2021.117206>
- 54 Mohapatra, M., Khatun, S. & Anand, S. Kinetics and thermodynamics of lead (II) adsorption on lateritic nickel ores of Indian origin. *Chem Eng J* **155**, 184-190 (2009). <https://doi.org/10.1016/j.cej.2009.07.035>
- 55 Diniz, V., Rath, G., Rath, S., Araujo, L. S. & Cunha, D. G. F. Competitive kinetics of adsorption onto activated carbon for emerging contaminants with contrasting physicochemical properties. *Environ Sci Pollut R* **29**, 42185-42200 (2022). <https://doi.org/10.1007/s11356-021-16043-2>
- 56 Hanna, M. W. & Sandoval, A. Nuclear magnetic resonance studies of complexes between caffeine and aromatic donors. *Biochim. Biophys. Acta* **155**, 433-436 (1968). [https://doi.org/https://doi.org/10.1016/0005-2787\(68\)90188-3](https://doi.org/https://doi.org/10.1016/0005-2787(68)90188-3)
- 57 Imai, Y. N., Inoue, Y., Nakanishi, I. & Kitaura, K. Amide- π Interactions Between Formamide and Benzene. *J Comput Chem* **30**, 2267-2276 (2009). <https://doi.org/10.1002/jcc.21212>
- 58 Salahshoori, I. *et al.* Advancements in wastewater Treatment: A computational analysis of adsorption characteristics of cationic dyes pollutants on amide Functionalized-MOF nanostructure MIL-53 (Al) surfaces. *Sep Purif Technol* **319** (2023). <https://doi.org/10.1016/j.seppur.2023.124081>
- 59 Zhang, G. *et al.* Another perspective to explain green tea cream: Utilizing engineered catechin-caffeine complex. *Food Res Int* **158** (2022). <https://doi.org/10.1016/j.foodres.2022.111542>
- 60 Dittmann, D. *et al.* Specific adsorption sites and conditions derived by thermal decomposition of activated carbons and adsorbed carbamazepine. *Sci Rep-Uk* **10** (2020). <https://doi.org/10.1038/s41598-020-63481-y>
- 61 Priyadarshi, R. *et al.* Sulfur recycling into value-added materials: a review. *Environ Chem Lett* **21**, 1673-1699 (2023). <https://doi.org/10.1007/s10311-023-01575-5>
- 62 Wang, Y. F. *et al.* Effect of sulfur source on photocatalytic degradation performance of CdS/MoS₂ prepared with one-step hydrothermal synthesis. *J Environ Sci* **65**, 347-355 (2018). <https://doi.org/10.1016/j.jes.2017.07.004>
- 63 Tufts, N. Q. *et al.* Photoactive Organo-Sulfur Polymers for Hydrogen Generation. *Chem-Eur J* **29** (2023). <https://doi.org/10.1002/chem.202203177>

Chapter 4.

Discussion

In recent years, our group has focused on the prioritization of pharmaceuticals, resulting in the selection of 12 contaminants of emerging concern (CECs) (acesulfame, acetaminophen, albendazole, carbamazepine, caffeine, diclofenac, hydrochlorothiazide, propranolol, ricobendazole, saccharin, sucralose, and sulfamethoxazole) for the initial phase of this thesis. These contaminants were monitored in raw sewage and effluent at the EPAR Capivari II using a bidimensional liquid chromatography coupled with mass spectrometry (LC-LC-MS/MS) method to support further prioritization efforts. It is important to note that the LC-LC-MS/MS method was developed and validated to quantify the 12 CECs in the water matrix, and the method parameters are presented in the supplementary materials of the manuscript “*Adsorption of recalcitrant contaminants of emerging concern onto activated carbon: A laboratory and pilot-scale study*” (Chapter 7: Annex).

As reported in “*Adsorption of recalcitrant contaminants of emerging concern onto activated carbon: A laboratory and pilot-scale study*”, 11 of the 12 prioritized CECs were detected in the raw sewage at the EPAR Capivari II, with ricobendazole (a metabolite of albendazole) being the only exception. This outcome validates the effectiveness of the prioritization process. While the EPAR Capivari II was not specifically designed for the removal of CECs, its advanced treatment train has demonstrated the capability to partially mitigate these substances (see **Figure 2**). Notably, three of the detected CECs (acesulfame, acetaminophen, and diclofenac) were not detected (< limit of quantification (LOQ)) in the treated effluent, whereas the other eight contaminants were only partially removed by the treatment process. These partial removals underscore the need for further advanced treatment technologies to effectively eliminate these contaminants and ensure water quality.

For further experiments, five of the eight CECs that were only partially removed in the initial treatment process were selected for in-depth study: caffeine, hydrochlorothiazide, saccharin, sulfamethoxazole, and sucralose. Caffeine was chosen due to its widespread presence in surface waters and its established use as an indicator of anthropogenic impact (Korekar, Kumar, and Ugale 2020; Li, Wen, *et al.* 2020; Paíga and Delerue-Matos 2017). Hydrochlorothiazide and sucralose were selected based on their high concentrations in the effluent of the EPAR Capivari II. Sucralose, a highly consumed artificial sweetener, is also non-metabolized by the human body and, unlike caffeine, is a synthetic molecule, making its detection in water bodies a clear marker of anthropogenic contamination (Oppenheimer *et al.* 2011). Saccharin, like sucralose, is an artificial sweetener, and there is a gap in the scientific literature regarding the removal of this class of contaminants, warranting further investigation. Finally, sulfamethoxazole, although detected at low concentrations, was

selected due to its antimicrobial properties, which pose a risk of contributing to the development of antimicrobial resistance genes in bacteria (Larcher and Yargeau 2012).

The World Health Organization (WHO) recommends that every direct potable reuse (DPR) treatment train includes multiple redundant processes to ensure robustness and reliability (WHO 2017). The pilot plant at EPAR Capivari II provides a platform to evaluate and select the most effective combination of treatments for DPR. The pilot plant was initially designed and studied by Hespanhol, Rodrigues, and Mierzwa (2019), who verified its operational feasibility for removing inorganic, microbiological, and certain organic contaminants (*e.g.*, *N-nitrosamines*). However, no studies were conducted on CECs. Considering the 5 CECs previously prioritized, unitary treatment units such as fixed-bed columns of granular activated carbon (GAC) and photoperoxidation (UV/H₂O₂) were effective in partially removing CECs (see “*Adsorption of recalcitrant contaminants of emerging concern onto activated carbon: A laboratory and pilot-scale study*”). However, reverse osmosis (RO) proved to be the most effective, reducing contaminant levels below the limit of quantification (<LOQ, ng/L levels) of the analytical method.

Both UV/H₂O₂ and GAC treatments are more susceptible to the influence of the water matrix compared to reverse osmosis (RO). This is because UV/H₂O₂ efficiency can be hindered by the presence of natural organic matter, which competes for hydroxyl radicals, while GAC's adsorption capacity can be reduced by the presence of competing organic compounds that occupy adsorption sites (Spina *et al.* 2021; Venancio *et al.* 2021; Diniz, Cunha, and Rath 2023; Diniz and Rath 2023). In contrast, RO functions as a physical barrier, effectively removing contaminants regardless of the water matrix composition by filtering them out at the molecular level (Lopera, Ruiz, and Alonso 2019). Due to these differences, RO was combined with both UV/ H₂O₂ and GAC in the treatment process, resulting in the highest removal rates of CECs, achieving levels <LOQ.

As the WHO (WHO 2017) recommends implementing a multi-barrier approach in DPR schemes to ensure that even if one process fails, the effluent maintains its quality, the combination of RO, UV/H₂O₂, and GAC was investigated. As expected, this multi-barrier approach effectively reduced CEC concentrations to <LOQ. In partnership with the Sociedade de Abastecimento de Água e Saneamento S/A (SANASA), the effluent from EPAR Capivari II and the effluent from the pilot plant (RO+UV/H₂O₂+GAC) were monitored according to the parameters established in GM/MS Ordinance No. 888 (Brazilian potability regulations). While the membrane bioreactor process produced high-quality effluent, certain parameters still exceeded the maximum permissible values

(MPVs). In contrast, the EPAR Capivari II + pilot plant (RO+UV/H₂O₂+GAC) met regulatory standards, including the removal of both inorganic and organic contaminants. For example, bacteria persisted in the EPAR Capivari II effluent, whereas the EPAR Capivari II + pilot plant significantly reduced heterotrophic bacteria and eliminated total coliforms, *Escherichia coli*, and *Pseudomonas aeruginosa*, demonstrating the effectiveness of this process in producing water suitable for potable reuse.

Although a robust treatment process has been established, further optimization is necessary to enhance the cost-effectiveness of the system. Given that activated carbon is widely recognized for its efficacy in removing CECs, the adsorption performance of the activated carbon used in the pilot plant (AC1) was investigated and compared with that of a commercially available alternative (AC2). This comparison was conducted through both batch (see “*Adsorption of recalcitrant contaminants of emerging concern onto activated carbon: A laboratory and pilot-scale study*”) and continuous flow studies (see “*Adsorption of aqueous phase contaminants of emerging concern by activated carbon: comparative fixed-bed column study and in situ regeneration methods*”) to evaluate the adsorption efficiency of the selected CECs. These studies aim to identify potential improvements in the process, which could lead to better contaminant removal and overall system efficiency.

Both activated carbons were comprehensively characterized using a range of analytical techniques, as detailed in the respective manuscripts. **Table 4** summarizes the key physical and chemical properties of the materials. Both activated carbons exhibit similar surface chemistry, characterized by the presence of carboxylic, lactonic, phenolic, and alkaline functional groups, resulting in comparable points of zero charge. Despite their similar pore sizes, AC2 possesses a larger surface area and pore volume, along with a greater particle size, which could have a significant impact on the adsorption behavior of these porous materials.

Laboratory-scale batch experiments revealed that AC2 exhibited superior adsorption capacities for the selected CECs compared to AC1. However, AC1 demonstrated a more rapid adsorption process, achieving equilibrium in 270 minutes, whereas AC2 required 480 minutes to reach equilibrium (**Figure 9**). To elucidate the adsorption kinetics, several kinetic models were evaluated, with the Elovich model providing the best fit for both activated carbons (see *Adsorption of recalcitrant contaminants of emerging concern onto activated carbon: A laboratory and pilot-scale study* for AC1 data and **Table 5** for AC2 data). The strong correlation with the Elovich model

suggests that the adsorption mechanism is predominantly governed by chemisorption, characterized by heterogeneous surface interactions and an increase in activation energy as adsorption sites become occupied (Diniz *et al.* 2022; Nwabue and Itumoh 2020). The model's fit implies that the adsorption process is not purely linear and is influenced by the progressively reduced availability of active sites as the reaction proceeds. These findings indicate that while AC2 offers higher overall adsorption capacity, the faster kinetics of AC1 may be advantageous in applications where rapid contaminant removal is critical.

Table 4: Properties of activated carbons (AC1 & AC2) determined by nitrogen gas (N_2) adsorption at 77 K and Boehm titration.

Parameters	AC1	AC2
Particle size (mm)	0.7 – 1.7	1.2 – 2.4
Specific surface area (m^2/g)	536.5	716.0
Total pore volume (cm^3/g)	0.349	0.504
Total micropore volume (cm^3/g)	0.265	0.365
Total mesopore volume (cm^3/g)	0.084	0.150
Average pore size (nm)	2.6	2.8
Isotherm class ^a	IV	IV
Hysteresis class ^a	H4	H4
Carboxylic groups (mEq/g)	0.5	0.4
Lactonic groups (mEq/g)	0.5	0.6
Phenolic groups (mEq/g)	0.2	0.3
Alkaline groups (mEq/g)	1.5	1.5
pH _{pzc}	9.2	9.3

^aSee Figure 4

Following the kinetic studies, adsorption isotherm experiments were conducted at the established equilibrium times to gain deeper insights into the adsorption characteristics of both activated carbons. The isotherm data were most accurately described by the Sips model, which is particularly suited for systems involving heterogeneous surfaces with a range of adsorption site affinities (Sips 1948). The Sips model, which integrates elements of both the Langmuir and Freundlich isotherms, confirmed that AC2 possesses a higher adsorption capacity for the CECs compared to AC1. This enhanced capacity is likely attributable to AC2's larger surface area and pore volume, which provide a greater number of active sites for adsorption.

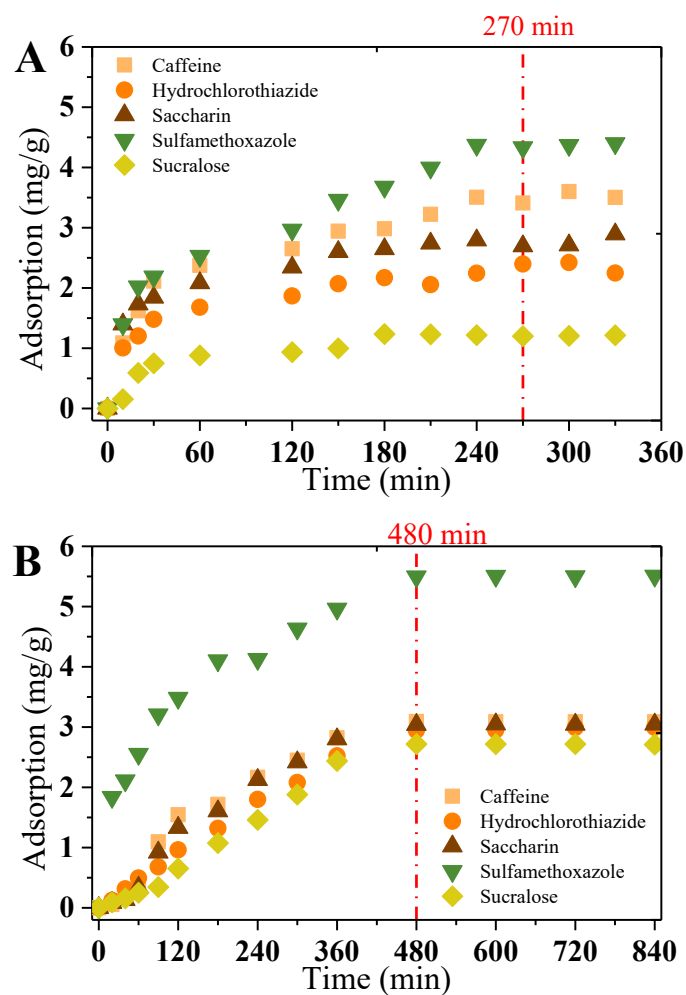


Figure 9: Adsorption kinetics of the selected contaminants of emerging concern (CECs) by AC1 (A) and AC2 (B). Initial concentration of 500 $\mu\text{g/L}$. Source: Author.

Table 5: Summary of Elovich model parameters for both AC1 and AC2

CECs	Elovich model parameters			
	α (mg/g min)	β (mg/g)	R^2	SSE
	AC1 / AC2	AC1 / AC2	AC1 / AC2	AC1 / AC2
Caffeine	0.308 / 0.019	1.396 / 0.728	0.988 / 0.950	0.169 / 0.981
Hydrochlorothiazide	0.436 / 0.012	2.492 / 0.600	0.987 / 0.971	0.071 / 0.512
Saccharin	1.149 / 0.017	2.385 / 0.683	0.994 / 0.950	0.050 / 0.992
Sulfamethoxazole	0.261 / 0.174	1.026 / 0.823	0.976 / 0.989	0.483 / 0.400
Sucralose	0.075 / 0.009	3.483 / 0.512	0.949 / 0.966	0.108 / 0.520

The Sips model's fit to the data indicates that the adsorption process on AC2 is characterized by an initial phase of high-affinity adsorption at low contaminant concentrations,

followed by a transition to more heterogeneous adsorption behavior as the surface sites become progressively occupied (Sips 1948; Kyzas *et al.* 2018). This model is particularly valuable in describing adsorption on materials where site heterogeneity plays a significant role, as it accounts for the decreasing affinity as more sites are filled (Al-Ghouti and Da'ana 2020). The higher adsorption potential of AC2, as predicted by the Sips model, suggests its suitability for applications requiring the removal of higher contaminant loads. However, the interplay between its higher capacity and slower kinetics, as observed in previous experiments, must be considered in optimizing treatment processes to balance efficiency with throughput.

Building on the insights gained from the batch process studies, it was essential to evaluate the performance of GAC in a more practical application, as most DPR plants utilize GAC in continuous flow systems rather than batch processes (Jeffrey, Yang, and Judd 2022). To this end, lab-scale columns were constructed and used to investigate the removal of CECs under conditions that closely mimic real-world operations (see “*Adsorption of aqueous phase contaminants of emerging concern by activated carbon: Comparative fixed-bed column study and in situ regeneration methods*”). Various operational parameters, including flow rate, bed height, and flow mode (*e.g.*, upflow vs. downflow), were systematically examined to understand their influence on the adsorption process. These studies aimed to optimize the column performance, ensuring that the GAC’s adsorption capacity observed in batch experiments could be effectively translated to continuous flow systems, thereby improving the overall efficiency and sustainability of DPR applications.

Understanding flow dynamics within these continuous flow columns is crucial for accurately assessing adsorption performance and optimizing operational parameters. To investigate this, an inert saline tracer (NaCl) was employed to determine the hydraulic retention time (HRT) and to identify any disturbances or preferential pathways under different operational configurations. The tracer data revealed that in the downflow mode, columns packed with AC1 exhibited longer HRT compared to those with AC2, likely due to the presence of preferential flow pathways in the AC2 columns. These pathways are attributed to AC2’s larger particle size, which creates more void spaces and channels within the column, reducing the contact time between contaminants and the adsorbent material. Conversely, in the upflow mode, where gravity’s influence is minimized, both activated carbons demonstrated similar retention times, with AC2 showing slightly longer HRT values. This suggests that in upflow configurations, the impact of particle size on flow dynamics is reduced, allowing for more uniform flow distribution and comparable retention times between the two activated carbons.

The effects of bed height and flow rate on the adsorption of CECs were also systematically studied in the lab-scale columns. Increasing the bed height resulted in longer saturation times, as more adsorbent material was available for contaminant removal (**Table 6**). However, this increase in bed height did not proportionally enhance the adsorption capacity. Although a greater number of active sites were theoretically available with a higher bed height, this did not necessarily translate into increased accessibility for the adsorbates (Wang *et al.* 2010). This finding suggests that the surface area of the activated carbons does not play a pivotal role in the adsorption of CECs in this context. Instead, the observed increase in the quantity of contaminants adsorbed was primarily due to the greater mass of activated carbon loaded into the columns, rather than an improvement in the adsorption efficiency or capacity.

Flow rate significantly impacts adsorption by affecting the contact time between the adsorbate and adsorbent (Ahmed and Hameed 2018). Slower flow rates allow more time for contaminants to interact with and be adsorbed in activated carbon, while higher flow rates lead to faster saturation due to rapid percolation and quicker occupation of active sites (**Table 7**). The reduced contact time between the activated carbon and contaminants at higher flow rates limited the adsorption process, resulting in lower adsorption capacities for all the contaminants studied. These findings underscore the importance of optimizing flow rate to balance throughput and adsorption efficiency, ensuring that sufficient contact time is maintained to maximize contaminant removal in continuous flow systems.

Table 6: Summary of breakthrough curve model parameters for both AC1 and AC2 at different bed heights and downflow mode.

	Q _{ads} (mg/g)	T _b (min)	T _s (min)	MTZ (cm)	Q _{ads} (mg/g)	T _b (min)	T _s (min)	MTZ (cm)	Q _{ads} (mg/g)	T _b (min)	T _s (min)	MTZ (cm)
Bed height	1.5 cm				2.5 cm				3.5 cm			
CECs	AC1											
Caffeine	1.73	203.8	117.6	0.63	1.61	314.4	235.3	0.63	1.41	387.8	294.1	0.85
Hydrochlorothiazide	1.13	138.1	58.8	0.86	1.20	243.0	146.9	0.99	1.20	344.1	264.5	0.81
Saccharin	1.18	145.0	58.8	0.89	1.21	245.8	176.3	0.71	1.21	345.0	264.5	0.82
Sulfamethoxazole	1.25	163.4	88.0	0.69	1.34	290.2	205.4	0.73	1.26	383.5	293.5	0.82
Sucralose	0.92	117.8	29.4	1.13	1.09	231.1	117.4	1.23	1.10	327.0	205.5	1.30
	AC2											
Caffeine	0.94	122.6	44.0	0.96	0.90	196.9	88.0	1.38	0.82	248.2	146.7	1.43
Hydrochlorothiazide	0.42	55.4	19.6	0.97	0.56	124.0	44.0	1.61	0.60	186.1	88.0	1.84
Saccharin	0.75	99.1	29.3	1.06	0.65	144.7	44.0	1.74	0.55	170.6	88.0	1.69
Sulfamethoxazole	0.99	131.8	29.3	1.17	0.75	167.3	58.7	1.62	0.70	217.3	117.3	1.61
Sucralose	0.57	78.9	4.9	1.41	0.42	99.1	19.5	2.01	0.42	136.6	43.9	2.38

Q_{ads} : Adsorption capacity; T_b : breakthrough time; T_s : saturation time; MTZ: mass transfer zone. Flow rate: 5 mL/min and theoretical initial concentration of the CECs: 2 mg/L.

Table 7: Summary of breakthrough curve model parameter for both AC1 and AC2 at different flow rates and downflow mode.

	Q _{ads} (mg/g)	T _b (min)	T _s (min)	MTZ (cm)	Q _{ads} (mg/g)	T _b (min)	T _s (min)	MTZ (cm)	Q _{ads} (mg/g)	T _b (min)	T _s (min)	MTZ (cm)
Flow rate	5 mL/min				8 mL/min				11 mL/min			
AC1												
Caffeine	1.41	387.8	294.1	0.85	0.98	196.0	146.6	0.88	0.94	136.4	88.0	1.24
Hydrochlorothiazide	1.20	344.1	264.5	0.81	0.44	90.2	58.6	1.23	0.16	24.3	19.5	0.69
Saccharin	1.21	345.0	264.5	0.82	0.42	87.7	58.6	1.16	0.14	20.8	19.5	0.22
Sulfamethoxazole	1.26	383.5	293.5	0.82	0.58	118.8	87.9	0.91	0.38	56.5	44.0	0.77
Sucralose	1.10	327.0	205.5	1.30	0.22	45.9	29.3	1.27	0.09	14.0	9.8	1.05
AC2												
Caffeine	0.82	248.2	146.7	1.43	0.32	64.6	44.0	1.12	0.15	21.9	14.6	1.17
Hydrochlorothiazide	0.60	186.1	88.0	1.84	0.13	27.8	14.6	1.66	0.06	9.0	4.9	1.59
Saccharin	0.55	170.6	88.0	1.69	0.13	28.3	14.6	1.69	0.08	13.1	3.9	2.46
Sulfamethoxazole	0.70	217.3	117.3	1.61	0.32	67.1	29.3	1.97	0.08	12.8	9.8	0.82
Sucralose	0.42	136.6	43.9	2.38	0.10	21.3	9.8	1.89	0.03	4.7	1.0	2.76

Q_{ads}: Adsorption capacity; T_b: breakthrough time; T_s: saturation time; MTZ: mass transfer zone. Bed height: 3.5 cm and theoretical initial concentration of the CECs: 2 mg/L.

When comparing the performance of both activated carbons in the downflow mode, AC1 consistently outperformed AC2 across all tested bed heights and flow rates. As demonstrated in the flow dynamics studies, despite AC2's higher surface area (see “*Adsorption of aqueous phase contaminants of emerging concern by activated carbon: Comparative fixed-bed column study and in situ regeneration methods*” for more details), its larger particle size led to the formation of preferential pathways within the columns. These pathways significantly reduced the HRT, thereby limiting the contact time between the contaminants and the adsorbent material. This reduction in HRT diminished the overall effectiveness of AC2 in adsorbing CECs. In contrast, AC1, with its smaller particle size and more uniform flow distribution, maintained longer HRTs and provided better contaminant removal efficiency, regardless of the operational parameters. This highlights the critical role of particle size in optimizing adsorption performance, particularly in downflow configurations where flow dynamics are more sensitive to the physical characteristics of the adsorbent.

To further investigate the impact of flow mode on the adsorption of contaminants in fixed-bed columns, the effect of bed height was also examined in the upflow mode (**Table 8**). The results mirrored those observed in the downflow mode: increasing the bed height led to longer saturation times but did not result in higher adsorption capacity. However, in the upflow mode, both activated carbons showed improved adsorption performance, with the increase being more pronounced for AC2. This enhancement is attributed to the elimination of preferential pathways, which were a significant issue in the downflow mode due to AC2's larger particle size. In the upflow configuration, where gravity's influence is minimized, the flow dynamics allowed for more uniform distribution of the contaminants across the adsorbent bed. Interestingly, despite AC2 having a 1.3 times larger surface area than AC1, the adsorption parameters for both activated carbons were similar. This suggests that in the upflow mode, the HRT was the dominant factor governing adsorption as the values for both activated carbons converged, highlighting the critical role of flow dynamics over the surface area in these systems.

Given that the goal of this study is to advance DPR, the impact of water composition on the removal of CECs was also explored (**Table 9**). Adsorption studies were conducted using three different water matrices: ultrapure water, post-MBR effluent from the EPAR Capivari II, and "reuse water" (treated water following the MBR + RO + UV/H₂O₂).

Table 8: Summary of breakthrough curve model parameters for both AC1 and AC2 at different bed heights and upflow mode.

	Q _{ads} (mg/g)	T _b (min)	T _s (min)	MTZ (cm)	Q _{ads} (mg/g)	T _b (min)	T _s (min)	MTZ (cm)	Q _{ads} (mg/g)	T _b (min)	T _s (min)	MTZ (cm)
Bed height	1.5 cm				2.5 cm				3.5 cm			
CECs	AC1											
Caffeine	1.57	230.0	175.6	0.35	1.54	378.3	321.9	0.37	1.33	453.7	409.8	0.34
Hydrochlorothiazide	1.26	176.2	87.9	0.75	1.32	307.8	234.4	0.60	1.17	380.1	322.3	0.53
Saccharin	1.35	187.5	87.9	0.80	1.31	306.1	234.4	0.59	1.21	394.2	351.6	0.38
Sulfamethoxazole	1.54	225.4	146.3	0.53	1.45	354.8	292.7	0.44	1.29	439.8	380.5	0.47
Sucralose	1.17	167.5	58.6	0.98	1.11	265.3	175.7	0.84	1.17	390.4	292.8	0.87
	AC2											
Caffeine	1.84	256.9	205.1	0.30	1.69	394.2	351.6	0.27	1.40	454.2	410.2	0.34
Hydrochlorothiazide	1.24	181.4	87.7	0.77	1.29	313.6	234.1	0.63	1.19	404.7	321.6	0.72
Saccharin	1.27	176.9	87.9	0.75	1.39	323.1	234.4	0.69	1.35	438.0	351.6	0.69
Sulfamethoxazole	1.59	227.5	146.4	0.53	1.56	370.4	292.8	0.52	1.37	457.5	380.7	0.59
Sucralose	1.23	175.7	58.6	1.00	1.32	315.4	205.0	0.87	1.25	416.6	322.1	0.79

Q_{ads} : Adsorption capacity; T_b : breakthrough time; T_s : saturation time; MTZ: mass transfer zone. Flow rate: 5 mL/min and theoretical initial concentration of the CECs: 2 mg/L .

Table 9: Summary of breakthrough curve model parameters for both AC1 and AC2 under different water composition.

	Q _{ads} (mg/g)	T _b (min)	T _s (min)	MTZ (cm)	Q _{ads} (mg/g)	T _b (min)	T _s (min)	MTZ (cm)	Q _{ads} (mg/g)	T _b (min)	T _s (min)	MTZ (cm)
Water matrice		Water				Post-MBR				Reuse water		
CECs		AC1										
Caffeine	1.41	387.8	294.1	0.85	0.7	146.3	232.5	1.30	1.1	264.0	333.6	0.75
Hydrochlorothiazide	1.20	344.1	264.5	0.81	0.5	58.7	163.0	2.24	1.0	205.3	316.0	1.23
Saccharin	1.21	345.0	264.5	0.82	0.5	58.5	186.8	2.40	0.9	204.9	295.9	1.08
Sulfamethoxazole	1.26	383.5	293.5	0.82	0.7	117.3	208.8	1.53	1.0	234.5	334.2	1.04
Sucralose	1.10	327.0	205.5	1.30	0.3	29.3	99.0	2.46	0.8	175.2	274.5	1.27
		AC2										
Caffeine	0.82	248.2	146.7	1.43	0.4	43.9	125.6	2.28	0.7	117.3	213.3	1.58
Hydrochlorothiazide	0.60	186.1	88.0	1.84	0.2	14.7	70.1	2.77	0.6	58.7	176.9	2.34
Saccharin	0.55	170.6	88.0	1.69	0.1	14.6	45.0	2.36	0.5	58.5	165.9	2.27
Sulfamethoxazole	0.70	217.3	117.3	1.61	0.3	20.3	109.2	2.85	0.6	87.9	194.0	1.91
Sucralose	0.42	136.6	43.9	2.38	0.1	3.9	35.2	3.01	0.3	19.5	117.0	2.92

Q_{ads}: Adsorption capacity; T_b: breakthrough time; T_s: saturation time; MTZ: mass transfer zone. Bed height: 3.5 cm, flow rate: 5 mL/min and theoretical initial concentration of the CECs: 2 mg/L

It is well-established that the use of more complex water matrices, such as those containing higher levels of organic matter, typically results in reduced adsorption efficiency (Sgroi *et al.* 2018). This is due to the competition between organic matter and contaminants for the active sites on activated carbon, which can significantly impair the removal of CECs. Since fixed-bed columns are commonly employed in reuse water treatment plants, understanding this impact is crucial for developing the most effective treatment protocols.

The adsorption studies demonstrated that the matrix with the highest purity, ultrapure water, yielded the most favorable parameters for contaminant removal, aligning with the principle that simpler water matrices with minimal organic matter led to more efficient adsorption onto activated carbon. In contrast, post-MBR effluent, which contains higher levels of organic matter, exhibited reduced adsorption performance due to competitive interactions for active sites on the activated carbon. Notably, pretreatment of the effluent, using RO and UV/H₂O₂, resulted in a marked improvement in the removal parameters. This enhancement underscores the effectiveness of pretreatment in mitigating the interference of organic matter and other contaminants. The improved adsorption capacity and overall removal efficiency achieved with pre-treated "reuse water" emphasize the significance of pretreatment processes in extending the operational lifespan of fixed-bed columns and enhancing their performance.

In addition to pretreatment strategies, the regeneration of activated carbon represents a viable alternative for improving the cost-effectiveness and sustainability of DPR plants. Regenerating the adsorbent can significantly reduce the frequency of carbon disposal, thereby minimizing operational costs and environmental impact. As demonstrated in "Adsorption of aqueous phase contaminants of emerging concern by activated carbon: Comparative fixed-bed column study and in situ regeneration methods", in-situ regeneration of the fixed-bed column was successfully achieved through a three-cycle process using a 100% ethanol solution. As an organic solvent, ethanol facilitates the physical displacement and solubilization of contaminants from the activated carbon. This process enhances the desorption efficiency, allowing for effective regeneration of the carbon and enabling its reuse. Combined with pretreatment strategies, such regeneration techniques are pivotal in extending the operational life of the adsorbent and improving the overall sustainability of DPR systems by reducing waste and associated costs.

Advancing the development of novel materials is also crucial for further enhancing the efficiency and sustainability of DPR systems. While traditional adsorbents offer effective

contaminant removal, they often fall short in simultaneous degradation, necessitating either disposal or regeneration. To overcome these limitations, current research is focusing on materials that integrate both adsorption and degradation functions, thereby optimizing contaminant removal and extending the operational lifespan of treatment systems.

With the aim to create innovative advanced materials for DPR systems, this study investigates two innovative approaches: anchoring titanium dioxide onto activated carbon (TiO₂/AC) and synthesizing porous sulfur polymers. The TiO₂/AC composite combines the adsorptive properties of activated carbon with the photocatalytic capabilities of titanium dioxide, enabling both removal and degradation of contaminants (see “Synthesis and characterization of TiO₂-carbon filter materials for water decontamination by adsorption-degradation processes”). Similarly, the synthesis of porous sulfur polymers through inverse vulcanization provides an advanced material with tunable porosity and chemical functionalities, designed to enhance both adsorption and degradation (see “Porous sulfur polymers for effective aqueous-phase organic contaminant removal”).

Building on the exploration of advanced materials, commercially available titanium dioxide photocatalysts, specifically PC500 and P25, were initially tested for their efficacy in degrading the CECs. The results demonstrated that PC500 – containing 100% anatase crystalline phase, outperformed P25 (80% anatase & 20% rutile) in terms of contaminant degradation. The anatase phase is particularly beneficial for photocatalysis due to its favorable band gap energy (~3.5 eV), which allows it to absorb UV light effectively and generate electron-hole pairs (Schneider *et al.* 2014). These pairs are crucial for initiating the redox reactions needed to break down organic pollutants. The higher anatase content in PC500 enhances its photocatalytic activity (Caianelo *et al.* 2022), making it more efficient in driving the degradation processes necessary for effective water purification.

While titanium dioxide is effective in degrading CECs, its nanometric size poses significant challenges for separation from the aqueous phase. This difficulty in separation raises environmental concerns, as these nanoparticles can bioaccumulate, leading to biomagnification in food webs (Shi *et al.* 2016; Li *et al.* 2022). To mitigate these issues, anchoring titanium dioxide onto activated carbon has been explored as a strategy to enhance both the photocatalytic efficiency and the ease of separation of titanium dioxide from aqueous media (Peñas-Garzón *et al.* 2020; Taoufik *et al.* 2019; Orha *et al.* 2017). Although this approach has been extensively investigated, the synthetic procedures for creating TiO₂/AC composites are not yet fully optimized. This study systematically

examined the impact of different titania precursors (titanium isopropoxide and titanium butoxide) and synthetic methods on the properties and photocatalytic efficiency of TiO₂/AC materials, aiming to develop a more effective and environmentally sustainable solution for contaminant removal in DPR systems.

Various methods for synthesizing titanium dioxide have been explored to enhance its photocatalytic properties and facilitate its integration with activated carbon (Akpan and Hameed 2010; Li Puma *et al.* 2008). Among the most prominent are the sol-gel, solvothermal, and hydrothermal methods. The sol-gel method involves the transition of a system from a liquid sol into a solid gel phase, allowing for precise control over the chemical composition and microstructure of the resulting titanium dioxide. This method is particularly advantageous for producing uniform and highly porous titanium dioxide particles, which are essential for maximizing surface area and photocatalytic efficiency (Akpan and Hameed 2010).

The solvothermal method, which involves the reaction of precursors in a solvent under high temperature and pressure, offers the benefit of producing well-crystallized titanium dioxide with controlled morphology (Inoue 2005). This technique allows for the synthesis of titanium dioxide with different crystalline phases, such as anatase and rutile, by adjusting the reaction parameters (Cargnello, Gordon, and Murray 2014). The hydrothermal method, a subset of solvothermal processes, is conducted in an aqueous medium, typically leading to the formation of anatase-phase titanium dioxide, which is highly active in photocatalysis due to its optimal band gap (Cargnello, Gordon, and Murray 2014; Caianelo *et al.* 2022). Moreover, microwave-assisted hydrothermal methods have gained attention as a rapid and energy-efficient alternative (Gao, Remón, and Matharu 2021). This technique uses microwave irradiation to accelerate the reaction kinetics, resulting in faster synthesis times and often yielding titanium dioxide with enhanced crystallinity and phase purity. The combination of microwave heating with hydrothermal conditions allows for the production of nanostructured titanium dioxide with tailored properties, making it an attractive option for improving the photocatalytic performance of TiO₂/AC composites in water treatment applications (Tian *et al.* 2015).

The eight TiO₂/AC composites synthesized through various methods were thoroughly characterized to assess their structural and surface properties. Despite sharing certain similarities, such as the exclusive presence of the anatase crystalline phase, the materials exhibited distinct differences in other aspects. For instance, variations in crystal size and surface area were observed

across the different synthesis techniques (see “*Synthesis and characterization of TiO₂-carbon filter materials for water decontamination by adsorption-degradation processes*”). The sol-gel method produced TiO₂/AC composites with the highest surface area, which is advantageous for adsorption processes as it provides more active sites for contaminant interaction. These differences underscore the influence of the synthesis method on the final properties of the TiO₂/AC materials, highlighting the importance of selecting appropriate synthesis conditions to tailor the composites for specific photocatalytic and adsorption applications.

The choice of titania precursors significantly impacted the final properties of the TiO₂/AC materials, with effects closely tied to the synthesis method. Titanium isopropoxide produced the best heterostructures when used with the sol-gel and microwave-assisted hydrothermal method with shorter hydrolysis time, while titanium butoxide was optimal for microwave-assisted hydrothermal method with the longest hydrolysis time. As the synthesis begins with the hydrolysis of the alkoxide bond in the precursor, leading to Ti–O–Ti bond formation, titanium butoxide, with its faster hydrolysis, tends to form larger agglomerates, resulting in lower surface area. Thus, titanium isopropoxide was preferred for methods requiring extended hydrolysis times, whereas titanium butoxide was better suited for quicker processes.

The synthesized TiO₂/AC materials were subsequently tested for their ability to remove the CECs. Hydrochlorothiazide and sulfamethoxazole were almost instantaneously removed, as seen in photolysis studies. For caffeine, saccharin, and sucralose, sucralose exhibited the highest removal rate, which was particularly noteworthy given its relatively low adsorption capacity in the AC1 material used as the titanium dioxide support. These results suggest that while adsorption played a role in contaminant removal, photocatalytic activity was the dominant factor influencing the efficiency of the TiO₂/AC materials.

Interestingly, when compared to titanium dioxide nanoparticles, the TiO₂/AC materials appeared to be less efficient in removing contaminants. However, when the removal capacity was normalized by the mass of titanium dioxide, a significant increase in photocatalytic efficiency was observed. For instance, the sol-gel method enhanced the photocatalytic efficiency of titanium dioxide by up to 10 times, likely due to the prolonged contact time between contaminants and the titanium dioxide nanoparticles facilitated by the activated carbon support. These findings underscore the potential of TiO₂/AC materials in optimizing contaminant removal through a synergistic combination of adsorption and photocatalysis.

The regenerative capacity of the synthesized TiO_2/AC materials was also evaluated, revealing a promising aspect for enhancing their cost-effectiveness in DPR systems. The materials demonstrated the ability to be regenerated and reused for up to four cycles without significant loss of photocatalytic efficiency. This stability across multiple cycles underscores their durability and potential as a sustainable alternative material for improving the overall effectiveness of DPR systems. The ability to maintain performance after regeneration not only reduces operational costs but also extends the functional lifespan of the materials, making them a viable option for long-term water treatment applications.

Another innovative approach for developing advanced materials for DPR systems can be the use of “inverse vulcanization” sulfur polymers. This relatively new class of polymers has already been explored for the removal of inorganic contaminants (Hasell *et al.* 2016; Bear *et al.* 2016; Amna and Alhssan 2024; Abraham, Kumar, and Alhassan 2018), but its potential for removing organic contaminants, such as CECs, remains largely unexplored. Sulfur polymers offer several advantages, including a scalable, solventless synthesis method that utilizes waste from petroleum refinement as a feedstock (Worthington, Kucera, and Chalker 2017). Additionally, these materials can be easily tailored and possess photocatalytic activity due to their high sulfur content (Upton *et al.* 2022). This study is pioneering in its investigation of sulfur polymers for the removal of CECs, using caffeine - a well-known emerging contaminant and anthropogenic marker - as a model contaminant.

The sulfur polymers were synthesized using the traditional thermal process (as proposed by Chung *et al.* (2013)) with 1,3-diisopropenylbenzene (DIB) serving as the crosslinker to stabilize the polymeric sulfur chains. To create porous materials that could support both adsorption and photodegradation processes, similar to the TiO_2/AC materials, pre-ground table salt (NaCl) was introduced into the liquid pre-polymer. After polymerization, the salt was removed by solubilization in water, leaving behind the desired porous structure. Various compositions of DIB and sulfur (by mass ratio) were synthesized and thoroughly characterized to confirm successful polymerization. The results revealed that while the DIB-to-sulfur ratio did not significantly impact the physical properties of the polymers (they exhibit similar surface area), it did influence their chemical properties, which in turn affected their adsorption and photodegradation efficiencies.

Batch adsorption studies further emphasized the role of DIB content in the adsorption of caffeine. These studies included detailed thermodynamic, kinetic, and isotherm analyses, which collectively demonstrated that higher DIB content correlated with increased adsorption capacity (see

the “*Porous sulfur polymers for effective aqueous-phase organic contaminant removal*” for more details). This relationship is likely due to the molecular structure of DIB, where its benzene rings facilitate aromatic interactions with caffeine, especially in the 7-nitrogen region (Hanna and Sandoval 1968). The adsorption models suggested site heterogeneity, indicating the presence of multiple active sites within the polymer matrix. Furthermore, thermodynamic analysis revealed adsorption energies greater than 80 kJ/mol, characteristic of an activated chemical process (Zanella *et al.* 2021), reinforcing the idea that the specific interactions between DIB and caffeine significantly enhance the material's adsorption efficiency.

In contrast, the photocatalytic activity was more pronounced in polymers with higher sulfur content. When sulfur is irradiated, it can generate a pair of photoinduced electron-hole pairs (h^+ and e^-), functioning similarly to TiO_2 as an indirect semiconductor (Li *et al.* 2020). This process involves two electronic bandgaps, at 4.4 eV and 2.6 eV, and leads to the production of hydroxyl radicals ($OH\cdot$), which are highly reactive and play a crucial role in the degradation of organic contaminants (Diniz *et al.* 2024b).

Lastly, when combining both adsorption and photodegradation processes, up to 92% of caffeine was successfully removed from the aqueous medium. Notably, for polymers with a higher DIB content, adsorption emerged as the dominant mechanism, whereas photodegradation played a more significant role in the removal process when sulfur-rich polymers were utilized. This differentiation underscores the tunable nature of sulfur polymers, where adjusting the DIB-to-sulfur ratio allows for a targeted approach in optimizing either adsorption or photodegradation processes, depending on the specific application requirements.

Both TiO_2/AC materials and sulfur polymers have shown promising potential in integrating adsorption and photodegradation processes within a single material, which is crucial for the efficient removal of CECs in water treatment. The dual functionality of these materials not only enhances contaminant removal but can also extend the operational lifespan of treatment systems by reducing the frequency of regeneration or replacement. This makes them strong candidates for advanced materials in DPR systems, where both cost-effectiveness and sustainability are paramount.

The findings presented in this thesis underscore the innovative nature of these materials, particularly in their ability to address the limitations of conventional single-function adsorbents or photocatalysts. The TiO_2/AC leverages the high surface area of activated carbon for adsorption, while the anchored TiO_2 facilitates the photodegradation of adsorbed contaminants. Similarly, sulfur

polymers, with their tunable chemical properties and inherent photocatalytic activity, offer a novel approach to contaminant removal, especially when designed with varying ratios of sulfur and crosslinkers like DIB.

However, it is important to note that the studies conducted here were primarily batch experiments performed in controlled water matrices with a limited variety of CECs. While these initial results are encouraging, they do not fully capture the complexities and challenges of real-world water treatment scenarios. For these materials to be considered viable alternatives in DPR systems, further research is needed, particularly in continuous flow systems such as fixed-bed columns or other reactor designs that mimic the conditions of full-scale water treatment plants.

Additionally, the long-term stability, regeneration capacity, and overall cost-effectiveness of these materials need to be thoroughly evaluated in practical applications. Understanding their behavior under varying water compositions, flow rates, and operational stresses will be critical in determining their feasibility for large-scale deployment in DPR systems. Future studies should also explore the scalability of the synthesis processes, and the potential environmental impacts associated with the use of these advanced materials.

In conclusion, while the TiO_2/AC composites and sulfur polymers developed in this thesis represent a significant step forward in water treatment technology, their full potential as advanced materials for DPR systems can only be realized through comprehensive, real-world testing and optimization.

Chapter 5.

Final Remarks

5.1. Summary of Research Contributions

This thesis presents advancements in the field of water treatment, focusing on the development and optimization of Direct Potable Reuse (DPR) systems through the integration of advanced materials and innovative treatment processes. A central achievement of this research was the prioritization of specific contaminants of emerging concern (CECs) by monitoring the effluent at the EPAR Capivari II wastewater treatment plant. For that, a bidimensional liquid chromatography coupled with mass spectrometry (LC-LC-MS/MS) method capable of detecting ng/L levels of CECs was developed and validated for monitoring 12 previously selected CECs. Caffeine, hydrochlorothiazide, saccharin, sulfamethoxazole, and sucralose were identified as priority CECs due to their high concentrations and recalcitrant properties, making them ideal targets for evaluating the effectiveness of various treatment methods.

Pilot plant studies demonstrated that reverse osmosis significantly reduced the concentrations of these target CECs, while photoperoxidation and adsorption processes provided partial removal. To meet the stringent safety requirements for DPR, these processes were combined into a comprehensive treatment train composed of osmose reverse, photoperoxidation, and adsorption. The integrated system (EPAR Capivari II + pilot plant) was monitored over several months, with the effluent parameters meeting the requirements of GM/MS Ordinance No. 888/2021 (Portaria GM/MS nº 888/2021) (Brazilian potability regulation). It is important to note that no chlorination of the effluent was performed; therefore, the effects of this final step must be studied before confirming the potability of the effluent, due to the risk of disinfection by-product formation.

A significant focus of the research was on adsorption, a critical process in water treatment. The activated carbon used in the pilot plant (AC1) was tested and compared with a commercial alternative (AC2) in both batch and continuous flow studies. Surface area was found to play a crucial role in the adsorption of CECs, with AC2 exhibiting superior adsorption capacities in batch studies. However, in continuous flow systems, the particle size of AC2 hindered removal efficiency in downflow studies due to the formation of preferential pathways within the column. Conversely, in upflow mode, AC2 demonstrated higher removal efficiency, consistent with its batch performance. Additionally, *in-situ* regeneration of the column using ethanol was shown to be feasible, enhancing the sustainability of the treatment process.

Aiming to enhance the performance of activated carbon and design an advanced hybrid material that combines both adsorption and photodegradation processes, this thesis explored the integration of titanium dioxide (TiO_2)-based photocatalysts with activated carbon. The anchoring of TiO_2 onto activated carbon significantly improved the photocatalytic degradation of the prioritized CECs, effectively leveraging the synergy between adsorption and photocatalysis. Notably, the sol-gel method using titanium isopropoxide as the precursor yielded the most effective TiO_2 /activated carbon composite, enhancing the efficiency of titanium dioxide up to 10 times compared to commercially available dispersed TiO_2 nanoparticles. Furthermore, the material demonstrated the ability to be regenerated for four cycles, further contributing to the cost-effectiveness and sustainability of DPR systems. This research underscores the importance of synthesis methods and precursor selection, revealing that key parameters such as surface area, porosity, and crystalline phase are critical in optimizing the performance of TiO_2 /activated carbon composites for water treatment applications.

Parallel to the development of TiO_2 /activated carbon materials, this thesis investigated the potential of inverse vulcanization sulfur polymers. These innovative materials, synthesized from elemental sulfur and unsaturated organic monomers, demonstrated a strong affinity for caffeine and exhibited intrinsic photocatalytic activity. Their versatility in addressing both metal ion adsorption (as already reported in the scientific literature) and CEC degradation positions them as a promising alternative to traditional materials in water treatment applications. Notably, the adsorption properties were closely linked to a higher content of the monomer 1,3-diisopropenylbenzene, while the photocatalytic activity was enhanced by a higher sulfur content in the polymer network. This relationship underscores the tailorability of these polymers to meet specific treatment needs. Furthermore, the alignment of these polymers with green chemistry principles enhances their appeal, offering a sustainable solution that minimizes environmental impact while maximizing performance.

5.2. Implications for Water Treatment Technologies

The advancements presented here showcased several implications for the future of water treatment technologies, particularly in the implementation of DPR systems. Beyond the batch adsorption studies, the continuous flow experiments highlighted the importance of selecting the activated carbon, as the particle size significantly influenced the adsorption efficiency of CECs in downflow mode. Additionally, it was also demonstrated that operating the system in upflow modes

can mitigate the impact of particle size, thereby enhancing overall performance. The integration of adsorption and photocatalysis within a single high porous material has the potential to minimize and address water purification challenges, reducing the costs of operation and final disposition of materials.

Moreover, the optimization of synthetic protocol offered a holistic approach to material design, where the method, precursor selection, and material properties were carefully evaluated to maximize the application requirements, which not only enhanced the efficiency but also contributed to the overall sustainability of water management strategies. It is also noteworthy that the versatility of the materials presented here ensures that they can be tailored for specific contaminants and operational conditions, ensuring that they can be adapted to a wide range of environmental contexts, from industrial wastewater treatment to municipal water reuse.

Additionally, the findings confirmed that CECs exhibit specific removal behaviors depending on the treatment technology employed. Consequently, DPR systems must be precisely tailored to the unique needs of each region. While a universal process might simplify implementation, this approach can lead to inefficiencies or unnecessary costs. Therefore, customized approaches are essential to achieving optimal performance and cost-effectiveness in DPR systems.

5.3. Challenges and Future Research Directions

While this thesis has made contributions to the research field, there are remaining challenges that warrant further investigation. One key challenge is the variability in chemical substance consumption (such as drugs, personal care products, and medicines), which differs across locations. This variability highlights the need for tailored, location-specific monitoring to ensure accurate results. Although five CECs were prioritized in this study, accurate monitoring in different regions will depend on the ongoing development of multiresidue analytical methods capable of detecting CECs at ng/L levels. Additionally, the detection and characterization of disinfection and degradation by-products require a tailored study using specialized equipment (high-resolution mass spectrometers), to ensure their effective removal by the treatment processes. In this case, indirect measurements (*e.g.*, toxicological tests and total organic carbon analysis) can provide an estimate of their presence or removal.

Another challenge is the scalability of the advanced materials presented in this thesis. While the laboratory-scale experiments have demonstrated promising results, scaling up production and application requires addressing issues related to material cost, production methods, and long-term stability. Therefore, future research should be done focusing on synthetic procedures on large scales to reduce costs and improve the durability of these materials in real-world conditions.

Another critical area for future research is the exploration of hybrid materials that combine multiple functionalities beyond adsorption and photocatalysis. For example, integrating antimicrobial properties into these materials could offer a comprehensive solution for pathogen removal in DPR systems, further enhancing water safety. Additionally, the development of novel catalysts that operate efficiently under visible light, as opposed to UV light, could expand the applicability of these technologies, while reduce the operational costs.

Furthermore, this thesis primarily focused on the performance of these materials in controlled environments and, although studies in real water matrices have been performed, future studies should focus on investigating their efficiency in various water matrices and for the removal of other contaminants beyond the ones studied here. This is essential for further understanding the interactions between different contaminants and the materials, and is essential for a successful application.

Finally, it is important to note that although DPR systems have been implemented worldwide, there is currently no legislation in Brazil that authorizes or regulates their use. Establishing such regulations would therefore require a collaborative effort among policymakers, researchers, and society to formalize DPR as a viable solution for addressing water scarcity. Additionally, monitoring CECs at ng/L levels demands specialized equipment and skilled personnel, necessitating substantial investment in both workforce training and infrastructure within the water treatment sector.

5.4. Broader Impact and Societal Relevance

As water scarcity and pollution intensify, the development of advanced water treatment technologies and the identification of prioritized CECs are essential for ensuring a safe, reliable, and sustainable water supply. This thesis focused on understanding and applied novel materials for water

decontamination. It also provided a kick-off list of CECs for future monitoring in Brazilian DPR schemes and outlined a treatment train capable of meeting Brazilian potability regulations.

The societal relevance of this research is further underscored by its potential to impact public health and environmental sustainability. By providing alternative materials for water decontamination, this thesis aligns with global efforts to reduce the environmental footprint of industrial processes, contributing to climate change mitigation and resource conservation. The adaptable material design approach ensures these technologies can meet diverse water treatment needs, paving the way for broader adoption of DPR systems worldwide.

5.5. Conclusion

In conclusion, this thesis presented an LC-LC-MS/MS method for monitoring CECs at ng/L concentrations. This method helped to prioritize contaminants for monitoring and supports the development of innovative materials for water treatment, especially in DPR systems. Key CECs identified include caffeine, hydrochlorothiazide, saccharin, sulfamethoxazole, and sucralose, emphasizing the need for targeted strategies to evaluate treatment efficiency. The research also demonstrated the potential of a treatment train that includes a membrane bioreactor, reverse osmosis, photoperoxidation, and adsorption processes in producing potable water. Combining adsorption and photocatalysis in a single material is a promising approach to enhance the efficiency and sustainability of potable reuse. The findings highlight the importance of a multidisciplinary approach to material design, considering environmental impact, scalability, and practical application. This ensures developed materials are effective not only in laboratory settings but also for large-scale use. As water treatment evolves, this thesis lays a solid foundation for future research and innovation. By integrating material science and engineering with analytical chemistry, this work improved monitoring processes essential for water treatment. These advancements are crucial for providing safe, clean water to support a growing global population while minimizing environmental effects. Ongoing development of novel materials and solutions will be vital in addressing 21st-century water security challenges.

Chapter 6.

References

- Abraham, A. M., S. V. Kumar, and S. M. Alhassan. 2018. 'Porous sulphur copolymer for gas-phase mercury removal and thermal insulation', *Chemical Engineering Journal*, 332: 1-7. <https://doi.org/10.1016/j.cej.2017.09.069>
- Adamson, A.W., and A.P. Gast. 1997. *Physical Chemistry of Surfaces* (John Wiley & Sons).
- Adán, C., A. Magnet, S. Fenoy, C. Pablos, C. del Aguila, and J. Marugán. 2018. 'Concomitant inactivation of *Acanthamoeba spp.* and *Escherichia coli* using suspended and immobilized TiO₂', *Water Research*, 144: 512-21. <https://doi.org/10.1016/j.watres.2018.07.060>
- Ahmed, M. B., J. L. Zhou, H. H. Ngo, W. S. Guo, and M. F. Chen. 2016. 'Progress in the preparation and application of modified biochar for improved contaminant removal from water and wastewater', *Bioresource Technology*, 214: 836-51. <https://doi.org/10.1016/j.biortech.2016.05.057>
- Ahmed, M. J., and B. H. Hameed. 2018. 'Removal of emerging pharmaceutical contaminants by adsorption in a fixed-bed column: A review', *Ecotoxicology and Environmental Safety*, 149: 257-66. <https://doi.org/10.1016/j.ecoenv.2017.12.012>
- Akpan, U. G., and B. H. Hameed. 2010. 'The advancements in sol-gel method of doped-TiO₂ photocatalysts', *Applied Catalysis a-General*, 375: 1-11. <https://doi.org/10.1016/j.apcata.2009.12.023>
- Al-Ghouti, M. A., and D. A. Da'ana. 2020. 'Guidelines for the use and interpretation of adsorption isotherm models: A review', *Journal of Hazardous Materials*, 393. <https://doi.org/10.1016/j.jhazmat.2020.122383>
- Al-Nuaim, M. A., A. A. Alwasiti, and Z. Y. Shnain. 2023. 'The photocatalytic process in the treatment of polluted water', *Chemical Papers*, 77: 677-701. <https://doi.org/10.1007/s11696-022-02468-7>
- Alex, A., N. K. Singha, and S. Choudhury. 2023. 'Exploring inverse vulcanization in lithium-sulfur batteries', *Current Opinion in Electrochemistry*, 39. <https://doi.org/10.1016/j.coelec.2023.101271>
- Alves, P. D. C., C. Rodrigues-Silva, A. R. Ribeiro, and S. Rath. 2021. 'Removal of low-calorie sweeteners at five Brazilian wastewater treatment plants and their occurrence in surface water', *Journal of Environmental Management*, 289. <https://doi.org/10.1016/j.jenvman.2021.112561>
- Amna, R., and S. M. Alhssan. 2024. 'Exploring porous sulfur copolymers for efficient removal of heavy metal ions from wastewater: A computational study', *Journal of Industrial and Engineering Chemistry*. 138: 365-79. <https://doi.org/10.1016/j.jiec.2024.04.014>
- Antunes, M., V. I. Esteves, R. Guégan, JS. Crespo, AN. Fernandes, and M. Giovanela. 2012. 'Removal of diclofenac sodium from aqueous solution by Isabel grape bagasse', *Chemical Engineering Journal*, 192: 114-21. <https://doi.org/10.1016/j.cej.2012.03.062>
- Apul, O. G., Q. L. Wang, Y. Zhou, and T. Karanfil. 2013. 'Adsorption of aromatic organic contaminants by graphene nanosheets: Comparison with carbon nanotubes and activated carbon', *Water Research*, 47: 1648-54. <https://doi.org/10.1016/j.watres.2012.12.031>
- Araújo, L. S. 2017. 'Comparação do desempenho de carvão ativado produzido a partir de diferentes matrizes para remoção de microcistina-LR de águas de abastecimento', Universidade de São Paulo. <https://doi.org/10.11606/D.18.2017.tde-13042017-105327>
- Araújo, LS., AR. Coutinho, MO. Alvarez-Mendez, RB. Moruzzi, MC. Calijuri, and DGF Cunha. 2018. 'Caracterização e avaliação de fatores que determinam a remoção de microcistina-LR em carvão ativado granular produzido a partir de diferentes matérias-primas', *Engenharia Sanitaria e Ambiental*, 23(6): 1131 - 42. <https://doi.org/10.1590/S1413-41522018177756>

- American Water Works Association (AWWA) -. 2011. *Water quality and treatment: a handbook on drinking water* (McGraw Hill Inc: USA).
- Ayyaru, S., and Y. H. Ahn. 2023. 'Novel sulfonated rGOHfO₂/PVDF hybrid nanocomposite ultrafiltration membrane towards direct potable reuse water production', *Journal of Cleaner Production*, 415. <https://doi.org/10.1016/j.jclepro.2023.137804>
- Baawain, M. S., A. Al-Mamun, H. Omidvarborna, A. Al-Sabti, and B. S. Choudri. 2020. 'Public perceptions of reusing treated wastewater for urban and industrial applications: challenges and opportunities', *Environment Development and Sustainability*, 22: 1859-71. <https://doi.org/10.1007/s10668-018-0266-0>
- Bacsik, Z., J. Mink, and G. Keresztury. 2004. 'FTIR spectroscopy of the atmosphere. I. Principles and methods', *Applied Spectroscopy Reviews*, 39: 295-363. <https://doi.org/10.1081/ASR-200030192>
- Barnes, J. L., A. S. Krishen, and H. F. Hu. 2021. 'Untapped Knowledge about Water Reuse: the Roles of Direct and Indirect Educational Messaging', *Water Resources Management*, 35: 2601-15. <https://doi.org/10.1007/s11269-021-02853-z>
- Bass, D. A., B. R. McFadden, M. Costanigro, and K. D. Messer. 2022. 'Implicit and Explicit Biases for Recycled Water and Tap Water', *Water Resources Research*, 58. <https://doi.org/10.1029/2021WR030712>
- Bear, J. C., J. D. McGettrick, I. P. Parkin, C. W. Dunnill, and T. Hasell. 2016. 'Porous carbons from inverse vulcanised polymers', *Microporous and Mesoporous Materials*, 232: 189-95. <https://doi.org/10.1016/j.micromeso.2016.06.021>
- Bedasa, Y. 2024. 'Is Africa's food insecurity linked to land use coverage, irrigation adoption and water scarcity?', *Irrigation and Drainage*, 73: 334-45. <https://doi.org/10.1002/ird.2873>
- Bekci, Z., Y. Seki, and M. K. Yurdakoc. 2006. 'Equilibrium studies for trimethoprim adsorption on montmorillonite KSF', *Journal of Hazardous Materials*, 133: 233-42. <https://doi.org/10.1016/j.jhazmat.2005.10.029>
- Berk, H., M. Kaya, M. Topcuoglu, N. Turkten, Y. Karatas, and A. Cihaner. 2023. 'Synthesis, characterization and application of high sulfur content polymeric materials from fatty acids', *Reactive & Functional Polymers*, 187. <https://doi.org/10.1016/j.reactfunctpolym.2023.105581>
- Blanchard, G., M. Maunaye, and G. Martin. 1984. 'Removal of Heavy-Metals from Waters by Means of Natural Zeolites', *Water Research*, 18: 1501-07. [https://doi.org/10.1016/0043-1354\(84\)90124-6](https://doi.org/10.1016/0043-1354(84)90124-6)
- Boehm, H. P. 1994. 'Some Aspects of the Surface-Chemistry of Carbon-Blacks and Other Carbons', *Carbon*, 32: 759-69. [https://doi.org/10.1016/0008-6223\(94\)90031-0](https://doi.org/10.1016/0008-6223(94)90031-0)
- . 2002. 'Surface oxides on carbon and their analysis: a critical assessment', *Carbon*, 40: 145-49. [https://doi.org/10.1016/S0008-6223\(01\)00165-8](https://doi.org/10.1016/S0008-6223(01)00165-8)
- Bohart, GS., and EQ. Adams. 1920. 'Behavior of charcoal towards chlorine', *Journal of Chemical Society*, 42: 523-29. <https://doi.org/10.1021/ja01448a01>
- Boyd, D. A., V. Q. Nguyen, C. C. McClain, F. H. Kung, C. C. Baker, J. D. Myers, M. P. Hunt, W. Kim, and J. S. Sanghera. 2019. 'Optical Properties of a Sulfur-Rich Organically Modified Chalcogenide Polymer Synthesized via Inverse Vulcanization and Containing an Organometallic Comonomer', *Acs Macro Letters*, 8: 113-16. <https://doi.org/10.1021/acsmacrolett.8b00923>
- Boyd, GE., AW. Adamson, and LS Meyers Jr. 1947. 'The exchange adsorption of ions from aqueous solutions by organite zeolithes. II. Kinetics', *J. Am. Chem. Soc.*, 69. <https://doi.org/10.1021/ja01203a066>

- Briche, S., M. Derqaoui, M. Belaiche, E. El Mouchtari, P. Wong-Wah-Chung, and S. Rafqah. 2020. 'Nanocomposite material from TiO₂ and activated carbon for the removal of pharmaceutical product sulfamethazine by combined adsorption/photocatalysis in aqueous media', *Environmental Science and Pollution Research*, 27: 25523-34. <https://doi.org/10.1007/s11356-020-08939-2>
- Brunauer, S., P. H. Emmett, and E. Teller. 1938. 'Adsorption of gases in multimolecular layers', *Journal of the American Chemical Society*, 60: 309-19. <https://doi.org/10.1021/ja01269a023>
- Cabrera-Lafaurie, W. A., F. R. Roman, and A. J. Hernandez-Maldonado. 2015. 'Single and multi-component adsorption of salicylic acid, clofibric acid, carbamazepine and caffeine from water onto transition metal modified and partially calcined inorganic-organic pillared clay fixed beds', *Journal of Hazardous Materials*, 282: 174-82. <https://doi.org/10.1016/j.jhazmat.2014.03.009>
- Caianelo, M., J. C. Espindola, V. Diniz, M. Spina, C. Rodrigues-Silva, and J. R. Guimaraes. 2022. 'Gatifloxacin photocatalytic degradation in different water matrices: Antimicrobial activity and acute toxicity reduction', *Journal of Photochemistry and Photobiology a-Chemistry*, 430. <https://doi.org/10.1016/j.jphotochem.2022.113973>
- Caianelo, M., C. Rodrigues-Silva, M. G. Maniero, V. Diniz, M. Spina, and J. R. Guimaraes. 2021. 'Evaluation of residual antimicrobial activity and acute toxicity during the degradation of gatifloxacin by ozonation', *Water Science and Technology*, 84: 225-36. <https://doi.org/10.2166/wst.2021.208>
- Cargnello, M., T. R. Gordon, and C. B. Murray. 2014. 'Solution-Phase Synthesis of Titanium Dioxide Nanoparticles and Nanocrystals', *Chemical Reviews*, 114: 9319-45. <https://doi.org/10.1021/cr500170p>
- Casas, N., J. Schell, R. Pini, and M. Mazzotti. 2012. 'Fixed bed adsorption of CO₂/H₂ mixtures on activated carbon: experiments and modeling', *Adsorption Science & Technology*, 18: 143-61. <https://doi.org/10.1007/s10450-012-9389-z>
- Chalker, J. M., M. J. H. Worthington, N. A. Lundquist, and L. J. Esdaile. 2019. 'Synthesis and Applications of Polymers Made by Inverse Vulcanization', *Topics in Current Chemistry*, 377. <https://doi.org/10.1007/s41061-019-0242-7>
- Chatterjee, A., and S. Schiewer. 2011. 'Biosorption of Cadmium(II) Ions by Citrus Peels in a Packed Bed Column: Effect of Process Parameters and Comparison of Different Breakthrough Curve Models', *Clean-Soil Air Water*, 39: 874-81. <https://doi.org/10.1002/clen.201000482>
- Chen, C. Y., S. W. Wang, H. Kim, S. Y. Pan, C. H. Fan, and Y. J. Lin. 2021. 'Non-conventional water reuse in agriculture: A circular water economy', *Water Research*, 199. <https://doi.org/10.1016/j.watres.2021.117193>
- Chen, H., B. Gao, and H. Li. 2014. 'Functionalization, pH, and ionic strength influenced sorption of sulfamethoxazole on graphene', *Journal of Environmental Chemical Engineering*, 2: 310-15. <https://doi.org/10.1016/j.jece.2013.12.021>
- Chen, T. W., L. Luo, S. H. Deng, G. Z. Shi, S. R. Zhang, Y. Z. Zhang, O. P. Deng, L. L. Wang, J. Zhang, and L. Y. Wei. 2018. 'Sorption of tetracycline on H₃PO₄ modified biochar derived from rice straw and swine manure', *Bioresource Technology*, 267: 431-37. <https://doi.org/10.1016/j.biortech.2018.07.074>
- Cheng, N., B. Wang, P. Wu, X. Lee, Y. Xing, M. Chen, and B. Gao. 2021. 'Adsorption of emerging contaminants from water and wastewater by modified biochar: A review', *Environmental Pollution*, 273. <https://doi.org/10.1016/j.envpol.2021.116448>
- Chien, S. H., and W. R. Clayton. 1980. 'Application of Elovich Equation to the Kinetics of Phosphate Release and Sorption in Soils', *Soil Science Society of America Journal*, 44: 265-68. <https://doi.org/10.2136/sssaj1980.03615995004400020013x>

- Chung, W. J., J. J. Griebel, E. T. Kim, H. Yoon, A. G. Simmonds, H. J. Ji, P. T. Dirlam, R. S. Glass, J. J. Wie, N. A. Nguyen, B. W. Guralnick, J. Park, A. Somogyi, P. Theato, M. E. Mackay, Y. E. Sung, K. Char, and J. Pyun. 2013. 'The use of elemental sulfur as an alternative feedstock for polymeric materials', *Nature Chemistry*, 5: 518-24. <https://doi.org/10.1038/nchem.1624>
- Collier, S. A., L. Deng, E. A. Adam, K. M. Benedict, E. M. Beshearse, A. J. Blackstock, B. B. Bruce, G. Derado, C. Edens, K. E. Fullerton, J. W. Gargano, A. L. Geissler, A. J. Hall, A. H. Havelaar, V. R. Hill, R. M. Hoekstra, S. C. Reddy, E. Scallan, E. K. Stokes, J. S. Yoder, and M. J. Beach. 2021. 'Estimate of Burden and Direct Healthcare Cost of Infectious Waterborne Disease in the United States', *Emerging Infectious Diseases*, 27: 140-49. <https://doi.org/10.3201/eid2701.190676>
- Cooney, D. O. 1999. *Adsorption design for wastewater treatment* (Lewis Publishers: Boca Raton, Fl.).
- Crank, J. 1956. *The Mathematics of Diffusion* (Oxford at the Clarendon Press).
- Cugusi, L., M. Meloni, M. Bergamin, S. Gobbo, A. Di Blasio, C. Conca, P. P. Bassareo, A. Piras, and P. Bandiera. 2023. 'Health effects of outdoor water sports in chronic disease: a scoping review', *Sport Sciences for Health*, 19: 1-15. <https://doi.org/10.1007/s11332-022-00989-y>
- D'Odorico, P., D. D. Chiarelli, L. Rosa, A. Bini, D. Zilberman, and M. C. Rulli. 2020. 'The global value of water in agriculture', *Proceedings of the National Academy of Sciences of the United States of America*, 117: 21985-93. <https://doi.org/10.1073/pnas.2005835117>
- Dale, J. J., V. Hanna, and T. Hasell. 2023. 'Manipulating Inverse Vulcanization Comonomers to Generate High-Tensile-Strain Polymers', *ACS Applied Polymer Materials*, 5: 6761-65. <https://doi.org/10.1021/acsapm.3c01378>
- Darweesh, T. M., and M. J. Ahmed. 2017. 'Batch and fixed bed adsorption of levofloxacin on granular activated carbon from date (Phoenix dactylifera L.) stones by KOH chemical activation', *Environmental Toxicology and Pharmacology*, 50: 159-66. <https://doi.org/10.1016/j.etap.2017.02.005>
- Deblonde, T., C. Cossu-Leguille, and P. Hartemann. 2011. 'Emerging pollutants in wastewater: A review of the literature', *International Journal of Hygiene and Environmental Health*, 214: 442-48. <https://doi.org/10.1016/j.ijheh.2011.08.002>
- Deere, J. R., S. Streets, M. D. Jankowski, M. Ferrey, Y. Chenaux-Ibrahim, M. Convertino, E. J. Isaac, N. B. D. Phelps, A. Primus, J. L. Servadio, R. S. Singer, D. A. Travis, M. Seth, and T. M. Wolf. 2021. 'A chemical prioritization process: Applications to contaminants of emerging concern in freshwater ecosystems (Phase I)', *Science of the Total Environment*, 772. <https://doi.org/10.1016/j.scitotenv.2021.146030>
- Di Bernardo, L., A. D. B. Dantas, and P. E. N Voltan. 2017. *Métodos e Técnicas de Tratamento de Água* (LDiBe: São Carlos).
- Diniz, V., J. C. Bear, S. Rath, and C. R. Crick. 2024a. 'Porous sulfur polymers for effective aqueous-phase organic contaminant removal', *Scientific Reports*, 14. <https://doi.org/10.1038/s41598-024-57856-8>
- . 2024b. 'UV-stable photoactive superhydrophobic coatings utilizing “inverse vulcanization” sulfur polymers', *Surfaces and Interfaces*, 51. <https://doi.org/10.1016/j.surfin.2024.104691>
- Diniz, V., D. G. F. Cunha, and S. Rath. 2023. 'Adsorption of recalcitrant contaminants of emerging concern onto activated carbon: A laboratory and pilot-scale study', *Journal of Environmental Management*, 325. <https://doi.org/10.1016/j.jenvman.2022.116489>
- Diniz, V., G. Rath, S. Rath, L. S. Araujo, and D. G. F. Cunha. 2022. 'Competitive kinetics of adsorption onto activated carbon for emerging contaminants with contrasting physicochemical properties', *Environmental Science and Pollution Research*, 29: 42185-200. <https://doi.org/10.1007/s11356-021-16043-2>

- Diniz, V., G. Rath, S. Rath, C. Rodrigues-Silva, J. R. Guimaraes, and D. G. F. Cunha. 2021. 'Long-term ecotoxicological effects of ciprofloxacin in combination with caffeine on the microalga *Raphidocelis subcapitata*', *Toxicology Reports*, 8: 429-35. <https://doi.org/10.1016/j.toxrep.2021.02.020>
- Diniz, V., and S. Rath. 2023. 'Adsorption of aqueous phase contaminants of emerging concern by activated carbon: Comparative fixed-bed column study and in situ regeneration methods', *Journal of Hazardous Materials*, 459. <https://doi.org/10.1016/j.jhazmat.2023.132197>
- Diniz, V., S. Rath, and C. R. Crick. 2023. 'Synthesis and characterization of TiO₂-carbon filter materials for water decontamination by adsorption-degradation processes', *Journal of Environmental Management*, 346. <https://doi.org/10.1016/j.jenvman.2023.118979>
- Diniz, V., G. M. Reyes, S. Rath, and D. G. F. Cunha. 2020. 'Caffeine reduces the toxicity of albendazole and carbamazepine to the microalgae *Raphidocelis subcapitata* (Sphaeropleales, Chlorophyta)', *International Review of Hydrobiology*, 105: 151-61. <https://doi.org/10.1002/iroh.201902024>
- do Vale, T. M. C., M. H. C. Spyrides, JB J. r. Cabral, L. D. B. Andrade, B. G. Bezerra, D. T. Rodrigues, and P. R. Mutti. 2024. 'Climate and water balance influence on agricultural productivity over the Northeast Brazil', *Theoretical and Applied Climatology*, 155: 879-900. <https://doi.org/10.1007/s00704-023-04664-1>
- Dop, R. A., D. R. Neill, and T. Hasell. 2021. 'Antibacterial Activity of Inverse Vulcanized Polymers', *Biomacromolecules*, 22: 5223-33. <https://doi.org/10.1021/acs.biomac.1c01138>
- Dubinin, M., and L. V. Radushkevich. 1947. 'Equation of the characteristic curve of activated charcoal', *Proceedings of the Academy of Sciences. Physical Chemistry Section USSR*, 55: 331-333.
- Eadie, G. S. 1942. 'The inhibition of cholinesterase by physostigmine and prostigmine', *Journal of Biological Chemistry*, 146: 85-93. [https://doi.org/10.1016/S0021-9258\(18\)72452-6](https://doi.org/10.1016/S0021-9258(18)72452-6)
- EMA. 2006. "European Medicine Agency Guideline on the Environmental Risk Assessment of Medicinal Products for Human Use: (EMA/CHMP/SWP/4447/00)." <https://www.ema.europa.eu/en/environmental-risk-assessment-medicinal-products-human-use-scientific-guideline>
- Ensano, B. M. B., L. Borea, V. Naddeo, M. D. G. de Luna, and V. Belgiorno. 2019. 'Control of emerging contaminants by the combination of electrochemical processes and membrane bioreactors', *Environmental Science and Pollution Research*, 26: 1103-12. <https://doi.org/10.1007/s11356-017-9097-z>
- Fan, S. S., Y. Wang, Z. Wang, J. Tang, J. Tang, and X. D. Li. 2017. 'Removal of methylene blue from aqueous solution by sewage sludge-derived biochar: Adsorption kinetics, equilibrium, thermodynamics and mechanism', *Journal of Environmental Chemical Engineering*, 5: 601-11. <https://doi.org/10.1016/j.jece.2016.12.019>
- Fan, Y., B. Wang, S. H. Yuan, X. H. Wu, J. Chen, and L. L. Wang. 2010. 'Adsorptive removal of chloramphenicol from wastewater by NaOH modified bamboo charcoal', *Bioresource Technology*, 101: 7661-64. <https://doi.org/10.1016/j.biortech.2010.04.046>
- Fawell, J., and C. N. Ong. 2012. 'Emerging Contaminants and the Implications for Drinking Water', *International Journal of Water Resources Development*, 28: 247-63. <https://doi.org/10.1080/07900627.2012.672394>
- Ferreira, D. C., I. Grazielle, R. C. Marques, and J. Gonçalves. 2021. 'Investment in drinking water and sanitation infrastructure and its impact on waterborne diseases dissemination: The Brazilian case', *Science of the Total Environment*, 779. <https://doi.org/10.1016/j.scitotenv.2021.146279>
- Freundlich, H. 1907. 'Kolloidfällung und Adsorption', *Angewandte chemie*, 20: 749-50. <https://doi.org/10.1002/ange.19070201805>

- Gao, Y., J. Remón, and A. S. Matharu. 2021. 'Microwave-assisted hydrothermal treatments for biomass valorisation: a critical review', *Green Chemistry*, 23: 3502-25. DOI <https://doi.org/10.1039/D1GC00623A>
- Gemeda, S. T., E. Springer, S. R. Gari, S. M. Birhan, and H. T. Bedane. 2021. 'The importance of water quality in classifying basic water services: The case of Ethiopia, SDG6.1, and safe drinking water', *Plos One*, 16. <https://doi.org/10.1371/journal.pone.0248944>
- Gerber, I. C., and P. Serp. 2020. 'A Theory/Experience Description of Support Effects in Carbon-Supported Catalysts', *Chemical Reviews*, 120: 1250-349. <https://doi.org/10.1021/acs.chemrev.9b00209>
- Goertzen, S. L., K. D. Theriault, A. M. Oickle, A. C. Tarasuk, and H. A. Andreas. 2010. 'Standardization of the Boehm titration. Part I. CO₂ expulsion and endpoint determination', *Carbon*, 48: 1252-61. <https://doi.org/10.1016/j.carbon.2009.11.050>
- Gomez, I., D. Mecerreyes, J. A. Blazquez, O. Leonet, H. Ben Youcef, C. M. Li, J. L. Gómez-Cámer, O. Bundarchuk, and L. Rodriguez-Martinez. 2016. 'Inverse vulcanization of sulfur with divinylbenzene: Stable and easy processable cathode material for lithium-sulfur batteries', *Journal of Power Sources*, 329: 72-78. <https://doi.org/10.1016/j.jpowsour.2016.08.046>
- Guo, T. J., J. Englehardt, and T. T. Wu. 2014. 'Review of cost versus scale: water and wastewater treatment and reuse processes', *Water Science and Technology*, 69: 223-34. <https://doi.org/10.2166/wst.2013.734>
- Guo, X. T., H. Dong, C. Yang, Q. Zhang, C. J. Liao, F. G. Zha, and L. M. Gao. 2016. 'Application of goethite modified biochar for tylosin removal from aqueous solution', *Colloids and Surfaces a-Physicochemical and Engineering Aspects*, 502: 81-88. <https://doi.org/10.1016/j.colsurfa.2016.05.015>
- Hagen, J. 2015. *Industrial Catalysis: A Practical Approach* (Wiley-Vch).
- Hanes, C. S. 1932. 'Studies on plant amylases. I. The effect of starch concentration upon the velocity of hydrolysis by the amylase of germinated barley.', *Biochemical Journal*, 26: 1406-21. <https://doi.org/10.1042/bj0261406>
- Hanna, M. W., and A. Sandoval. 1968. 'Nuclear Magnetic Resonance Studies of Complexes between Caffeine and Aromatic Donors', *Biochimica Et Biophysica Acta*, 155: 433-36. [https://doi.org/10.1016/0005-2787\(68\)90188-3](https://doi.org/10.1016/0005-2787(68)90188-3)
- Hartley, K., C. Tortajada, and A. K. Biswas. 2019. 'A formal model concerning policy strategies to build public acceptance of potable water reuse', *Journal of Environmental Management*, 250. <https://doi.org/10.1016/j.jenvman.2019.109505>
- Hasell, T., D. J. Parker, H. A. Jones, T. McAllister, and S. M. Howdle. 2016. 'Porous inverse vulcanised polymers for mercury capture', *Chemical Communications*, 52: 5383-86. <https://doi.org/10.1039/C6CC00938G>
- Hespanhol, I., R. Rodrigues, and J. C. Mierzwa. 2019. 'Direct potable water reuse – Technical feasibility study using a pilot plant', *Revista DAE*, 67: 103-15. <https://doi.org/10.4322/dae.2019.026>
- Hill Jr, C. G., and T. W. Root. 2014. *Introduction to Chemical Engineering Kinetics and Reactor Design* (Wiley).
- Ho, Y. S., and G. McKay. 1999. 'Pseudo-second order model for sorption processes', *Process Biochemistry*, 34: 451-65. [https://doi.org/10.1016/S0032-9592\(98\)00112-5](https://doi.org/10.1016/S0032-9592(98)00112-5)
- Howe, K., D. Hand, J. C. Crittenden, R. Trussel, and G. Tchobanoglous. 2012. *Principles of water treatment* (John Wiley & Sons: New Jersey).
- Hu, Q. L., and Z. Y. Zhang. 2019. 'Application of Dubinin-Radushkevich isotherm model at the solid/solution interface: A theoretical analysis', *Journal of Molecular Liquids*, 277: 646-48. <https://doi.org/10.1016/j.molliq.2019.01.005>

- Huang, Z., E. L. Nya, V. Cao, W. Gwenzi, M. A. Rahman, and C. Noubactep. 2021. 'Universal Access to Safe Drinking Water: Escaping the Traps of Non-Frugal Technologies', *Sustainability*, 13. <https://doi.org/10.3390/su13179645>
- Inglezakis, VJ, and SG Pouloupoulos. 2006. *Adsorption, ion exchange and catalysis design of operations and environmental applications*. (Elsevier Science). <https://doi.org/10.1016/B978-0-444-52783-7.X5000-9>
- Inoue, M. 2005. 'Solvothermal Synthesis.' in B. Lee and S. Komarneni (eds.), *Chemical Processing of Ceramics* (Taylor & Francis).
- Jacobs, PA., EM. Flanigen, JC. Jansen, and H. van Bekkum. 2001. *Introduction to Zeolite Science and Practice* (Elsevier).
- Jaerger, S., A. dos Santos, A. N. Fernandes, and C. A. P. Almeida. 2015. 'Removal of p-Nitrophenol from Aqueous Solution Using Brazilian Peat: Kinetic and Thermodynamic Studies', *Water Air and Soil Pollution*, 226. <https://doi.org/10.1007/s11270-015-2500-9>
- Jang, H. M., S. Yoo, Y. K. Choi, S. Park, and E. Kan. 2018. 'Adsorption isotherm, kinetic modeling and mechanism of tetracycline on Pinus taeda-derived activated biochar', *Bioresource Technology*, 259: 24-31. <https://doi.org/10.1016/j.biortech.2018.03.013>
- Jaria, G., M. A. O. Lourenco, C. P. Silva, P. Ferreira, M. Otero, V. Calisto, and V. I. Esteves. 2020. 'Effect of the surface functionalization of a waste-derived activated carbon on pharmaceuticals' adsorption from water', *Journal of Molecular Liquids*, 299. <https://doi.org/10.1016/j.molliq.2019.112098>
- Jeffrey, P., Z. Yang, and S. J. Judd. 2022. 'The status of potable water reuse implementation', *Water Research*, 214. <https://doi.org/10.1016/j.watres.2022.118198>
- Jiang, N., R. Shang, S. G. J. Heijman, and L. C. Rietveld. 2020. 'Adsorption of triclosan, trichlorophenol and phenol by high-silica zeolites: Adsorption efficiencies and mechanisms', *Separation and Purification Technology*, 235. <https://doi.org/10.1016/j.seppur.2019.116152>
- Jiang, Q., and Z. Wen. 2011. *Thermodynamics of Materials* (Springer-Verlag Berlin Heidelberg).
- Jing, X. R., Y. Y. Wang, W. J. Liu, Y. K. Wang, and H. Jiang. 2014. 'Enhanced adsorption performance of tetracycline in aqueous solutions by methanol-modified biochar', *Chemical Engineering Journal*, 248: 168-74. <https://doi.org/10.1016/j.cej.2014.03.006>
- Jodar-Abellan, A., M. I. López-Ortiz, and J. Melgarejo-Moreno. 2019. 'Wastewater Treatment and Water Reuse in Spain. Current Situation and Perspectives', *Water*, 11. <https://doi.org/10.3390/w11081551>
- Jung, C., L. K. Boateng, J. R. V. Flora, J. Oh, M. C. Braswell, A. Son, and Y. Yoon. 2015. 'Competitive adsorption of selected non-steroidal anti-inflammatory drugs on activated biochars: Experimental and molecular modeling study', *Chemical Engineering Journal*, 264: 1-9. <https://doi.org/10.1016/j.cej.2014.11.076>
- Jung, K. W., T. U. Jeong, J. W. Choi, K. H. Ahn, and S. H. Lee. 2017. 'Adsorption of phosphate from aqueous solution using electrochemically modified biochar calcium-alginate beads: Batch and fixed-bed column performance', *Bioresource Technology*, 244: 23-32. <https://doi.org/10.1016/j.biortech.2017.07.133>
- Juntgen, H. 1986. 'Activated Carbon as Catalyst Support - a Review of New Research Results', *Fuel*, 65: 1436-46. [https://doi.org/10.1016/0016-2361\(86\)90120-1](https://doi.org/10.1016/0016-2361(86)90120-1)
- Kaiser, F. A. C., A. R. Ribeiro, and C. C. Montagner. 2024. 'Environmental and socioeconomic aspects related to the acceptance of direct potable reuse in a metropolitan city in Brazil', *Journal of Cleaner Production*, 466. <https://doi.org/10.1016/j.jclepro.2024.142897>
- Karimi, M., M. Tabiee, S. Karami, V. Karimi, and E. Karamidehkordi. 2024. 'Climate change and water scarcity impacts on sustainability in semi-arid areas: Lessons from the South of Iran', *Groundwater for Sustainable Development*, 24. <https://doi.org/10.1016/j.gsd.2023.101075>

- Keller, A. A., Y. M. Su, and D. Jassby. 2022. 'Direct Potable Reuse: Are We Ready? A Review of Technological, Economic, and Environmental Considerations', *ACS Es&T Engineering*, 2: 273-91. <https://doi.org/10.1021/acsestengg.1c00258>
- Kennedy, S. J., J. C. Wheeler, C. Osuch, and E. Wasserman. 1983. 'Free-Radical Concentration in Doped Sulfur - Theory and Experiment', *Journal of Physical Chemistry*, 87: 3961-66. <https://doi.org/10.1021/j100243a033>
- Kleine, T. S., N. A. Nguyen, L. E. Anderson, S. Namnabat, E. A. LaVilla, S. A. Showghi, P. T. Dirlam, C. B. Arrington, M. S. Manchester, J. Schwiegerling, R. S. Glass, K. Char, R. A. Norwood, M. E. Mackay, and J. Pyun. 2016. 'High Refractive Index Copolymers with Improved Thermomechanical Properties via the Inverse Vulcanization of Sulfur and 1,3,5-Triisopropenylbenzene', *ACS Macro Letters*, 5: 1152-56. <https://doi.org/10.1021/acsmacrolett.6b00602>
- Klinar, D. 2016. 'Universal model of slow pyrolysis technology producing biochar and heat from standard biomass needed for the techno-economic assessment', *Bioresource Technology*, 206: 112-20. <https://doi.org/10.1016/j.biortech.2016.01.053>
- Korekar, G., A. Kumar, and C. Ugale. 2020. 'Occurrence, fate, persistence and remediation of caffeine: a review', *Environmental Science and Pollution Research*, 27: 34715-33. <https://doi.org/10.1007/s11356-019-06998-8>
- Kumar, KV. 2006. 'Comments on "Adsorption of acid dye onto organobentonite"', *Journal of Hazardous Materials*, 137: 638-39. <https://doi.org/10.1016/j.jhazmat.2006.03.056>
- Kyzas, G. Z., E. A. Deliyanni, K. A. Matis, N. K. Lazaridis, D. N. Bikiaris, and A. C. Mitropoulos. 2018. 'Emerging nanocomposite biomaterials as biomedical adsorbents: an overview', *Composite Interfaces*, 25: 415-54. <https://doi.org/10.1080/09276440.2017.1361716>
- Lagergren, S. 1898. 'About the theory of so-called adsorption of soluble substances', *Kungliga Svenska Vetenskapsakademiens, Handlingar, Band*, 24: 1-39.
- Lahnsteiner, J., P. van Rensburg, and J. Esterhuizen. 2018. 'Direct potable reuse - a feasible water management option', *Journal of Water Reuse and Desalination*, 8: 14-28. <https://doi.org/10.2166/wrd.2017.172>
- Langmuir, I. 1918. 'The Adsorption of Gases on Plane Surfaces of Glass, Mica and Platinum.', *Journal of the American Chemical Society*, 40: 1361-403. <https://doi.org/10.1021/ja02242a004>
- Larcher, S., and V. Yargeau. 2012. 'Biodegradation of sulfamethoxazole: current knowledge and perspectives', *Applied Microbiology and Biotechnology*, 96: 309-18. <https://doi.org/10.1007/s00253-012-4326-3>
- Largitte, L., and R. Pasquier. 2016. 'A review of the kinetics adsorption models and their application to the adsorption of lead by an activated carbon', *Chemical Engineering Research & Design*, 109: 495-504. <https://doi.org/10.1016/j.cherd.2016.02.006>
- Lazaro, L. L. B., S. Abram, L. L. Giatti, P. Sinisgalli, and P. R. Jacobi. 2023. 'Assessing water scarcity narratives in Brazil-Challenges for urban governance', *Environmental Development*, 47. <https://doi.org/10.1016/j.envdev.2023.100885>
- Levenspiel, O. 1999. *Engenharia das Reações Químicas* (Blucher: São Paulo).
- Leyva-Ramos, R., and C. J. Geankoplis. 1985. 'Model Simulation and Analysis of Surface-Diffusion of Liquids in Porous Solids', *Chemical Engineering Science*, 40: 799-807. [https://doi.org/10.1016/0009-2509\(85\)85032-6](https://doi.org/10.1016/0009-2509(85)85032-6)
- Li, D. D., J. W. O'Brien, B. J. Tschärke, P. M. Choi, F. Ahmed, J. Thompson, J. F. Mueller, H. W. Sun, and K. V. Thomas. 2021. 'Trends in artificial sweetener consumption: A 7-year wastewater-based epidemiology study in Queensland, Australia', *Science of the Total Environment*, 754. <https://doi.org/10.1016/j.scitotenv.2020.142438>

- Li, D., J. W. O'Brien, B. J. Tschärke, P. M. Choi, Q. Zheng, F. Ahmed, J. Thompson, J. Li, J. F. Mueller, H. Sun, and K. V. Thomas. 2020. 'National wastewater reconnaissance of artificial sweetener consumption and emission in Australia', *Environment International*, 143. <https://doi.org/10.1016/j.envint.2020.105963>
- Li, M., Y. Z. Zhang, S. Feng, X. X. Zhang, Y. L. Xi, and X. L. Xiang. 2022. 'Bioaccumulation and biomagnification effects of nano-TiO₂ in the aquatic food chain', *Ecotoxicology*, 31: 1023-34. <https://doi.org/10.1007/s10646-022-02572-0>
- Li Puma, G. L., A. Bono, D. Krishnaiah, and J. G. Collin. 2008. 'Preparation of titanium dioxide photocatalyst loaded onto activated carbon support using chemical vapor deposition: A review paper', *Journal of Hazardous Materials*, 157: 209-19. <https://doi.org/10.1016/j.jhazmat.2008.01.040>
- Li, R. N., Z. W. Wang, J. L. Guo, Y. Li, H. Y. Zhang, J. M. Zhu, and X. Y. Xie. 2018. 'Enhanced adsorption of ciprofloxacin by KOH modified biochar derived from potato stems and leaves', *Water Science and Technology*, 77: 1127-36. <https://doi.org/10.2166/wst.2017.636>
- Li, S. L., J. Wen, B. S. He, J. Wang, X. M. Hu, and J. Liu. 2020. 'Occurrence of caffeine in the freshwater environment: Implications for ecopharmacovigilance', *Environmental Pollution*, 263. <https://doi.org/10.1016/j.envpol.2020.114371>
- Li, Y. Z., Y. Li, Y. Liu, Y. F. Wu, J. Q. Wu, B. Wang, H. Ye, H. N. Jia, X. Wang, L. H. Li, M. X. Zhu, H. R. Ding, Y. Lai, C. Q. Wang, J. Dick, and A. H. Lu. 2020. 'Photoreduction of inorganic carbon(plus IV) by elemental sulfur: Implications for prebiotic synthesis in terrestrial hot springs', *Science Advances*, 6. <https://doi.org/10.1126/sciadv.abc3687>
- Lim, T. T., P. S. Yap, M. Srinivasan, and A. G. Fane. 2011. 'TiO₂/AC Composites for Synergistic Adsorption-Photocatalysis Processes: Present Challenges and Further Developments for Water Treatment and Reclamation', *Critical Reviews in Environmental Science and Technology*, 41: 1173-230. <https://doi.org/10.1080/10643380903488664>
- Lineweaver, H., and D. Burk. 1934. 'The determination of enzyme dissociation constants', *Journal of the American Chemical Society*, 56: 658-66. <https://doi.org/10.1021/ja01318a036>
- Liu, J. L., B. Q. Zhou, H. Zhang, J. Ma, B. Mu, and W. B. Zhang. 2019. 'A novel Biochar modified by Chitosan-Fe/S for tetracycline adsorption and studies on site energy distribution', *Bioresource Technology*, 294. <https://doi.org/10.1016/j.biortech.2019.122152>
- Liu, L., E. Lopez, L. Dueñas-Orsorio, L. Stadler, Y. F. Xie, P. J. J. Alvarez, and Q. L. Li. 2020. 'The importance of system configuration for distributed direct potable water reuse', *Nature Sustainability*, 3: 548-55. <https://doi.org/10.1038/s41893-020-0518-5>
- Lopera, A. E. C., S. G. Ruiz, and J. M. Q. Alonso. 2019. 'Removal of emerging contaminants from wastewater using reverse osmosis for its subsequent reuse: Pilot plant', *Journal of Water Process Engineering*, 29. <https://doi.org/10.1016/j.jwpe.2019.100800>
- Lowell, S., J. E. Shields, M. A. Thomas, and M. Thommes. 2004. *Characterization of Porous Solids and Powders: Surface Area, Pore Size and Density* (Springer). <https://doi.org/10.1007/978-1-4020-2303-3>
- Lu, X. Q. 2008. 'Comment on "Thermodynamic and isotherm studies of the biosorption of Cu(II), Pb(II), and Zn(II) by leaves of saltbush (Atriplex canescens)"', *Journal of Chemical Thermodynamics*, 40: 739-40. <https://doi.org/10.1016/j.jct.2007.11.014>
- Luhar, I., S. Luhar, M. M. A. Abdullah, R. A. Razak, P. Vazureanu, A. V. Sandu, and P. D. Matasaru. 2021. 'A State-of-the-Art Review on Innovative Geopolymer Composites Designed for Water and Wastewater Treatment', *Materials*, 14. <https://doi.org/10.3390/ma14237456>
- Luo, J., Q. Zhang, M. Cao, L. Wu, J. Cao, F. Fang, C. Li, Z. Xue, and Q. Feng. 2019. 'Ecotoxicity and environmental fates of newly recognized contaminants-artificial sweeteners: A review',

- Science of the Total Environment*, 653: 1149-60. <https://doi.org/10.1016/j.scitotenv.2018.10.445>
- Malet, P., and G. Munuera. 1989. 'Temperature-Programmed Desorption Study of Activated Chemisorption Involving a Precursor State - Desorption of Water from TiO₂', *Journal of the Chemical Society-Faraday Transactions I*, 85: 4157-66. <https://doi.org/10.1039/F19898504157>
- Marson, E. O., C. E. S. Paniagua, O. Gomes, B. R. Goncalves, V. M. Silva, I. A. Ricardo, M. C. V. M. Starling, C. C. Amorim, and A. G. Trovo. 2022. 'A review toward contaminants of emerging concern in Brazil: Occurrence, impact and their degradation by advanced oxidation process in aquatic matrices', *Science of the Total Environment*, 836. <https://doi.org/10.1016/j.scitotenv.2022.155605>
- McBain, J. W. 1909. 'The mechanism of the adsorption ("sorption") of hydrogen by carbon.', *Philosophical Magazine*, 18: 916-35. <https://doi.org/10.1080/14786441208636769>
- McLintock, I. S. 1967. 'The Elovich equation in chemisorption kinetics', *Nature*, 216: 1204-05. <https://doi.org/10.1038/2161204a0>
- Menendez, J. A., M. J. Illangomez, C. A. Leon Y Leon, and L. R. Radovic. 1995. 'On the Difference between the Isoelectric Point and the Point of Zero Charge of Carbons', *Carbon*, 33: 1655-57. [https://doi.org/10.1016/0008-6223\(95\)96817-R](https://doi.org/10.1016/0008-6223(95)96817-R)
- Mesones, S., E. Mena, M. J. López-Muñoz, C. Adán, and J. Marugán. 2020. 'Synergistic and antagonistic effects in the photoelectrocatalytic disinfection of water with TiO₂ supported on activated carbon as a bipolar electrode in a novel 3D photoelectrochemical reactor', *Separation and Purification Technology*, 247. <https://doi.org/10.1016/j.seppur.2020.117002>
- Meyer, B. 1976. 'Elemental Sulfur', *Chemical Reviews*, 76: 367-88. <https://doi.org/10.1021/cr60301a003>
- Mineiro, C., F. Catozzo, and E. Pelizzetti. 1992. 'Role of adsorption in photocatalyzed reactions of organic molecules in aqueous titania suspensions', *Langmuir*, 8: 481-86. <https://doi.org/10.1021/la00038a029>
- Mohapatra, N. K. 2023. 'Geopolitics of water securitisation in Central Asia', *Geojournal*, 88: 897-916. <https://doi.org/10.1007/s10708-022-10661-0>
- Moreno-Piraján, J. C. 2011. *Thermodynamics - Interaction Studies - Solids, Liquids and Gases* (IntechOpen). <https://doi.org/10.5772/823>
- Mukhopadhyay, A., S. Duttagupta, and A. Mukherjee. 2022. 'Emerging organic contaminants in global community drinking water sources and supply: A review of occurrence, processes and remediation', *Journal of Environmental Chemical Engineering*, 10. <https://doi.org/10.1016/j.jece.2022.107560>
- Müller, F., L. S. Lisboa, and J. M. Chalker. 2023. 'Inverse Vulcanized Polymers for Sustainable Metal Remediation', *Advanced Sustainable Systems*, 7. <https://doi.org/10.1002/adsu.202300010>
- Nagabhatla, N., P. Pouramin, R. Brahmabhatt, C. Fioret, T. Glickman, K. B. Newbold, and V. Smakhtin. 2020. "Water and Migration: A Global Overview." In *UNU-INWEH Report Series*. Hamilton, Canada: United Nations University Institute for Water, Environment and Health.
- Nazari, G., H. Abolghasemi, M. Esmaeli, and E. S. Pouya. 2016. 'Aqueous phase adsorption of cephalixin by walnut shell-based activated carbon: A fixed-bed column study', *Applied Surface Science*, 375: 144-53. <https://doi.org/10.1016/j.apsusc.2016.03.096>
- Ngo, M. T. T., B. Q. Diep, H. Sano, Y. Nishimura, S. Boivin, H. Kodamatani, H. Takeuchi, S. C. W. Sakti, and T. Fujioka. 2022. 'Membrane distillation for achieving high water recovery for potable water reuse', *Chemosphere*, 288. <https://doi.org/10.1016/j.chemosphere.2021.132610>
- Nwabue, F. I., and E. J. Itumoh. 2020. 'Adsorption isotherm and kinetic modeling of a novel procedure for physical modification of silica gel using aqueous solutions of 4,4'-(1,2-

- ethanediyldinitrilo)bis-(2-pentanone) for preconcentration of Ni(II) ion', *Separation Science and Technology*, 55: 2919-32. <https://doi.org/10.1080/01496395.2019.1659821>
- Onjia, A. E., and S. K. Milonjic. 2003. 'Influence of the background electrolyte on the point of zero charge of chromium(III)-oxide', *Materials Science Forum*, 413: 87-91. <https://doi.org/10.4028/www.scientific.net/MSF.413.87>
- Oppenheimer, J., A. Eaton, M. Badruzzaman, A. W. Haghani, and J. G. Jacangelo. 2011. 'Occurrence and suitability of sucralose as an indicator compound of wastewater loading to surface waters in urbanized regions', *Water Research*, 45: 4019-27. <https://doi.org/10.1016/j.watres.2011.05.014>
- Orha, C., R. Pode, F. Manea, C. Lazau, and C. Bandas. 2017. 'Titanium dioxide-modified activated carbon for advanced drinking water treatment', *Process Safety and Environmental Protection*, 108: 26-33. <https://doi.org/10.1016/j.psep.2016.07.013>
- Paíga, P., and C. Delerue-Matos. 2017. 'Anthropogenic contamination of Portuguese coastal waters during the bathing season: Assessment using caffeine as a chemical marker', *Marine Pollution Bulletin*, 120: 355-63. <https://doi.org/10.1016/j.marpolbul.2017.05.030>
- Papirer, E., R. Lacroix, J. B. Donnet, G. Nanse, and P. Fioux. 1994. 'Xps Study of the Halogenation of Carbon-Black .1. Bromination', *Carbon*, 32: 1341-58. [https://doi.org/10.1016/0008-6223\(94\)90121-X](https://doi.org/10.1016/0008-6223(94)90121-X)
- Patel, M., R. Kumar, K. Kishor, T. Mlsna, C. U. Pittman, and D. Mohan. 2019. 'Pharmaceuticals of Emerging Concern in Aquatic Systems: Chemistry, Occurrence, Effects, and Removal Methods', *Chemical Reviews*, 119: 3510-673. <https://doi.org/10.1021/acs.chemrev.8b00299>
- Paunovic, O., S. Pap, S. Maletic, M. A. Taggart, N. Boskovic, and M. T. Sekulic. 2019. 'Ionisable emerging pharmaceutical adsorption onto microwave functionalised biochar derived from novel lignocellulosic waste biomass', *Journal of Colloid and Interface Science*, 547: 350-60. <https://doi.org/10.1016/j.jcis.2019.04.011>
- Peiris, C., S. R. Gunatilake, T. E. Mlsna, D. Mohan, and M. Vithanage. 2017. 'Biochar based removal of antibiotic sulfonamides and tetracyclines in aquatic environments: A critical review', *Bioresource Technology*, 246: 150-59. <https://doi.org/10.1016/j.biortech.2017.07.150>
- Peñas-Garzón, M., A. Gómez-Avilés, C. Belver, J. J. Rodriguez, and J. Bedia. 2020. 'Degradation pathways of emerging contaminants using TiO₂-activated carbon heterostructures in aqueous solution under simulated solar light', *Chemical Engineering Journal*, 392. <https://doi.org/10.1016/j.cej.2020.124867>
- Peng, H. B., B. Pan, M. Wu, Y. Liu, D. Zhang, and B. S. Xing. 2012. 'Adsorption of ofloxacin and norfloxacin on carbon nanotubes: Hydrophobicity- and structure-controlled process', *Journal of Hazardous Materials*, 233: 89-96. <https://doi.org/10.1016/j.jhazmat.2012.06.058>
- Perez-Marin, A. B., V. M. Zapata, J. F. Ortuno, M. Aguilar, J. Saez, and M. Llorens. 2007. 'Removal of cadmium from aqueous solutions by adsorption onto orange waste', *Journal of Hazardous Materials*, 139: 122-31. <https://doi.org/10.1016/j.jhazmat.2006.06.008>
- Pivetta, R. C., C. Rodrigues-Silva, A. R. Ribeiro, and S. Rath. 2020. 'Tracking the occurrence of psychotropic pharmaceuticals in Brazilian wastewater treatment plants and surface water, with assessment of environmental risks', *Science of the Total Environment*, 727. <https://doi.org/10.1016/j.scitotenv.2020.138661>
- Porto, R. S., R. S. B. Pinheiro, and S. Rath. 2021. 'Leaching of benzimidazole antiparasitics in soil columns and in soil columns amended with sheep excreta', *Environmental Science and Pollution Research*, 28: 59040-49. <https://doi.org/10.1007/s11356-020-08389-w>
- Porto, R. S., C. Rodrigues-Silva, J. Schneider, and S. Rath. 2019. 'Benzimidazoles in wastewater: Analytical method development, monitoring and degradation by photolysis and ozonation',

- Journal of Environmental Management*, 232: 729-37. <https://doi.org/10.1016/j.jenvman.2018.11.121>
- Puri, M., K. Gandhi, and M. S. Kumar. 2023. 'Emerging environmental contaminants: A global perspective on policies and regulations', *Journal of Environmental Management*, 332. <https://doi.org/10.1016/j.jenvman.2023.117344>
- Putra, E. K., R. Pranowo, J. Sunarso, N. Indraswati, and S. Ismadji. 2009. 'Performance of activated carbon and bentonite for adsorption of amoxicillin from wastewater: mechanisms, isotherms and kinetics', *Water Research*, 43: 2419-30. <https://doi.org/10.1016/j.watres.2009.02.039>
- Quesada, H. B., A. T. A. Baptista, L. F. Cusioli, D. Seibert, C. D. Bezerra, and R. Bergamasco. 2019. 'Surface water pollution by pharmaceuticals and an alternative of removal by low-cost adsorbents', *Chemosphere*, 222: 766-80. <https://doi.org/10.1016/j.chemosphere.2019.02.009>
- Reddy, K. R., V. Kandou, R. Havrelock, A. R. El-Khattabi, T. Cordova, M. D. Wilson, B. Nelson, and C. Trujillo. 2023. 'Reuse of Treated Wastewater: Drivers, Regulations, Technologies, Case Studies, and Greater Chicago Area Experiences', *Sustainability*, 15. <https://doi.org/10.3390/su15097495>
- Redlich, O., and D. L. Peterson. 1959. 'A Useful Adsorption Isotherm', *Journal of Physical Chemistry*, 63: 1024-24.
- Richardson, S. D., and S. Y. Kimura. 2020. 'Water Analysis: Emerging Contaminants and Current Issues', *Analytical Chemistry*, 92: 473-505. <https://doi.org/10.1021/acs.analchem.9b05269>
- Ritchie, AG. 1977. 'Alternative to the Elovich equation for the kinetics of adsorption of gases on solids', *Journal of the Chemical Society, Faraday Transactions 1: Physical Chemistry in Condensed Phases*, 73: 1650-53. <https://doi.org/10.1039/F19777301650>
- Ritter, L., K. Solomon, P. Sibley, K. Hall, P. Keen, G. Mattu, and B. Linton. 2002. 'Sources, pathways, and relative risks of contaminants in surface water and groundwater: A perspective prepared for the Walkerton inquiry', *Journal of Toxicology and Environmental Health-Part a-Current Issues*, 65: 1-142. <https://doi.org/10.1080/152873902753338572>
- Rodrigues-Silva, C., R. S. Porto, S. G. dos Santos, J. Schneider, and S. Rath. 2019. 'Fluoroquinolones in Hospital Wastewater: Analytical Method, Occurrence, Treatment with Ozone and Residual Antimicrobial Activity Evaluation', *Journal of the Brazilian Chemical Society*, 30: 1447-57. <https://doi.org/10.21577/0103-5053.20190040>
- Rodriguez-Liebana, J. A., A. Lopez-Galindo, C. J. de Cisneros, A. Galvez, M. Rozalen, R. Sanchez-Espejo, E. Caballero, and A. Pena. 2016. 'Adsorption/desorption of fungicides in natural clays from Southeastern Spain', *Applied Clay Science*, 132: 402-11. <https://doi.org/10.1016/j.clay.2016.07.006>
- Rodriguez-Reinoso, F., and A. Sepúlveda-Escribano. 2009. 'Carbon as Catalyst Support.' in P. Serp and J. K. Figueiredo (eds.), *Carbon Materials for Catalysis* (Wiley: Hoboken, New Jersey).
- Roginsky, S., and Zeldovich. YB. 1934. 'The catalytic oxidation of carbon monoxide on manganese dioxide', *Acta Phys. Chem. USSR*, 1.
- Rosinger, A. Y. 2023. 'Water Needs, Water Insecurity, and Human Biology', *Annual Review of Anthropology*, 52: 93-113. <https://doi.org/10.1146/annurev-anthro-052721-090331>
- Rouquerol, F., J. Rouquerol, K. Sing, P. Llewellyn, and G. Maurin. 2014. *Adsorption by powders and Porous Solids Principles, Methodology and Applications* (Elsevier). <https://doi.org/10.1016/B978-0-12-598920-6.X5000-3>
- Ruthven, D. M. 1984. *Principles of adsorption and adsorption processes* (Wiley).
- Saha, P., and S. Chowdhury. 2011. 'Insight Into Adsorption Thermodynamics.' in M. Tadashi (ed.), *Thermodynamics* (IntechOpen). <https://doi.org/10.5772/13474>
- SANASA. "EPAR CAPIVARI II.". <https://cetesb.sp.gov.br/wp-content/uploads/sites/33/2018/08/Folder-EPAR-Capivari-II.pdf>

- Santhosh, C., V. Velmurugan, G. Jacob, S. K. Jeong, A. N. Grace, and A. Bhatnagar. 2016. 'Role of nanomaterials in water treatment applications: A review', *Chemical Engineering Journal*, 306: 1116-37. <https://doi.org/10.1016/j.cej.2016.08.053>
- Scanlon, B. R., S. Fakhreddine, A. Rateb, I. de Graaf, J. Famiglietti, T. Gleeson, R. Q. Grafton, E. Jobbagy, S. Kebede, S. R. Kolusu, L. F. Konikow, D. Long, M. Mekonnen, H. M. Schmied, A. Mukherjee, A. MacDonald, R. C. Reedy, M. Shamsudduha, C. T. Simmons, A. L. Sun, R. G. Taylor, K. G. Villholth, C. J. Vörösmarty, and C. M. Zheng. 2023. 'Global water resources and the role of groundwater in a resilient water future', *Nature Reviews Earth & Environment*, 4: 351-51. <https://doi.org/10.1038/s43017-022-00378-6>
- Scatchard, G. 1949. 'The Attractions of Proteins for Small Molecules and Ions', *Annals of the New York Academy of Sciences*, 51: 660-72. <https://doi.org/10.1111/j.1749-6632.1949.tb27297.x>
- Schimmoller, L. J., M. J. Kealy, and S. K. Foster. 2015. 'Triple bottom line costs for multiple potable reuse treatment schemes', *Environmental Science-Water Research & Technology*, 1: 644-58. <https://doi.org/10.1039/C5EW00044K>
- Schneider, J., M. Matsuoka, M. Takeuchi, J. L. Zhang, Y. Horiuchi, M. Anpo, and D. W. Bahnemann. 2014. 'Understanding TiO₂ Photocatalysis: Mechanisms and Materials', *Chemical Reviews*, 114: 9919-86. <https://doi.org/10.1021/cr5001892>
- Sgroi, M., T. Anumol, P. Roccaro, F. G. A. Vagliasindi, and S. A. Snyder. 2018. 'Modeling emerging contaminants breakthrough in packed bed adsorption columns by UV absorbance and fluorescing components of dissolved organic matter', *Water Research*, 145: 667-77. <https://doi.org/10.1016/j.watres.2018.09.018>
- Shamoon, A., A. Haleem, S. Bahl, M. Javaid, S. B. Garg, R. C. Sharma, and J. Garg. 2022. 'Environmental impact of energy production and extraction of materials - a review', *Materials Today-Proceedings*, 57: 936-41. <https://doi.org/10.1016/j.matpr.2022.03.159>
- Shankar, P., S. Ahuja, and K. Sriram. 2013. 'Non-nutritive sweeteners: review and update', *Nutrition*, 29: 1293-9.
- Shi, X. M., Z. X. Li, W. Chen, L. W. Qiang, J. C. Xia, M. Chen, L. Y. Zhu, and P. J. J. Alvarez. 2016. 'Fate of TiO₂ nanoparticles entering sewage treatment plants and bioaccumulation in fish in the receiving streams', *NanoImpact*, 3-4: 96-103. <https://doi.org/10.1016/j.impact.2016.09.002>
- Silva, DA, RP Cavalcante, EB Barbosa, AM Junior, SC Oliveira, and RF Dantas. 2021. 'Combined AOP/GAC/AOP systems for secondary effluent polishing: Optimization, toxicity and disinfection', *Separation and Purification Technology*, 263. <https://doi.org/10.1016/j.seppur.2021.118415>
- Silva, M.A.C. 2006. 'Avaliação experimental e modelagem do processo contínuo de adsorção do preto remazol B em coluna de leito fixo de carvão ativado', Universidade Federal de Pernambuco. <https://repositorio.ufpe.br/handle/123456789/6707>
- Sips, R. 1948. 'On the Structure of a Catalyst Surface', *The Journal of Chemical Physics*, 16: 490-95. <https://doi.org/10.1063/1.1746922>
- Smaranda, C., M. C. Popescu, D. Bulgariu, T. Malutan, and M. Gavrilescu. 2017. 'Adsorption of organic pollutants onto a Romanian soil: Column dynamics and transport', *Process Safety and Environmental Protection*, 108: 108-20. <https://doi.org/10.1016/j.psep.2016.06.027>
- Soller, J. A., S. E. Eftim, and S. P. Nappier. 2018. 'Direct potable reuse microbial risk assessment methodology: Sensitivity analysis and application to State log credit allocations', *Water Research*, 128: 286-92. <https://doi.org/10.1016/j.watres.2017.10.034>

- Song, JY., and SH. Jhung. 2017. 'Adsorption of pharmaceuticals and personal care products over metalorganic frameworks functionalized with hydroxyl groups: quantitative analyses of H-bonding in adsorption', *Chemical Engineering Journal*, 322: 366-74. <https://doi.org/10.1016/j.cej.2017.04.036>
- Sonobe, HG. 2018. 'Remoção de microcistina por filtros de carvão ativado granular: aplicação de modelos matemáticos para obtenção de parâmetros de dimensionamento', Universidade de São Paulo. <https://doi.org/10.11606/D.18.2018.tde-19062018-165550>
- Sophia, A. C., and E. C. Lima. 2018. 'Removal of emerging contaminants from the environment by adsorption', *Ecotoxicology and Environmental Safety*, 150: 1-17. <https://doi.org/10.1016/j.ecoenv.2017.12.026>
- Spina, M., W. Venancio, C. Rodrigues-Silva, R. C. Pivetta, V. Diniz, S. Rath, and J. R. Guimaraes. 2021. 'Degradation of antidepressant pharmaceuticals by photoperoxidation in diverse water matrices: a highlight in the evaluation of acute and chronic toxicity', *Environmental Science and Pollution Research*, 28: 24034-45. <https://doi.org/10.1007/s11356-020-11657-4>
- Srivastava, S., and P. Goyal. 2010. *Novel biomaterials: decontamination of toxic metals from wastewater* (Springer Science & Business Media). <https://doi.org/10.1007/978-3-642-11329-1>
- Taheran, M. , M. Naghdi, S. K. Brar, M. Verma, and R. T. Surampalli. 2018. 'Emerging contaminants: Here today, there tomorrow!', *Environmental Nanotechnology, Monitoring & Management*, 10: 122-26. <https://doi.org/10.1016/j.enmm.2018.05.010>
- Tan, K. L., and B. H. Hameed. 2017. 'Insight into the adsorption kinetics models for the removal of contaminants from aqueous solutions', *Journal of the Taiwan Institute of Chemical Engineers*, 74: 25-48. <https://doi.org/10.1016/j.jtice.2017.01.024>
- Taoufik, N., A. Elmchaouri, F. Anouar, S. A. Korili, and A. Gil. 2019. 'Improvement of the adsorption properties of an activated carbon coated by titanium dioxide for the removal of emerging contaminants', *Journal of Water Process Engineering*, 31. <https://doi.org/10.1016/j.jwpe.2019.100876>
- Thomas, H. C. 1944. 'Heterogeneous ion exchange in a flowing system', *Journal of the American Chemical Society*, 66: 1664-66. <https://doi.org/10.1021/ja01238a017>
- Tian, F., Z. S. Wu, Q. Y. Chen, Y. J. Yan, G. Cravotto, and Z. L. Wu. 2015. 'Microwave-induced crystallization of AC/TiO₂ for improving the performance of rhodamine B dye degradation', *Applied Surface Science*, 351: 104-12. <https://doi.org/10.1016/j.apsusc.2015.05.133>
- Tran, H. N., H. P. Chao, and S. J. You. 2018. 'Activated carbons from golden shower upon different chemical activation methods: Synthesis and characterizations', *Adsorption Science & Technology*, 36: 95-113. <https://doi.org/10.1177/02636174166848>
- Tran, H. N., S. J. You, and H. P. Chao. 2016. 'Thermodynamic parameters of cadmium adsorption onto orange peel calculated from various methods: A comparison study', *Journal of Environmental Chemical Engineering*, 4: 2671-82. <https://doi.org/10.1016/j.jece.2016.05.009>
- Tran, H. N., S. J. You, A. Hosseini-Bandegharai, and H. P. Chao. 2017. 'Mistakes and inconsistencies regarding adsorption of contaminants from aqueous solutions: A critical review', *Water Research*, 120: 88-116. <https://doi.org/10.1016/j.watres.2017.04.014>
- Upton, R. L., R. A. Dop, E. Sadler, A. M. Lunt, D. R. Neill, T. Hasell, and C. R. Crick. 2022. 'Investigating the viability of sulfur polymers for the fabrication of photoactive, antimicrobial, water repellent coatings', *Journal of Materials Chemistry B*, 10: 4153-62. <https://doi.org/10.1039/D2TB00319H>
- Varga, M., M. Elabadsa, E. Tatar, and V. G. Mihucz. 2019. 'Removal of selected pharmaceuticals from aqueous matrices with activated carbon under batch conditions', *Microchemical Journal*, 148: 661-72. <https://doi.org/10.1016/j.microc.2019.05.038>

- Velarde, L., M. S. Nabavi, E. Escalera, M. L. Antti, and F. Akhtar. 2023. 'Adsorption of heavy metals on natural zeolites: A review', *Chemosphere*, 328. <https://doi.org/10.1016/j.chemosphere.2023.138508>
- Venancio, W. A. L., C. Rodrigues-Silva, M. Spina, V. Diniz, and J. R. Guimaraes. 2021. 'Degradation of benzimidazoles by photoperoxidation: metabolites detection and ecotoxicity assessment using *Raphidocelis subcapitata* microalgae and *Vibrio fischeri*', *Environmental Science and Pollution Research*, 28: 23742-52. <https://doi.org/10.1007/s11356-020-11294-x>
- Villarin, M. C., and S. Merel. 2020. 'Paradigm shifts and current challenges in wastewater management', *Journal of Hazardous Materials*, 390. <https://doi.org/10.1016/j.jhazmat.2020.122139>
- Wallmann, L., J. Krampe, J. Lahnsteiner, E. Radu, P. van Rensburg, K. Slipko, M. Wogerbauer, and N. Kreuzinger. 2021. 'Fate and persistence of antibiotic-resistant bacteria and genes through a multi-barrier treatment facility for direct potable reuse', *Water Reuse*, 11: 373-90. <https://doi.org/10.2166/wrd.2021.097>
- Wang, J., Y. B. Sun, J. W. Feng, L. Xin, and J. Z. Ma. 2016. 'Degradation of triclocarban in water by dielectric barrier discharge plasma combined with TiO₂/activated carbon fibers: Effect of operating parameters and byproducts identification', *Chemical Engineering Journal*, 300: 36-46. <https://doi.org/10.1016/j.cej.2016.04.041>
- Wang, X. J., Z. H. Hu, Y. J. Chen, G. H. Zhao, Y. F. Liu, and Z. B. Wen. 2009. 'A novel approach towards high-performance composite photocatalyst of TiO₂ deposited on activated carbon', *Applied Surface Science*, 255: 3953-58. <https://doi.org/10.1016/j.apsusc.2008.10.083>
- Wang, Y. F., J. X. Zhu, H. O. Huang, and H. H. Cho. 2015. 'Carbon nanotube composite membranes for microfiltration of pharmaceuticals and personal care products: Capabilities and potential mechanisms', *Journal of Membrane Science*, 479: 165-74.
- Wang, Y. Z., and A. X. Wu. 2008. 'pi-pi interaction in aromatic supramolecular system', *Chinese Journal of Organic Chemistry*, 28: 997-1011. <https://doi.org/10.1016/j.memsci.2015.01.034>
- Wang, Z. Y., X. D. Yu, B. Pan, and B. S. Xing. 2010. 'Norfloxacin Sorption and Its Thermodynamics on Surface-Modified Carbon Nanotubes', *Environmental Science & Technology*, 44: 978-84. <https://doi.org/10.1021/es902775u>
- Weber, WJ., and JC. Morris. 1963. 'Kinetics of adsorption on carbon from solution', *Journal of the Sanitary Engineering Division*, 89: 31-60. <https://doi.org/10.1061/JSEDAI.000043>
- Westall, F., and A. Brack. 2018. 'The Importance of Water for Life', *Space Science Reviews*, 214. <https://doi.org/10.1007/s11214-018-0476-7>
- Whelan, M. J., C. Linstead, F. Worrall, S. J. Ormerod, I. Durance, A. C. Johnson, D. Johnson, M. Owen, E. Wiik, N. J. K. Howden, T. P. Burt, A. Boxall, C. D. Brown, D. M. Oliver, and D. Tickner. 2022. 'Is water quality in British rivers "better than at any time since the end of the Industrial Revolution"?', *Science of the Total Environment*, 843. <https://doi.org/10.1016/j.scitotenv.2022.157014>
- World Health Organization (WHO). 2017. "Potable reuse : Guidance for producing safe drinking-water." <https://www.who.int/publications/i/item/9789241512770>
- Worch, E. 2012. *Adsorption Technology in Water Treatment* (De Gruyter).
- Worthington, M. J. H., R. L. Kucera, and J. M. Chalker. 2017. 'Green chemistry and polymers made from sulfur', *Green Chemistry*, 19: 2748-61. <https://doi.org/10.1039/C7GC00014F>
- Wu, F-C., R-L. Tseng, and R-S. Juang. 2009. 'Characteristics of Elovich equation used for the analysis of adsorption kinetics in dye-chitosan systems', *Chemical Engineering Journal*, 150: 366-73. <https://doi.org/10.1016/j.cej.2009.01.014>

- Wu, J., J. Lu, C. Zhang, Z. H. Zhang, and X. Y. Min. 2019. 'Adsorptive Removal of Tetracyclines and Fluoroquinolones Using Yak Dung Biochar', *Bulletin of Environmental Contamination and Toxicology*, 102: 407-12. <https://doi.org/10.1007/s00128-018-2516-0>
- Xie, L., D. L. Yang, Q. Y. Lu, H. Zhang, and H. B. Zeng. 2020. 'Role of molecular architecture in the modulation of hydrophobic interactions', *Current Opinion in Colloid & Interface Science*, 47: 58-69. <https://doi.org/10.1016/j.cocis.2019.12.001>
- Yan, P. Y., W. Zhao, B. W. Zhang, L. Jiang, S. Petcher, J. A. Smith, D. J. Parker, A. I. Cooper, J. X. Lei, and T. Hasell. 2020. 'Inverse Vulcanized Polymers with Shape Memory, Enhanced Mechanical Properties, and Vitrimers Behavior', *Angewandte Chemie-International Edition*, 59: 13371-78. <https://doi.org/10.1002/anie.202004311>
- Yianatos, J., L. Vinnett, I. Panire, M. Alvarez-Silva, and F. Diaz. 2017. 'Residence time distribution measurements and modelling in industrial flotation columns', *Minerals Engineering*, 110: 139-44. <https://doi.org/10.1016/j.mineng.2017.04.018>
- Yoon, Y. H., and J. H. Nelson. 1984a. 'Application of gas adsorption kinetics--II. A theoretical model for respirator cartridge service life and its practical applications', *American Industrial Hygiene Association Journal*, 45: 517-24. <https://doi.org/10.1080/15298668491400205>
- . 1984b. 'Application of gas adsorption kinetics. I. A theoretical model for respirator cartridge service life', *American Industrial Hygiene Association Journal*, 45: 509-16. <https://doi.org/10.1080/15298668491400197>
- Yu, F., J. Ma, and S. Han. 2014. 'Adsorption of tetracycline from aqueous solutions onto multi-walled carbon nanotubes with different oxygen contents', *Scientific Reports*, 4. <https://doi.org/10.1038/srep05326>
- Yu, F., S. N. Sun, S. Han, J. Zheng, and J. Ma. 2016. 'Adsorption removal of ciprofloxacin by multi-walled carbon nanotubes with different oxygen contents from aqueous solutions', *Chemical Engineering Journal*, 285: 588-95. <https://doi.org/10.1016/j.cej.2015.10.039>
- Yu, J. G., X. H. Zhao, H. Yang, X. H. Chen, Q. Yang, L. Y. Yu, J. H. Jiang, and X. Q. Chen. 2014. 'Aqueous adsorption and removal of organic contaminants by carbon nanotubes', *Science of the Total Environment*, 482: 241-51. <https://doi.org/10.1016/j.scitotenv.2014.02.129>
- Zaiat, M. 2005. "Fundamentos de cinética e análise de reatores aplicados ao tratamento de águas residuárias: notas de aula." In. São Carlos: Escola de Engenharia de São Carlos. <http://repositorio.eesc.usp.br/handle/RIEESC/6109>
- Zanella, H. G., L. Spessato, G. K. P. Lopes, J. T. C. Yokoyama, M. C. Silva, P. S. C. Souza, A. Ronix, A. L. Cazetta, and V. C. Almeida. 2021. 'Caffeine adsorption on activated biochar derived from macrophytes (*Eichornia crassipes*)', *Journal of Molecular Liquids*, 340. <https://doi.org/10.1016/j.molliq.2021.117206>
- Zhang, C. S., L. Liu, M. H. Zhao, H. W. Rong, and Y. Xu. 2018. 'The environmental characteristics and applications of biochar', *Environmental Science and Pollution Research*, 25: 21525-34. <https://doi.org/10.1007/s11356-018-2521-1>
- Zhang, D., B. Pan, M. Wu, B. Wang, H. Zhang, H. B. Peng, D. Wu, and P. Ning. 2011. 'Adsorption of sulfamethoxazole on functionalized carbon nanotubes as affected by cations and anions', *Environmental Pollution*, 159: 2616-21. <https://doi.org/10.1016/j.envpol.2011.05.036>
- Zhang, P. L., S. Yin, and T. Sato. 2009. 'Synthesis of high-activity TiO₂ photocatalyst via environmentally friendly and novel microwave assisted hydrothermal process', *Applied Catalysis B-Environmental*, 89: 118-22. <https://doi.org/10.1016/j.apcatb.2008.12.002>
- Zhao, L., J. H. Deng, P. Z. Sun, J. S. Liu, Y. Ji, N. Nakada, Z. Qiao, H. Tanaka, and Y. K. Yang. 2018. 'Nanomaterials for treating emerging contaminants in water by adsorption and photocatalysis: Systematic review and bibliometric analysis', *Science of the Total Environment*, 627: 1253-63. <https://doi.org/10.1016/j.scitotenv.2018.02.006>

- Zhao, Y. X., S. M. Liu, D. Elsworth, Y. D. Jiang, and J. Zhu. 2014. 'Pore Structure Characterization of Coal by Synchrotron Small-Angle X-ray Scattering and Transmission Electron Microscopy', *Energy & Fuels*, 28: 3704-11. <https://doi.org/10.1021/ef500487d>
- Zhu, Z. Y., J. W. Xie, M. C. Zhang, Q. Zhou, and F. Q. Liu. 2016. 'Insight into the adsorption of PPCPs by porous adsorbents: Effect of the properties of adsorbents and adsorbates', *Environmental Pollution*, 214: 524-31. <https://doi.org/10.1016/j.envpol.2016.04.070>
- Zhuo, N., Y. Lan, W. Yang, Z. Yang, X. Li, X. Zhou, Y. Liu, J. Shen, and X. Zhang. 2017. 'Adsorption of three selected pharmaceuticals and personal care products (PPCPs) onto MIL-101(Cr)/natural polymer composite beads', *Separation and Purification Technology*, 177: 272-80. <https://doi.org/10.1016/j.seppur.2016.12.041>
- Zodrow, K. R., Qilin L., R. M. Buono, W. Chen, G. Daigger, L. Dueñas-Osorio, M. Elimelech, X. Huang, G. Jiang, J.-H. Kim, B. E. Logan, D. L. Sedlak, P. Westerhoff, and P. J. J. Alvarez. 2017. 'Advanced Materials, Technologies, and Complex Systems Analyses: Emerging Opportunities to Enhance Urban Water Security', *Environmental Science & Technology*, 51: 10274-81. <https://doi.org/10.1021/acs.est.7b01679>

Chapter 7.

Annexes

DECLARAÇÃO

As cópias dos documentos de minha autoria ou de minha coautoria, já publicados ou submetidos para publicação em revistas científicas ou anais de congressos sujeitos a arbitragem, que constam da minha Tese de Doutorado, intitulada “Advanced Hybrid Materials for Direct Potable Reuse as Alternatives to Activated Carbon for Removal of Contaminants of Emerging Concern” não infringem os dispositivos da Lei nº 9.610/98, nem o direito autoral de qualquer editora.

Campinas, 11 de março de 2025

Autor R.G. nº 46820015-0

Orientadora RMN nº V069242H

15/07/2024, 09:03

Rightslink® by Copyright Clearance Center



Adsorption of recalcitrant contaminants of emerging concern onto activated carbon: A laboratory and pilot-scale study

Author: Vinícius Diniz, Davi Gasparini Fernandes Cunha, Susanne Rath
Publication: Journal of Environmental Management
Publisher: Elsevier
Date: 1 January 2023

© 2022 Elsevier Ltd. All rights reserved.

Journal Author Rights

Please note that, as the author of this Elsevier article, you retain the right to include it in a thesis or dissertation, provided it is not published commercially. Permission is not required, but please ensure that you reference the journal as the original source. For more information on this and on your other retained rights, please visit: <https://www.elsevier.com/about/our-business/policies/copyright#Author-rights>

BACK

CLOSE WINDOW

© 2024 Copyright - All Rights Reserved | Copyright Clearance Center, Inc. | Privacy statement | Data Security and Privacy
| For California Residents | Terms and ConditionsComments? We would like to hear from you. E-mail us at
customercare@copyright.com

15/07/2024, 09:06

Rightslink® by Copyright Clearance Center







Adsorption of aqueous phase contaminants of emerging concern by activated carbon: Comparative fixed-bed column study and in situ regeneration methods

Author: Vinicius Diniz, Susanne Rath

Publication: Journal of Hazardous Materials

Publisher: Elsevier

Date: 5 October 2023

© 2023 Elsevier B.V. All rights reserved.

Journal Author Rights

Please note that, as the author of this Elsevier article, you retain the right to include it in a thesis or dissertation, provided it is not published commercially. Permission is not required, but please ensure that you reference the journal as the original source. For more information on this and on your other retained rights, please visit: <https://www.elsevier.com/about/our-business/policies/copyright#Author-rights>

BACKCLOSE WINDOW

© 2024 Copyright - All Rights Reserved | Copyright Clearance Center, Inc. | Privacy statement | Data Security and Privacy
| For California Residents | Terms and ConditionsComments? We would like to hear from you. E-mail us at
customer.care@copyright.com

15/07/2024, 09:07

Rightslink® by Copyright Clearance Center





Synthesis and characterization of TiO₂-carbon filter materials for water decontamination by adsorption-degradation processes

Author: Vinidius Diniz, Colin R. Crick, Susanne Rath

Publication: Journal of Environmental Management

Publisher: Elsevier

Date: 15 November 2023

© 2023 Elsevier Ltd. All rights reserved.

Journal Author Rights

Please note that, as the author of this Elsevier article, you retain the right to include it in a thesis or dissertation, provided it is not published commercially. Permission is not required, but please ensure that you reference the journal as the original source. For more information on this and on your other retained rights, please visit: <https://www.elsevier.com/about/our-business/policies/copyright#Author-rights>

BACKCLOSE WINDOW

© 2024 Copyright - All Rights Reserved | Copyright Clearance Center, Inc. | Privacy statement | Data Security and Privacy
| For California Residents | Terms and ConditionsComments? We would like to hear from you. E-mail us at
customerCare@copyright.com



15/07/2024, 09:08

Rightslink® by Copyright Clearance Center



RightsLink



SPRINGER NATURE

Porous sulfur polymers for effective aqueous-phase organic contaminant removal

Author: Vinicius Dintz et al
Publication: Scientific Reports
Publisher: Springer Nature
Date: Apr 7, 2024
Copyright © 2024, The Author(s)

Creative Commons

This is an open access article distributed under the terms of the [Creative Commons CC BY](#) license, which permits unrestricted use, distribution, and reproduction in any medium, provided the original work is properly cited.
You are not required to obtain permission to reuse this article.
To request permission for a type of use not listed, please contact [Springer Nature](#)

© 2024 Copyright - All Rights Reserved | [Copyright Clearance Center, Inc.](#) | [Privacy statement](#) | [Data Security and Privacy](#)
| [For California Residents](#) | [Terms and Conditions](#)Comments? We would like to hear from you. E-mail us at customercare@copyright.com

Supplementary Material: Adsorption of recalcitrant contaminants of emerging concern onto activated carbon: a laboratory and pilot-scale study

Vinicius Diniz^{1,*}, Davi Gasparini Fernandes Cunha², Susanne Rath¹

¹Department of Analytical Chemistry, Institute of Chemistry, University of Campinas, Rua Josué de Castro, Cidade Universitária, Campinas, SP, 13083-970, Brazil

²São Carlos School of Engineering, Department of Hydraulics and Sanitation, University of São Paulo, Avenida Trabalhador São-Carlense, Centro, São Carlos, SP, 13566-590, Brazil

*Author for correspondence: *viniciusdiniz994@gmail.com*

Supplementary text:

Chemicals and reagents

Analytical standards of acetaminophen (ACE) ($\geq 99.0\%$), acesulfame (ACF) ($\geq 99.0\%$), albendazole (ABZ) (99.3%), caffeine (CAF) (99.0%), diclofenac (DCF) ($\geq 99.0\%$), hydrochlorothiazide (HTZ) (99.7%), propranolol (PRP) ($\geq 99.0\%$), ricobendazole (RBZ) ($\geq 98.0\%$), saccharin (SAC) (99.6%), sulfamethoxazole (SMX) ($\geq 99.0\%$), and sucralose (SUC) (99.4%) were purchased from Sigma-Aldrich (USA). Carbamazepine (CMZ) ($\geq 98\%$) was obtained from Toronto Research chemicals (Canada). The physicochemical data of the contaminants of emerging concern are shown on Table S1. The internal standards albendazole-d3 (99.3%), caffeine-d3 (99.0%), diclofenac-d4 (99.0%), and sulfadimethoxin-d3 (99.3%) were purchased from Sigma-Aldrich (USA).

Dimethylformamide (DMF), ammonium acetate (HPLC grade), and methanol (MeOH) (HPLC grade) were obtained from Labsynth (Brazil), Merck (USA), and J.T. Baker (USA), respectively. Hydrochloric acid (35%), potassium chloride (p.a.), sodium bicarbonate (p.a.), sodium carbonate (p.a.), sodium hydroxide (p.a.), acetic acid (p.a.), boric acid (p.a.), and phosphoric acid (85%) were purchased from Synth (Brazil).

Activated carbon characterization

The AC was characterized by adsorption/desorption isotherm of nitrogen at 77 K in a mercury porosimeter PoreMaster (Quantachrome) and surface area analyzer NOVA 4200e (Quantachrome). Previously to the analysis, the AC was degassed at 150 °C under a vacuum chamber for 24 h. The specific surface area (SSA_{BET}) and pore size distribution were calculated using the BET theory and BJH methods. The structural, morphological, and chemical composition by scanning electron microscopy (SEM) and energy-dispersive X-ray spectroscopy (EDX) were evaluated by a field-emission scanning microscope (Jeol J6360 LV). Thermogravimetric analyses were carried out in a TGA-2950 (TA instruments) with a heating ratio of 10 °C min⁻¹. The pH_{ZPC} was determined according to the procedure described by Larous & Meniai (2016). Briefly, a 500 mL solution of 0.01 mol L⁻¹ NaCl was equally divided into 100 mL glass vessels (50 mL for vessel), and the pH of each vessel was adjusted between 2 and 12. Then, 200 mg of AC were introduced into each vessel, and the mixtures were kept under controlled temperature (25 °C) for 48 h to determine the final pH.

X-ray diffraction (XRD) spectrum of the AC were acquired with a XRD-7000 (SHIMADZU) diffractometer using a copper anode ($K\alpha$ radiation). Confocal Raman spectroscopy

studies were carried out on a T64000 (Horiba) spectrometer equipped with a 532 nm laser with a grating of 1800 grooves per mm² and slit of 100 μ m, resulting in a spectral resolution of 2.9 cm⁻¹. Fourier Transformed Infrared spectroscopy (FTIR) was conducted in a CARY 630 (Agilent) spectrophotometer. Finally, Boehm's titration method was used to determine the surface groups on the AC sample (Oickle *et al.*, 2010). The method is a reliable procedure determining acidic (lactonic, phenolic and carboxylic) and basic groups.

Pilot plant operation

The pilot plant receives the effluent of the wastewater treatment plant (WWTP) in the equalizer tank 1 (ET1), which has a hydraulic detention time (HDT) of 20 min. The biological air filter installed is to avoid the growth of the microbiological community in the ET1. To analyze the efficiency of the granular activated carbon fixed-bed column (GAC), it is necessary to open the water valves (V4 and V5) and turn on the pump (P1). The effluent flows to ET2 (HDT 6 min), and P4 pumps the effluent to the ultraviolet reactor (which is turned off). The effluent percolated through the activated carbon fixed-bed column (GAC) with V9 closed and V10 open, then collected in V11. The photoperoxidation process (UV/H₂O₂) is operated initially similarly; however, P3 pumps hydrogen peroxide (H₂O₂) into ET2, which is in constant agitation due to the water flows. So, P4 pumps the mixture (effluent + H₂O₂) to the UV reactor, which now is turned on, and with V10 closed and V9 open, it is possible to collect UV/H₂O₂ in V11.

On the other hand, to analyze the reverse osmosis process, V3 is opened, and P2 is turned on, instead of V4, V5, and P1. It is possible to collect the fraction removed by reverse osmosis (RO) in V8; however, to analyze RO + GAC or RO + UV/H₂O₂, it is necessary to configure the pilot plant after ET2, such as when evaluating each process (*i.e.*, GAC or UV/H₂O₂) alone. Finally, to analyze the combination RO + UV/H₂O₂ + GAC, it is necessary to close V9, open V10, and keep the UV reactor on, collecting the sample in V11.

Supplementary tables:

Table S1: Physicochemical characteristics of the contaminants of emerging concern (CECs)

CECs	Chemical structure ¹	Molar mass (g/mol)	Solubility in water (25 C) (g L ⁻¹)	Log K _{ow}	pKa
Albendazole		265.3 ¹	0.04 ^{1,2}	3.14 ¹ 1.27 ²	6.9 ²
Acetaminophen		151.2 ¹	30.3 ¹ 14.0 ²	0.46 ^{1,2}	4.4 / 9.4 ²
Acesulfame		201.2 ¹	270.0 ²	-1.3 ²	2.0 ²
Caffeine		194.2 ¹	21.6 ²	-0.07 ^{1,2}	0.7 / 10.4 ²
Carbamazepine		236.3 ¹	0.02 ¹ 0.04 ²	2.45 ^{1,2}	13.9 ²
Diclofenac		268.1 ¹	0.005 ¹ 0.002 ²	4.51 ^{1,2}	3.9 ²
Hydrochlorothiazide		297.7 ¹	1.3 ¹ 0.7 ²	-0.07 ^{1,2}	7.9 / 9.2 ²
Propranolol		259.3 ¹	0.22 ¹ 0.06 ²	3.48 ^{1,2}	9.4 ²
Ricobendazole		281.3 ¹	1.3 ¹	1.27 ^{1,2}	2.0 / 7.1 ³
Saccharin		183.2 ¹	0.8 ¹	0.91 ^{1,2}	1.3 ²
Sulfamethoxazole		253.3 ¹	4.0 ¹	0.89 ^{1,2}	1.6 / 5.7 ²
Sucralose		397.6 ¹	22.7 ^{1,2}	-1.00 ^{1,2}	11.9 ³

¹ChemSpider (<http://www.chemspider.com/Default.aspx>);²PubChem(<https://pubchem.ncbi.nlm.nih.gov>);³HMDB(<https://hmdb.ca/>).

Table S2: Details of the Chromatographic method.

Quaternary solvent manager (QSM)				
Time (min)	Water (% v/v)	Methanol (% v/v)	Acetonitrile (% v/v)	Flow rate (mL min ⁻¹)
0	100	0	0	1.00
0.25	100	0	0	
2.0	100	0	0	
2.01	10	45	45	
2.8	100	0	0	
3.5	100	0	0	
Binary solvent manager (BSM)				
Time (min)	Water ^a (% v/v)	Methanol (% v/v)	Flow rate (mL min ⁻¹)	
0	50	50	0.35	
0.25	50	50		
2.0	5	95		
2.5	5	95		
3	50	50		
3.5	50	50		
a: added of 5 mmol of ammonium acetate				
Other parameters				
Injection volume (μL)			250	
Loading period (min)			0 - 0.25	
Elution time (min)			0.25 - 2	
ESI source		Positive and Negative		
Desolvation temperature (°C)			350	
Desolvation gas flow rate (L h ⁻¹)			600	
Cone gas flow rate (L h ⁻¹)			75	
Capillary voltage (kV)			1.3 ^b and 2.0 ^c	
b: positive mode; c: negative mode				

Analysis parameters

The limit of quantification (Table S3) was determined by analyzing water samples spiked with decreasing concentrations of the contaminants of emerging concern (CECs), until a signal-to-noise ratio of 10 was obtained. The recovery was determined with the fortification of effluent of the wastewater treatment plant with 5 μg L⁻¹ of each CEC.

Table S3: Analysis parameters of contaminants of emerging concern (CECs).

CECs	Limit of quantification ($\mu\text{g L}^{-1}$)	Linear range on monitoring ($\mu\text{g L}^{-1}$)	Linear range on adsorption ($\mu\text{g L}^{-1}$)	Recovery (%) N = 6
Acesulfame	1.0	1 – 100	NA	75.4 – 81.9
Acetaminophen	0.5	0.5 - 10	NA	75.2 – 80.0
Albendazole	0.1	0.1 – 10	NA	111.8 – 117.9
Caffeine	0.1	0.1 – 10	5 – 600	99.6 – 100.5
Carbamazepine	0.01	0.01 – 10	NA	102.1 – 108.2
Diclofenac	0.5	0.5 - 10	NA	85.9 – 91.9
Hydrochlorothiazide	1.0	1 – 30	5 - 600	105.8 – 122.9
Propranolol	0.5	0.5 - 10	NA	93.2 – 118.4
Ricobendazole	0.5	0.5 – 10	NA	91.6 – 104.3
Saccharin	1.0	1 – 100	5 – 600	95.6 – 102.2
Sucralose	1.0	1 – 100	5 – 600	98.7 – 101.3
Sulfamethoxazole	0.1	0.1 - 10	5 - 600	86.3 – 101.0
NA: Non-analyzed.				

Table S4: Error analysis

Coefficient of determination (R^2)	$R^2 = 1 - \frac{\sum (q_{exp} - q_{cal})^2}{\sum (q_{exp} - q_{mean})^2}$
Sum of squared error (SSE)	$SSE = \sqrt{\frac{\sum (q_{exp} - q_{cal})^2}{N}}$

q_{exp} , q_{cal} and q_{mean} are the the experimental adsorption capacity, calculated adsorption capacity and mean of experimental value, respectively, and N is the number of measurements.

Table S5: *Water quality parameters.*

Parameter	Influent of the pilot plant (effluent of the wastewater treatment plant)	Effluent of the pilot plant (OR + UV/H ₂ O ₂ + GAC)
Color (mg Pt-Co L ⁻¹)	46	<15
pH	7.59	6.66
Turbidity (NTU)	0.2	0.1
Conductivity (μS cm ⁻¹)	622.0	14.8
Biological oxygen demand (mg L ⁻¹)	<1	<1
Chemical oxygen demand (mg L ⁻¹)	32	15
Total phosphorus (mg-P L ⁻¹)	3.90	<0.05
Ammoniacal Nitrogen (mg L ⁻¹)	< 0.01	< 0.01
Total Kjeldahl Nitrogen (mg L ⁻¹)	2.16	0.90
Nitrate Nitrogen (mg L ⁻¹)	4.29	0.27
Nitrite Nitrogen	<0.015	<0.015

RO: Reverse osmosis; UV/H₂O₂: Photoperoxidation; GAC: Activated carbon fixed-bed column.

Table S6: Adsorption models

Model	Equation	Units
Experimental	$q_{exp} = \frac{(C_i - C_t)}{m} V$	q_{exp} (mg g ⁻¹); C_i and C_t (mg L ⁻¹); m (g); and V (L)
Pseudo-first order (PFO)	$q_{exp} = q_{cal}(1 - e^{-k_1 t})$	q_{exp} and q_{cal} (mg g ⁻¹); k_1 (min ⁻¹); and t (min)
Pseudo-second order (PSO)	$q_{exp} = \frac{q_{cal}^2 k_2 t}{1 + q_{cal} k_2 t}$	q_{exp} and q_{cal} (mg g ⁻¹); k_2 (mg g ⁻¹ min ⁻¹); and t (min)
Elovich	$q_{exp} = \frac{1}{\beta} \ln(1 + \alpha \beta t)$	q_{exp} (mg g ⁻¹); α (mg g ⁻¹ min ⁻¹); β (mg g ⁻¹ min ⁻¹); and t (min)
Intraparticle diffusion	$q_{exp} = k_i \sqrt{t} + C$	q_{exp} (mg g ⁻¹); k_i (mg g ⁻¹ min ^{-0.5}); C (dimensionless); and t (min)
Film Diffusion	$\ln\left(1 - \frac{q_t}{q_e}\right) = -k_{fd} t$	q_t and q_e (mg g ⁻¹); k_{fd} (min ⁻¹); and t (min)
Langmuir	$q_{exp} = \frac{q_{cal} k_L C_t}{1 + k_L C_t}$ $R_L = \frac{1}{1 + k_L q_{cal} C_i}$	q_{exp} and q_{cal} (mg g ⁻¹); k_L (L mg ⁻¹); C_t (mg L ⁻¹); and R_L (dimensionless)
Freundlich	$q_{exp} = k_F C_t^{\frac{1}{n}}$	q_{exp} (mg g ⁻¹); k_F (mg/g)/(mg/L) ⁿ ; C_t (mg L ⁻¹); and n (dimensionless)
Sips	$q_{exp} = \frac{q_{cal} (k_s c_t)^n}{(k_s c_t)^n + 1}$	q_{exp} and q_{cal} (mg g ⁻¹); k_s (L mg ⁻¹); C_t (mg L ⁻¹); and n (dimensionless)
Redlich-Peterson	$q_{exp} = \frac{k_{RP} C_t}{1 + \alpha_{RP} C_t^g}$	q_{exp} (mg g ⁻¹); k_{RP} (L g ⁻¹); C_t (mg L ⁻¹); and α_{RP} (mg L ⁻¹) ^g ; and g (dimensionless)
Dubinin-Radushkevich	$\ln(q_{exp}) = -k_{DR} \varepsilon^2 + \ln(q_{cal})$ $\varepsilon = RT \ln\left(1 + \frac{1}{C_e}\right)$ $E = \frac{1}{\sqrt{2 k_{DR}}}$	q_{exp} and q_{cal} (mg g ⁻¹); k_{DR} (mol ² kJ ⁻²); ε (kJ mol ⁻¹); C_e (mg L ⁻¹); E (kJ mol ⁻¹); R (J mol ⁻¹ K ⁻¹); and T (K)

Table S7: Microcrystalline structural parameters of the activated carbon.

Structural parameters	2 Θ_{002}	2 Θ_{100}
Interlayer spacing (nm)	0.367	0.205
Half maximum width of peak (rad)	0.126	0.090
Crystallite size (nm)	1.137	3.398
Number of layers	4	100
Effective crystallite dimension (nm)		2.177
Structural strain		0.190

Table S8: Comparative data regarding sorption parameters for contaminants of emerging concern onto activated carbon.

Contaminant of Emerging Concern	Adsorbent/Initial concentration	Water matrix	Main results	Reference
Caffeine	Coconut-Shell based Activated carbon / 0.5 mg L ⁻¹	Water	$q_{cal} = 91 \text{ mg g}^{-1}$ $E = 13.9 \text{ kJ mol}^{-1}$	Diniz et al. (2022)
Caffeine	<i>Pinnus sp.</i> Based Activated carbon / 0.5 mg L ⁻¹	Water	$q_{cal} = 63 \text{ mg g}^{-1}$ $E = 14.5 \text{ kJ mol}^{-1}$	Diniz et al. (2022)
Caffeine	Pineapple plant leaves based Activated carbon / 500 mg L ⁻¹	Water	$q_{cal} = 155.5 \text{ mg g}^{-1}$ $E = 18.5 \text{ kJ mol}^{-1}$	Beltrame et al. (2018)
Caffeine	Sargassum (sp) based Activated carbon / 20 mg L ⁻¹	Water	$q_{cal} = 221.6 \text{ mg g}^{-1}$	Francoeur et al. (2021)
Caffeine	Babassu based Activated carbon / 100 mg L ⁻¹	Water	$q_{cal} = 212.4 \text{ mg g}^{-1}$	Couto Jr et al. (2014)
Caffeine	Peanut shell based Activated carbon / 10 mg L ⁻¹	Water	$q_{cal} = 122.3 - 134.0 \text{ mg g}^{-1}$	Medina et al. (2021)
Hydrochlorothiazide	Powder activated carbon / 0.2 mg L ⁻¹	Simulated water (organic matter = 1400 mg L ⁻¹)	$q_{cal} = 0.383 - 0.484 \text{ mg g}^{-1}$	Duygan et al. (2021)
Saccharin	Activated carbon / 500 mg L ⁻¹	Water	$q_{cal} = 6.2 \text{ mg g}^{-1}$	Song et al. (2018)
Sulfamethoxazole	Coal based Activated carbon / 10 – 20 mg L ⁻¹	Water	$q_{cal} = 185.2 \text{ mg g}^{-1}$ $E = 0.7 \text{ kJ mol}^{-1}$	Çaliskan and Gokturk (2010)
Sulfamethoxazole	Core-shell activated carbon / 5 - 100 mg L ⁻¹	Water	$q_{cal} = 6.4 \text{ mg g}^{-1}$	Ndagijimana et al. (2019)
Sulfamethoxazole	Powder activated carbon / 5 - 100 mg L ⁻¹	Water	$q_{cal} = 86.0 \text{ mg g}^{-1}$	Ndagijimana et al. (2019)
Sulfamethoxazole	Mineral based activated carbon / 1 mg L ⁻¹	Water	$q_{cal} = 58.3 \text{ mg g}^{-1}$	Tonucci et al. (2015)
Sulfamethoxazole	<i>Pinnus sp.</i> Based activated carbon / 1 mg L ⁻¹	Water	$q_{cal} = 130.7 \text{ mg g}^{-1}$	Tonucci et al. (2015)

q_{cal} is the adsorption capacity and E is the mean adsorption energy

Table S9: Summary of Langmuir, Freundlich, and Redlich-Peterson isotherms parameters of selected marker contaminants of emerging concern adsorption onto activated carbon on the water.

Model	Parameter	Caffeine	Hydrochlorothiazide	Saccharin	Sulfamethoxazole	Sucralose
Langmuir	k_L (L mg ⁻¹)	0.0213	0.0181	0.0073	0.0178	0.0054
	q_{cal} (mg g ⁻¹)	3.03	1.98	3.60	4.95	1.22
	R_L	0.09	0.12	0.30	0.13	0.36
	R^2	0.961	0.909	0.893	0.930	0.848
	SSE	0.23282	0.11829	0.60835	1.42195	0.01356
Freundlich	k_F (mg/g)/(mg/L) ⁿ	0.45	0.36	0.17	0.44	0.10
	n	3.20	3.72	2.11	2.43	2.85
	R^2	0.982	0.910	0.853	0.872	0.838
	SSE	0.10811	0.11618	0.83796	2.60777	0.01451
Redlich-Peterson	k_{RP} (L g ⁻¹)	0.23072	0.06904	0.01797	0.05948	0.00374
	α_{RP} (mg L ⁻¹)L ^g	0.34496	0.0898	2.58E-05	7.02E-04	2.72E-05
	g	0.75113	0.84884	1.89196	1.51484	1.71447
	R^2	0.984	0.916	0.923	0.954	0.857
	SSE	0.09799	0.10923	0.43883	0.93764	0.01281

Table S10: Summary of Langmuir, Freundlich, and Redlich-Peterson isotherms parameters of selected marker contaminants of emerging concern adsorption onto activated carbon on the wastewater treatment plant effluent.

Model	Parameter	Caffeine	Hydrochlorothiazide	Saccharin	Sulfamethoxazole	Sucralose
Langmuir	K_L (L mg ⁻¹)	0.0020	0.0010	0.0042	0.0113	0.0040
	q_{cal} (mg g ⁻¹)	4.63	4.99	2.15	3.75	1.04
	R_L	0.94	1.99	0.50	0.18	0.48
	R^2	0.811	0.852	0.823	0.975	0.758
	SSE	0.7611	0.22978	0.19896	0.24674	0.02336
Freundlich	K_F (mg/g)/(mg/L) ⁿ	0.04	0.01	0.07	0.25	0.05
	n	1.47	1.26	1.97	2.32	2.36
	R^2	0.780	0.842	0.781	0.910	0.731
	SSE	0.88524	0.24466	0.2458	0.88541	0.02599
Redlich-Peterson	K_{RP} (L g ⁻¹)	0.00709	0.00409	0.00574	0.03165	0.00228
	α_{RP} (mg L ⁻¹) ^g	4.9148E-15	1.35856E-15	1.34E-08	8.34E-04	5.03E-08
	g	5.35078	5.40639	2.99224	1.3913	2.65331
	R^2	0.892	0.873	0.889	0.990	0.802
	SSE	0.43625	0.19591	0.1244	0.09745	0.01911

Table S11: Concentration of the contaminants of emerging concern (CECs) on the influent of the pilot plant.

CECs	Concentration (ng L ⁻¹) ± standard deviation
Caffeine	1,626.0 ± 564.1
Hydrochlorothiazide	9,265.4 ± 3,471.1
Saccharin	2,978.2 ± 280.6
Sulfamethoxazole	577.4 ± 52.2
Sucralose	36,305.2 ± 15,931.8

Supplementary Figures:

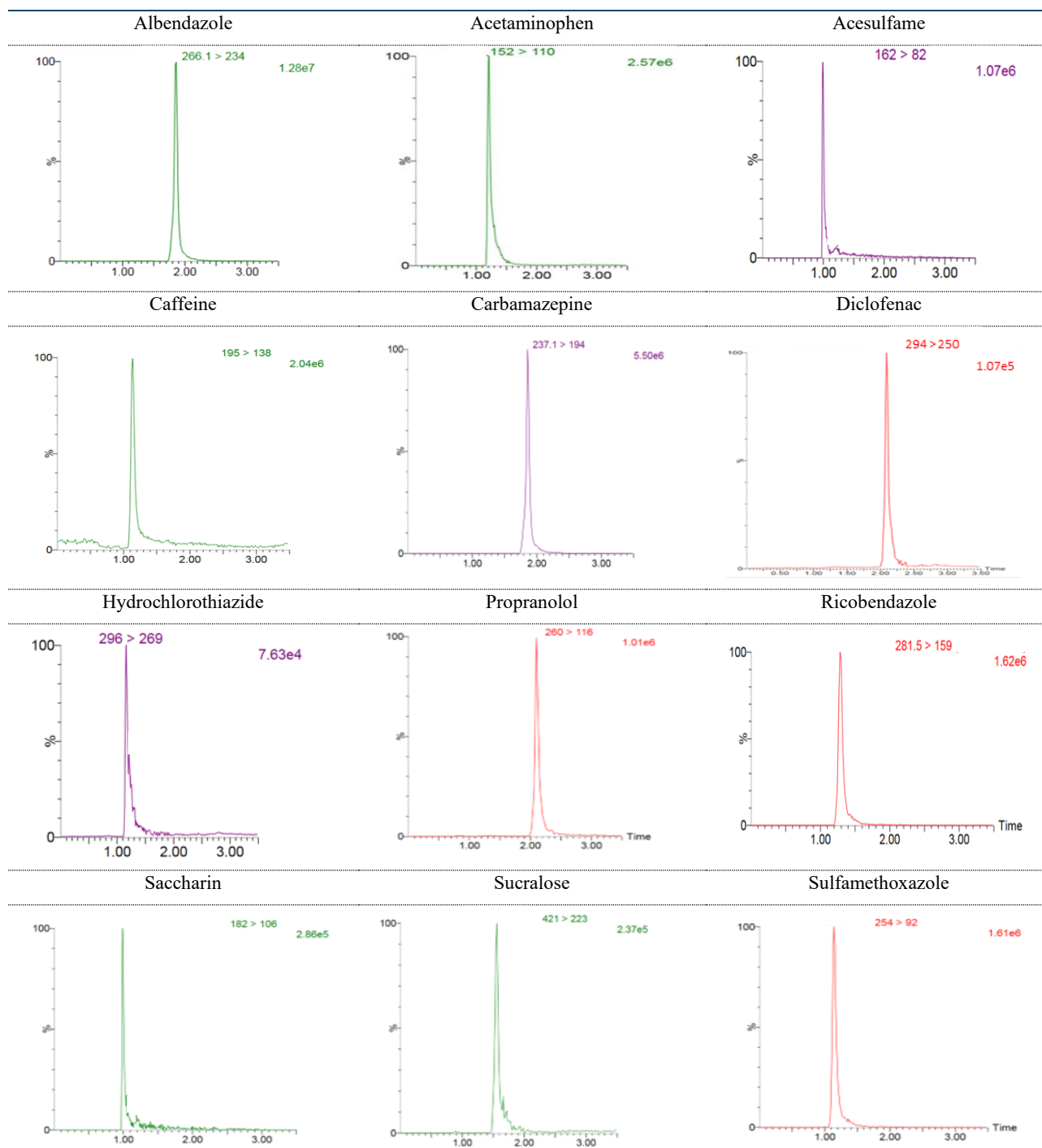


Figure S1: Chromatogram obtained from SPE-UHPLC-MS/MS. UPLC® CSH C18 column (130 Å, 1.7 µm, 2.1 × 100 mm). Chromatographic conditions: mobile phase composed of methanol:water (50:30, v/v) with 5 mmol L⁻¹ of ammonium acetate. Flow rate: 0.35 mL min⁻¹. Column temperature: 40 °C. Injection volume: 250 µL. Online SPE conditions: XBridge C8 column. Loading solvent: methanol:water (0:100, v/v), flow rate 1.0 mL min⁻¹, loading volume 0.25 mL. Concentration of drugs of interest: 5 µg L⁻¹.

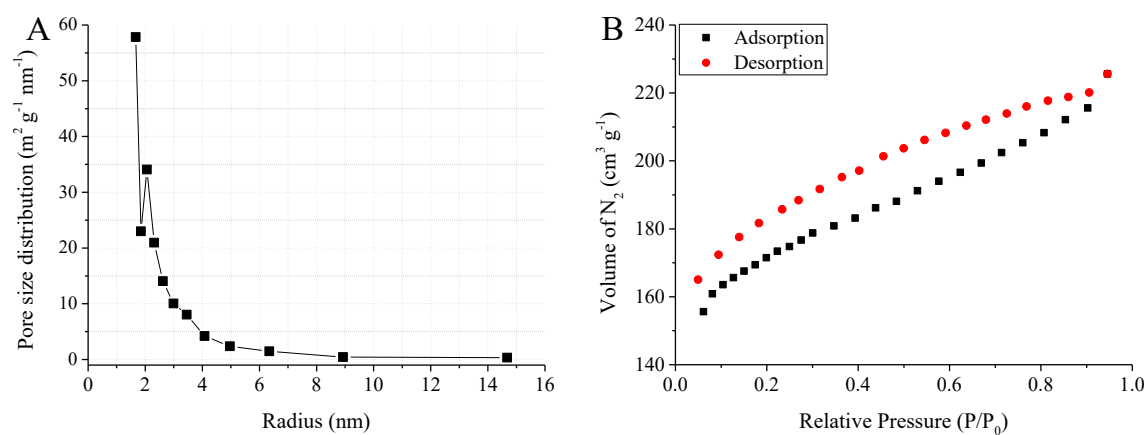


Figure S2: Pore size distribution (A) and N_2 -isotherm (B) of the activated carbon.

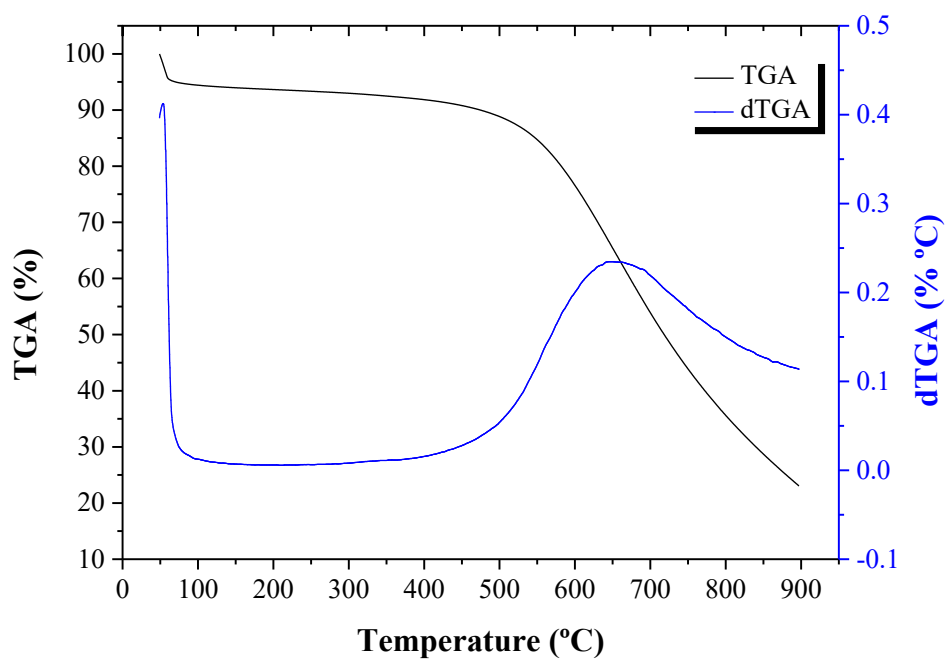


Figure S3: Thermogravimetric analysis of the activated carbon.

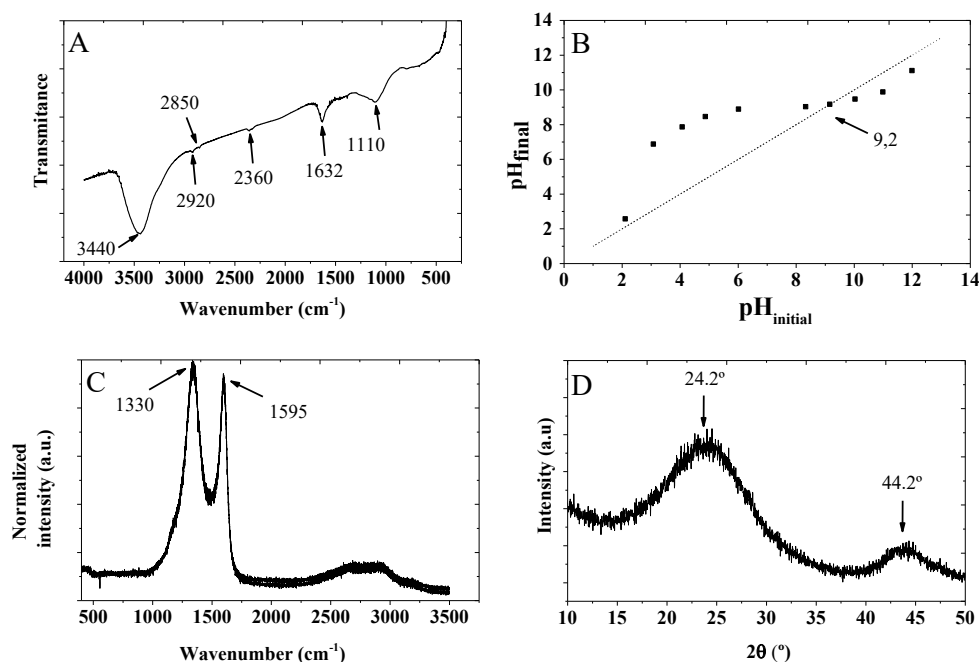


Figure S4: Fourier Transformed Infrared spectroscopy spectrum (A), pH_{PZC} (B) Raman spectrum (C), and X-ray diffraction spectrum (D) of the activated carbon.

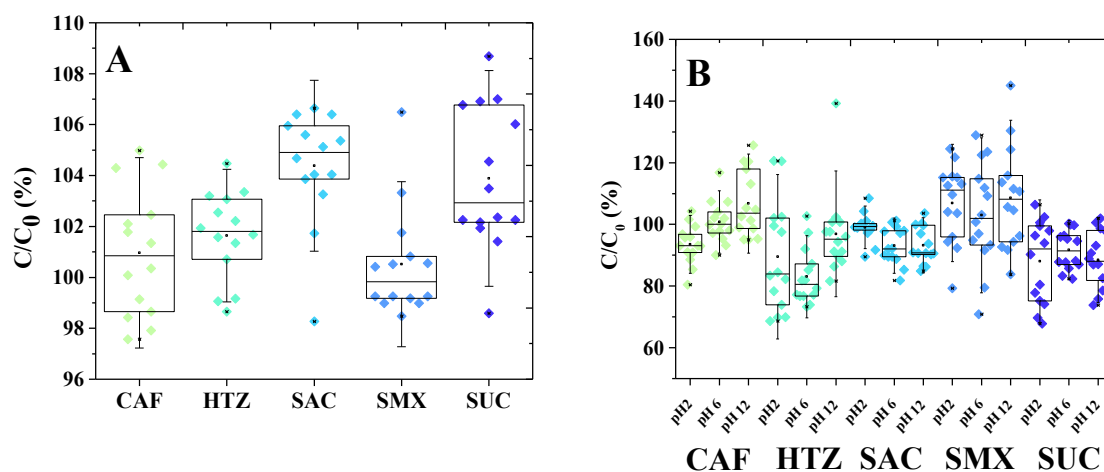


Figure S5: Box-chart of stability of the caffeine (CAF), hydrochlorothiazide (HTZ), saccharin (SAC), sulfamethoxazole (SMX), and sucralose (SUC) under time (A) and different pH (B). Each data is showed by a specific point, the boxplot indicates 25-75% deviation, and the whiskers the 1.5 calculated standard deviation.

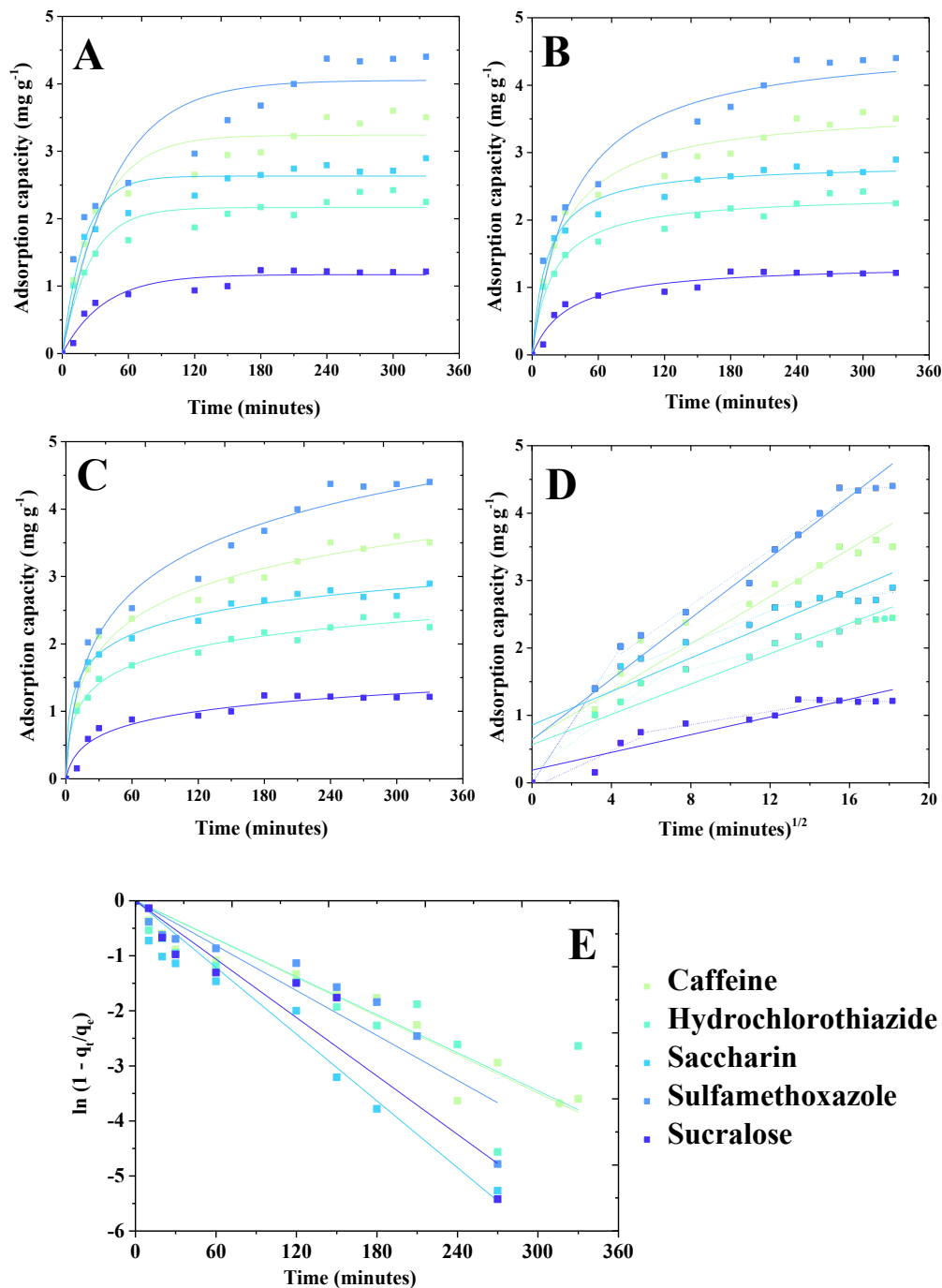


Figure S6: Adsorption kinetics of selected marker contaminants of emerging concern onto activated carbon by fitting the pseudo-first order (A), pseudo-second order (B), Elovich (C), intraparticle diffusion (D) and film diffusion (E) models.

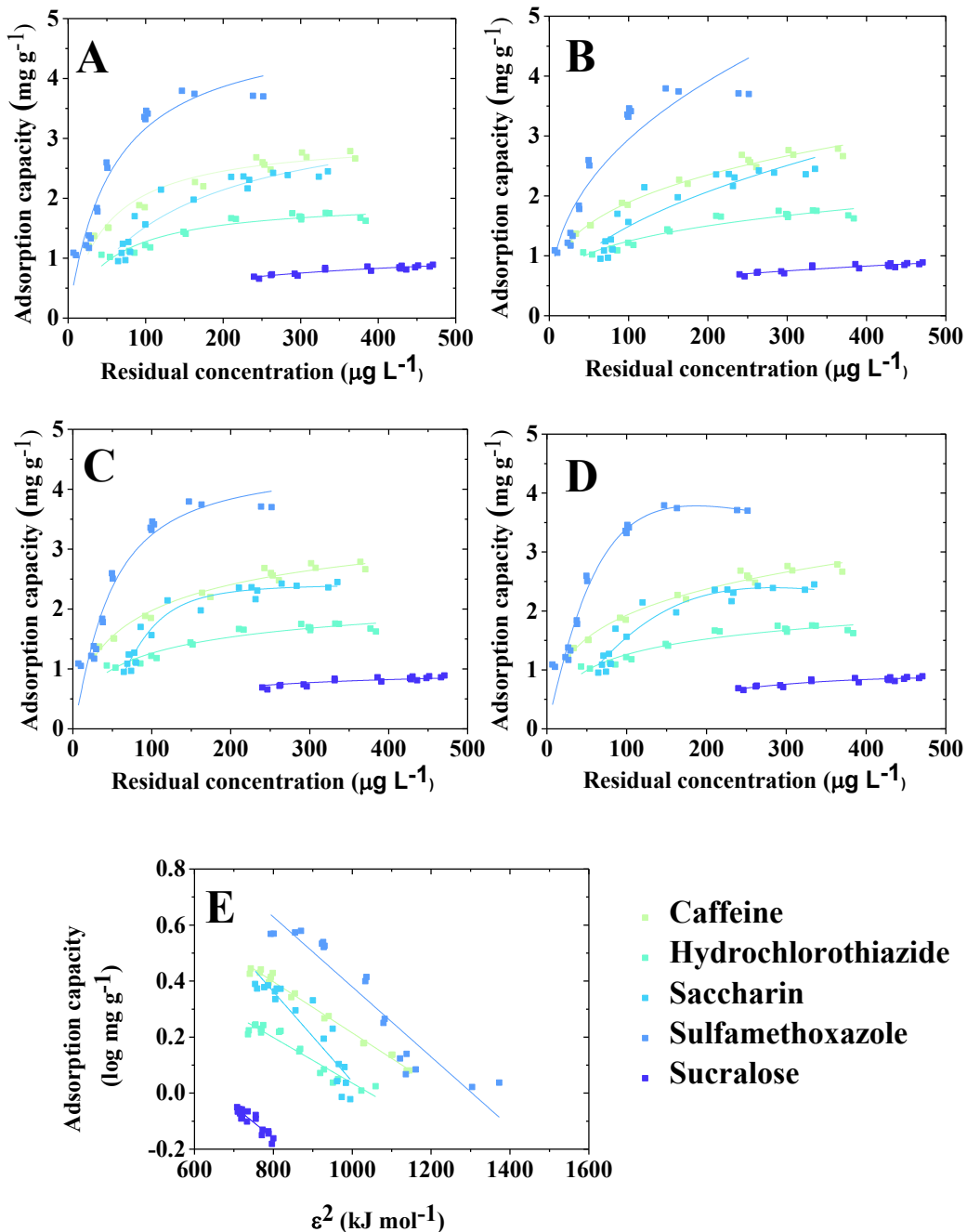


Figure S7: Adsorption isotherms of selected marker contaminants of emerging concern onto activated carbon by fitting the Langmuir (A), Freundlich (B), Redlich-Peterson (C), Sips (D), and Dubinin-Radsukevich (E) models.

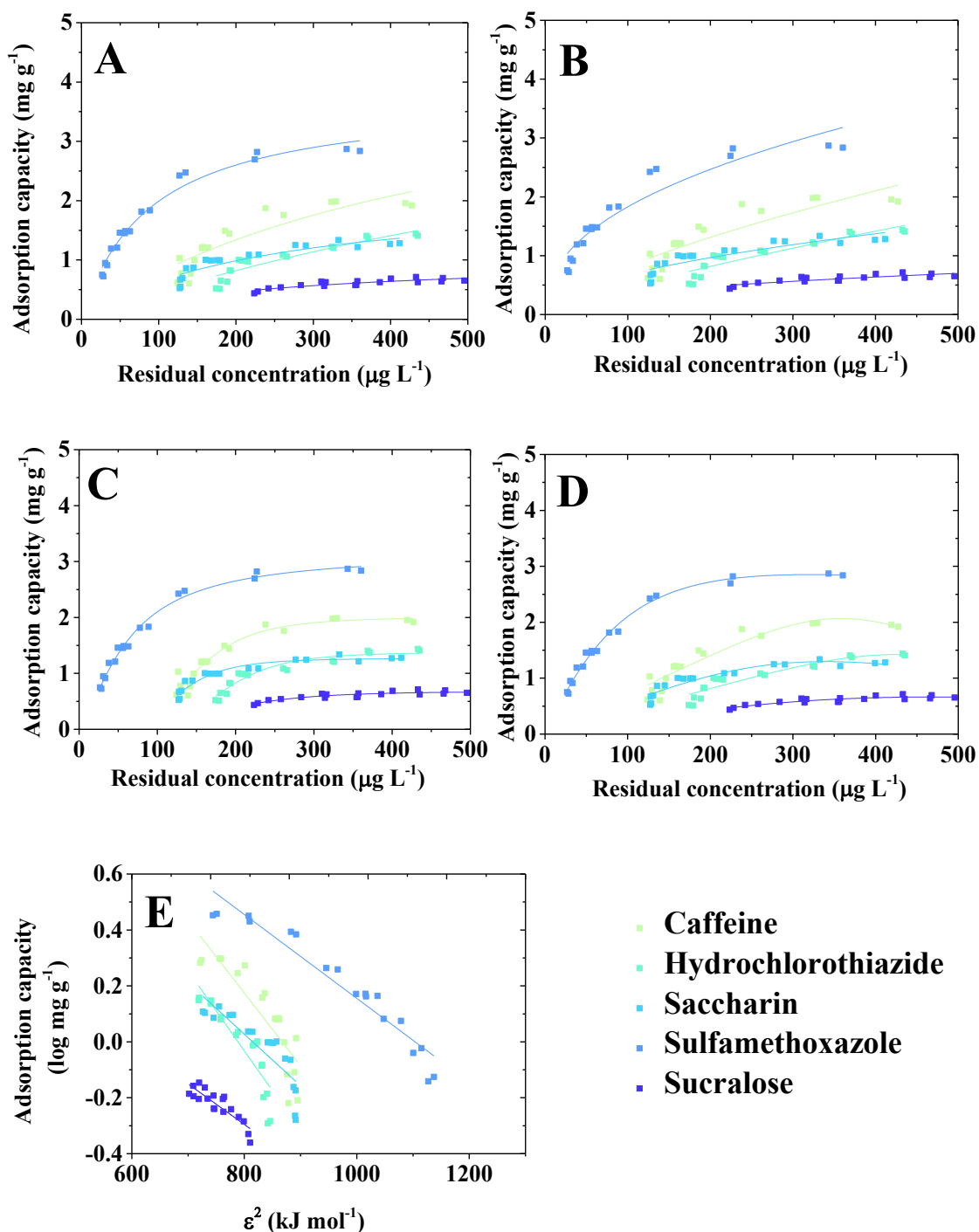


Figure S8: Adsorption isotherms on the wastewater treatment plant effluent of selected marker contaminants of emerging concern onto activated carbon by fitting the Langmuir (A), Freundlich (B), Redlich-Peterson (C), Sips (D), and Dubinin-Radsukovich (E) models.

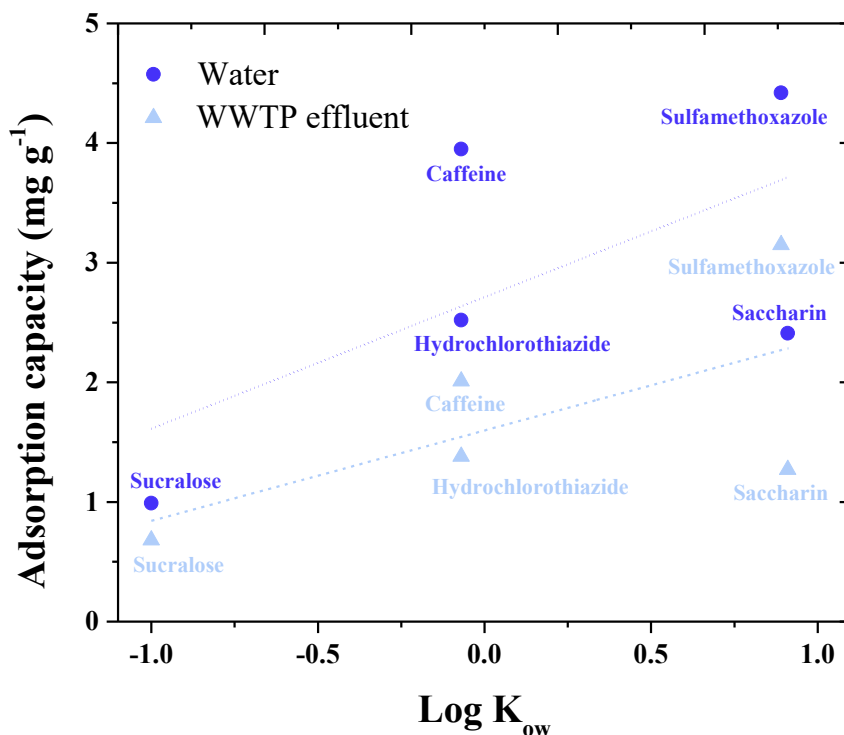


Figure S9: Adsorption capacity (estimated by Sips model) onto activated carbon versus Log K_{ow} of the contaminants of emerging concern. WWTP, wastewater treatment plant.

References

- Beltrame, K. K., Cazetta, A. L., Souza, P. S. C., Spessato, L., Silva, T. L., Almeida, V. C. (2018). Adsorption of caffeine on mesoporous activated carbon fibers prepared from pineapple plant leaves. *Ecotoxicology and Environmental Safety*, 147. <https://doi.org/10.1016/j.ecoenv.2017.08.034>
- Couto Jr, O. M., Matos, I., Fonseca, I. M., Arroyo, P. A., Silva, E. A., Barros, M. A. S. D. (2014). Effect of solution pH and influence of water hardness on caffeine adsorption onto activated carbons. *The Canadian Journal of Chemical Engineering*, 93. <https://doi.org/10.1002/cjce.22104>
- Çaliskan, E., Gokturk, S. (2010). Adsorption Characteristics of Sulfamethoxazole and Metronidazole on Activated Carbon. *Separation Science and Technology*, 45. <https://doi.org/10.1080/01496390903409419>
- Diniz, V., Rath, G., Rath, S., Araujo, L. S., & Cunha, D. G. F. (2022). Competitive kinetics of adsorption onto activated carbon for emerging contaminants with contrasting physicochemical properties. *Environmental Science and Pollution Research*, 29(28), 42185-42200. <https://doi.org/10.1007/s11356-021-16043-2>
- Duygan, B. D. O., Udert, K. M., Remmele, A., Mc Ardell, C. S. (2021). Removal of pharmaceuticals from human urine during storage, aerobic biological treatment, and activated carbon adsorption to produce a safe fertilizer. *Resources, Conservation and Recycling*, 166. <https://doi.org/10.1016/j.resconrec.2020.105341>
- Francoeur, M., Ferino-Pérez, A., Yacou, C., Jean-Marius, C., Emmanuel, E., Chérémoud, Y., Jauregui-Haza, U., Gaspard, S. (2021). Activated carbon synthesized from Sargassum (sp) for

adsorption of caffeine: Understanding the adsorption mechanism using molecular modeling. *Journal of Environmental Chemical Engineering*, 9. <https://doi.org/10.1016/j.jece.2020.104795>

Larous, S., & Meniai, A. H. (2016). Adsorption of Diclofenac from aqueous solution using activated carbon prepared from olive stones. *International Journal of Hydrogen Energy*, 41(24), 10380-10390. <https://doi.org/10.1016/j.ijhydene.2016.01.096>

Medina, F., M., O., Aguiar, M. B., Parolo, M. E., Avena, M. J. (2021). Insights of competitive adsorption on activated carbon of binary caffeine and diclofenac solutions. *Journal of Environmental Management*, 278. <https://doi.org/10.1016/j.jenvman.2020.111523>

Ndagijimana, P., Liu, X., Yu, G., Wang, Y. (2019). Synthesis of a novel core-shell-structure activated carbon material and its application in sulfamethoxazole adsorption. *Journal of Hazardous Materials*, 368. <https://doi.org/10.1016/j.jhazmat.2019.01.093>

Oickle, A. M., Goertzen, S. L., Hopper, K. R., Abdalla, Y. O., & Andreas, H. A. (2010). Standardization of the Boehm titration: Part II. Method of agitation, effect of filtering and dilute titrant. *Carbon*, 48(12), 3313-3322. <https://doi.org/10.1016/j.carbon.2010.05.004>

Song, J. Y., Bhadra, B. N., Khan, N. A., Jhung, H. S. (2018). Adsorptive removal of artificial sweeteners from water using porous carbons derived from metal azolate framework-6. *Microporous and Mesoporous Materials*, 260. <https://doi.org/10.1016/j.micromeso.2017.10.021>

Tonucci, M. C., Gurgel, L. V. A., Aquino, S. F. (2015). Activated carbons from agricultural byproducts (pine tree and coconut shell), coal, and carbon nanotubes as adsorbents for removal of sulfamethoxazole from spiked aqueous solutions: Kinetic and thermodynamic studies. *Industrial Crops and Products*, 74. <https://doi.org/10.1016/j.indcrop.2015.05.003>

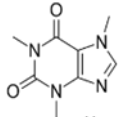
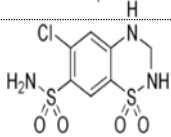
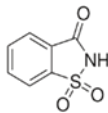
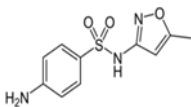
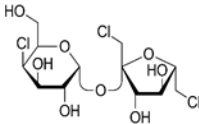
Supplementary information: Adsorption of aqueous phase contaminants of emerging concern by activated carbon: comparative fixed-bed column study and in situ regeneration methods

Vinicius Diniz^{1,*}, Susanne Rath¹

¹ Department of Analytical Chemistry, Institute of Chemistry, University of Campinas.
Address: Rua Josué de Castro s/n. Zip Code 13083-970. Cidade Universitária, Campinas, SP, Brasil.

*Author for correspondence: *viniciusdiniz994@gmail.com*

Table S1: Physicochemical characteristics of the contaminants of emerging concern (CECs)

CECs	Chemical structure ¹	Molar mass (g/mol)	Solubility in water (25 C) (g L ⁻¹)	Log K _{ow}	pKa
Caffeine		194.21	21.62	-0.07 ^{1,2}	0.7 / 10.4 ²
Hydrochlorothiazide		297.71	1.31 / 0.72	-0.07 ^{1,2}	7.9 / 9.2 ²
Saccharin		183.21	0.81	0.91 ^{1,2}	1.32
Sulfamethoxazole		253.31	4.01	0.89 ^{1,2}	1.6 / 5.7 ²
Sucralose		397.61	22.7 ^{1,2}	-1.00 ^{1,2}	11,9 ³

¹ChemSpider (<http://www.chemspider.com/Default.aspx>); ²PubChem(<https://pubchem.ncbi.nlm.nih.gov/>); ³HMDB(<https://hmdb.ca/>).

Table S2: Details of the Chromatographic method

Time (min)	Water ^a	Methanol	Flow rate
	(% v/v)	(% v/v)	(mL min ⁻¹)
0	40	60	0.3
2	40	60	
a: 0.1% of formic acid			
Injection volume (μL)			5
ESI source			Positive and negative
Desolvation temperature (°C)			350
Desolvation gas flow rate (L h ⁻¹)			600
Cone gas flow rate (L h ⁻¹)			75
Capillary voltage (kV)			1.3 for positive and 2 for negative

Supplementary Material: Adsorption of aqueous phase contaminants of emerging concern by activated carbon: comparative fixed-bed column study and in situ regeneration methods

The limit of quantification (Table S3) was determined by analyzing water samples spiked with decreasing concentrations of the CECs, until a signal-to-noise ratio of 10 was obtained. The recovery was determined with the fortification of effluent of the wastewater treatment plant with 1 mg L⁻¹ of each CEC.

Table S3: Analysis parameters

CECs	Limit of quantification (mg L ⁻¹)	Linear range on adsorption (mg L ⁻¹)	Recovery (%)
			N = 5
Caffeine	0.01	0.1 – 3	95.6 – 103.5
Hydrochlorothiazide	0.1	0.1 – 3	97.8 – 112.3
Saccharin	0.1	0.1 – 3	90.6 – 107.2
Sucralose	0.1	0.1 – 3	97.7 – 110.3
Sulfamethoxazole	0.01	0.1 – 3	96.3 – 101.3

Table S4: Water quality parameters.

Parameter	WWTP effluent	Reuse water
Color (mg Pt-Co L ⁻¹)	46	<15
pH	7.59	6.66
Turbidity (NTU)	0.2	0.1
Conductivity (μS cm ⁻¹)	622	14.8
Biological oxygen demand (mg L ⁻¹)	<1	<1
Chemical oxygen demand (mg L ⁻¹)	32	15
Total phosphorus (mg-P L ⁻¹)	3.9	<0.05
Ammoniacal Nitrogen (mg L ⁻¹)	< 0.01	< 0.01
Total Kjeldahl Nitrogen (mg L ⁻¹)	2.16	0.9
Nitrate Nitrogen (mg L ⁻¹)	4.29	0.27
Nitrite Nitrogen	<0.015	<0.015

Table S5: Parameters of the Thomas, Bohart-Adams, and Yoon-Nelson models.

Kinetic model	a	b
	$\frac{k_T q_{ads,T} m_{ads}}{Q}$	$k_T C_0$
Thomas model	Where: k_T is Thomas model constant (L/mg min), $q_{ads,T}$ is the Thomas maximum adsorption capacity (mg/g), m_{ads} is the mass of AC (g), and Q is the flow rate (L/min)	Where: k_T is Thomas model constant (L/mg min) and C_0 is inlet concentration (mg/L)
	$\frac{k_{BA} N_0 H}{v}$	$k_{BA} C_0$
Bohart-Adams	Where: k_{BA} is Bohart-Adams model constant (L/mg min), N_0 is the volumetric capacity of maximal adsorption (mg/L-AC), H is height of the AC in the column (cm), and v is the migration speed (cm/min)	Where: k_{BA} is Bohart-Adams model constant (L/mg min) and C_0 is inlet concentration (mg/L)
	τk_{YN}	k_{YN}
Yoon-Nelson	Where: k_{YN} is Yoon-Nelson model constant (1/min) and τ is the time required to maintain 50% of the initial AC in its original form (min)	Where: k_{YN} is Yoon-Nelson model constant (1/min)

Table S6: Error analysis

Determination coefficient (R^2)	$R^2 = 1 - \frac{\sum (q_{exp} - q_{cal})^2}{\sum (q_{exp} - q_{mean})^2}$
Sum of squared error (SSE)	$SSE = \sqrt{\frac{\sum (q_{exp} - q_{cal})^2}{N}}$

q_{exp} , q_{cal} and q_{mean} are the experimental adsorption capacity, calculated adsorption capacity and mean of experimental value, respectively, and N is the number of measurements.

Table S7: AC2 characterization parameters

Specific surface area ($m^2 g^{-1}$)	716
Total pore volume ($cm^3 g^{-1}$)	0.504
Total micropore volume ($cm^3 g^{-1}$)	0.365
Average pore size (nm)	2.8
pH _{PCZ}	9.3

Table S8: Summary of the isotherm parameters for the adsorption of the studied contaminants of emerging concern onto activated carbon.

Model	Parameter	CAF	HTZ	SAC	SMX	SUC
Sips	K_s (L mg ⁻¹)	0.01054	0.03487	0.0064	0.01916	0.00794
	Adsorption capacity (mg g ⁻¹)	5.32687	3.89091	4.32544	6.17809	2.53146
	n	0.44591	0.85211	1.08789	0.72783	1.42232
	R^2	0.984	0.982	0.924	0.960	0.977
	SSE	0.17989	0.23007	0.694	1.19417	0.06778
Dubinin-Radsukevich	KDR	0.000021	0.000041	0.000128	0.000057	0.000079
	Mean adsorption Energy (kJ mol ⁻¹)	27.31366	24.35721	17.57085	23.03413	18.10741
	R^2	0.98523	0.96349	0.90929	0.94512	0.95921
	SSE	0.006	0.019	0.042	0.041	0.009

Table S9 (Part 1 of 5): Summary of the adsorption parameters for the Bohart-Adams, Thomas, Yoon-Nelson, and BCT modeling for the adsorption of the studied contaminants of emerging concern onto activated carbon.

Flow direction		Downflow																
Flow rate (mL min ⁻¹)		5																
Bed Height (cm)		1.5																
Activated carbon (AC)	Contaminants of Emerging Concern (CECs)	Bohart-Adams model				Thomas model				Yoon-Nelson model				BTC modelling				
		KBA (L/min mg)	N0 (mg/L-AC)	R2	SSE	KT (L/min*mg)	qads,T (mg/g)	R2	SSE	KYN (1/min)	τ (min)	qads,YN (mg/g)	R2	SSE	qads (mg/g)	tB (min)	tS (min)	MTZ (cm)
AC1	Caffeine	0.005	1394.0	0.942	0.114	0.015	1.64	0.998	0.023	0.035	205.4	1.74	0.998	0.012	1.73	203.8	117.6	0.63
	Hydrochlorothiazide	0.005	1097.3	0.915	0.161	0.014	1.12	0.999	0.018	0.034	140.0	1.14	0.999	0.007	1.13	138.1	58.8	0.86
	Saccharin	0.005	1106.6	0.930	0.125	0.014	1.16	0.998	0.021	0.033	145.2	1.18	0.998	0.010	1.18	145.0	58.8	0.89
	Sulfamethoxazole	0.004	1237.0	0.913	0.176	0.014	1.31	0.998	0.020	0.035	164.0	1.25	0.998	0.009	1.25	163.4	88.0	0.69
	Sucralose	0.005	966.1	0.923	0.126	0.013	0.93	0.997	0.025	0.032	116.5	0.91	0.997	0.014	0.92	117.8	29.4	1.13
AC2	Caffeine	0.004	1006.5	0.872	0.270	0.014	0.91	0.992	0.036	0.032	120.8	0.93	0.992	0.036	0.94	122.6	44.0	0.96
	Hydrochlorothiazide	0.006	617.2	0.765	0.435	0.033	0.39	0.996	0.016	0.074	51.8	0.39	0.996	0.016	0.42	55.4	19.6	0.97
	Saccharin	0.006	781.6	0.924	0.112	0.016	0.75	0.995	0.025	0.036	100.2	0.75	0.995	0.025	0.75	99.1	29.3	1.06
	Sulfamethoxazole	0.005	1034.6	0.929	0.123	0.012	1.00	0.997	0.013	0.026	132.9	1.00	0.997	0.013	0.99	131.8	29.3	1.17
	Sucralose	0.005	756.7	0.871	0.192	0.015	0.54	0.991	0.033	0.033	72.3	0.52	0.991	0.033	0.57	78.9	4.9	1.41

Supplementary Material: Adsorption of aqueous phase contaminants of emerging concern by activated carbon: comparative fixed-bed column study and in situ regeneration methods

Table S9 (Part 2 of 5): Summary of the adsorption parameters for the Bohart-Adams, Thomas, Yoon-Nelson, and BCT modeling for the adsorption of the studied contaminants of emerging concern onto activated carbon.

Flow direction		Downflow																
Flow rate (mL min ⁻¹)		5																
Bed Height (cm)		2.5																
Activated carbon (AC)	Contaminants of Emerging Concern (CECs)	Bohart-Adams model				Thomas model				Yoon-Nelson model				BTC modelling				
		KBA (L/min mg)	N0 (mg/L-AC)	R2	SSE	KT (L/min*mg)	qads,T (mg/g)	R2	SSE	KYN (1/min)	τ (min)	qads,YN (mg/g)	R2	SSE	qads (mg/g)	tB (min)	tS (min)	MTZ (cm)
AC1	Caffeine	0.004	1182.7	0.945	0.120	0.014	1.54	0.997	0.013	0.033	319.0	1.63	0.997	0.013	1.61	314.4	235.3	0.63
	Hydrochlorothiazide	0.004	1002.2	0.943	0.125	0.012	1.19	0.998	0.010	0.029	246.9	1.21	0.998	0.010	1.20	243.0	146.9	0.99
	Saccharin	0.005	933.6	0.952	0.086	0.016	1.21	0.997	0.016	0.039	250.7	1.23	0.997	0.016	1.21	245.8	176.3	0.71
	Sulfamethoxazole	0.004	1096.6	0.937	0.132	0.016	1.42	0.998	0.010	0.038	293.8	1.36	0.998	0.010	1.34	290.2	205.4	0.73
	Sucralose	0.005	926.7	0.955	0.086	0.014	1.14	0.998	0.011	0.033	236.0	1.11	0.998	0.011	1.09	231.1	117.4	1.23
AC2	Caffeine	0.005	748.7	0.970	0.035	0.012	0.89	0.998	0.011	0.026	199.5	0.91	0.998	0.011	0.90	196.9	88.0	1.38
	Hydrochlorothiazide	0.005	607.7	0.888	0.230	0.015	0.56	0.999	0.007	0.033	124.7	0.56	0.999	0.007	0.56	124.0	44.0	1.61
	Saccharin	0.005	628.2	0.949	0.084	0.013	0.66	0.996	0.021	0.028	147.7	0.66	0.996	0.021	0.65	144.7	44.0	1.74
	Sulfamethoxazole	0.005	701.5	0.938	0.116	0.013	0.75	0.998	0.008	0.030	168.0	0.75	0.998	0.008	0.75	167.3	58.7	1.62
	Sucralose	0.005	533.5	0.890	0.193	0.014	0.45	0.996	0.017	0.032	101.5	0.43	0.996	0.017	0.42	99.1	19.5	2.01

Supplementary Material: Adsorption of aqueous phase contaminants of emerging concern by activated carbon: comparative fixed-bed column study and in situ regeneration methods

Table S9 (Part 3 of 5): Summary of the adsorption parameters for the Bohart-Adams, Thomas, Yoon-Nelson, and BCT modeling for the adsorption of the studied contaminants of emerging concern onto activated carbon.

Flow direction		Downflow																
Flow rate (mL min ⁻¹)		5																
Bed Height (cm)		3.5																
Activated carbon (AC)	Contaminants of Emerging Concern (CECs)	Bohart-Adams model				Thomas model				Yoon-Nelson model				BTC modelling				
		KBA (L/min mg)	N0 (mg/L-AC)	R2	SSE	KT (L/min*mg)	qads _T (mg/g)	R2	SSE	KYN (1/min)	τ (min)	qads _{YN} (mg/g)	R2	SSE	qads (mg/g)	tB (min)	tS (min)	MTZ (cm)
AC1	Caffeine	0.005	974.0	0.939	0.126	0.018	1.35	0.997	0.009	0.044	394.2	1.44	0.997	0.009	1.41	387.8	294.1	0.85
	Hydrochlorothiazide	0.004	906.0	0.937	0.143	0.015	1.20	0.998	0.008	0.037	348.7	1.22	0.998	0.008	1.20	344.1	264.5	0.81
	Saccharin	0.004	908.5	0.948	0.112	0.014	1.20	0.996	0.014	0.033	350.6	1.23	0.996	0.014	1.21	345.0	264.5	0.82
	Sulfamethoxazole	0.005	977.6	0.962	0.074	0.013	1.34	0.995	0.016	0.031	390.0	1.28	0.995	0.016	1.26	383.5	293.5	0.82
	Sucralose	0.005	856.6	0.976	0.043	0.013	1.15	0.995	0.019	0.031	335.8	1.13	0.995	0.019	1.10	327.0	205.5	1.30
AC2	Caffeine	0.004	677.2	0.958	0.085	0.011	0.81	0.996	0.016	0.025	251.1	0.83	0.996	0.016	0.82	248.2	146.7	1.43
	Hydrochlorothiazide	0.004	552.6	0.929	0.151	0.014	0.61	0.998	0.008	0.031	188.8	0.61	0.998	0.008	0.60	186.1	88.0	1.84
	Saccharin	0.005	501.3	0.931	0.132	0.015	0.56	0.999	0.007	0.035	172.8	0.56	0.999	0.007	0.55	170.6	88.0	1.69
	Sulfamethoxazole	0.006	569.8	0.968	0.053	0.015	0.71	0.997	0.017	0.034	220.8	0.71	0.997	0.017	0.70	217.3	117.3	1.61
	Sucralose	0.005	439.7	0.911	0.170	0.015	0.44	0.999	0.007	0.034	137.2	0.42	0.999	0.007	0.42	136.6	43.9	2.38

Supplementary Material: Adsorption of aqueous phase contaminants of emerging concern by activated carbon: comparative fixed-bed column study and in situ regeneration methods

Table S9 (Part 4 of 5): Summary of the adsorption parameters for the Bohart-Adams, Thomas, Yoon-Nelson, and BCT modeling for the adsorption of the studied contaminants of emerging concern onto activated carbon.

Flow direction		Downflow																
Flow rate (mL min ⁻¹)		8																
Bed Height (cm)		3.5																
Activated carbon (AC)	Contaminants of Emerging Concern (CECs)	Bohart-Adams model				Thomas model				Yoon-Nelson model				BTC modelling				
		KBA (L/min mg)	N0 (mg/L-AC)	R2	SSE	KT (L/min*mg)	qads _T (mg/g)	R2	SSE	KYN (1/min)	τ (min)	qads _{YN} (mg/g)	R2	SSE	qads (mg/g)	tB (min)	tS (min)	MTZ (cm)
AC1	Caffeine	0.010	691.1	0.945	0.068	0.035	0.93	0.998	0.011	0.074	195.0	0.98	0.998	0.011	0.98	196.0	146.6	0.88
	Hydrochlorothiazide	0.007	483.5	0.816	0.375	0.042	0.44	0.998	0.008	0.088	91.1	0.45	0.998	0.008	0.44	90.2	58.6	1.23
	Saccharin	0.009	410.9	0.861	0.233	0.058	0.42	0.998	0.009	0.121	88.4	0.42	0.998	0.009	0.42	87.7	58.6	1.16
	Sulfamethoxazole	0.014	434.9	0.954	0.046	0.059	0.57	0.998	0.009	0.125	118.2	0.58	0.998	0.009	0.58	118.8	87.9	0.91
	Sucralose	0.013	250.0	0.793	0.283	0.078	0.22	0.998	0.009	0.164	46.5	0.22	0.998	0.009	0.22	45.9	29.3	1.27
AC2	Caffeine	0.011	332.8	0.828	0.251	0.114	0.29	0.996	0.019	0.239	59.6	0.30	0.996	0.019	0.32	64.6	44.0	1.12
	Hydrochlorothiazide	0.019	164.0	0.800	0.284	0.119	0.13	0.997	0.013	0.249	27.7	0.13	0.997	0.013	0.13	27.8	14.6	1.66
	Saccharin	0.021	166.0	0.877	0.157	0.080	0.15	0.997	0.014	0.169	32.3	0.15	0.997	0.014	0.13	28.3	14.6	1.69
	Sulfamethoxazole	0.011	336.2	0.859	0.187	0.043	0.31	0.998	0.010	0.090	65.6	0.31	0.998	0.010	0.32	67.1	29.3	1.97
	Sucralose	0.025	126.4	0.853	0.155	0.096	0.11	0.995	0.020	0.202	23.2	0.11	0.995	0.020	0.10	21.3	9.8	1.89

Supplementary Material: Adsorption of aqueous phase contaminants of emerging concern by activated carbon: comparative fixed-bed column study and in situ regeneration methods

Table S9 (Part 5 of 5): Summary of the adsorption parameters for the Bohart-Adams, Thomas, Yoon-Nelson, and BCT modeling for the adsorption of the studied contaminants of emerging concern onto activated carbon.

Flow direction		Downflow																
Flow rate (mL min ⁻¹)		11																
Bed Height (cm)		3.5																
Activated carbon (AC)	Contaminants of Emerging Concern (CECs)	Bohart-Adams model				Thomas model				Yoon-Nelson model				BTC modelling				
		KBA (L/min mg)	N0 (mg/L-AC)	R2	SSE	KT (L/min*mg)	qads _T (mg/g)	R2	SSE	KYN (1/min)	τ (min)	qads _{YN} (mg/g)	R2	SSE	qads (mg/g)	tB (min)	tS (min)	MTZ (cm)
AC1	Caffeine	0.013	598.9	0.923	0.090	0.069	0.77	0.936	0.335	0.148	114.8	0.80	0.936	0.335	0.94	136.4	88.0	1.24
	Hydrochlorothiazide	0.017	222.6	0.685	0.574	0.295	0.17	0.998	0.009	0.626	25.9	0.18	0.998	0.009	0.16	24.3	19.5	0.69
	Saccharin	0.018	225.4	0.713	0.484	0.244	0.18	0.997	0.015	0.519	26.9	0.18	0.997	0.015	0.14	20.8	19.5	0.22
	Sulfamethoxazole	0.017	358.6	0.860	0.156	0.139	0.38	0.997	0.013	0.296	57.5	0.39	0.997	0.013	0.38	56.5	44.0	0.77
	Sucralose	0.066	77.9	0.800	0.237	0.595	0.09	0.996	0.013	1.264	12.9	0.09	0.996	0.013	0.09	14.0	9.8	1.05
AC2	Caffeine	0.015	218.8	0.682	0.537	0.297	0.13	0.997	0.011	0.623	20.5	0.14	0.997	0.011	0.15	21.9	14.6	1.17
	Hydrochlorothiazide	0.024	102.3	0.622	0.560	0.428	0.06	0.996	0.010	0.898	9.1	0.06	0.996	0.010	0.06	9.0	4.9	1.59
	Saccharin	0.087	59.1	0.931	0.055	0.398	0.06	0.996	0.010	0.835	9.6	0.06	0.996	0.010	0.08	13.1	3.9	2.46
	Sulfamethoxazole	0.085	78.6	0.941	0.054	0.467	0.10	0.997	0.008	0.980	14.6	0.10	0.997	0.008	0.08	12.8	9.8	0.82
	Sucralose	0.078	37.6	0.728	0.234	0.630	0.02	0.994	0.011	1.323	3.6	0.02	0.994	0.011	0.03	4.7	1.0	2.76

Supplementary Material: Adsorption of aqueous phase contaminants of emerging concern by activated carbon: comparative fixed-bed column study and in situ regeneration methods

Table S10 (Part 1 of 3): Summary of the adsorption parameters for the Bohart-Adams, Thomas, Yoon-Nelson, and BCT modeling for the adsorption of the studied contaminants of emerging concern onto activated carbon.

Flow direction										Upflow								
Flow rate (mL min ⁻¹)										5								
Bed Height (cm)										1.5								
Activated carbon (AC)	Contaminants of Emerging Concern (CECs)	Bohart-Adams model				Thomas model				Yoon-Nelson model				BTC modelling				
		KBA (L/min mg)	N0 (mg/L-AC)	R2	SSE	KT (L/min*mg)	qads,T (mg/g)	R2	SSE	KYN (1/min)	τ (min)	qads,YN (mg/g)	R2	SSE	qads (mg/g)	tB (min)	tS (min)	MTZ (cm)
AC1	Caffeine	0.006	1341.7	0.928	0.150	1.689	0.02	0.996	0.020	0.048	241.0	1.65	0.996	0.020	1.57	230.0	175.6	0.35
	Hydrochlorothiazide	0.005	1099.9	0.950	0.089	1.246	0.01	0.997	0.015	0.031	177.8	1.28	0.997	0.015	1.26	176.2	87.9	0.75
	Saccharin	0.006	1109.9	0.959	0.068	1.359	0.02	0.997	0.017	0.040	194.0	1.39	0.997	0.017	1.35	187.5	87.9	0.80
	Sulfamethoxazole	0.005	1341.0	0.936	0.133	1.624	0.02	0.997	0.018	0.037	231.9	1.59	0.997	0.018	1.54	225.4	146.3	0.53
	Sucralose	0.005	1087.4	0.935	0.125	1.188	0.02	0.998	0.012	0.033	169.5	1.19	0.998	0.012	1.17	167.5	58.6	0.98
AC2	Caffeine	0.005	1462.0	0.909	0.206	1.832	0.02	0.998	0.013	0.048	261.8	1.88	0.998	0.013	1.84	256.9	205.1	0.30
	Hydrochlorothiazide	0.006	1105.9	0.960	0.068	1.288	0.02	0.996	0.021	0.032	184.0	1.26	0.996	0.021	1.24	181.4	87.7	0.77
	Saccharin	0.004	1187.5	0.891	0.257	1.244	0.02	0.998	0.008	0.036	177.8	1.27	0.998	0.008	1.27	176.9	87.9	0.75
	Sulfamethoxazole	0.005	1341.4	0.930	0.145	1.625	0.02	0.998	0.010	0.039	232.2	1.62	0.998	0.010	1.59	227.5	146.4	0.53
	Sucralose	0.005	1106.9	0.963	0.062	1.257	0.01	0.997	0.017	0.029	179.6	1.26	0.997	0.017	1.23	175.7	58.6	1.00

Supplementary Material: Adsorption of aqueous phase contaminants of emerging concern by activated carbon: comparative fixed-bed column study and in situ regeneration methods

Table S10 (Part 2 of 3): Summary of the adsorption parameters for the Bohart-Adams, Thomas, Yoon-Nelson, and BCT modeling for the adsorption of the studied contaminants of emerging concern onto activated carbon.

Flow direction										Upflow								
Flow rate (mL min ⁻¹)										5								
Bed Height (cm)										2.5								
Activated carbon (AC)	Contaminants of Emerging Concern (CECs)	Bohart-Adams model				Thomas model				Yoon-Nelson model				BTC modelling				
		KBA (L/min mg)	N0 (mg/L-AC)	R2	SSE	KT (L/min*mg)	qads,T (mg/g)	R2	SSE	KYN (l/min)	τ (min)	qads,YN (mg/g)	R2	SSE	qads (mg/g)	tB (min)	tS (min)	MTZ (cm)
AC1	Caffeine	0.007	1129.4	0.946	0.090	0.026	1.62	0.996	0.013	0.055	386.9	1.58	0.996	0.013	1.54	378.3	321.9	0.37
	Hydrochlorothiazide	0.006	971.6	0.944	0.101	0.023	1.32	0.998	0.011	0.047	314.7	1.35	0.998	0.011	1.32	307.8	234.4	0.60
	Saccharin	0.006	972.3	0.959	0.073	0.018	1.31	0.994	0.025	0.038	313.1	1.34	0.994	0.025	1.31	306.1	234.4	0.59
	Sulfamethoxazole	0.008	1058.6	0.964	0.054	0.024	1.51	0.996	0.014	0.050	362.1	1.48	0.996	0.014	1.45	354.8	292.7	0.44
	Sucralose	0.005	888.9	0.950	0.096	0.017	1.13	0.998	0.009	0.036	269.3	1.13	0.998	0.009	1.11	265.3	175.7	0.84
AC2	Caffeine	0.006	1988.7	0.897	0.221	0.037	1.68	0.997	0.010	0.077	401.1	1.72	0.997	0.010	1.69	394.2	351.6	0.27
	Hydrochlorothiazide	0.005	1721.5	0.937	0.139	0.018	1.35	0.997	0.012	0.037	320.3	1.31	0.997	0.012	1.29	313.6	234.1	0.63
	Saccharin	0.005	1733.9	0.950	0.099	0.018	1.39	0.996	0.017	0.038	331.7	1.43	0.996	0.017	1.39	323.1	234.4	0.69
	Sulfamethoxazole	0.007	1880.1	0.959	0.070	0.021	1.60	0.995	0.018	0.044	380.6	1.60	0.995	0.018	1.56	370.4	292.8	0.52
	Sucralose	0.005	1737.2	0.963	0.072	0.015	1.37	0.996	0.019	0.031	325.1	1.37	0.996	0.019	1.32	315.4	205.0	0.87

Supplementary Material: Adsorption of aqueous phase contaminants of emerging concern by activated carbon: comparative fixed-bed column study and in situ regeneration methods

Table S10 (Part 3 of 3): Summary of the adsorption parameters for the Bohart-Adams, Thomas, Yoon-Nelson, and BCT modeling for the adsorption of the studied contaminants of emerging concern onto activated carbon.

Flow direction										Upflow								
Flow rate (mL min ⁻¹)										5								
Bed Height (cm)										3.5								
Activated carbon (AC)	Contaminants of Emerging Concern (CECs)	Bohart-Adams model				Thomas model				Yoon-Nelson model				BTC modelling				
		KBA (L/min mg)	N0 (mg/L-AC)	R2	SSE	KT (L/min*mg)	qads _T (mg/g)	R2	SSE	KYN (1/min)	τ (min)	qads _{YN} (mg/g)	R2	SSE	qads (mg/g)	tB (min)	tS (min)	MTZ (cm)
AC1	Caffeine	922.602	0.0	0.959	0.056	0.031	1.39	0.992	0.017	0.064	463.9	1.36	0.992	0.017	1.33	453.7	409.8	0.34
	Hydrochlorothiazide	848.425	0.0	0.912	0.199	0.024	1.15	0.997	0.012	0.051	385.3	1.18	0.997	0.012	1.17	380.1	322.3	0.53
	Saccharin	812.630	0.0	0.952	0.066	0.032	1.20	0.996	0.013	0.067	402.3	1.24	0.996	0.013	1.21	394.2	351.6	0.38
	Sulfamethoxazole	918.076	0.0	0.957	0.068	0.024	1.35	0.993	0.016	0.051	450.1	1.32	0.993	0.016	1.29	439.8	380.5	0.47
	Sucralose	854.341	0.0	0.945	0.109	0.021	1.19	0.996	0.012	0.044	398.9	1.20	0.996	0.012	1.17	390.4	292.8	0.87
AC2	Caffeine	2246.208	0.0	0.912	0.184	0.031	1.39	0.994	0.012	0.064	462.7	1.42	0.994	0.012	1.40	454.2	410.2	0.34
	Hydrochlorothiazide	2113.333	0.0	0.955	0.095	0.015	1.24	0.995	0.015	0.033	413.5	1.21	0.995	0.015	1.19	404.7	321.6	0.72
	Saccharin	2237.892	0.0	0.939	0.135	0.019	1.34	0.994	0.013	0.040	447.4	1.38	0.994	0.013	1.35	438.0	351.6	0.69
	Sulfamethoxazole	2258.883	0.0	0.952	0.087	0.022	1.40	0.993	0.012	0.045	467.7	1.40	0.993	0.012	1.37	457.5	380.7	0.59
	Sucralose	2125.856	0.0	0.959	0.079	0.017	1.28	0.995	0.013	0.036	425.7	1.28	0.995	0.013	1.25	416.6	322.1	0.79

Supplementary Material: Adsorption of aqueous phase contaminants of emerging concern by activated carbon: comparative fixed-bed column study and in situ regeneration methods

Table S11 (Part 1 of 2): Summary of the adsorption parameters for the Bohart-Adams, Thomas, Yoon-Nelson, and BCT modeling for the adsorption of the studied contaminants of emerging concern onto activated carbon.

Flow direction										Upflow								
Flow rate (mL min ⁻¹)										5								
Bed Height (cm)										3.5								
Water Matrice										Wastewater treatment plant effluent								
Activated carbon (AC)	Contaminants of Emerging Concern (CECs)	Bohart-Adams model				Thomas model				Yoon-Nelson model				BTC modelling				
		KBA (L/min mg)	N0 (mg/L-AC)	R2	SSE	KT (L/min*mg)	qads,T (mg/g)	R2	SSE	KYN (1/min)	τ (min)	qads,YN (mg/g)	R2	SSE	qads (mg/g)	tB (min)	tS (min)	MTZ (cm)
AC1	Caffeine	0.006	561.0	0.977	0.029	0.015	0.73	0.997	0.017	0.032	236.1	0.69	0.997	0.017	0.7	146.3	232.5	1.30
	Hydrochlorothiazide	0.005	476.8	0.936	0.122	0.014	0.51	0.999	0.007	0.030	165.8	0.54	0.999	0.007	0.5	58.7	163.0	2.24
	Saccharin	0.005	530.4	0.946	0.109	0.013	0.59	0.997	0.015	0.028	191.2	0.56	0.997	0.015	0.5	58.5	186.8	2.40
	Sulfamethoxazole	0.006	541.8	0.962	0.066	0.015	0.66	0.996	0.021	0.033	215.2	0.68	0.996	0.021	0.7	117.3	208.8	1.53
	Sucralose	0.007	315.8	0.890	0.185	0.023	0.31	0.998	0.010	0.050	99.8	0.29	0.998	0.010	0.3	29.3	99.0	2.46
AC2	Caffeine	0.006	373.1	0.937	0.096	0.015	0.39	0.998	0.008	0.033	127.6	0.37	0.998	0.008	0.4	43.9	125.6	2.28
	Hydrochlorothiazide	0.005	301.1	0.807	0.337	0.020	0.19	0.987	0.053	0.042	63.3	0.20	0.987	0.053	0.2	14.7	70.1	2.77
	Saccharin	0.008	202.8	0.765	0.364	0.038	0.13	0.994	0.025	0.080	42.9	0.13	0.994	0.025	0.1	14.6	45.0	2.36
	Sulfamethoxazole	0.006	365.7	0.919	0.133	0.015	0.35	0.995	0.026	0.031	113.8	0.36	0.995	0.026	0.3	20.3	109.2	2.85
	Sucralose	0.010	154.8	0.815	0.225	0.038	0.11	0.996	0.017	0.081	36.8	0.11	0.996	0.017	0.1	3.9	35.2	3.01

Supplementary Material: Adsorption of aqueous phase contaminants of emerging concern by activated carbon: comparative fixed-bed column study and in situ regeneration methods

Table S11 (Part 2 of 2): Summary of the adsorption parameters for the Bohart-Adams, Thomas, Yoon-Nelson, and BCT modeling for the adsorption of the studied contaminants of emerging concern onto activated carbon.

Flow direction										Upflow								
Flow rate (mL min ⁻¹)										5								
Bed Height (cm)										3.5								
Water Matrice										Reuse water								
Activated carbon (AC)	Contaminants of Emerging Concern (CECs)	Bohart-Adams model				Thomas model				Yoon-Nelson model				BTC modelling				
		KBA (L/min mg)	N0 (mg/L-AC)	R2	SSE	KT (L/min*mg)	qads,T (mg/g)	R2	SSE	KYN (1/min)	τ (min)	qads,YN (mg/g)	R2	SSE	qads (mg/g)	tB (min)	tS (min)	MTZ (cm)
AC1	Caffeine	0.006	766.8	0.956	0.080	0.019	1.06	0.997	0.012	0.040	343.2	1.10	0.997	0.012	1.1	264.0	333.6	0.75
	Hydrochlorothiazide	0.004	804.9	0.946	0.130	0.011	0.98	0.997	0.010	0.024	319.7	1.03	0.997	0.010	1.0	205.3	316.0	1.23
	Saccharin	0.005	706.9	0.950	0.097	0.018	0.93	0.998	0.011	0.039	303.0	0.89	0.998	0.011	0.9	204.9	295.9	1.08
	Sulfamethoxazole	0.004	810.7	0.961	0.085	0.013	1.05	0.995	0.020	0.027	340.4	1.07	0.995	0.020	1.0	234.5	334.2	1.04
	Sucralose	0.006	656.2	0.972	0.048	0.016	0.86	0.997	0.016	0.035	281.2	0.82	0.997	0.016	0.8	175.2	274.5	1.27
AC2	Caffeine	0.004	576.7	0.935	0.142	0.014	0.65	0.998	0.011	0.030	215.7	0.69	0.998	0.011	0.7	117.3	213.3	1.58
	Hydrochlorothiazide	0.004	523.3	0.940	0.121	0.011	0.54	0.995	0.025	0.023	178.2	0.57	0.995	0.025	0.6	58.7	176.9	2.34
	Saccharin	0.004	510.7	0.898	0.242	0.014	0.51	0.999	0.007	0.030	168.1	0.49	0.999	0.007	0.5	58.5	165.9	2.27
	Sulfamethoxazole	0.005	528.8	0.949	0.098	0.014	0.60	0.998	0.012	0.029	196.8	0.62	0.998	0.012	0.6	87.9	194.0	1.91
	Sucralose	0.005	407.2	0.892	0.222	0.015	0.37	0.997	0.015	0.032	121.4	0.35	0.997	0.015	0.3	19.5	117.0	2.92

Supplementary Material: Adsorption of aqueous phase contaminants of emerging concern by activated carbon: comparative fixed-bed column study and in situ regeneration methods

Table S12 (Part 1 of 2): Summary of the adsorption parameters for the Bohart-Adams, Thomas, Yoon-Nelson, and BCT modeling for the adsorption of the studied contaminants of emerging concern onto activated carbon.

Flow direction		Upflow																
Flow rate (mL min ⁻¹)		5																
Bed Height (cm)		3.5																
Water Matrice		Wastewater treatment plant effluent																
Activated carbon (AC)	Contaminants of Emerging Concern (CECs)	Bohart-Adams model				Thomas model				Yoon-Nelson model				BTC modelling				
		KBA (L/min mg)	N0 (mg/L-AC)	R2	SSE	KT (L/min*mg)	qads,T (mg/g)	R2	SSE	KYN (l/min)	τ (min)	qads,YN (mg/g)	R2	SSE	qads (mg/g)	tB (min)	tS (min)	MTZ (cm)
AC1	Caffeine	0.061	54.7	0.962	0.058	0.158	0.07	0.997	0.013	0.021	351.1	0.07	0.997	0.013	0.07	208.5	348.6	1.41
	Hydrochlorothiazide	0.049	46.5	0.876	0.226	0.163	0.05	0.993	0.028	0.022	238.5	0.05	0.993	0.028	0.05	118.8	246.0	1.81
	Saccharin	0.046	44.7	0.841	0.361	0.228	0.04	0.993	0.032	0.031	214.1	0.04	0.993	0.032	0.04	118.6	221.8	1.63
	Sulfamethoxazole	0.049	53.1	0.903	0.192	0.158	0.06	0.994	0.027	0.021	297.0	0.05	0.994	0.027	0.05	178.9	300.5	1.42
	Sucralose	0.052	38.8	0.824	0.360	0.245	0.04	0.998	0.009	0.033	189.9	0.04	0.998	0.009	0.04	89.4	193.5	1.88
AC2	Caffeine	0.055	39.1	0.841	0.312	0.254	0.04	0.997	0.012	0.034	200.6	0.04	0.997	0.012	0.04	119.0	203.1	1.45
	Hydrochlorothiazide	0.046	37.8	0.790	0.465	0.241	0.03	0.997	0.011	0.033	170.7	0.04	0.997	0.011	0.04	59.4	170.0	2.28
	Saccharin	0.043	36.5	0.781	0.535	0.240	0.03	0.996	0.017	0.032	154.4	0.03	0.996	0.017	0.03	59.3	153.3	2.15
	Sulfamethoxazole	0.105	26.9	0.941	0.095	0.333	0.03	0.994	0.028	0.045	164.3	0.03	0.994	0.028	0.03	59.9	164.1	2.22
	Sucralose	0.076	26.2	0.902	0.175	0.250	0.03	0.996	0.018	0.034	131.5	0.03	0.996	0.018	0.03	39.7	132.8	2.45

Supplementary Material: Adsorption of aqueous phase contaminants of emerging concern by activated carbon: comparative fixed-bed column study and in situ regeneration methods

Table S12 (Part 2 of 2): Summary of the adsorption parameters for the Bohart-Adams, Thomas, Yoon-Nelson, and BCT modeling for the adsorption of the studied contaminants of emerging concern onto activated carbon.

Flow direction										Upflow								
Flow rate (mL min-1)										5								
Bed Height (cm)										3.5								
Water Matrice										Reuse water								
Activated carbon (AC)	Contaminants of Emerging Concern (CECs)	Bohart-Adams model				Thomas model				Yoon-Nelson model				BTC modelling				
		KBA (L/min mg)	N0 (mg/L-AC)	R2	SSE	KT (L/min*mg)	qads,T (mg/g)	R2	SSE	KYN (1/min)	τ (min)	qads,YN (mg/g)	R2	SSE	qads (mg/g)	tB (min)	tS (min)	MTZ (cm)
AC1	Caffeine	0.056	75.7	0.970	0.050	0.156	0.10	0.995	0.011	0.021	526.9	0.10	0.995	0.011	0.10	358.7	524.5	1.11
	Hydrochlorothiazide	0.048	67.6	0.948	0.098	0.143	0.08	0.998	0.006	0.019	432.0	0.09	0.998	0.006	0.09	237.5	428.9	1.56
	Saccharin	0.037	73.0	0.931	0.159	0.114	0.08	0.996	0.012	0.015	435.5	0.09	0.996	0.012	0.09	208.1	427.5	1.80
	Sulfamethoxazole	0.054	75.1	0.965	0.064	0.164	0.10	0.996	0.011	0.022	518.4	0.10	0.996	0.011	0.10	358.5	514.3	1.06
	Sucralose	0.057	53.8	0.926	0.133	0.180	0.06	0.998	0.009	0.024	330.4	0.07	0.998	0.009	0.07	208.5	329.4	1.28
AC2	Caffeine	0.050	60.6	0.936	0.122	0.154	0.07	0.997	0.011	0.030	215.7	0.04	0.997	0.011	0.07	209.5	373.6	1.54
	Hydrochlorothiazide	0.052	46.0	0.870	0.258	0.211	0.05	0.995	0.021	0.023	178.2	0.04	0.995	0.021	0.05	148.6	252.1	1.44
	Saccharin	0.068	40.5	0.883	0.189	0.272	0.04	0.998	0.010	0.030	168.1	0.04	0.998	0.010	0.05	148.8	238.6	1.32
	Sulfamethoxazole	0.041	58.4	0.895	0.254	0.142	0.06	0.994	0.025	0.029	196.8	0.04	0.994	0.025	0.06	179.5	317.6	1.52
	Sucralose	0.063	32.4	0.849	0.285	0.254	0.03	0.998	0.010	0.032	121.4	0.03	0.998	0.010	0.04	89.2	166.4	1.63

Supplementary Material: Adsorption of aqueous phase contaminants of emerging concern by activated carbon: comparative fixed-bed column study and in situ regeneration methods

Table S13: Adsorption capacity (mg/g) of each contaminant of emerging concern on activated carbon 1.

Contaminants of emerging concern	Ethanol:water	Ethanol:water	Ethanol	Water at pH 2	Water at pH 10
	(10:90, v/v)	(50:50, v/v)			
	Cycles 1 / 2 / 3	Cycles 1 / 2 / 3			
Caffeine	1.49 / 0.87 / 0.07	1.38 / 1.44 / 0.79	1.36 / 1.54 / 1.32	1.27 / 0.17 / 0.03	1.36 / 0.96 / 0.71
Hydrochlorothiazide	1.04 / 0.16 / 0.02	0.94 / 0.69 / 0.39	0.89 / 0.98 / 0.83	0.96 / 0.76 / 0.41	0.93 / 0.88 / 0.73
Saccharin	0.86 / 0.35 / 0.03	0.88 / 0.84 / 0.57	0.93 / 1.01 / 0.92	0.92 / 0.25 / 0.15	0.93 / 0.22 / 0.18
Sulfamethoxazole	0.98 / 0.97 / 0.35	1.20 / 1.50 / 1.41	1.06 / 1.32 / 1.49	1.22 / 0.98 / 0.58	1.30 / 1.27 / 1.07
Sucralose	0.75 / 0.06 / 0.05	0.64 / 0.18 / 0.12	0.71 / 0.42 / 0.26	0.73 / 0.06 / 0.03	0.71 / 0.30 / 0.23
Total	5.12 / 2.41 / 0.52	5.05 / 4.65 / 3.28	4.95 / 5.27 / 4.81	5.11 / 2.22 / 1.22	5.24 / 3.63 / 2.92

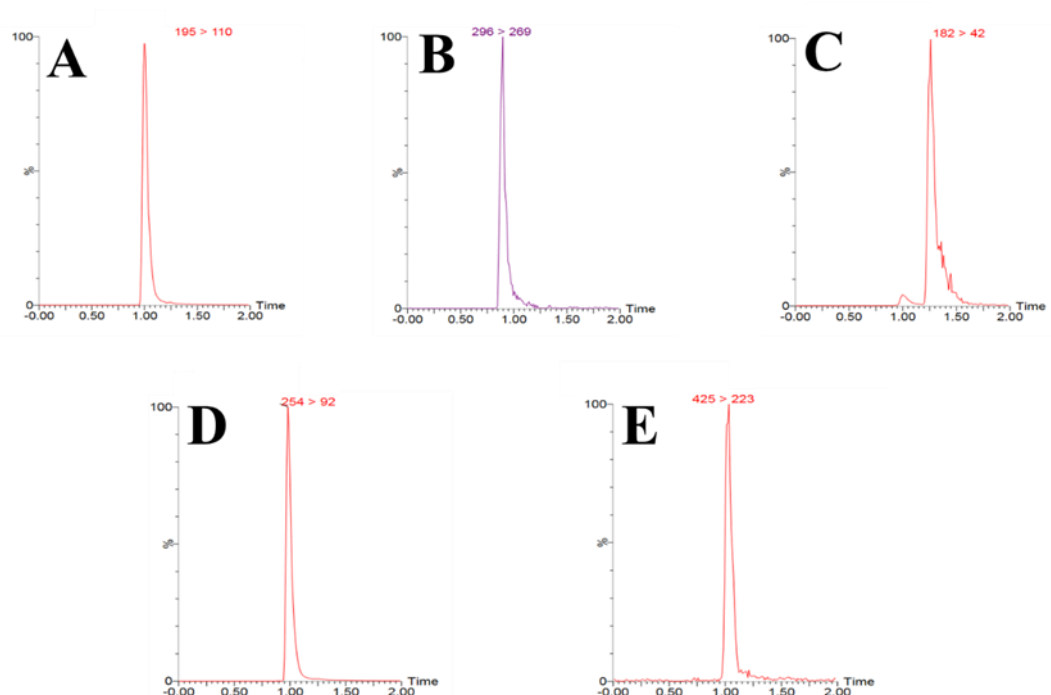


Figure S1: Chromatogram obtained from UHPLC-MS/MS. UPLC® CSH C18 column (130 Å, 1.7 µm, 2.1 × 100 mm). Chromatographic conditions: mobile phase composed of methanol:water (60:40, v/v) with 0.1% of formic acid. Flow rate: 0.3 mL min⁻¹. Column temperature: 40 °C. Injection volume: 5 µL. Caffeine (A); Hydrochlorothiazide (B); Saccharin (C); Sulfamethoxazole (D); and Sucralose (E).

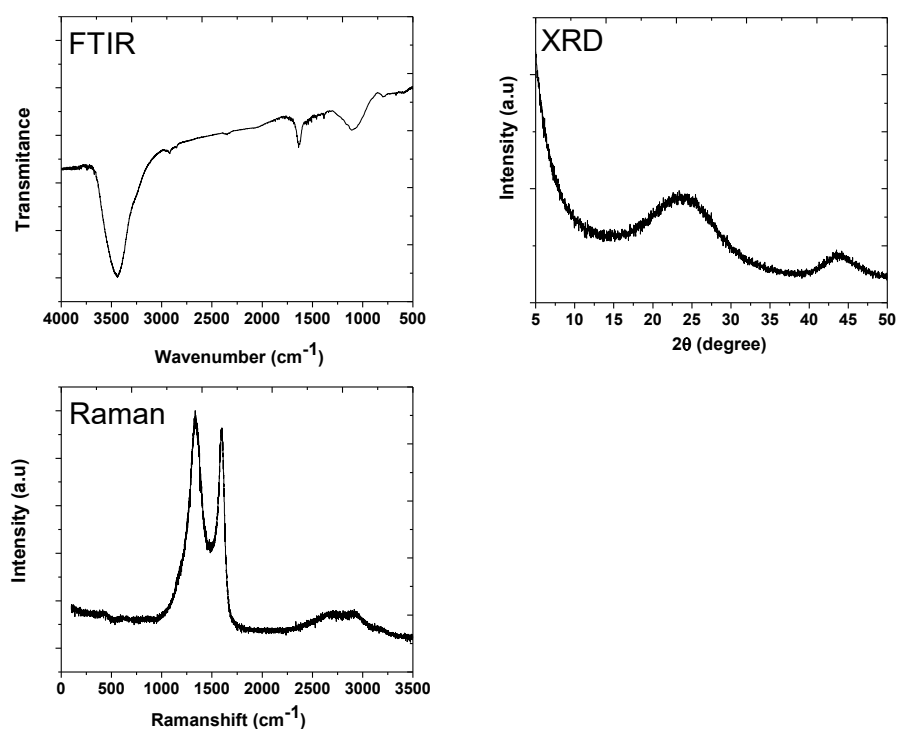


Figure S2: FTIR spectra, XRD spectra, and Raman spectra of the activated carbon 2 (AC2).

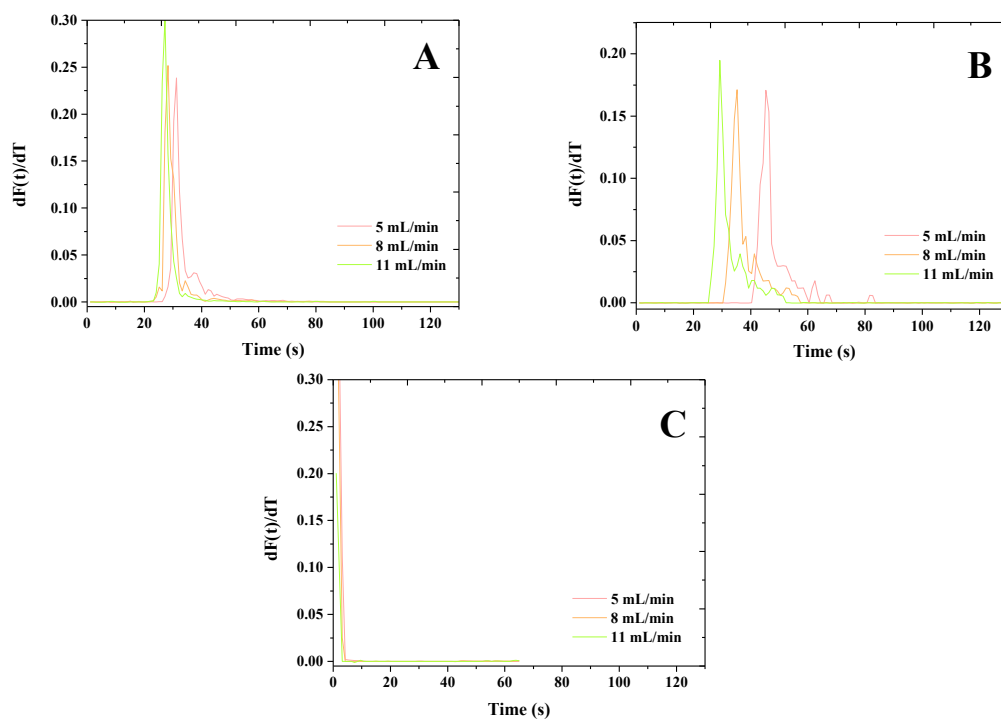


Figure S3: Curve E of the empty bed column time for the downflow (A), upflow (B), and for the determination of the dead volume (C).

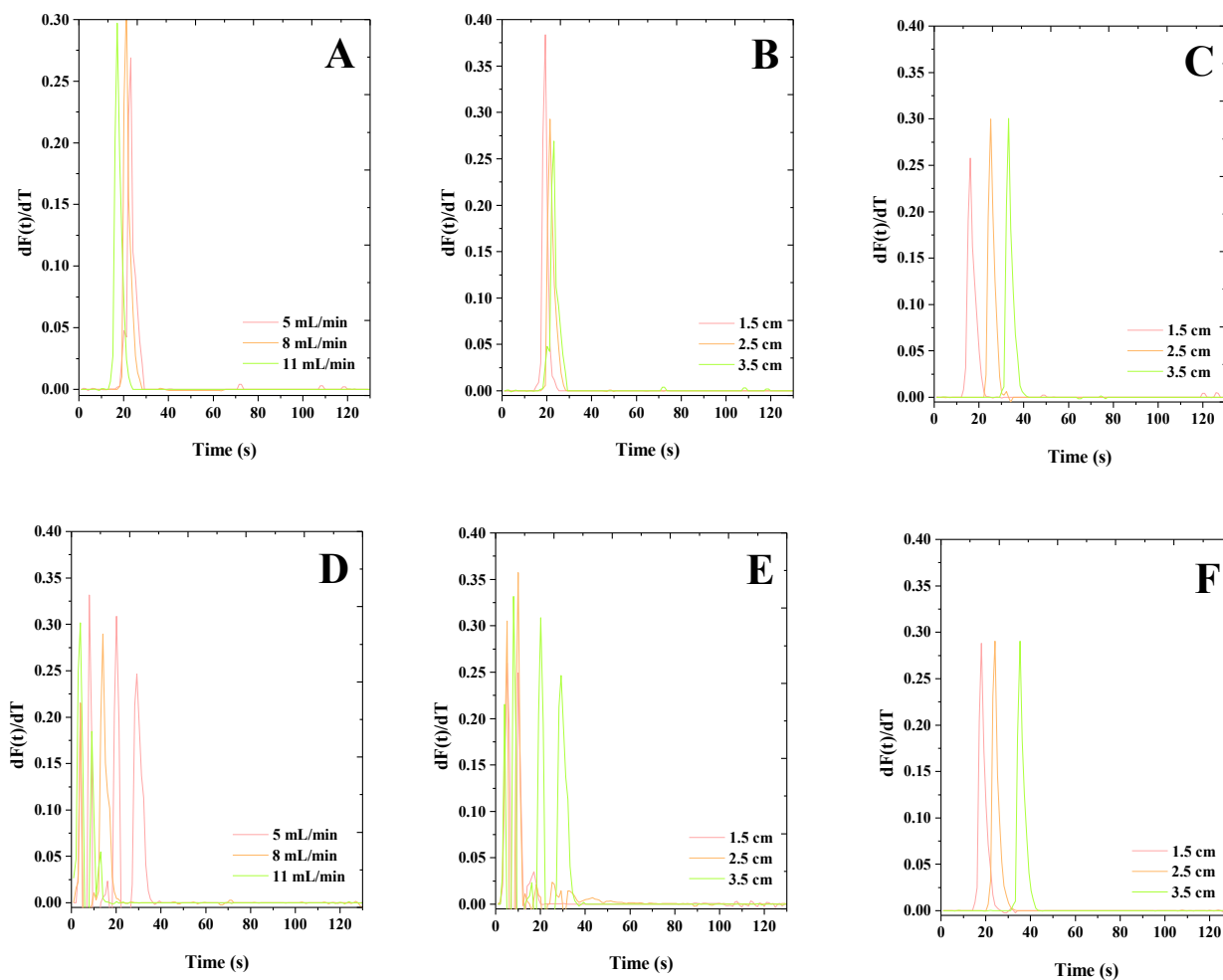


Figure S4: Curve E of each experiment configuration. (A) flow rate variation for the AC1; (B) bed depth variation for the AC1; (C) bed height variation for the AC1 (upflow mode); (D) flow rate variation for the AC2; (E) bed height variation for the AC2; (F) bed height variation for the AC2 (upflow mode).

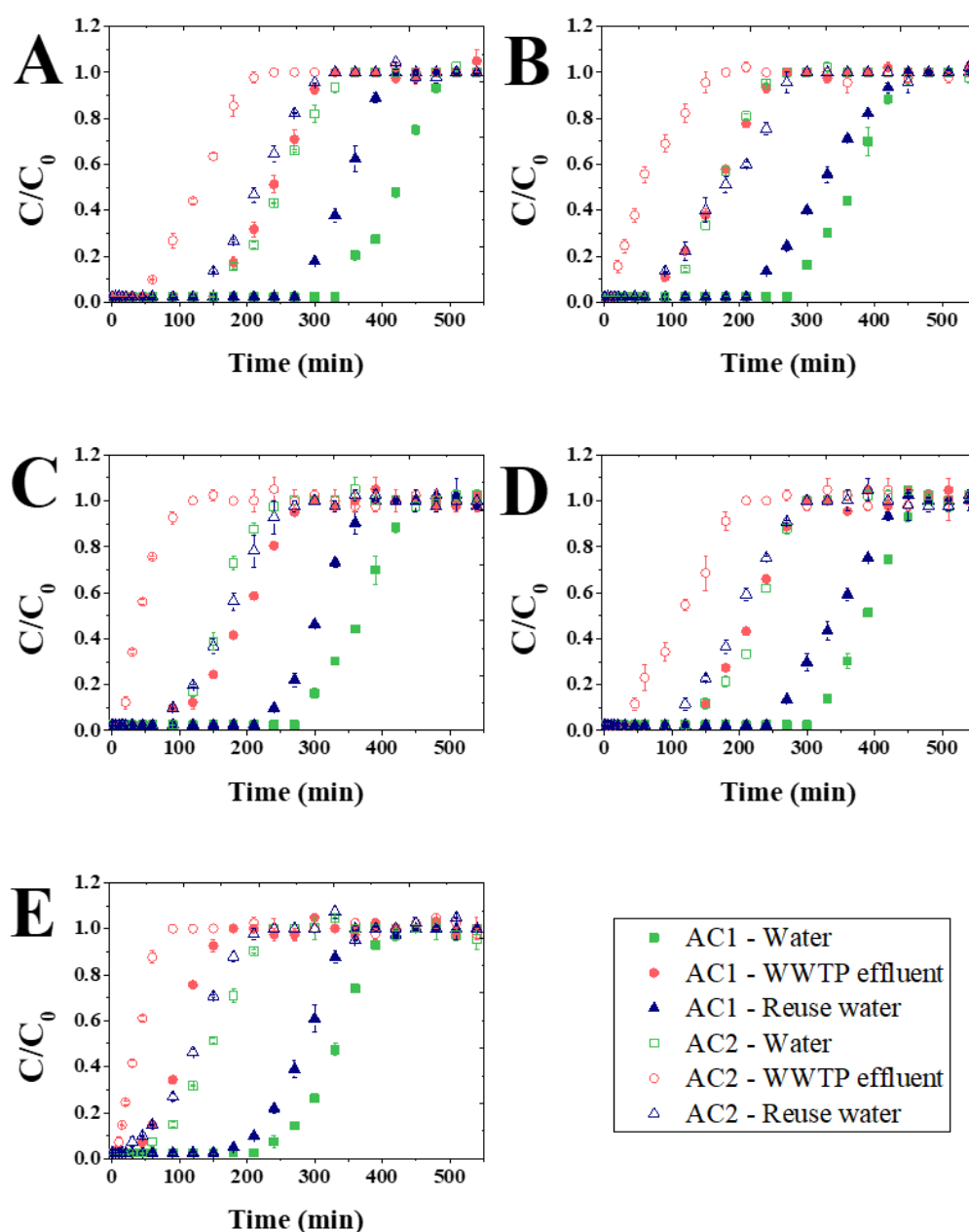


Figure S5: The breakthrough curve of CAF (A), HTZ (B), SAC (C), SMX (D), and SUC (E) sorption onto AC1 and AC2 at different water composition (bed height = 3.5 cm, $C_0 = 2$ mg/L, and flow rate = 5 mL/min, and down-flow mode).

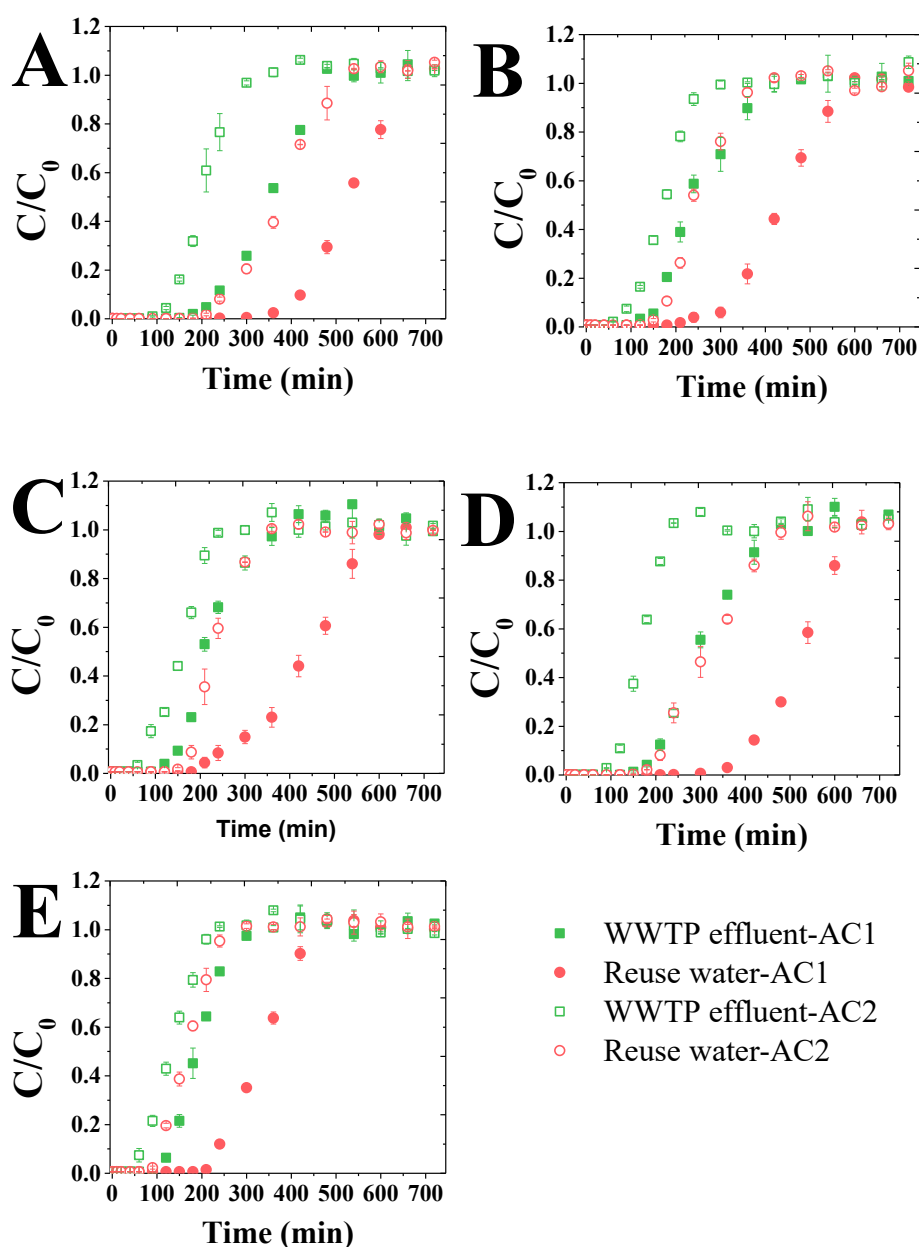


Figure S6: The breakthrough curve of CAF (A), HTZ (B), SAC (C), SMX (D), and SUC (E) sorption onto AC1 and AC2 at different water composition (bed height = 3.5 cm, $C_0 = 0.1$ mg/L, and flow rate = 5 mL/min, and down-flow mode).

Text T1: Activated carbon characterization

The AC was characterized by adsorption/desorption isotherm of nitrogen at 77 K in a mercury porosimeter PoreMaster (Quantachrome) and surface area analyzer NOVA 4200e (Quantachrome). Previously to the analysis, the AC was degassed at 150 °C under a vacuum chamber for 24 h. The specific surface area (ASEBET) and pore size distribution were calculated using the BET theory and BJH methods. The pHZPC was determined according to the procedure described by Larous & Meniai (2016).

X-ray diffraction (XRD) spectra of the AC were acquired with a XRD-7000 (SHIMADZU) diffractometer using a copper anode ($K\alpha$ radiation). Confocal Raman spectroscopy studies were carried out on a T64000 (Horiba) spectrometer equipped with a 532 nm laser with a grating of 1800 grooves per mm² and slit of 100 μ m, resulting in a spectral resolution of 2.9 cm⁻¹. Fourier Transformed Infrared spectroscopy (FTIR) was conducted in a CARY 630 (Agilent) spectrophotometer. Boehm's titration method was used to determine the surface groups on the AC sample (Oickle *et al.*, 2010). The method is a reliable procedure determining acidic (lactonic, phenolic and carboxylic) and basic groups.

Larous, S., & Meniai, A. H. (2016). Adsorption of Diclofenac from aqueous solution using activated carbon prepared from olive stones. *International Journal of Hydrogen Energy*, 41(24), 10380-10390. <https://doi.org/10.1016/j.ijhydene.2016.01.096>

Oickle, A. M., Goertzen, S. L., Hopper, K. R., Abdalla, Y. O., & Andreas, H. A. (2010). Standardization of the Boehm titration: Part II. Method of agitation, effect of filtering and dilute titrant. *Carbon*, 48(12), 3313-3322. <https://doi.org/10.1016/j.carbon.2010.05.004>

Supplementary information: Synthesis and characterization of TiO₂-carbon filter materials for water decontamination by adsorption-degradation processes

Vinicius Diniz^{1,*}, Colin R Crick², Susanne Rath¹

¹ Department of Analytical Chemistry, Institute of Chemistry, University of Campinas.
Address: Rua Josué de Castro s/n. Zip Code 13083-970. Cidade Universitária, Campinas, SP, Brasil.

² School of Engineering and Materials Science, Queen Mary University of London. Mile End Road, E1 4NS, London, UK.

*Author for correspondence: *viniciusdiniz994@gmail.com*

Figures

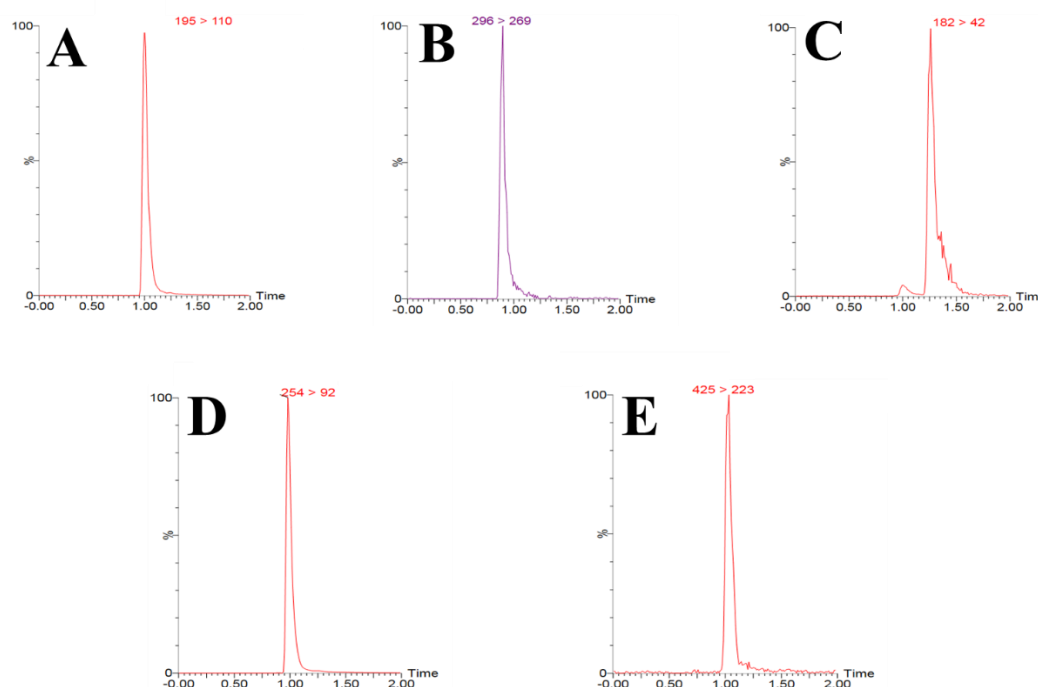


Figure S1: Chromatogram obtained from UHPLC-MS/MS. UPLC® CSH C18 column (130 Å, 1.7 µm, 2.1 × 100 mm). Chromatographic conditions: mobile phase composed of methanol:water (60:40, v/v) with 0.1% of formic acid. Flow rate: 0.3 mL min⁻¹. Column temperature: 40 °C. Injection volume: 10 µL. Caffeine (A); Hydrochlorothiazide (B); Saccharin (C); Sulfamethoxazole (D); and Sucralose (E).

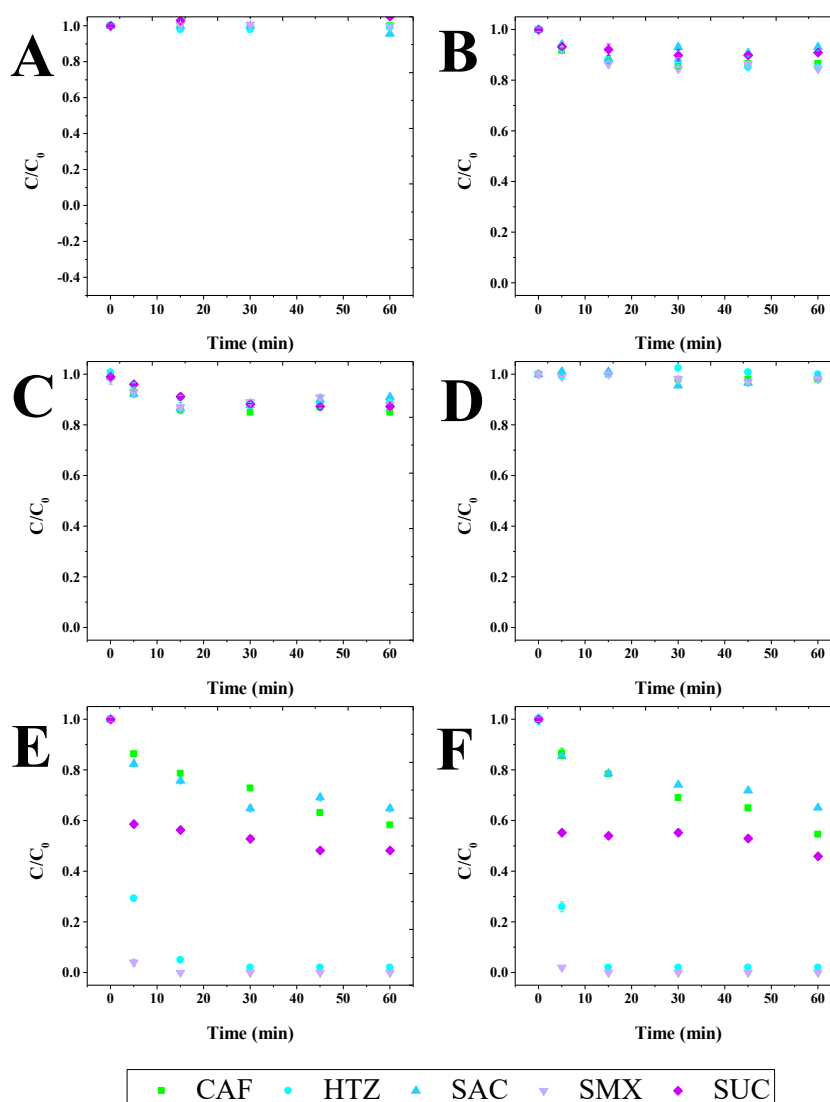


Figure S2: Removal of caffeine (CAF), hydrochlorothiazide (HTZ), saccharin (SAC), sulfamethoxazole (SMX), and sucralose (SUC). (A) Hydrolysis. (B) P25 (50 mg/L) adsorption studies. (C) PC500 (50 mg/L) adsorption studies. (D) UV-A (8W) irradiation studies. (E) UV-C (8 W) irradiation studies. (F) UV-C (16 W) irradiation studies. Initial concentration of the contaminants = 2 mg L^{-1} .

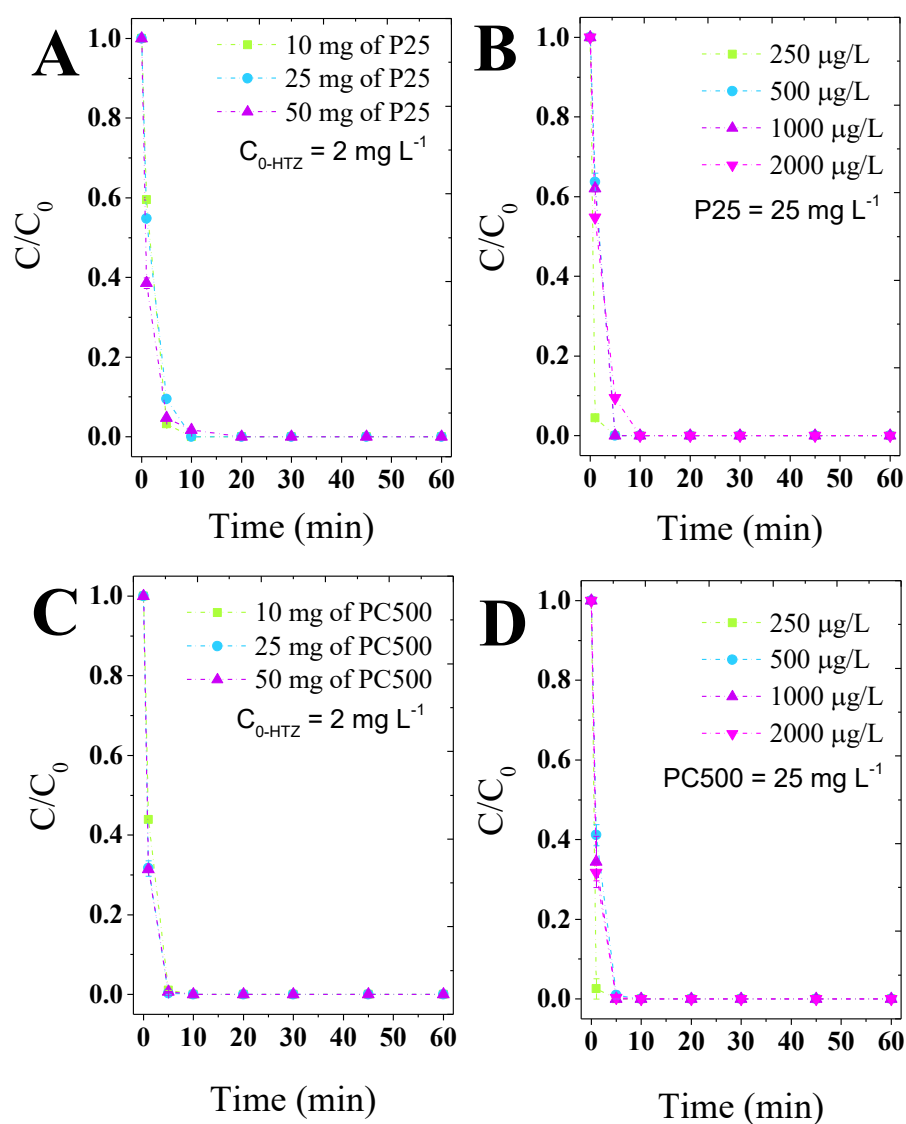


Figure S3: Photocatalysis of hydrochlorothiazide by TiO_2 -P25 (A and B) and TiO_2 -PC500 (C and D). $C_{0\text{-HTZ}}$: initial concentration of hydrochlorothiazide.

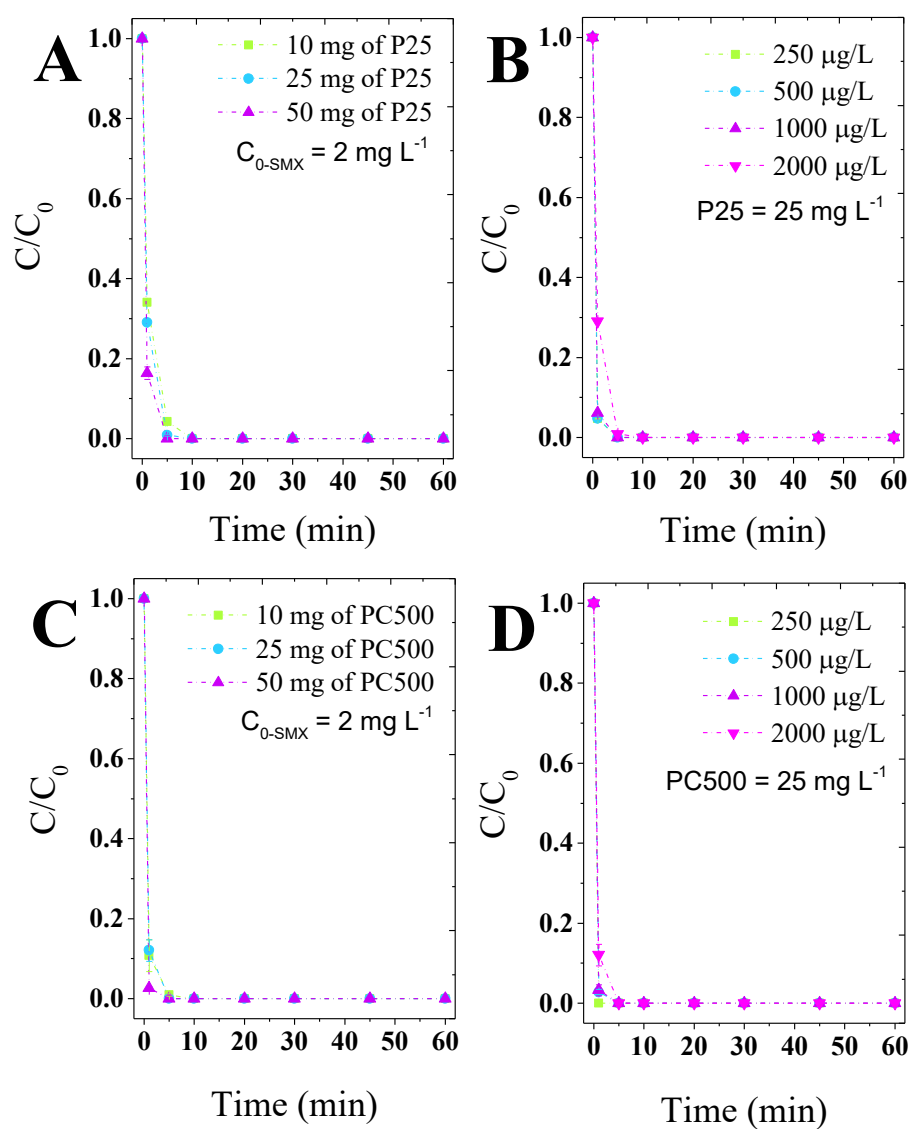


Figure S4: Photocatalysis of sulfamethoxazole by TiO_2 -P25 (A and B) and TiO_2 -PC500 (C and D). $C_{0\text{-SMX}}$: initial concentration of sulfamethoxazole.

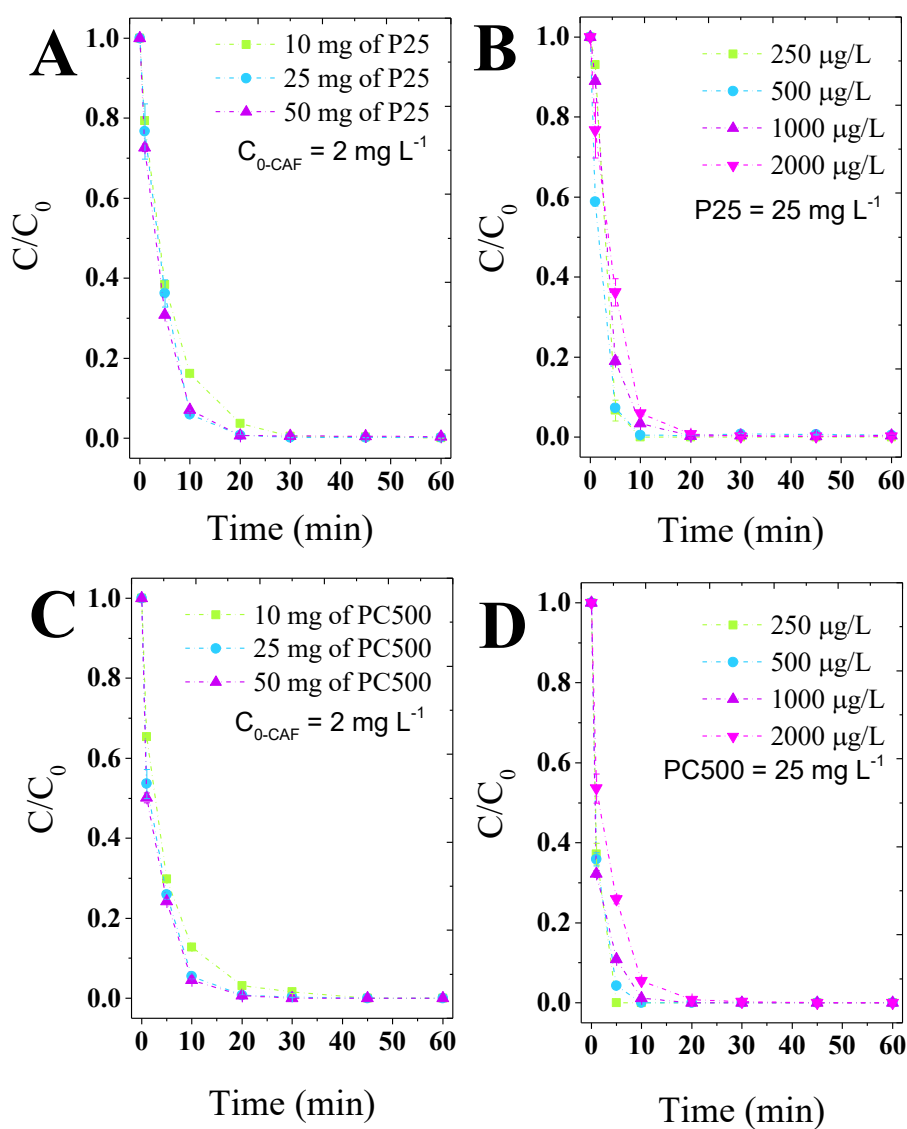


Figure S5: Photocatalysis of caffeine by TiO_2 -P25 (A and B) and TiO_2 -PC500 (C and D). $C_{0\text{-CAF}}$: initial concentration of caffeine.

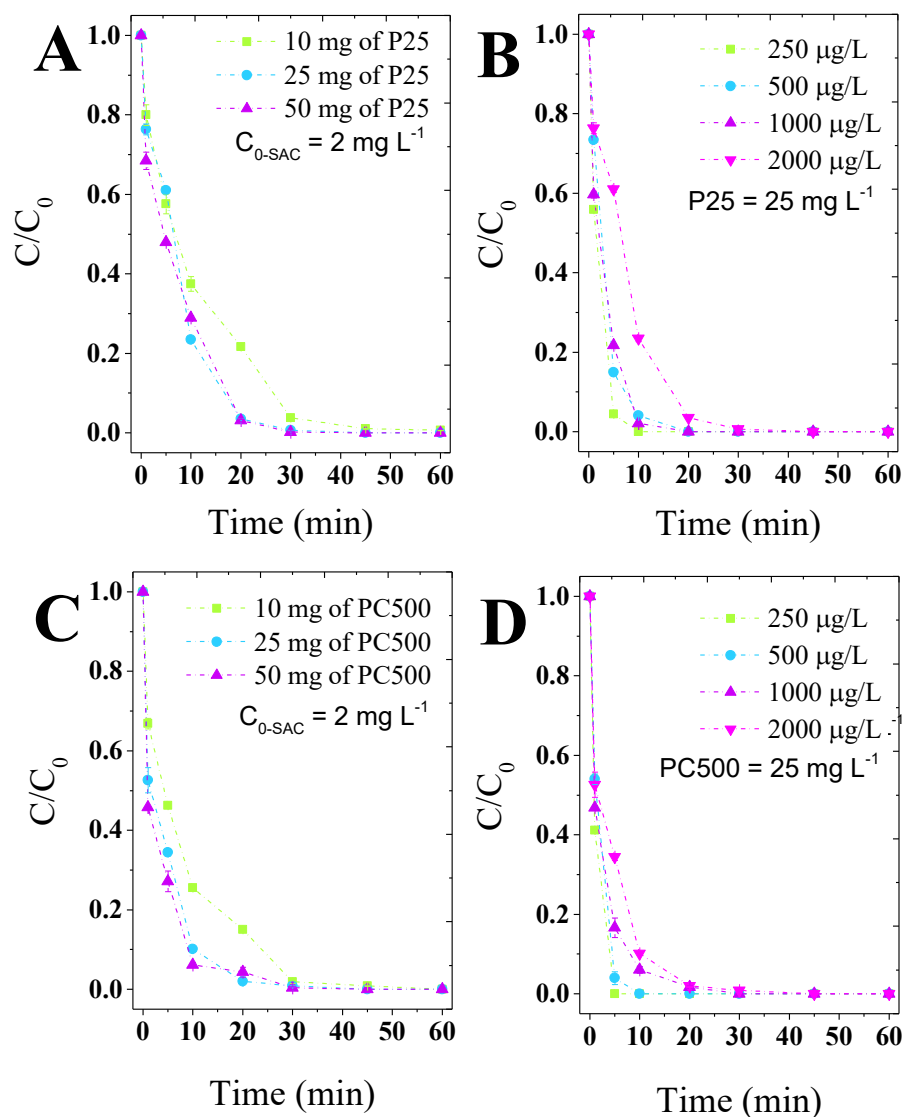


Figure S6: Photocatalysis of saccharin by TiO_2 -P25 (A and B) and TiO_2 -PC500 (C and D). C_{0-SAC} : initial concentration of saccharin.

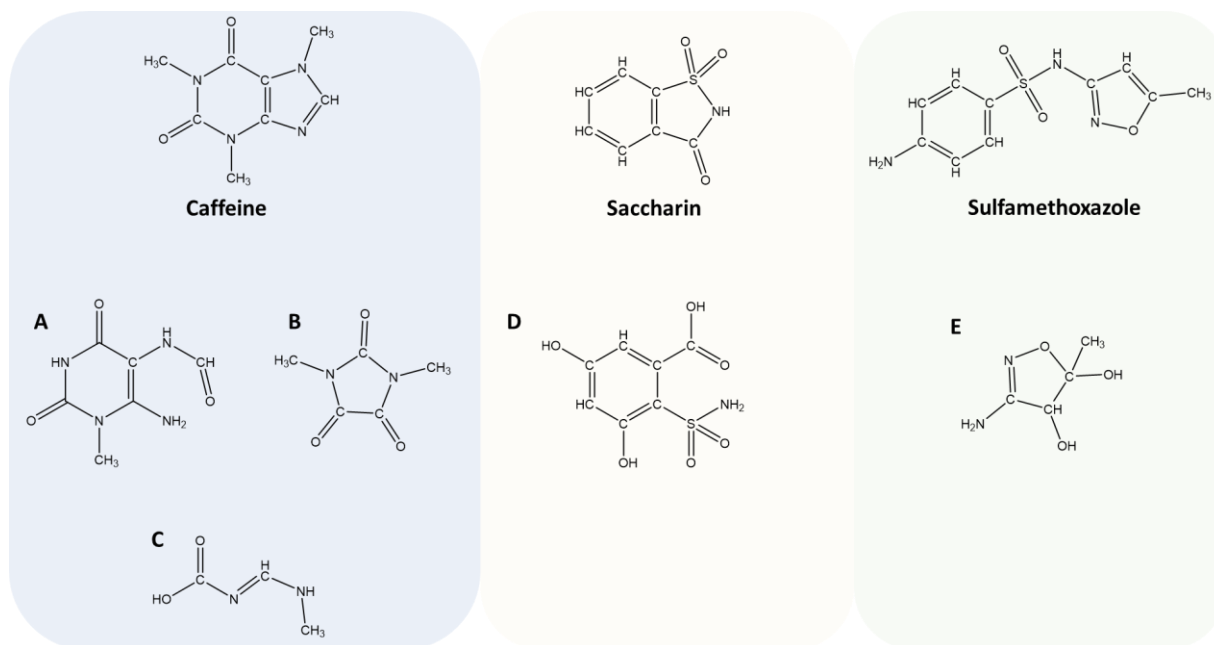


Figure S7: Structural formula of caffeine, saccharin, and sulfamethoxazole, and proposed structural formulas for the degradation products that remained in the solution after 60 min of photocatalysis. Adapted from: ^a Manoli et al. (2017), ^b Chuang et al. (2011), ^c Dalmazio et al. (2005), ^d Davididou et al. (2018), and ^e Hu et al. (2007)

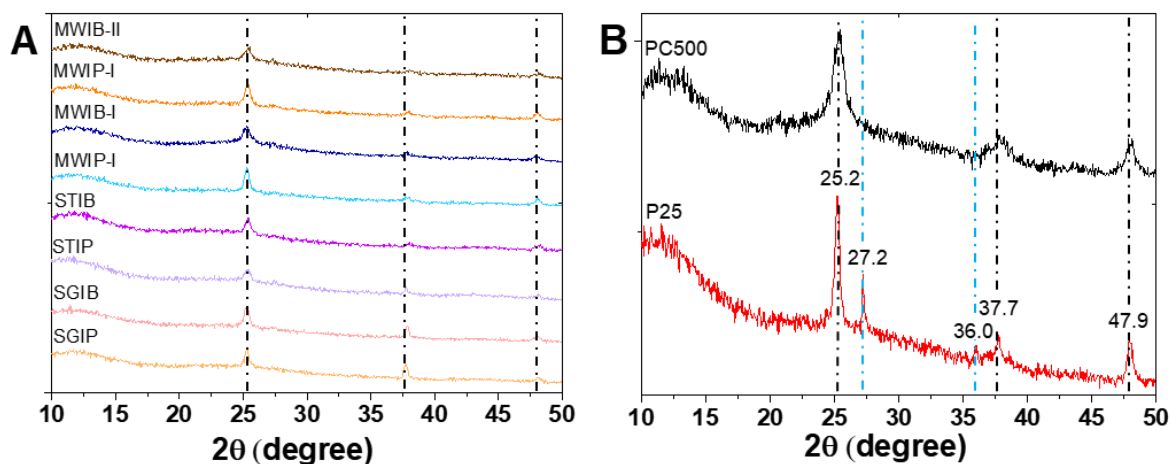


Figure S8: XRD patterns of the (A) TiO₂/AC heterostructures and (B) pristine P25 and PC500. The dotted black lines are related to anatase peaks, and the dotted blue lines are related to rutile peaks.

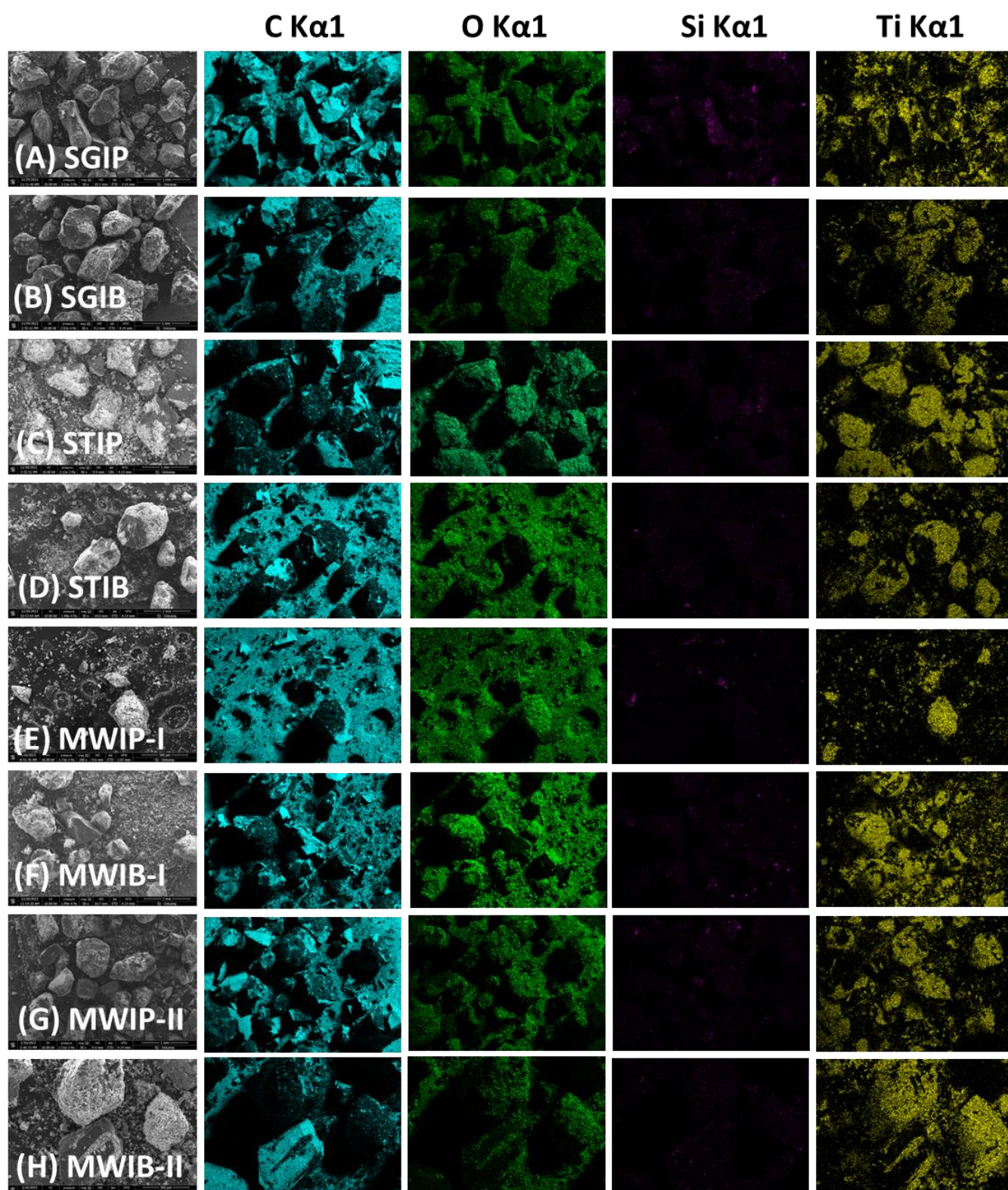


Figure S9: Elemental mapping of (A) SGIP, (B) SGIB, (C) STIP, (D) STIB, (E) MWIP-I, (F) MWIB-I, (G) MWIP-II, and (H) MWIB-II, and their respective SEM images

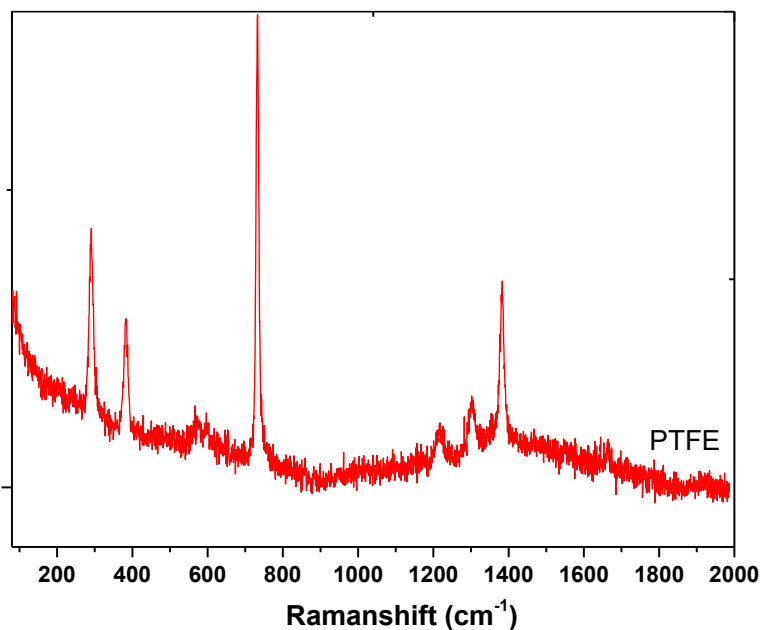


Figure S10: Raman spectrum of polytetrafluoroethylene (PTFE).

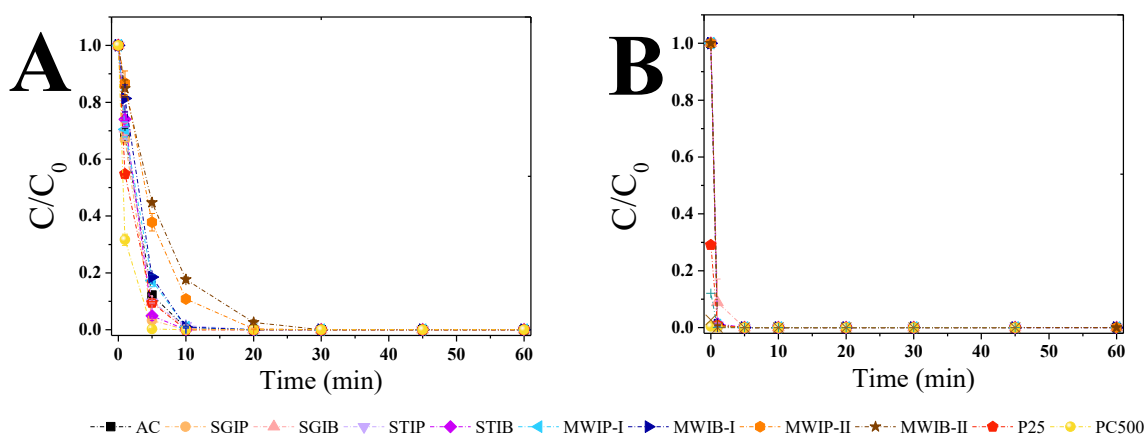


Figure S11: Removal of hydrochlorothiazide (A) and sulfamethoxazole (B) by the TiO_2/AC heterostructures, pristine AC under UV-C, $\text{TiO}_2\text{-P25}$, and $\text{TiO}_2\text{-PC500}$ under UV-C (8 W) irradiation. Initial concentration of the contaminants = 2 mg L^{-1} . TiO_2/AC heterostructure = 25 mg L^{-1} .

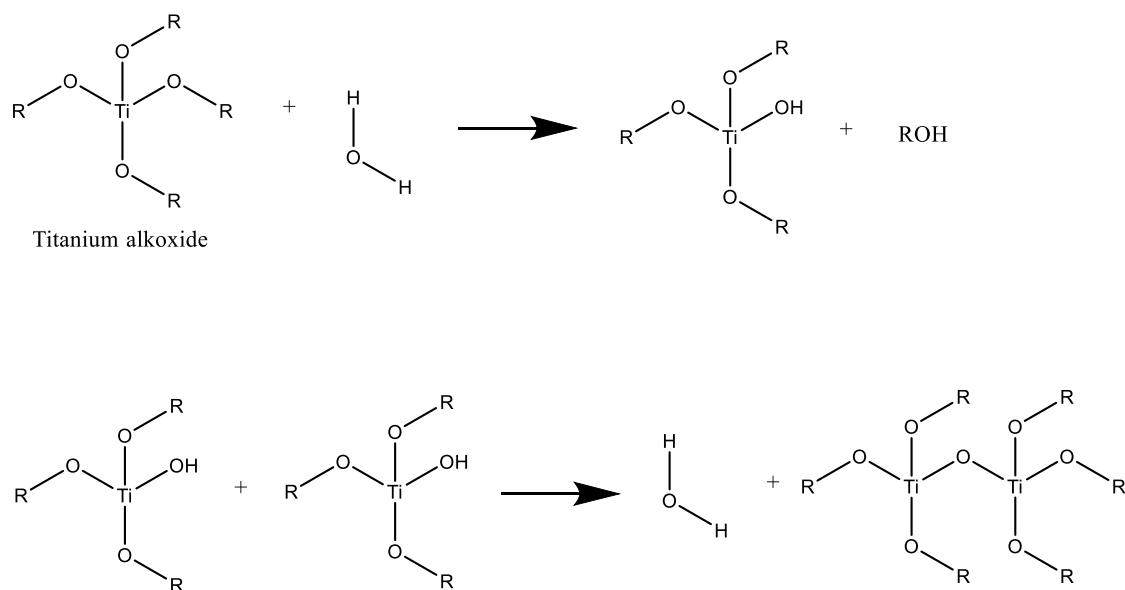


Figure S12: Hydrolysis and water condensation reactions of titanium alkoxide. *R* is an alkane chain.

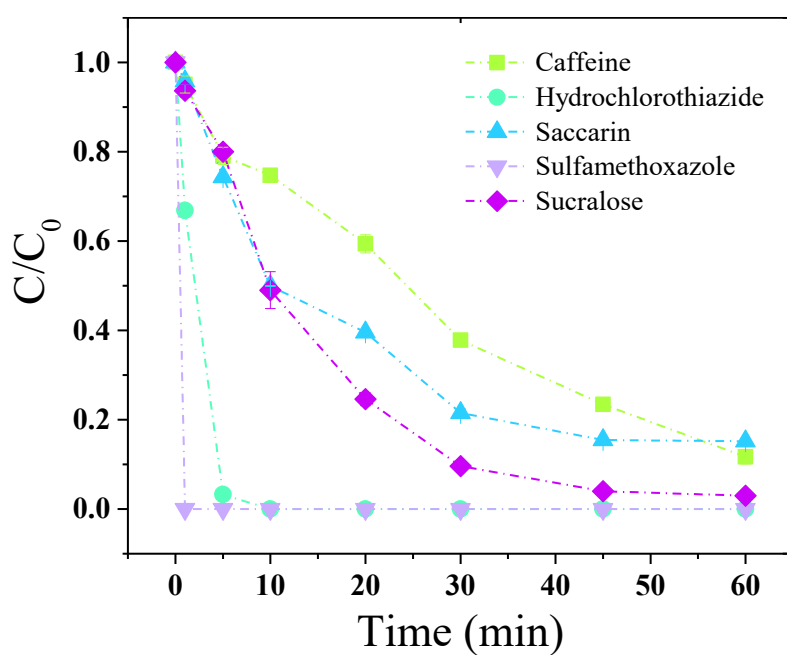


Figure S13: Removal of the contaminants by the SGIP heterostructure under UV-C (8 W) irradiation. The initial concentration of the contaminants = 2 mg L⁻¹ and material = 25 mg L⁻¹.

Tables

Table S1: Accurate mass (m/z) values obtained for the contaminants and its proposed photocatalytic degradation products after TiO_2 exposure.

Name	Proposed Formula $[\text{M-H}]^+$ or $[\text{M-H}]^-$	Calculated m/z	Exact m/z	Error (ppm)
Caffeine	$\text{C}_8\text{H}_{11}\text{N}_4\text{O}_2$	195.087641	195.08765	-0.0456
CAF-1	$\text{C}_3\text{H}_7\text{O}_2\text{N}_2$	103.05056	103.05024	3.105281
CAF-2	$\text{C}_4\text{H}_9\text{N}_2\text{O}_2$	117.066063	117.06585	1.815218
CAF-3	$\text{C}_5\text{H}_7\text{N}_2\text{O}_3$	143.04512	143.04512	0
CAF-4	$\text{C}_7\text{H}_9\text{N}_4\text{O}_2$	181.072141	181.072	0.781063
CAF-5	$\text{C}_7\text{H}_9\text{N}_4\text{O}_3$	197.066866	197.06692	-0.27402
CAF-6	$\text{C}_7\text{H}_{11}\text{N}_4\text{O}_3$	199.082456	199.08257	-0.57137
CAF-7	$\text{C}_5\text{H}_{11}\text{N}_4\text{O}_3$	211.08249	211.0825	-0.04737
CAF-8	$\text{C}_8\text{H}_{13}\text{N}_4\text{O}_3$	213.09805	213.0982	-0.7039
CAF-9	$\text{C}_8\text{H}_{11}\text{N}_4\text{O}_4$	227.077318	227.07748	-0.71194
CAF-10	$\text{C}_8\text{H}_{13}\text{N}_4\text{O}_4$	229.092938	229.09313	-0.83622
CAF-d ₃	$\text{C}_8\text{H}_8\text{N}_4\text{O}_2\text{D}_3$	198.10635	198.10648	-0.65621
Hydrochlorothiazide	$\text{C}_7\text{H}_7\text{ClN}_3\text{S}_2\text{O}_4$	295.9572	295.9561	3.589121
HTZ-1	$\text{C}_7\text{H}_8\text{N}_3\text{S}_2\text{O}_5$	277.9756	277.97434	4.514805
HTZ-2	$\text{C}_7\text{H}_5\text{ClN}_3\text{S}_2\text{O}_4$	279.9913	279.9899	4.881128
HTZ-3	$\text{C}_7\text{H}_6\text{ClN}_3\text{S}_2\text{O}_5$	293.9418	293.94085	3.150294
Saccharin	$\text{C}_7\text{H}_4\text{NO}_3\text{S}$	181.9909	181.9906	1,269907
SAC-1	$\text{C}_7\text{H}_4\text{NO}_4\text{S}$	197.9864	197.9855	4.577355
SAC-2	$\text{C}_7\text{H}_4\text{NO}_6\text{S}$	229.9764	229.9758	2.391556
SAC-3	$\text{C}_7\text{H}_6\text{NO}_6\text{S}$	231.9921	231.991	4.69738
Sulfamethoxazole	$\text{C}_{10}\text{H}_{12}\text{N}_3\text{O}_3\text{S}$	254.0592	254.0594	-0.92006
SMX-1	$\text{C}_4\text{H}_7\text{N}_2\text{O}_4\text{S}$	179.0122	179.0121	0.353794
SMX-2	$\text{C}_6\text{H}_9\text{NO}_5\text{S}$	203.9961	203.9961	-0.06536
SMX-3	$\text{C}_7\text{H}_6\text{N}_3\text{O}_4\text{S}$	228.0074	228.0074	0
SMX-4	$\text{C}_{10}\text{H}_{10}\text{N}_3\text{O}_4\text{S}$	268.0392	268.0387	1.977327
SMX-5	$\text{C}_{10}\text{H}_{12}\text{N}_3\text{O}_4\text{S}$	270.054	270.0543	-1.12323
SMX-6	$\text{C}_{10}\text{H}_{11}\text{N}_2\text{O}_5\text{S}$	271.0375	271.0383	-3.0623
SMX-7	$\text{C}_{10}\text{H}_{10}\text{N}_3\text{O}_5\text{S}$	284.0334	284.0336	-0.59852
SMX-8	$\text{C}_{10}\text{H}_{12}\text{N}_3\text{O}_5\text{S}$	286.049	286.0489	0.291325
SMX-9	$\text{C}_{10}\text{H}_{14}\text{N}_3\text{O}_5\text{S}$	288.0647	288.0649	-0.69429
SMX-10	$\text{C}_{10}\text{H}_{11}\text{N}_3\text{O}_4\text{SNa}$	292.0359	292.0363	-1.26697
SMX-11	$\text{C}_4\text{H}_7\text{ON}_2$	99.05563	99.05529	3.407188
SMX-12	$\text{C}_{10}\text{H}_{14}\text{O}_5\text{N}_3\text{S}$	288.0647	288.0649	-0.72102
SMX-13	$\text{C}_7\text{H}_{10}\text{O}_3\text{N}_3\text{S}$	216.0436	216.0437	-0.55544
SMX-14	$\text{C}_6\text{H}_8\text{O}_3\text{NS}$	174.022	174.0219	0.316052
SMX-15	$\text{C}_4\text{H}_9\text{O}_3\text{N}_2$	133.0609	133.0608	0.620017
SMX-16	$\text{C}_6\text{H}_8\text{O}_4\text{NS}$	190.0168	190.0169	-0.49118

Supplementary information: Synthesis and characterization of TiO_2 -carbon filter materials for water decontamination by adsorption-degradation processes

Sucralose	$C_{12}H_{19}Cl_3O_8$	419.0035	419.0038	-0.5698
SUC-1	$C_{12}H_{16}Cl_2O_8Na$	381.0111	381.0111	0.056866
SUC-2	$C_{12}H_{17}Cl_3O_8Na$	416.9882	416.9881	0.16787
SUC-3	$C_{12}H_{19}Cl_3O_{10}Na$	450.9937	450.9936	0.12417
SUC-4	$C_{12}H_{19}Cl_3O_9Na$	434.9985	434.9987	-0.34483
SUC-5	$C_6H_{11}O_3Cl_2$	201.0071	201.008	-4.59372
SUC-6	$C_6H_{10}O_5Cl$	197.0207	197.0211	-2.41937
SUC-7	$C_6H_{10}O_4Cl_2Na$	238.9846	238.9848	-1.11583
SUC-8	$C_{12}H_{19}O_{11}Cl_3Na$	466.9885	466.9885	-0.00535

Table S2: Values of the first order kinetic constant (min^{-1}) of contaminants removal under UV-C irradiation light with the TiO_2/AC heterostructures and pristine AC.

Material	Hydrochlorothiazide	Sulfamethoxazole
Pristine AC	0.401 ± 0.009	5.037 ± 0.000
SGIP	0.475 ± 0.037	*
SGIB	0.403 ± 0.021	2.424 ± 0.000
STIP	0.412 ± 0.017	4.709 ± 0.000
STIB	0.413 ± 0.045	4.257 ± 0.000
MWIP-I	0.355 ± 0.007	4.731 ± 0.000
MWIB-I	0.303 ± 0.025	4.740 ± 0.000
MWIP-II	0.197 ± 0.009	4.770 ± 0.000
MWIB-II	0.167 ± 0.003	4.836 ± 0.000

* Fit did not converge since SMX totally was removed before the first sampling time.

References

- Chuang, L. C., C. H. Luo, S. W. Huang, Y. C. Wu, and Y. C. Huang. 2011. 'Photocatalytic Degradation Mechanism and Kinetics of Caffeine in Aqueous Suspension of Nano- TiO_2 ', *Advances in Key Engineering Materials*, 214: 97-102.
- Dalmazio, I., L. S. Santos, R. P. Lopes, M. N. Eberlin, and R. Augusti. 2005. 'Advanced oxidation of caffeine in water: On-line and real-time monitoring by electrospray ionization mass spectrometry', *Environmental Science & Technology*, 39: 5982-88.
- Davididou, K., C. McRitchie, M. Antonopoulou, I. Konstantinou, and E. Chatzisyseon. 2018. 'Photocatalytic degradation of saccharin under UV-LED and blacklight irradiation', *Journal of Chemical Technology and Biotechnology*, 93: 269-76.
- Hu, L. H., P. M. Flanders, P. L. Miller, and T. J. Strathmann. 2007. 'Oxidation of sulfamethoxazole and related antimicrobial agents by TiO_2 photocatalysis', *Water Research*, 41: 2612-26.
- Manoli, K., G. Nakhla, A. K. Ray, and V. K. Sharma. 2017. 'Oxidation of Caffeine by Acid-activated Ferrate(VI): Effect of Ions and Natural Organic Matter', *Aiche Journal*, 63: 4998-5006.

Supplementary Information: Porous sulfur polymers for effective aqueous-phase organic contaminant removal

Vinicius Diniz^{1,2}, Joseph C. Bear³, Susanne Rath² and Colin R. Crick^{1*}

¹School of Engineering and Materials Sciences, Queen Mary University of London, London, E1 4NS, UK

²Institute of Chemistry, University of Campinas, 13083-970 Campinas, Brazil

³School of Life Sciences, Pharmacy and Chemistry, Kingston University, Penrhyn Road, Kingston-upon-Thames, KT1 2EE, UK

*Author for correspondence: *c.crick@qmul.ac.uk*

LIST OF FIGURES

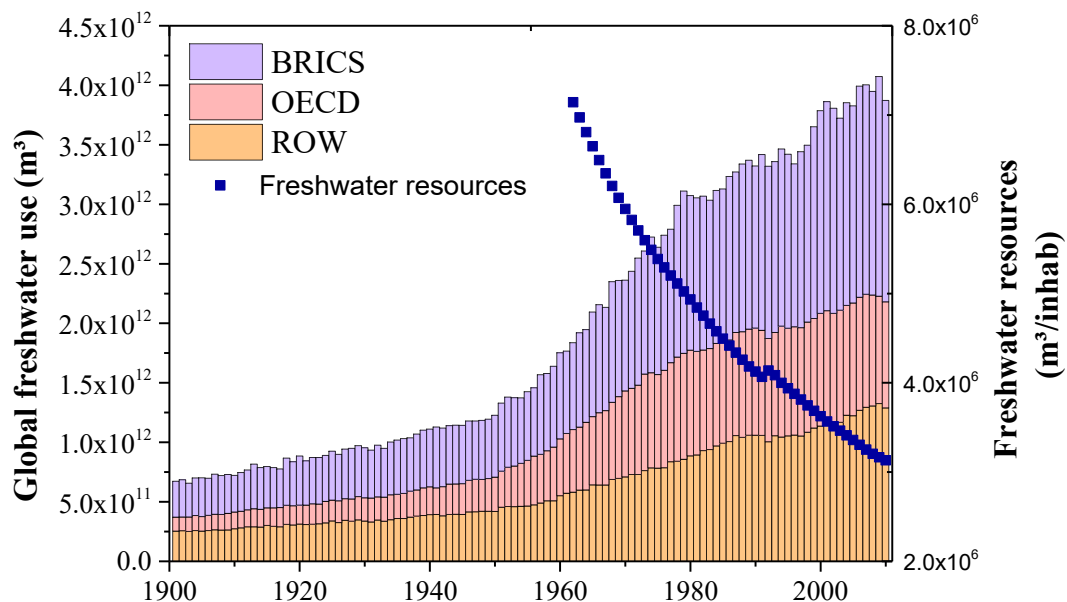


Figure S1: Global freshwater withdrawals for agricultural, industrial, and domestic uses by aggregated regional groupings (left side). Renewable internal freshwater resources flows refer to internal renewable resources (internal river flows and groundwater from rainfall) (right side). OECD members are defined as countries who were members in 2010 and their membership was carried back in time. BRICS countries are Brazil, Russia, India, China and South Africa. ROW refers to the Rest of the World, excluding OECD and BRICS countries. Data source Our world in data ¹.

¹Our World in Data, <https://ourworldindata.org/>, (accessed 07th of August, 2023).

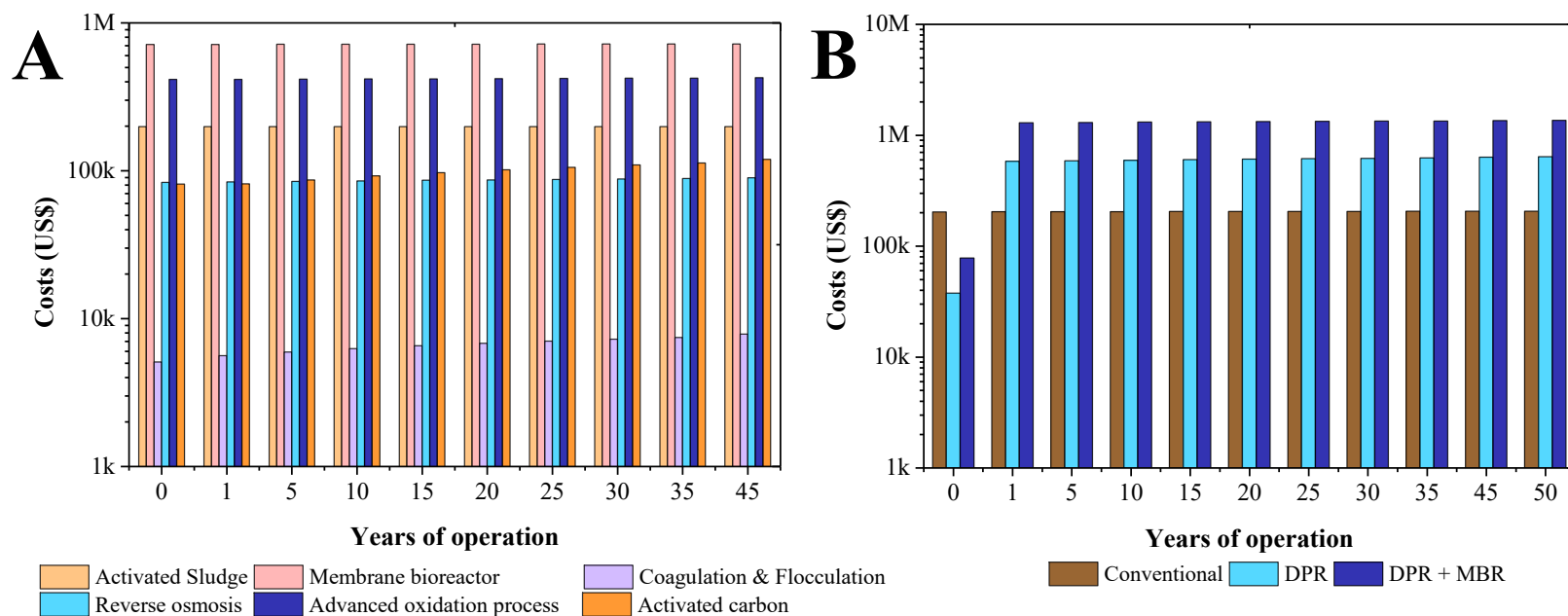


Figure S2: Approximate cost for (A) each treatment process considering a production of 100 m³/day of potable water and (B) considering a convention approach (activated sludge + coagulation & flocculation), general direct potable reuse (DPR, reverse osmosis + mineralization + activated carbon), and general DPR + membrane bioreactor (MBR). The calculations were based on the work of Guo et al.¹

¹T. J. Guo, J. Englehardt and T. T. Wu, *Water Sci Technol*, 2014, **69**, 223-234.

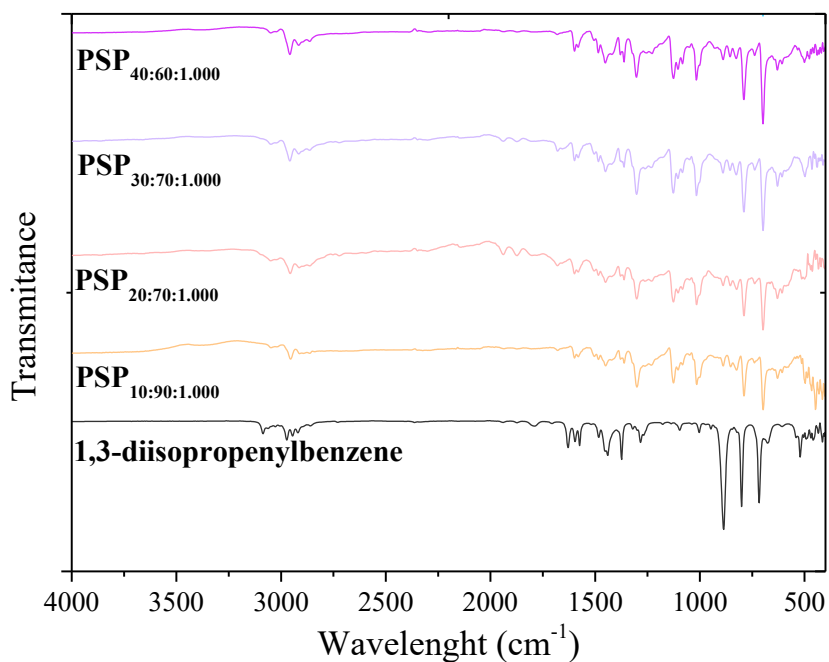


Figure S3: Fourier Transform Infrared (FTIR) spectra of the 1,3-diisopropenylbenzene (DIB) monomer and porous sulfur polymer (PSP) synthesized considering different sulfur/DIB ratios and 1.000 g of table salt after water treatment. $\text{PSP}_{X:Y:Z} = X\%[\text{DIB}]:Y\%[\text{S}_8]:Z\text{g}[\text{NaCl}]$.

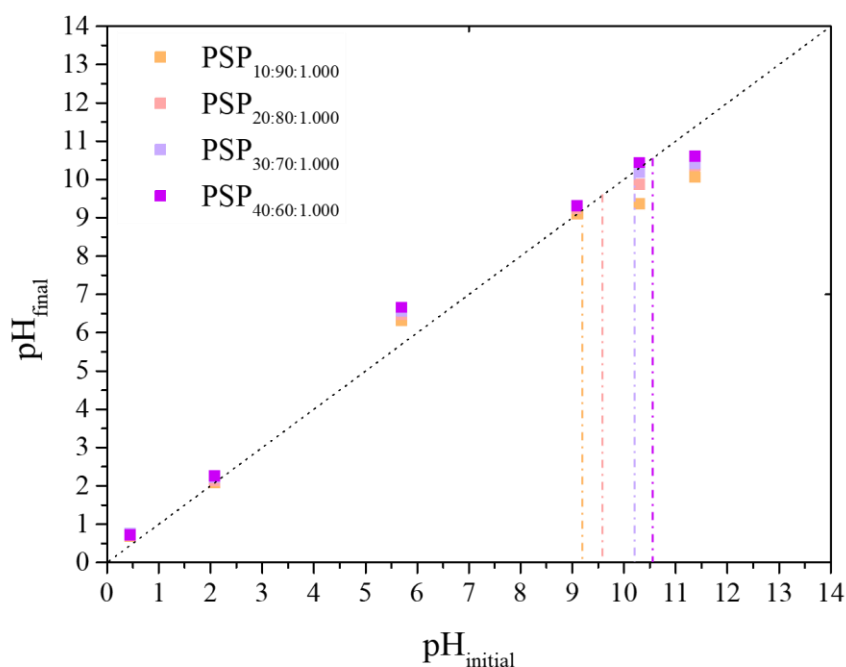


Figure S4: Point of zero charge of the porous sulfur polymers (PSPs) synthesized considering different sulfur/1,3-diisopropenylbenzene (DIB) monomer ratios. $\text{PSP}_{X:Y:Z} = X\%[\text{DIB}]:Y\%[\text{S}_8]:Z\text{g}[\text{NaCl}]$.

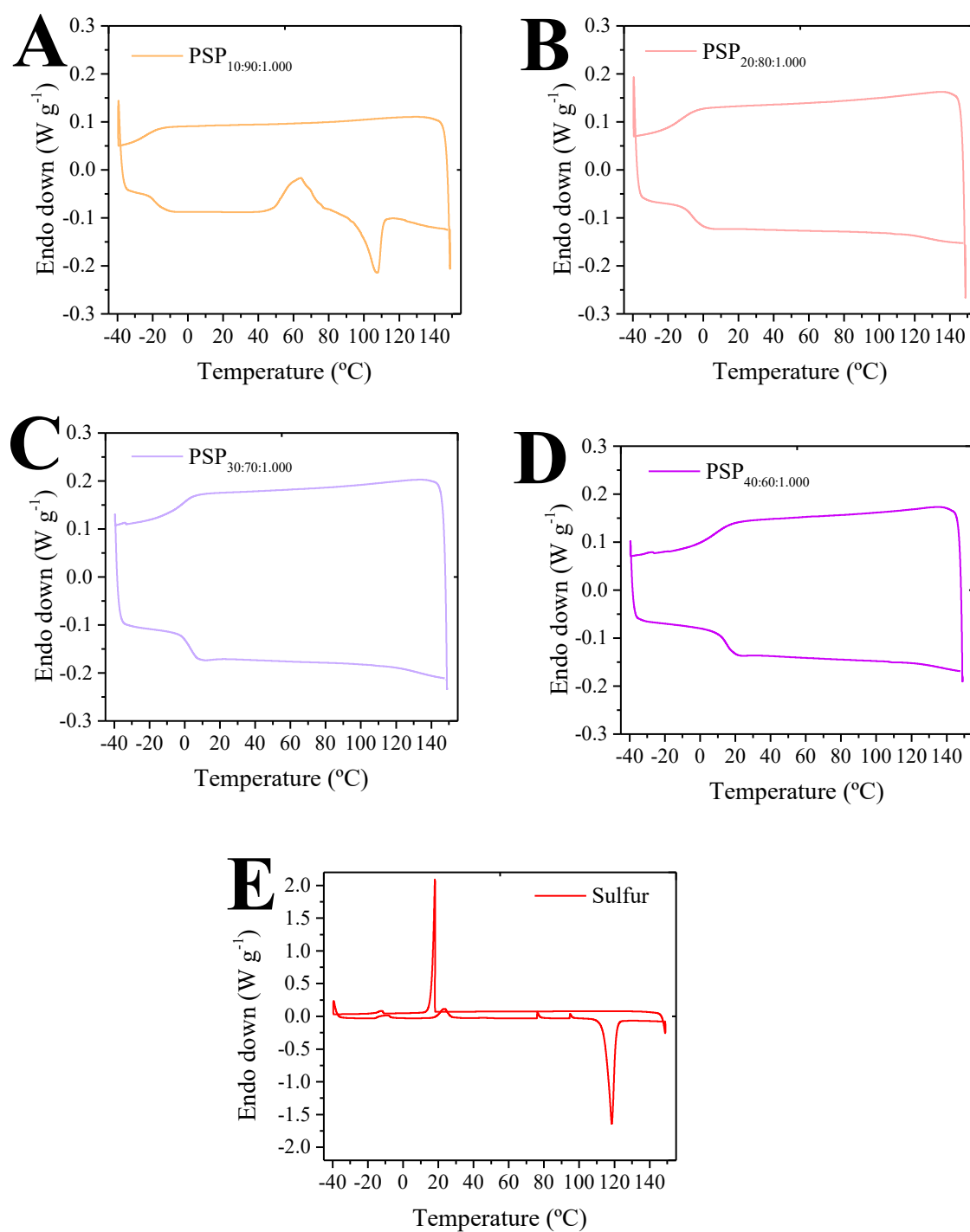


Figure S5: Differential Scanning Calorimetry (DSC) thermograms of 2nd cycles of (A) PSP_{10:90:1.000}, (B) PSP_{20:80:1.000}, (C) PSP_{30:70:1.000}, (D) PSP_{40:60:1.000}, (E) Pure sulfur. PSP_{X:Y:Z} = X%[DIB]:Y%[S₈]:Zg[NaCl].

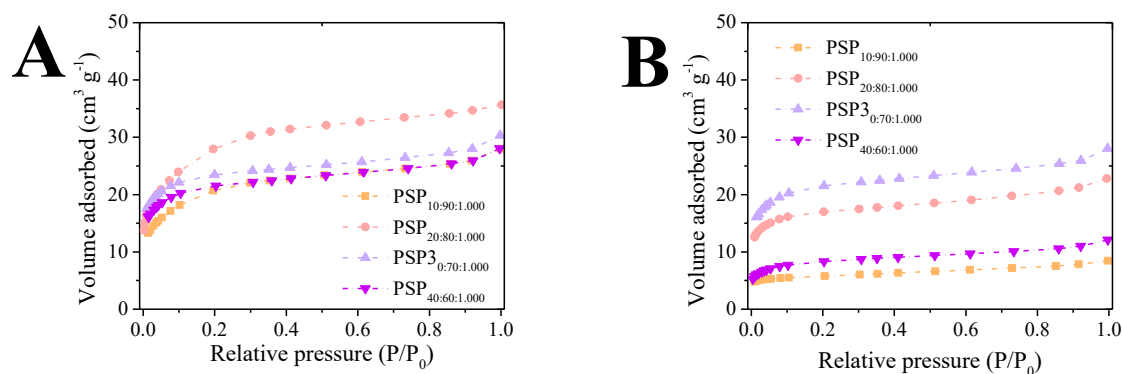


Figure S6: Nitrogen adsorption isotherms of the porous sulfur polymers (PSPs). $PSP_{X:Y:Z} = X\%[DIB]:Y\%[S_8]:Zg[NaCl]$.

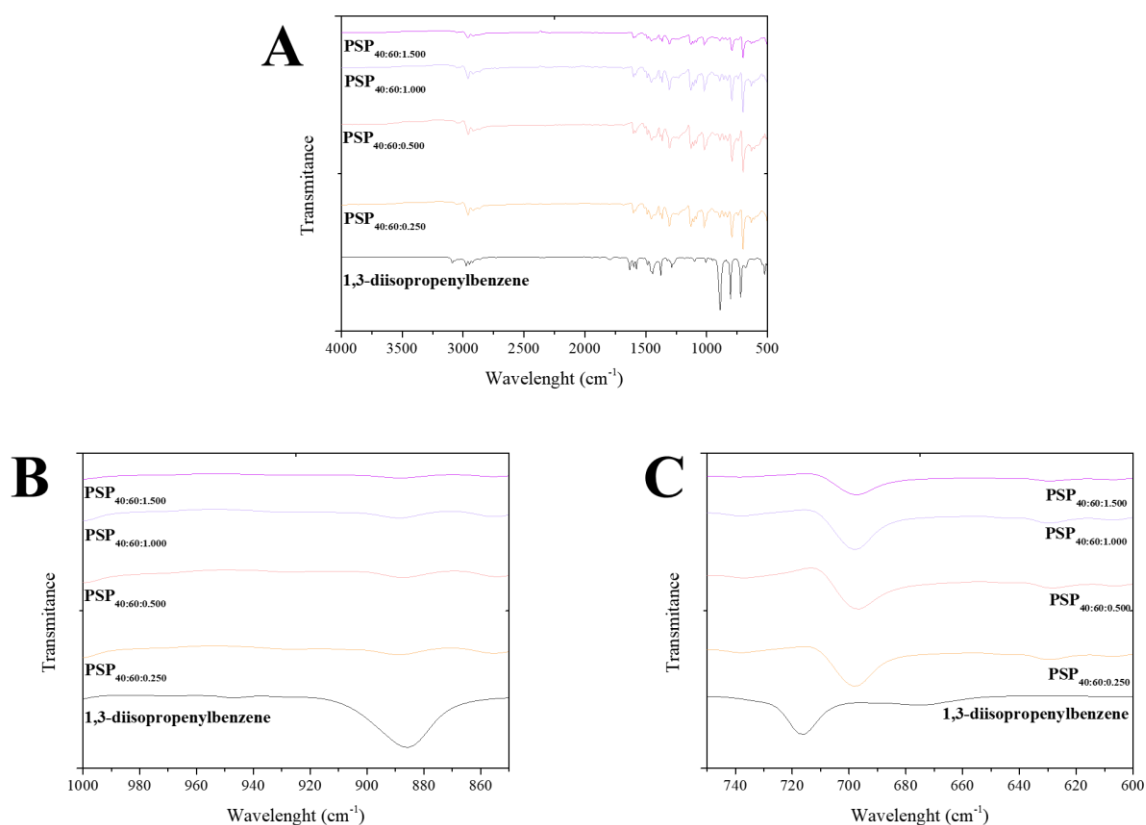


Figure S7: Fourier Transform Infrared (FTIR) spectra of the 1,3-diisopropenylbenzene (DIB) monomer and porous sulfur polymer (PSP) synthesized different amounts of salt. $PSP_{X:Y:Z} = X\%[DIB]:Y\%[S_8]:Zg[NaCl]$.

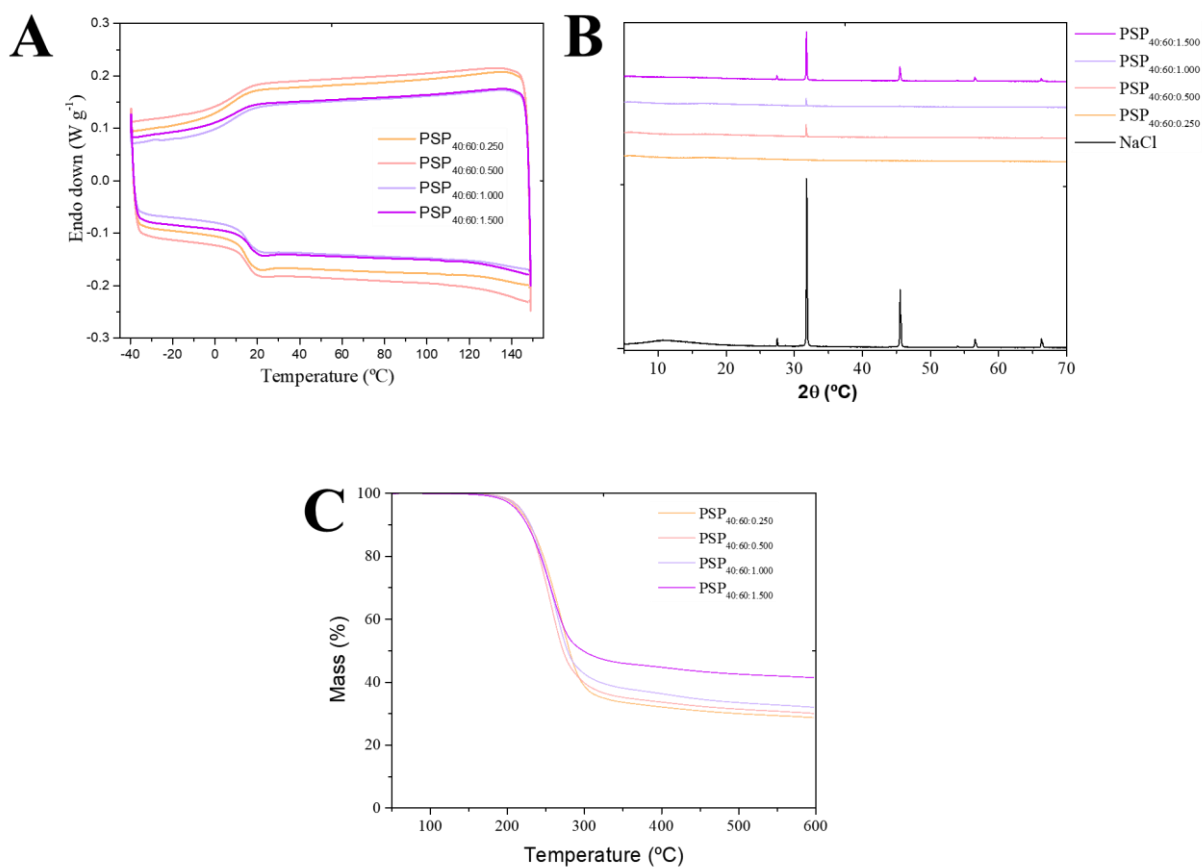


Figure S8: (A) Powder X-ray Diffraction, (B) Thermogravimetric analysis thermograms, and (C) Differential Scanning Calorimetry thermograms of the 1,3-diisopropenylbenzene monomer and porous sulfur polymers (PSPs) synthesized considering different amounts of salt. $PSP_{X:Y:Z} = X\%[DIB]:Y\%[S_8]:Zg[NaCl]$.

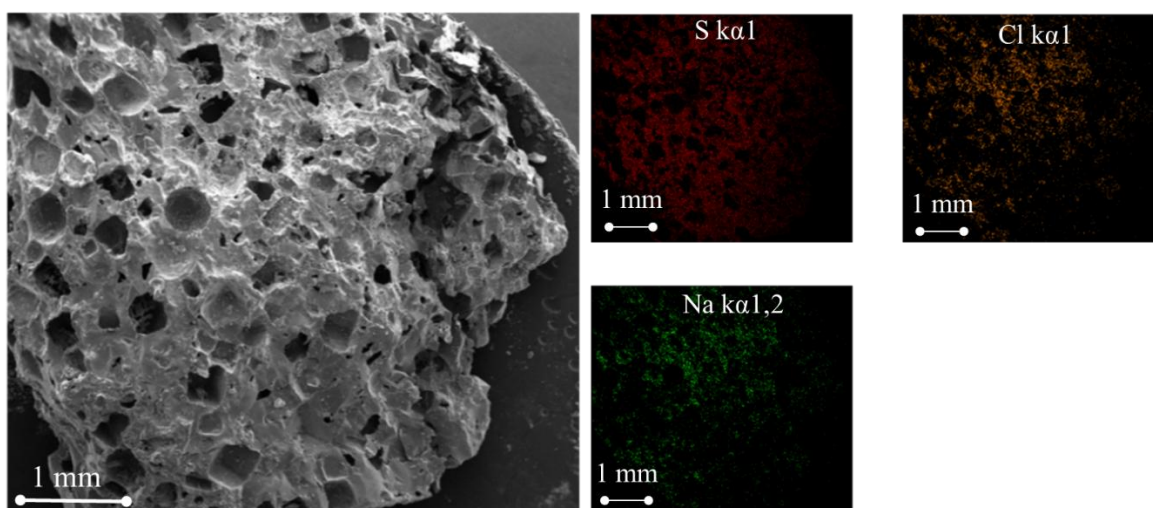


Figure S9: Scanning Electron Microscopy micrographs of $PSP_{40:60:1.500}$ after water treatment (insight image shows the Na, Cl, and S elemental mapping). $PSP_{X:Y:Z} = X\%[DIB]:Y\%[S_8]:Zg[NaCl]$.

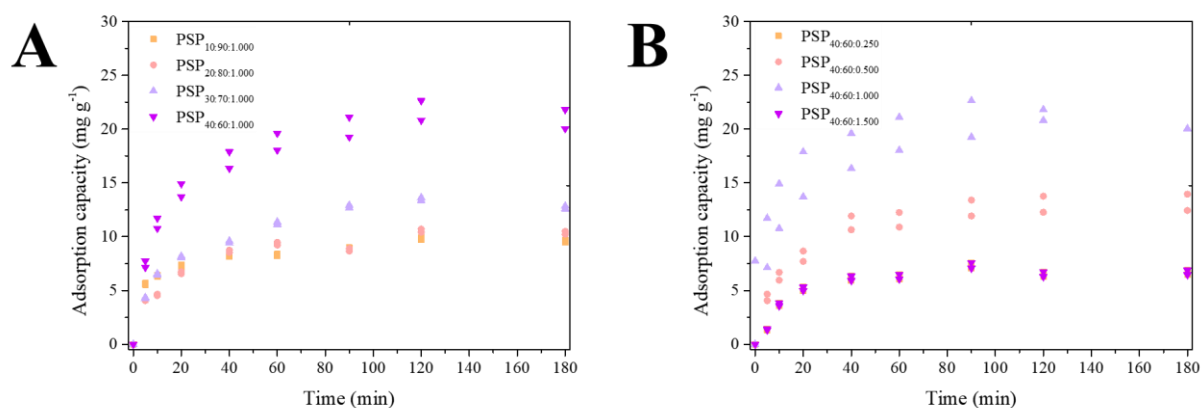


Figure S10: Adsorption kinetics of caffeine onto the porous sulfur polymers (PSPs). $PSP_{X:Y:Z} = X\%[DIB]:Y\%[S_8]:Zg[NaCl]$. Initial concentration of caffeine 7.5 mg/L and PSP loading 250 mg/L

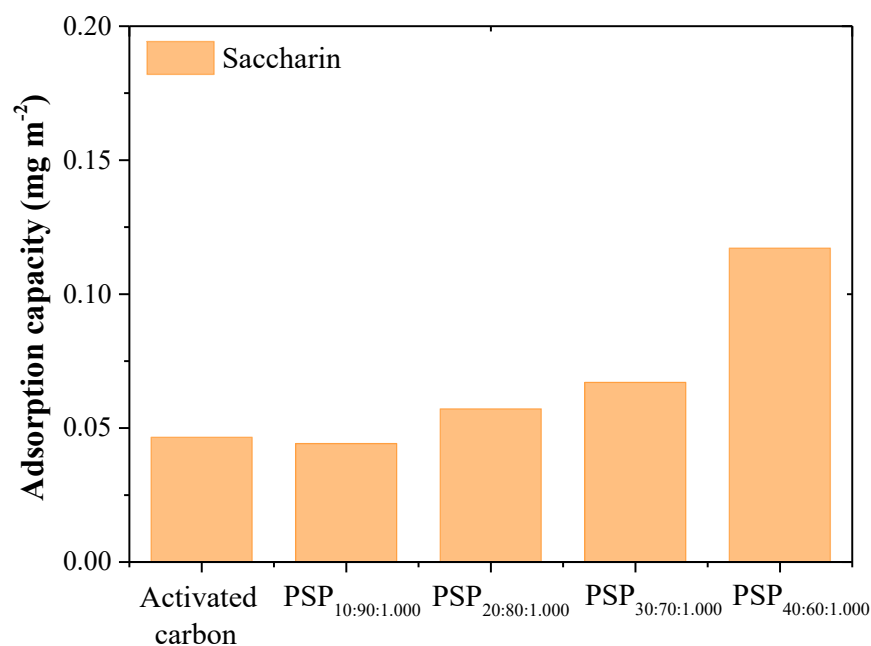


Figure S11: Normalized adsorption capacity of saccharin onto activated carbon and porous sulfur polymers. $PSP_{X:Y:Z} = X\%[DIB]:Y\%[S_8]:Zg[NaCl]$. Initial concentration of saccharin 7.5 mg/L and PSP loading 250 mg/L

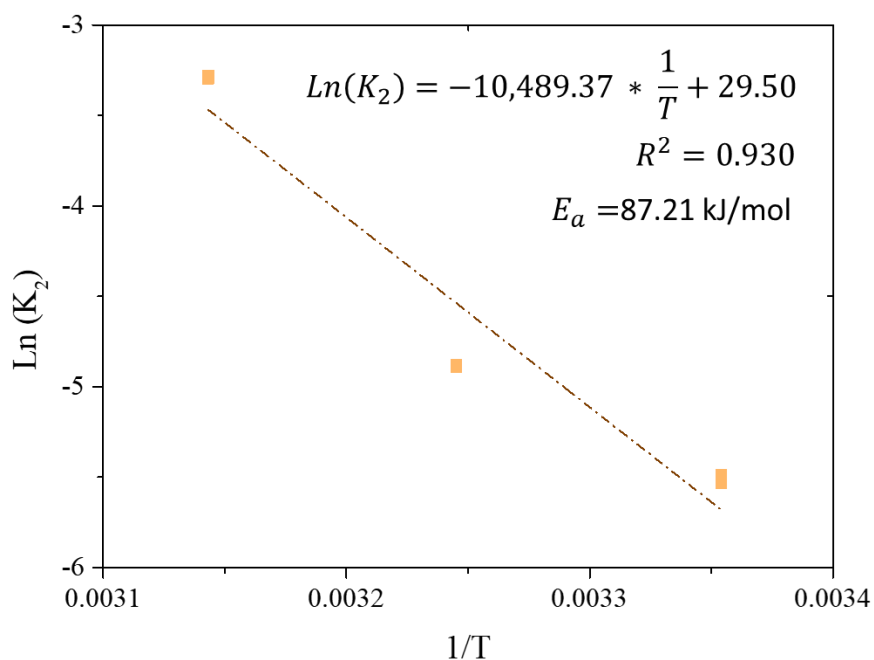


Figure S12: Influence of temperature on thermodynamic adsorption of caffeine and Arrhenius equation plot for adsorption of caffeine on $PSP_{40:60:1.000}$. $PSP_{X:Y:Z} = X\%[DIB]:Y\%[S_8]:Zg[NaCl]$.

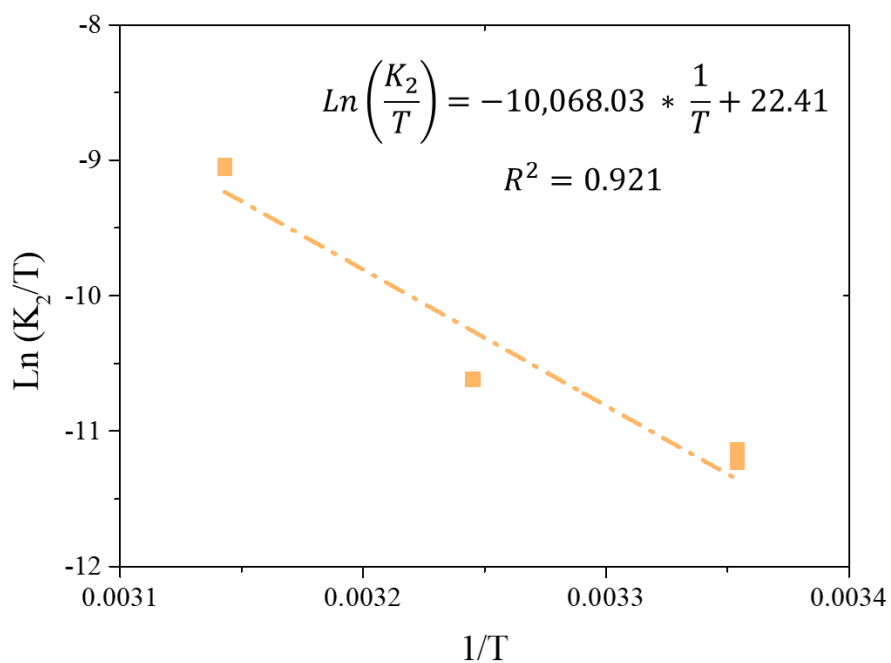


Figure S13: Influence of temperature on thermodynamic adsorption of caffeine and Eyring equation plot for adsorption of caffeine on $PSP_{40:60:1.000}$. $PSP_{X:Y:Z} = X\%[DIB]:Y\%[S_8]:Zg[NaCl]$.

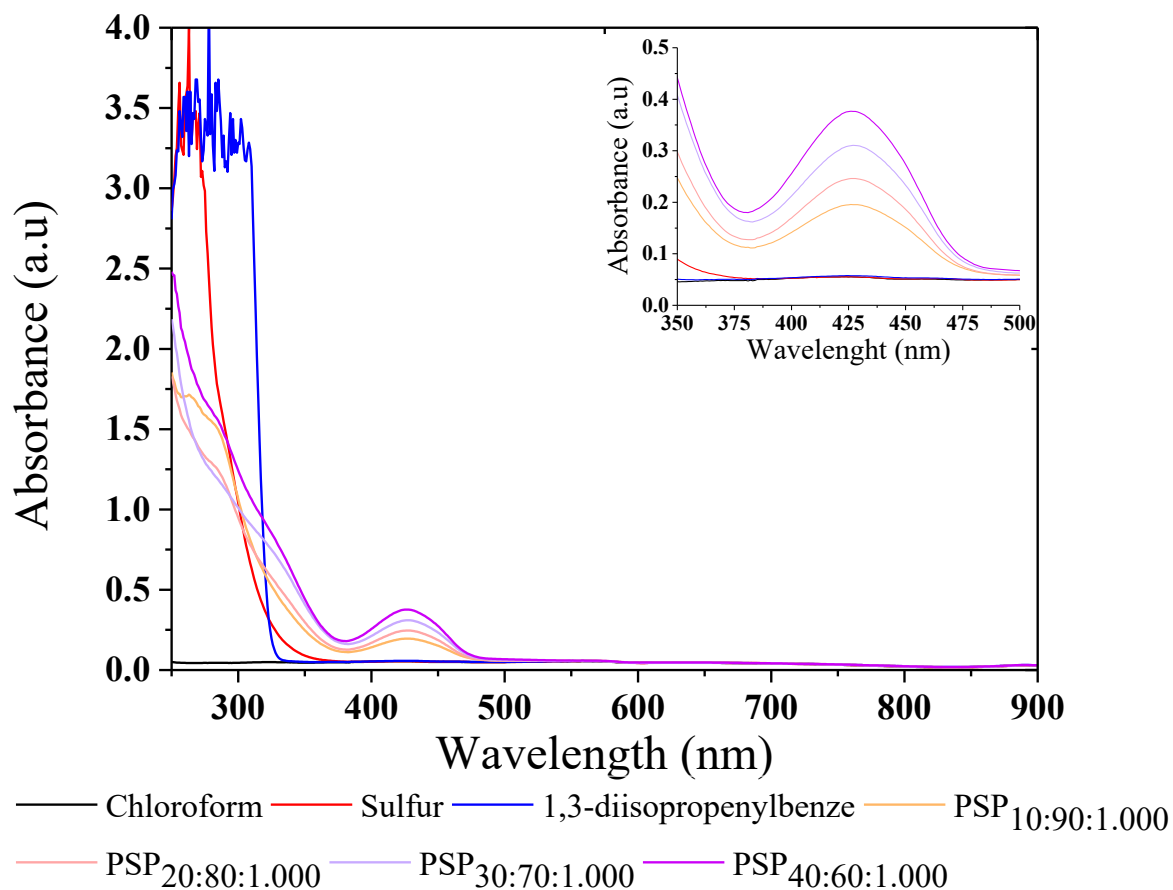


Figure S14: Ultraviolet-visible spectra of porous sulphur polymers (PSPs) from 900–250 nm, 1,3-diisopropenylbenzene (DIB), and sulfur dissolved in chloroform (5 ng/mL). The inset graph shows a zoom of the 500–350 nm region of the spectra. PSP_{X:Y:Z} = X%[DIB]:Y%[S₈]:Zg[NaCl].

LIST OF TABLES

Table S1: EDS spectra values of the PSP_{40:60:1.000} before and after water treatment, respectively.

PSP _{40:60:1.000}	Sulfur (%)	Chlorine (%)	Sodium (%)
Before water treatment	42.2 (0.3)	35.9 (0.3)	21.9 (0.3)
After water treatment	89.2 (0.3)	6.8 (0.2)	3.9 (0.2)

PSP_{X:Y:Z} = X%[DIB]:Y%[S₈]:Zg[NaCl].

Table S2: Surface area of the porous sulfur polymers.

1,3-Diisopropenylbenzene (%)	Sulfur (%)	Table salt (g)	Surface area (m ² g ⁻¹)
10	90	1.000	69.55
20	80	1.000	69.21
30	70	1.000	64.30
40	60	1.000	61.30
40	60	0.250	22.03
40	60	0.500	52.43
40	60	1.500	29.30

Table S3: Comparison of adsorption capacity of different adsorbents for caffeine.

Material	Initial Concentration (mg L ⁻¹)	Normalized adsorption capacity (mg m ²)	Reference
Activated carbon	7.5	0.067	This work
PSP _{10:90:1.000}	7.5	0.140	This work
PSP _{20:80:1.000}	7.5	0.153	This work
PSP _{30:70:1.000}	7.5	0.210	This work
PSP _{40:60:1.000}	7.5	0.355	This work
PSP _{40:60:0.250}	7.5	0.333	This work
PSP _{40:60:0.500}	7.5	0.252	This work
PSP _{40:60:1.500}	7.5	0.322	This work
Activated carbon	100.0	0.075	1
Activated carbon	500.0	0.159	2
Activated carbon	0.5	0.064	3
Activated carbon	120.0	0.216	4

PSPX:Y:Z = X%[DIB]:Y%[S₈]:Zg[NaCl].

1. K. K. Beltrame, A. L. Cazetta, P. S. C. de Souza, L. Spessato, T. L. Silva and V. C. Almeida, *Ecotox Environ Safe*, 2018, 147, 64-71.

Supplementary information: Porous sulfur polymers for effective aqueous-phase organic contaminant removal

2. H. G. Zanella, L. Spessato, G. K. P. Lopes, J. T. C. Yokoyama, M. C. Silva, P. S. C. Souza, A. Ronix, A. L. Cazetta and V. C. Almeida, J Mol Liq, 2021, 340.

3. V. Diniz, G. Rath, S. Rath, L. S. Araujo and D. G. F. Cunha, Environ Sci Pollut R, 2022, 29, 42185-42200.

4. G. Labuto, A. P. Carvalho, A. S. Mestre, M. S. dos Santos, H. R. Modesto, T. D. Martins, S. G. Lemos, H. D. T. da Silva, E. N. V. M. Carrilho and W. A. Carvalho, Sustain Chem Pharm, 2022, 28.

LIST OF EQUATIONS

Kinetics models

$q_i = q_{ads} (1 - e^{-k_1 t})$	Pseudo-first order model
$q_i = \frac{q_{ads}^2 k_2 t}{1 + k_2 q_{ads} t}$	Pseudo-second model
$q_i = \frac{1}{\beta} \ln (1 + \alpha \beta t)$	Elovich model
$q_i = k_i \sqrt{t} + C$	Intraparticle diffusion model
$\ln \left(1 - \frac{i}{q_{ads}} \right) = -k_{fd} t$	Film diffusion model

Where q_i (mg g^{-1}) represents the adsorption amount at the time of t (min), q_{ads} (mg g^{-1}) is the adsorption potential and t is time (min). k_1 (min^{-1}), k_2 (g mgmin^{-1}), k_i ($\text{mg g}^{-1} \text{min}^{-0.5}$) are the adsorption rate constants of the pseudo-first-order, pseudo-second order and Intraparticle diffusion model, respectively. C is a constant involving the liquid film thickness. α ($\text{mg g}^{-1} \text{min}^{-1}$) and β (mg g^{-1}) are the parameters of the Elovich model.

Isotherm models

$$q_i = \frac{q_{ads} K_L C_e}{1 + K_L C_e}$$

Langmuir model

$$q_i = K_F C_e^{\frac{1}{n}}$$

Freundlich model

$$q_i = \frac{K_{RP} C_e}{1 + \alpha_{RP} C_e^g}$$

Redlich-Peterson model

$$q_i = \frac{q_{ads} (K_S C_e)^n}{(K_S C_e)^n + 1}$$

Sips model

$$\ln(q_i) = -k_{DR} \varepsilon^2 + \ln(q_{ads})$$

$$\varepsilon = RT \ln \left(1 + \frac{1}{C_e/C_s} \right)$$

Dubinin-Radushkevich model

$$E = \frac{1}{\sqrt{2 k_{DR}}}$$

Where K_L ($L \text{ mg}^{-1}$), K_F ($((\text{mg/g})/(\text{mg/L})^n)$), and K_{RP} ($L \text{ mg}^{-1}$), and K_S ($L \text{ mg}^{-1}$) are the Langmuir, Freundlich, Redlich-Peterson, and Sips model constants, C_e (mg L^{-1}) is the concentration at equilibrium, $1/n$ is a constant related to the adsorption strength and n represents the inhomogeneity of the adsorbent. The closer the value of n is to 1, the more uniform the adsorbent surface is³³. α_{RP} ($(\text{mg L}^{-1})^g$) and g are also constant of the Redlich- Peterson model.

K_{DR} ($\text{mol}^2 \text{ kJ}^{-2}$) is the constant of the Dubinin-Radushkevich model. ε (kJ mol^{-1}) is the Polanyi potential. C_s is the solubility of caffeine in water at 25°C (21.7 g L^{-1}). E is the free energy (kJ mol^{-1}).

Thermodynamics models

$Ln(K_2) = -\frac{E_a}{RT} + Ln(A)$	Arrhenius model
$Ln\left(\frac{K_2}{T}\right) = -\frac{\Delta H^\#}{RT} + \left(Ln\left(\frac{k_b}{h}\right) + \frac{\Delta S^\#}{R}\right)$	Eyring model

Where A was the Arrhenius constant, R is the gas constant ($8.314 \text{ J mol}^{-1} \text{ K}^{-1}$) and T is the temperature (K). $\Delta H^\#$ is the standard enthalpy (J mol^{-1}), $\Delta S^\#$ is the entropy of activation ($\text{J mol}^{-1} \text{ K}^{-1}$), k_b is the Boltzman constant ($1.3807 \times 10^{-23} \text{ J K}^{-1}$), and h is the plank constant ($6.6261 \times 10^{-34} \text{ Js}$).